




ADVERTIMENT. L'accés als continguts d'aquesta tesi queda condicionat a l'acceptació de les condicions d'ús establertes per la següent llicència Creative Commons:  http://cat.creativecommons.org/?page_id=184

ADVERTENCIA. El acceso a los contenidos de esta tesis queda condicionado a la aceptación de las condiciones de uso establecidas por la siguiente licencia Creative Commons:  <http://es.creativecommons.org/blog/licencias/>

WARNING. The access to the contents of this doctoral thesis it is limited to the acceptance of the use conditions set by the following Creative Commons license:  <https://creativecommons.org/licenses/?lang=en>



Universitat Autònoma de Barcelona
Departament de Bioquímica i Biologia Molecular
and
Institut de Biotecnologia i Biomedicina (IBB)

Preventing α -Synuclein aggregation.
Finding disease modifying molecules
for Parkinson's disease

Samuel Peña Díaz



Universitat Autònoma de Barcelona
Departament de Bioquímica i Biologia Molecular
and
Institut de Biotecnologia i Biomedicina (IBB)

Preventing α -Synuclein aggregation. Finding disease modifying molecules for Parkinson's disease

Doctoral thesis submitted by Samuel Peña Díaz as candidate for the degree of Ph-D in Biochemistry, Molecular Biology and Biomedicine from the Universitat Autònoma de Barcelona (UAB).

The work described here has been developed at the Department of Biochemistry and Molecular Biology and at the Institute of Biotechnology and Biomedicine (IBB), under the supervision of Prof. Salvador Ventura Zamora.

Samuel Peña Díaz

Prof. Salvador Ventura Zamora

Bellaterra, September 2022

Summary (English)

Neurodegenerative disorders, such as Parkinson's or Alzheimer's diseases, are one of the biggest health challenges in modern society. The lack of effective treatments and early-diagnosis techniques, together with the gradual aging population, contributes to worsening these conditions, significantly impacting society and the healthcare system. Therefore, developing new diagnostic and therapeutic techniques is a necessary goal. Many neurodegenerative disorders are characterised by the presence of intra/extracellular proteinaceous accumulations, often because of the formation of highly ordered aggregates named amyloids, which exhibit toxicity and transmission capacities. In particular, Parkinson's disease is characterised by the loss of dopaminergic cells in *substantia nigra pars compacta*, which induces motor deficits, causing bradykinesia, tremor or rigidity. Although the cause of Parkinson's disease remains unknown, affected tissues exhibit intracellular accumulations of proteins, whose main components are amyloid forms of α -Synuclein.

This protein, characterised by its disordered nature, is preferentially located at the presynaptic termini as a soluble monomer. Nevertheless, in pathological conditions, α -Synuclein establishes intermolecular interactions that lead to the formation of insoluble amyloids fibrils. These fibrillar aggregates alter cellular homeostasis and accumulate into Lewy's bodies or neurites, kidnapping several cellular components along the process. Moreover, intermediates formed during aggregation, as oligomers or protofibrils, have been described as toxic and transmissible entities that induce cell death and cell-to-cell spreading of the pathology. Unfortunately, the complexity and heterogeneity of this process have hindered the development of effective therapies and diagnostic tools for Parkinson's Disease.

The present thesis attempts to develop effective molecules that prevent α -Synuclein aggregation, reducing amyloid toxicity and spreading. By implementing a robust technique for the screening of large chemical libraries we have discovered and characterised different molecular chaperones that efficiently halt α -Synuclein *in vitro* aggregation. In addition, the work here described elucidates the inhibitory mechanism and the properties of the obtained molecules. We also clarified the structures or steps of the process targeted by the compounds, their minimum effective concentration, and their effect on familiar variants of Parkinson's disease. Furthermore, as α -Synuclein can adopt multiple amyloid conformations depending on the environmental conditions, this thesis also addresses if the molecules inhibitory capacity is consistent against different amyloid strains. Altogether, the final goal of this work is to identify, validate and characterize the mechanisms of action of different molecular scaffolds that can be potentially evolved into disease-modifying drugs with neuroprotective activity.

Resum (Catalá)

Les malalties neurodegeneratives, com el Parkinson o l'Alzheimer, són un dels reptes més grans de la societat moderna. La manca de tractaments efectius i tècniques de diagnòstic precoç, juntament amb l'envelliment gradual de la població, contribueix a agreujar aquesta situació, impactant significativament en la societat i els sistemes de salut. Per tant, desenvolupar noves tècniques diagnòstiques i terapèutiques és un objectiu imperatiu. Nombrosos trastorns neurodegeneratius es distingeixen per la presència d'acumulacions proteiques intra/extracel·lulars com a conseqüència de la formació d'agregats molt ordenats anomenats amiloides, que presenten una gran toxicitat i capacitat de transmissió. En particular, la malaltia de Parkinson es caracteritza per la pèrdua de cèl·lules dopaminèrgiques a la substància negra pars compacta el que indueix un important dèficit motor que provoca bradicinèsia, tremolor o rigidesa. Tot i que es desconeix la causa de la malaltia de Parkinson, els teixits afectats presenten acumulacions intracel·lulars de proteïnes, els components principals de les quals són les estructures amiloides de l' α -Sinucleïna.

Aquesta proteïna, caracteritzada per la seva naturalesa desordenada, es localitza preferentment als extrems presinàptics com a monòmer soluble. Tot i això, en condicions patològiques, l' α -Sinucleïna estableix interaccions intermoleculars que condueixen a la formació de fibrilles amiloides insolubles. Aquests agregats fibril·lars alteren significativament l'homeòstasi cel·lular i s'acumulen als cossos de Lewy o neurites, segregant diversos components cel·lulars al llarg del procés. A més, les estructures intermèdies formades durant l'agregació, com ara oligòmers o protofibril·les, s'han descrit com a entitats tòxiques i transmissibles que indueixen la mort cel·lular i la propagació de la patologia de cèl·lula a cèl·lula. Malauradament, la complexitat i l'heterogeneïtat d'aquest procés han dificultat el desenvolupament de teràpies i diagnòstics efectius per a la malaltia de Parkinson.

Aquesta tesi pretén desenvolupar molècules efectives que impedeixin l'agregació de proteïnes, redueixin la toxicitat i la propagació de l'amiloides. En implementar una tècnica robusta per a l'anàlisi de grans biblioteques químiques, hem descobert i caracteritzat diferents xaperones moleculars potents que obstaculitzen de manera eficient l'agregació in vitro de α -Sinucleïna. A més, el treball aquí descrit aclareix el mecanisme inhibitori i les propietats de les molècules obtingudes. També aclarim les estructures o passos del procés abordat pels compostos, la concentració mínima efectiva i el seu efecte en variants familiars de la malaltia de Parkinson. A més, com que l' α -Sinucleïna pot adoptar múltiples conformacions amiloides depenent de les condicions ambientals, aquesta tesi també se centra a discernir si la capacitat inhibidora d'aquestes molècules és consistent davant de diferents ceps amiloides. En conjunt, l'objectiu final d'aquest treball és identificar validar i caracteritzar els mecanismes d'acció de diferents estructures moleculars, que poden evolucionar potencialment a fàrmacs modificats de la malaltia, presentant una activitat neuroprotectora

Resumen (Español)

Las enfermedades neurodegenerativas, como el Parkinson o el Alzheimer, son uno de los mayores desafíos de la sociedad moderna. La falta de tratamientos efectivos y técnicas de diagnóstico precoz, junto con el paulatino envejecimiento de la población, contribuye a agravar esta situación, impactando significativamente en la sociedad y los sistemas de salud. Por lo tanto, desarrollar nuevas técnicas diagnósticas y terapéuticas es un objetivo imperativo. Numerosos trastornos neurodegenerativos se distinguen por la presencia de acumulaciones proteicas intra/extracelulares como consecuencia de la formación de agregados muy ordenados denominados amiloides, que presentan una gran toxicidad y capacidad de transmisión. En particular, la enfermedad de Parkinson se caracteriza por la pérdida de células dopaminérgicas en la *sustancia negra pars compacta* lo que induce un importante déficit motor que provoca bradicinesia, temblor o rigidez. A pesar de que se desconoce la causa de la enfermedad de Parkinson, los tejidos afectados presentan acumulaciones intracelulares de proteínas, cuyo principal componente son las estructuras amiloides de la α -Sinucleína.

Esta proteína, caracterizada por su naturaleza desordenada, se localiza preferentemente en los extremos presinápticos como monómero soluble. Sin embargo, en condiciones patológicas, la α -Sinucleína establece interacciones intermoleculares que conducen a la formación de fibrillas amiloides insolubles. Estos agregados fibrilares alteran significativamente la homeostasis celular y se acumulan en los cuerpos de Lewy o neuritas, secuestrando varios componentes celulares a lo largo del proceso. Además, las estructuras intermedias formadas durante la agregación, como oligómeros o protofibrillas, se han descrito como entidades tóxicas y transmisibles que inducen la muerte celular y la propagación de la patología de célula a célula. Desafortunadamente, la complejidad y heterogeneidad de este proceso han dificultado el desarrollo de terapias y diagnósticos efectivos para la enfermedad de Parkinson.

La presente tesis pretende desarrollar moléculas efectivas que impidan la agregación de proteínas, reduciendo la toxicidad y propagación del amiloide. Al implementar una técnica robusta para el análisis de grandes bibliotecas químicas, hemos descubierto y caracterizado diferentes chaperonas moleculares potentes que detienen de manera eficiente la agregación *in vitro* de α -Sinucleína. Además, el trabajo aquí descrito aclara el mecanismo inhibitorio y las propiedades de las moléculas obtenidas. También aclaramos las estructuras o pasos del proceso abordados por los compuestos, su concentración mínima efectiva y su efecto en variantes familiares de la enfermedad de Parkinson. Además, como la α -Sinucleína puede adoptar múltiples conformaciones amiloides dependiendo de las condiciones ambientales, esta tesis también se centra en discernir si la capacidad inhibidora de estas moléculas es consistente frente a diferentes cepas amiloides. En conjunto, el objetivo final de este trabajo es identificar, validar y caracterizar los mecanismos de acción de diferentes estructuras moleculares, que pueden evolucionar potencialmente a fármacos modificadores de la enfermedad, presentando una actividad neuroprotectora.

List of publications

This thesis is composed by the following published articles:

1. Jordi Pujols[†], **Samuel Peña-Díaz**[†], María Conde-Giménez, Francisca Pinheiro, Susanna Navarro, Javier Sancho and Salvador Ventura
High-throughput screening methodology to identify alpha-synuclein aggregation inhibitors. *Int. J. Mol. Sci.* 2017, 18, 478
2. Jordi Pujols[†], **Samuel Peña-Díaz**[†], Diana F. Lázaro, Francesca Peccati, Francisca Pinheiro, Danilo González, Anita Carija, Susanna Navarro, María Conde-Giménez, Jesús García, Salvador Guardiola, Ernest Giralt, Xavier Salvatella, Javier Sancho, Mariona Sodupe, Tiago Fleming Outeiro, Esther Dalfó, and Salvador Ventura
Small molecule inhibits α -Synuclein aggregation, disrupts amyloid fibrils, and prevents degeneration of dopaminergic neurons. *PNAS*. 2018, 115 (41), 10481-10486
3. **Samuel Peña-Díaz**[†], Jordi Pujols[†], María Conde-Giménez, Anita Čarija, Esther Dalfo, Jesús García, Susanna Navarro, Francisca Pinheiro, Jaime Santos, Xavier Salvatella, Javier Sancho and Salvador Ventura
ZPD-2, a small compound that inhibits α -Synuclein amyloid aggregation and its seeded polymerization. *Front. Mol. Neurosci.* 2019, 12:306
4. **Samuel Peña-Díaz**[†], Jordi Pujols[†], Francisca Pinheiro, Jaime Santos, Irantzu Pallarés, Susanna Navarro, María Conde-Giménez, Javier García, Xavier Salvatella, Esther Dalfó, Javier Sancho, Salvador Ventura
Inhibition of α -Synuclein Aggregation and Mature Fibril Disassembling With a Minimalistic Compound, ZPDm. *Front. Bioeng. Biotechnol.* 2020, 16;8:588947
5. **Samuel Peña-Díaz**[†], Jordi Pujols[†], Eftychia Vasili, Francisca Pinheiro, Jaime Santos, Zoe Mangano-Artuñedo, Tiago F. Outeiro and Salvador Ventura
The small aromatic compound SynuClean-D inhibits the aggregation and seeded polymerization of multiple α -Synuclein strains. *JBC*. 2022, 298(5) 101902

[†] Both authors contributed equally to the work.

Other co-first authored and related articles that are not part of this thesis:

1. **Samuel Peña-Díaz**, Jordi Pujols, Salvador Ventura
Small molecules to prevent the neurodegeneration caused by α -Synuclein aggregation. *Neural Regen. Res.* 2020, 15(12):2260-2261
2. **Samuel Pena-Díaz**, Salvador Ventura
One ring is sufficient to inhibit α -Synuclein aggregation. *Neural Regen Res.* 2022, 17(3):508-511

Other articles that are not part of this thesis:

1. Jordi Pujols, **Samuel Peña-Díaz**, and Salvador Ventura
AGGRESKAN3D: toward the prediction of the aggregation propensities of protein structures. *Computational Drug Discovery and Design*. 2018, pp 427-443
2. Jordi Pujols, **Samuel Peña-Díaz**, Irantzu Pallarès and Salvador Ventura
Chemical chaperones as novel drugs for Parkinson's disease. *Trends. Mol. Med.* 2020, 26, 4, 408-421
3. Serena Vittorio, Ilenia Adornato, Rosaria Gitto, **Samuel Peña-Díaz**, Salvador Ventura, Laura De Luca

- Rational design of small molecules able to inhibit α -Synuclein amyloid aggregation for the treatment of Parkinson's disease. *J. Enzyme. Inhib. Med. Chem.* 2020, 35(1):1727-173
4. Jaime Santos, Pablo Gracia, Susanna Navarro, **Samuel Peña-Díaz**, Jordi Pujols, Nunilo Cremades, Irantzu Pallarès, Salvador Ventura
 α -Helical peptidic scaffolds to target α -Synuclein toxic species with nanomolar affinity. *Nat. Commun.* 2021, 12(1):3752
 5. Alejandro Mahía, **Samuel Peña-Díaz**, Susanna Navarro, Juan José Galano-Frutos, Irantzu Pallarés, Jordi Pujols, María D Díaz-de-Villegas, José A Gálvez, Salvador Ventura, Javier Sancho
Design, synthesis and structure-activity evaluation of novel 2-pyridone-based inhibitors of α -Synuclein aggregation with potentially improved BBB permeability. *Bioorg. Chem.* 2021, 117:105472
 6. Federica Quaglia, Bálint Mészáros, Edoardo Salladini, András Hatos, Rita Pancsa, Lucía B Chemes, Mátyás Pajkos, Tamas Lazar, **Samuel Peña-Díaz**, Jaime Santos, et al.
DisProt in 2022: improved quality and accessibility of protein intrinsic disorder annotation. *Nucleic Acids Res.* 2022, 50(D1):D480-D487
 7. Rosaria Gitto, Serena Vittorio, Federica Bucolo, **Samuel Peña-Díaz**, Rosalba Siracusa, Salvatore Cuzzocrea, Salvador Ventura, Rosanna Di Paola, Laura De Luca
Discovery of Neuroprotective Agents Based on a 5-(4-Pyridinyl)-1,2,4-triazole Scaffold. *ACS Chem. Neurosci.* 2022, 13(5):581-586

Abbreviations

6-OHDA	6-hydroxydopamine
α -Syn	α -Synuclein
AD	Alzheimer's disease
AADC	L-Amino Acid Decarboxylase
AADC	Aromatic amino acid decarboxylase
AFM	Atomic Force Microscopy
APRs	Aggregation Prone Regions
ARTN	Artemin
BBB	Blood-Brain Barrier
CD	Circular Dichroism
CNS	Central Nervous System
COMT	Catechol-O-methyltransferase
CR	Congo Red
CRH	Corticotropin-Releasing Hormone
Cryo-EM	Cryo Electron Microscopy
csg	Curli Specific Genes
cv	Column Volumes
DA	Dopaminergic
DBS	Deep Brain Stimulation
DLB	Dementia with Lewy Body
DPP	3,5-diphenyl-pyrazole
EGCG	Epigallocatechin gallate
FTIR	Fourier Transformer Infra-Red
GAD	Glutamic Acid Decarboxylase
GCH	GTP Cyclohydroxylase
GDNF	Glial Cell-line Derived Neurotrophic Factor
GFP	Green Fluorescent Protein
IDP	Intrinsically disordered protein
L4	Fourth larval stage
LBs	Lewy bodies
L-DOPA	L-3,4-dihydroxyphenylalanine
LMTM	Leuco-Methylthionium bis(hydromethanesulphonate)
LN _s	Lewy neurites
MAOB	Monoamine oxidase-B

MPTP	1-methyl-4-phenyl-1,2,3,6-tetrahydropyridine
MS	Motor Symptoms
MSA	Multiple System Atrophy
MT	Methylthioninium
MTC	Methylthioninium chloride
NAC	Non Amyloid Component
NGM	Nematode Growth Media
NMR	Nuclear Magnetic Resonance
NMS	Non-Motor Symptoms
NRTN	Neurtinin
PBS	Phosphate-Buffered Saline
PD	Parkinson's disease
PET	Positron Emission Tomography
PGC1 α	Peroxisome proliferator-activated receptor- γ co-activator 1 α
PK	Proteinase K
PMCA	Protein Misfolding Cyclic Amplification
PMEL	Premelanosome protein
PNS	Peripheral Nervous System
PrP	Prion protein
PSMs	Phenol-Soluble Modulins
PSPN	Persephin
SAR	Structure-Activity Relationship
SC-D	SynuClean-D
SDS-PAGE	Sodium Dodecyl Sulfate Polyacrylamide Gel Electrophoresis
SNc	Substantia Nigra pars compacta
SPECT	Single Photon Emission Computed Tomography
ssNMR	solid-state Nuclear Magnetic Resonance
TEM	Transmission Electron Microscopy
TH	Tyrosine Hydroxylase
Th-T	Thioflavin-T
UPDRS	Unified Parkinson's Diseases Ratings Scale
VEGF	Vascular Endothelial Growth Factor
WT	Wild-type
YFP	Yellow Fluorescent Protein

Contents

1. Introduction	1
1.1. Aggregation, a protein landscape beyond folding	1
1.1.1. <i>Folding or aggregation? A conflict of proteins</i>	1
1.1.2. <i>Insights on protein aggregation</i>	5
1.1.3. <i>Amyloids: functional or dangerous?.....</i>	7
1.2. Parkinson's disease	10
1.2.1. <i>Historical overview</i>	10
1.2.2. <i>Symptomatology</i>	12
1.2.3. <i>Risk factors and molecular mechanisms</i>	13
1.2.4. <i>Alpha-synuclein</i>	17
1.2.5. <i>Current diagnosis and treatments.....</i>	20
1.3. Other synucleinopathies	28
1.3.1. <i>Multiple system atrophy (MSA).....</i>	28
1.3.2. <i>Dementia with Lewy's bodies (DLB)</i>	30
2. Research objectives.....	31
2.1. Chapter 1. High-throughput screening methodology to identify alpha-synuclein aggregation inhibitors	31
2.2. Chapter 2. Small molecule inhibits α-Synuclein aggregation, disrupts amyloid fibrils, and prevents degeneration of dopaminergic neurons.....	31
2.3. Chapter 3. ZPD-2, a Small Compound That Inhibits α-Synuclein Amyloid Aggregation and Its Seeded Polymerization	32
2.4. Chapter 4. Inhibition of α-Synuclein Aggregation and Mature Fibril Disassembling With a Minimalistic Compound, ZPDm	32

2.5. Chapter 5. The small aromatic compound SynuClean-D inhibits the aggregation and seeded polymerization of multiple α -Synuclein strains	33
3. Chapters	34
3.1. Chapter 1. High-throughput screening methodology to identify alpha-synuclein aggregation inhibitors	34
3.2. Chapter 2. Small molecule inhibits α -Synuclein aggregation, disrupts amyloid fibrils, and prevents degeneration of dopaminergic neurons.....	47
3.3. Chapter 3. ZPD-2, a Small Compound That Inhibits α -Synuclein Amyloid Aggregation and Its Seeded Polymerization	54
3.4. Chapter 4. Inhibition of α -Synuclein Aggregation and Mature Fibril Disassembling With a Minimalistic Compound, ZPDm	67
3.5. Chapter 5. The small aromatic compound SynuClean-D inhibits the aggregation and seeded polymerization of multiple α -Synuclein strains	80
4. Concluding remarks.....	92
4.1. Chapter 1. High-throughput screening methodology to identify alpha-synuclein aggregation inhibitors	92
4.2. Chapter 2. Small molecule inhibits α -Synuclein aggregation, disrupts amyloid fibrils, and prevents degeneration of dopaminergic neurons.....	92
4.3. Chapter 3. ZPD-2, a Small Compound That Inhibits α -Synuclein Amyloid Aggregation and Its Seeded Polymerization	93
4.4. Chapter 4. Inhibition of α -Synuclein Aggregation and Mature Fibril Disassembling With a Minimalistic Compound, ZPDm	94
4.5. Chapter 5. The small aromatic compound SynuClean-D inhibits the aggregation and seeded polymerization of multiple α -Synuclein strains	95

5. Annex: Supplementary information	96
5.1. Chapter 2. Small molecule inhibits α -Synuclein aggregation, disrupts amyloid fibrils, and prevents degeneration of dopaminergic neurons.....	96
5.2. Chapter 3. ZPD-2, a Small Compound That Inhibits α -Synuclein Amyloid Aggregation and Its Seeded Polymerization	119
5.3. Chapter 4. Inhibition of α -Synuclein Aggregation and Mature Fibril Disassembling With a Minimalistic Compound, ZPDm	126
5.4. Chapter 5. The small aromatic compound SynuClean-D inhibits the aggregation and seeded polymerization of multiple α -Synuclein strains	130
6. References	140

1. Introduction

1.1. Aggregation, a protein landscape beyond folding

Proteins and peptides are natural polymers essentially constituted by a combination of 20 different amino acids (**Fig. 1A**). They play a key role in most cellular processes, and their chemical and physical properties vary depending on their amino acid side chains ¹. Traditionally, it has been considered that proteins need to adopt a particular three-dimensional structure, known as native conformation, from an initially unstructured conformation (unfolded state), in order to develop their biological functions. This complex process is called protein folding ² and it is encoded in the amino acid sequence of the protein, as demonstrated by Christian B. Anfinsen ³. Anfinsen's theory considered that this native structure was the thermodynamic global minimum of Gibbs energy in physiological conditions and, thus, the most stable conformation of a protein ³. However, recent evidence indicates that more stable states, like aggregates, can be adopted under certain conditions ^{4,5}.

1.1.1. *Folding or aggregation? A conflict of proteins*

Proteins are biological macromolecules with a large variety of lengths and properties. They constitute the basic machinery of all living organisms as they are required in a multitude of molecular functions such as signalling, transport, structure, catalysis, or gene regulation ^{1,6}. Proteins are synthesised in the ribosomes as a combination of multiple amino acids, whose side chains determine their properties (**Fig. 1A**). The distribution of these residues on the sequence dictates protein function and conformation ⁶. To perform their biological role, proteins need to acquire a unique three-dimensional organisation or native state in a process called protein folding ², which is driven by non-covalent interactions between neighbouring residues in the protein sequence.

These non-covalent interactions between residues give rise to different hierarchical levels of organisation (**Fig. 1B**) ⁶. The first level or primary structure corresponds to the linear sequence of amino acids that starts from the amino-terminal end (N-terminal) and finishes in the carboxyl-terminal end (C-terminal). This sequence is maintained by peptide bonds, covalent interactions between the N-terminal and the C-terminal ends of adjacent residues ⁶. The next level of organisation, called secondary structure, accounts for the local three-dimensional distributions of protein residues, mostly as α -helices or β -sheets, preferentially sustained by intramolecular hydrogen bonds. The spatial packing of these secondary structures into a compact conformation leads to the tertiary structure. Hydrogen bonds, Van der Waals forces, electrostatic interactions and disulphide bonds are some of the intramolecular contacts that facilitate the formation of this three-dimensional architecture. In some cases, non-covalent intermolecular contacts between independent, folded polypeptides form the basis for a higher level of organization, the quaternary structure ⁶. However, not all proteins present a quaternary structure. Despite protein folding is a key biological process tightly controlled by various machineries such as chaperones, numerous errors can occur. These non-native interactions conduct to the formation of misfolded, aberrant structures related to human disorders as Parkinson's (PD) or Alzheimer's diseases (AD) ⁷⁻¹¹.

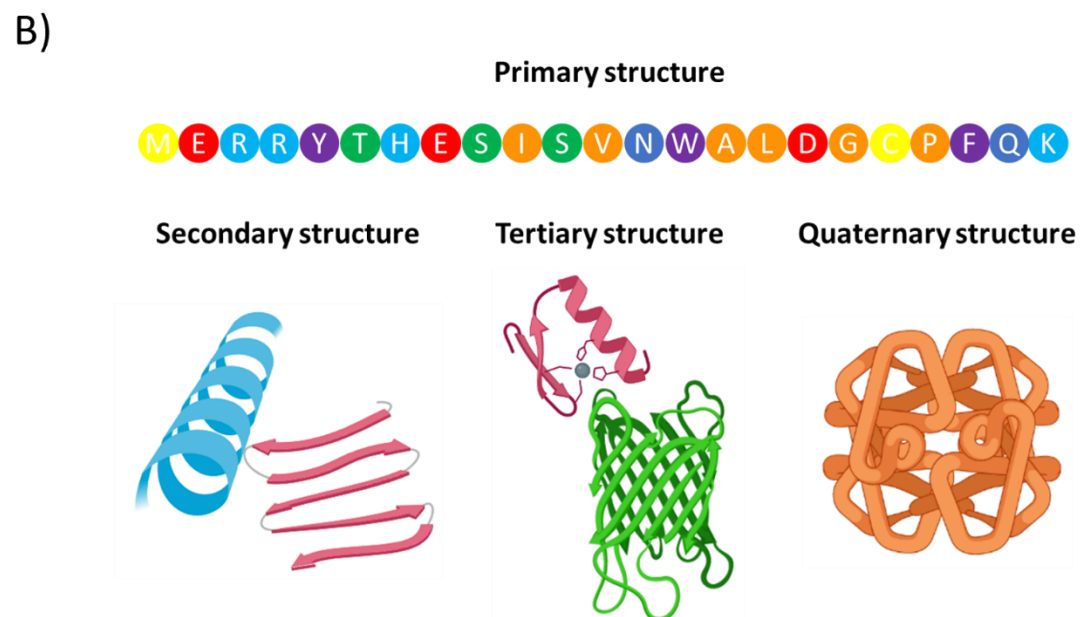
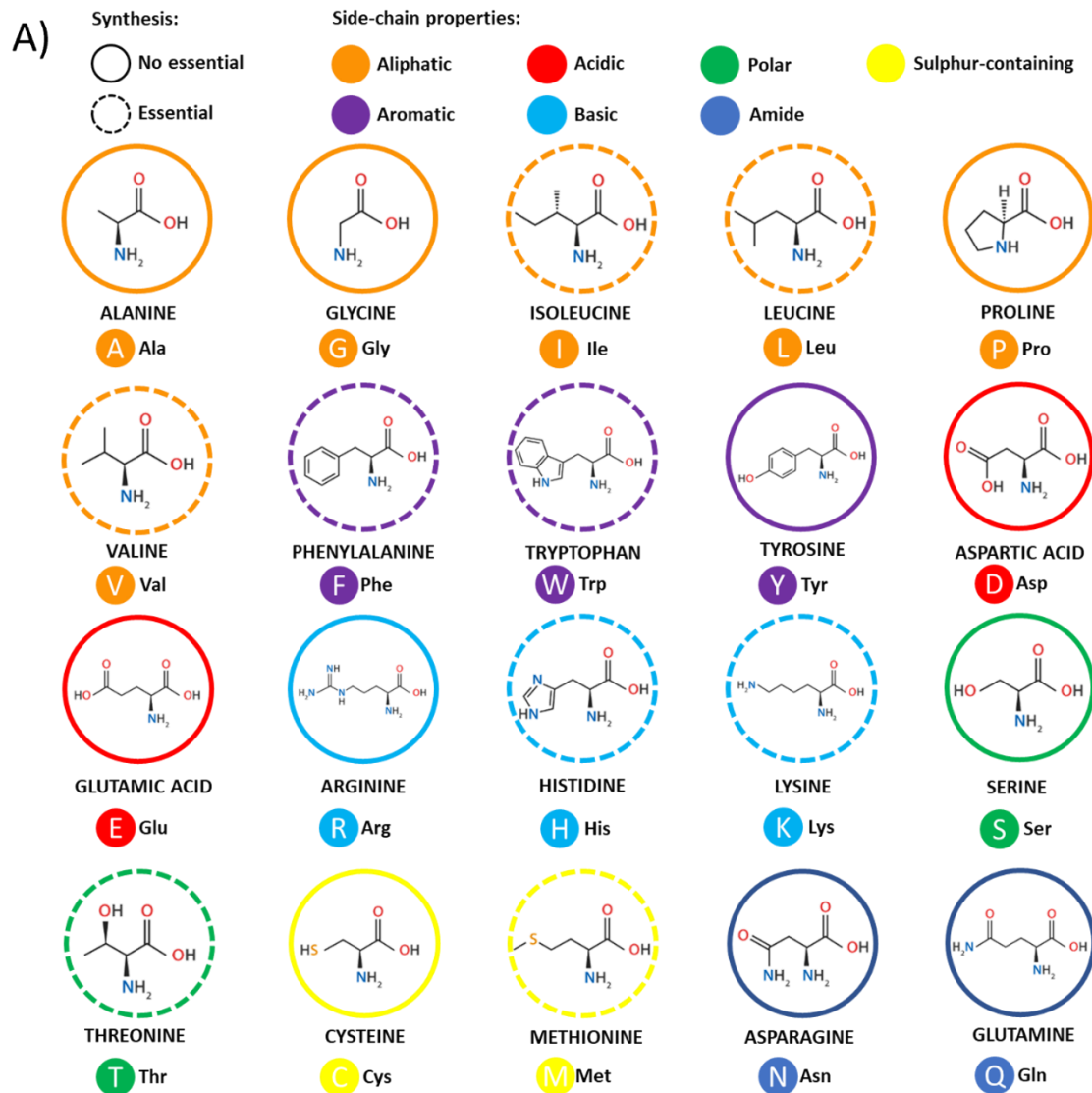


Figure 1. Protein structural basis. (A) Schematic representation of amino acid structure classified according to the side-chains properties and the capacities to be synthesised by the organism. (B) Overview of the hierarchical levels of protein organisation.

Understanding how proteins fold into their native, three-dimensional conformations from their primary structures has been a puzzling challenge over the years and even today it continues to cause controversy. Since the first experiments on protein folding, numerous models have been proposed to explain this process. Christian B. Anfinsen pioneered this field in the 1960s with an analysis of the folding and unfolding of ribonuclease A, which concluded that the amino acid composition dictates the structural arrangement of the protein [3,12](#). Moreover, Anfinsen suggested that protein folding was a spontaneous process under physiological conditions. Thus, folded (and functional) states should correspond to the most stable architecture of a protein and the Gibbs free energy minimum [3](#). Years later, Cyrus Levinthal observed that the time a protein would require for obtaining the native conformation by arbitrary interactions does not match with the observed milli-second folding processes [13](#). This suggested that protein folding follows a selective pathway driven by specific native interactions and the formation of intermediate conformations from which the native structure will originate [13](#). Since that moment, researchers have proposed different models to explain how protein folding occurs. One of the first described models, called nucleation-growth mechanism, stated that for a protein to fold, a first region should establish native interactions forming an initial folded nucleus that progressively includes residues from the unfolded regions [14](#). A second model, called framework mechanism, suggested that protein folding is preceded by the formation of secondary structures that later interact to form the final three-dimensional structure [15-17](#). Another proposed mechanism, the hydrophobic collapse, argues that the folding process is dominated by hydrophobic interactions that compact the protein structure and facilitate the formation of native interactions [18,19](#). These two last models were widely accepted as they consider the existence of folding intermediates. Nevertheless, during the 90s a new and unifying model was proposed. This new model was called the nucleation-collapse mechanism and suggested that protein folding is preceded by the formation of a folding nucleus driven by hydrophobic collapse [20-22](#). In other words, the hydrophobic collapse of a protein induces the formation of a partially folded structures, named molten globules, which would finally lead to the native structure [20-22](#).

All in all, protein folding is a process dominated by kinetic and thermodynamic basis and directed by intramolecular contacts. During this process, proteins tend to achieve a global energetic minimal, the Gibbs minimal energy, to remain in a stable native conformation [23,24](#). The formation of native interactions is translated into a favourable enthalpy of the process, counterbalanced by the negative entropy. Throughout this process, several different conformations with multiple energy levels can be observed [23,25](#). This diversity is frequently represented by theoretical diagrams called energy landscapes. Among different models, the most popular to represent this process is the folding-funnel scheme (**Fig. 2**). The folding-funnel model represents folding and aggregation from unfolded states as a function of energy, considering multiple pathways for such processes and thus, different intermediates [23,25,26](#). Furthermore, the shape of the funnel varies depending on protein sequence and the environmental conditions [24,27](#), with large proteins presenting a more complex profile and larger number of intermediates [28](#). According to the folding-funnel model, folding intermediates, and partially folded proteins occupy an intermediate energetic level, while native and aggregated (either amyloid or amorphous) forms represent the lowest energetic conformations [29,30](#).

Nonetheless, not all the proteins acquire a three-dimensional arrangement and some unstructured polypeptidic sequences are functional, thus challenging the structure-function paradigm [31-34](#). These proteins are named intrinsically disordered proteins (IDPs) and include

polypeptides with different levels of disorder, ranging from fully disordered to partially unstructured [31-34](#). All IDPs are characterised by their flexibility and plasticity, which confer the capacity to perform a variety of functions, as signalling or regulation, and to establish weak transient interactions with multiple partners [31,32,35,36](#). Interestingly, some IDPs have been described to adopt a defined three-dimensional structure upon binding to specific partners [37-40](#). Of note, IDPs have been estimated to cover a 15-45 % of the proteins in eukaryotic cells [32,41,42](#) and are connected with multiple disorders as PD or AD. IDPs residues are constantly exposed to the solvent and ready to form intermolecular contacts that, in some cases, can lead to aberrant interactions. As an evolutionary strategy to maintain their solubility and reduce aggregation, these proteins are enriched in polar residues and β -breakers (Pro and Gly) with a scarce number of hydrophobic and non-polar amino acids [43-45](#).

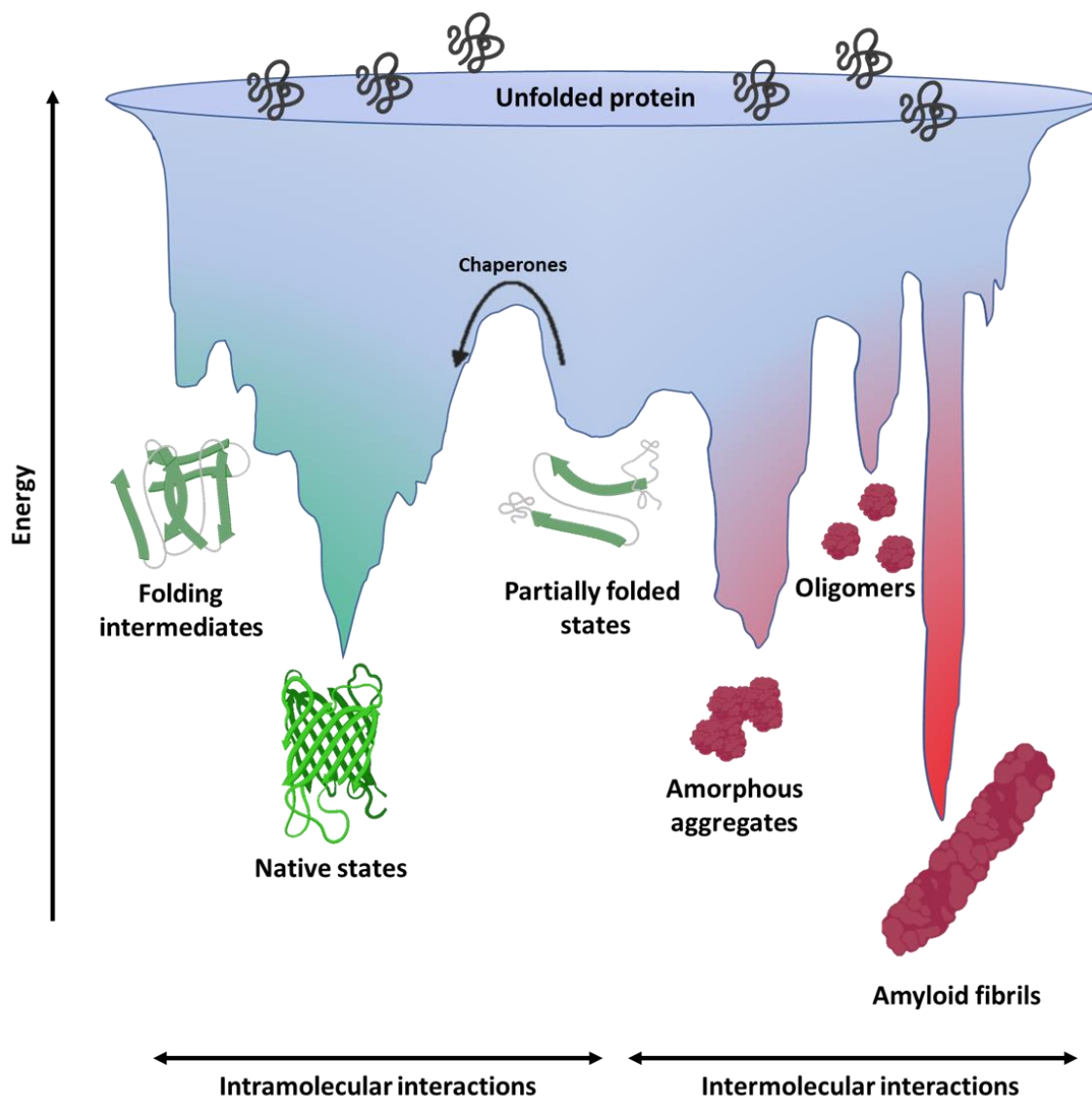


Figure 2. Schematic representation of the hypothetical energy landscape of protein folding and misfolding. Protein folding is an energetically favourable process driven by intramolecular contacts (green) with different intermediate structures as energetic pockets and the native state as an energetic minimal conformation. Nevertheless, intermolecular interactions lead to aggregated structures (amorphous or amyloids) that constitute the lowest energetic conformations (red) of the system.

Regardless the strict control to which it is subjected, protein folding is a complex process that may suffer mistakes. This erroneous folding drives to a loss of function, as the

protein is not achieving its native and active conformation, but also to the formation of a myriad of abnormal and stable conformations named aggregates, which may exert a toxic effect. During evolution, organisms have developed strategies to facilitate folding and prevent or reduce aggregation [46,47](#). One of the most relevant examples are the molecular chaperones, which assist the conformational protein folding, by reducing non-native interactions, and the refolding of misfolded or abnormal structures [48,49](#). Hsp70 family constitutes the best characterised group of molecular chaperones [49](#). Aided by Hsp40 chaperones [50](#), these proteins bind and stabilise unfolded proteins, preventing aggregation, until the folded structure is achieved [50-52](#). Moreover, cells have developed alternative mechanisms as the ubiquitin-proteasome system and autophagosomes, which degrade misfolded protein and aggregates [30,49,53](#). When these mechanisms fail, there is an accumulation of partially folded and misfolded proteins that could establish intermolecular contacts and then aggregate. Overall, protein folding and protein aggregation are competitive processes driven by hydrophobicity and the formation of hydrogen bonds. In normal conditions, hydrophobic regions are buried in the native structure. Nevertheless, mistakes during folding, environmental factors, genetic variations and even the dynamic nature of proteins expose these non-polar regions to the solvent, facilitating non-native intermolecular interactions [46,54,55](#).

1.1.2. Insights on protein aggregation

Despite protein aggregation is an heterogenous process that conduces to the formation of multiple structures, one of them has attracted most of the attention. Amyloid aggregates are characterised by a fibrillar morphology that can be detected using Transmission Electron Microscopy (TEM) or Atomic Force Microscopy (AFM) [56,57](#). Interestingly, although different unrelated sequences can form amyloid fibrils with diverse general conformations, they all share a common, highly ordered architecture. These aggregates are composed by a cross β -sheet structure sustained by parallel or antiparallel β -sheets that run perpendicularly to the fibril axis [58](#). Such unique configuration has been frequently recognised by a singular X-Ray diffraction pattern [57](#), but also with the appearance of a band at 1625 cm^{-1} in Fourier Transformer Infra-Red (FTIR) spectroscopy or the typical β minimum at 217 nm in the Circular Dichroism (CD) analysis [56](#). New techniques as solid-state Nuclear Magnetic Resonance (ssNMR) or Cryo Electron Microscopy (CryoEM) have allowed a more detailed analysis of the structural characteristics of these amyloids [59-61](#). Moreover, amyloid fibrils present a peculiar binding to different dyes as Thioflavin-T (Th-T) or Congo Red (CR). These dyes specifically bind to these cross β -sheet structures, changing their structural and spectral properties [62,63](#).

Regarding the structural determinants underlying amyloid formation, this process seems to be governed by the hydrophobicity and the propensity to form β -sheet secondary structures [64,65](#). Accordingly, the sequence composition considerably impacts the susceptibility to form amyloid structures (**Table 1**) [2,66](#). Hydrophobic and non-polar residues increase the aggregation propensity, while polar and β -breakers residues negatively impact the formation of aggregates [67,68](#). Furthermore, the net charge of the polypeptidic chain plays an important role in the aggregation as charged residues generate repulsion forces weakening intermolecular contacts [64,65,69](#). Notwithstanding, the protein sequence is crucial for aggregation, the sequential and structural distribution of these residues are playing an even more important role [70](#). It has been widely described that short regions of the proteins, named Aggregation Prone Regions (APRs) or Hot-spots, modulate and drive the aggregation process [67,71,72](#). APRs are mainly composed by hydrophobic residues that, in normal conditions, constitute the hydrophobic core of native structured proteins and drive the folding process

[48,55,73](#). However, the exposure of APRs to the solvent is translated into the aggregation of the protein [74](#). Therefore, these regions are frequently flanked by gatekeepers residues (charged or β -breakers) that reduce their intrinsic aggregation propensity [67](#).

Table 1. Amino acid properties and aggregation. Classification of the different amino acid depending on their side chain properties and its aggregation propensity

Code	Amino acid	Abbreviation	Side chain	Aggregation propensity [†]
F	Phenylalanine	Phe	Aromatic	1,754
W	Tryptophan	Trp	Aromatic	1,037
Y	Tyrosine	Tyr	Aromatic	1,159
A	Alanine	Ala	Hydrophobic	-0,036
I	Isoleucine	Ile	Hydrophobic	1,822
L	Leucine	Leu	Hydrophobic	1,38
M	Methionine	Met	Hydrophobic	0,91
V	Valine	Val	Hydrophobic	1,594
D	Aspartic acid	Asp	Negative charge	-1,836
E	Glutamic acid	Glu	Negative charge	-1,412
N	Asparagine	Asn	Polar uncharged	-1,302
Q	Glutamine	Gln	Polar uncharged	-1,231
S	Serine	Ser	Polar uncharged	-0,294
T	Threonine	Thr	Polar uncharged	-0,159
H	Histidine	His	Positive charge	-1,033
K	Lysine	Lys	Positive charge	-0,931
R	Arginine	Arg	Positive charge	-1,24
P	Proline	Pro	Rigid	-0,334
G	Glycine	Gly	Slight	-0,535
C	Cysteine	Cys	Thiol group	0,604

[†] Data obtained experimentally [75](#)

The abovementioned intrinsic determinants are highly modulated by environmental factors as pH, ionic strength, or temperature. The ionic strength and the pH influence in similar way the aggregation propensity as both impact the net charge of the protein. In the first case, the ionic charge of the medium can shield the charges of the side chains of the residues, thus precluding electrostatic repulsions [76-78](#). Regarding the pH, it modulates the degree of protonation of the side chains of the residues, which is why it also determines their charge and the repulsion between residues [79](#). Moreover, pH and temperature can alter the stability of the protein promoting the exposure of the hydrophobic regions of the protein that are buried in the native state.

Since the discovery of amyloid structures, understanding the mechanism underlying their formation has become a baffling challenge. Different mechanisms of protein aggregation have been proposed along the years as the Templated assembly [80](#) or the Monomer-directed conversion [81](#). Despite all these alternatives, the model that explains better the kinetics of the aggregation process is the nucleation-dependent polymerisation. Protein aggregation follows a three step process that can be represented as a sigmoidal curve (**Fig. 3**) [82](#). During the first step, a thermodynamically unfavourable process called nucleation, protein monomers assemble adopting cross- β structures, constituting the prefibrillar species, like oligomers, that nucleate the aggregation process. In the second step, the elongation phase, the accumulation, and maturation of these nuclei leads to an exponential, thermodynamically favourable growth of the aggregate forming fibrils through constant addition of monomeric protein. As the monomers exhaust, the elongation rate decreases, and the system enters an equilibrium between fibril formation and dismantling. During this saturation phase, fibrils can laterally interact leading to mature fibrils made of multiple protofilaments. In general, this process is

strongly influenced by the monomeric protein concentration, as higher concentrations facilitate monomer-monomer interactions. In addition, pre-formed aggregates can accelerate the reaction, acting as the nuclei or seeds of the process and reducing or abrogating the lag phase (**Fig. 3**) [83-86](#).

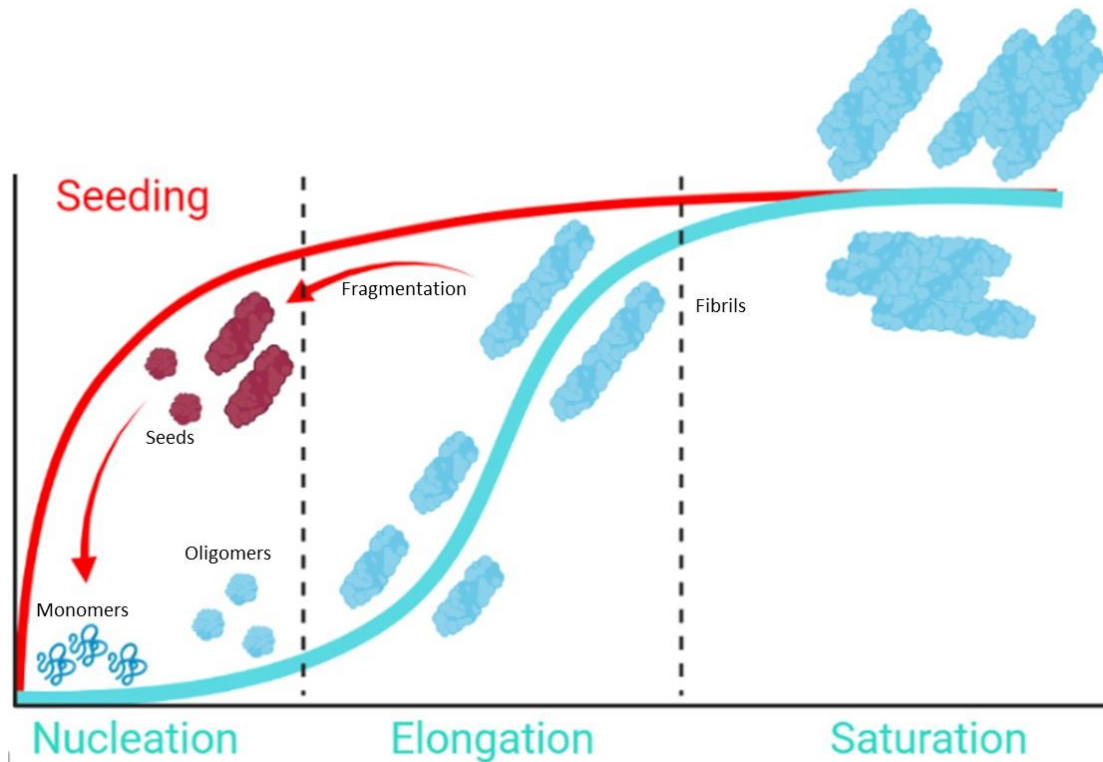


Figure 3. Schematic aggregation profile. The aggregation kinetic of most of the proteins can be dissected into three main phases (blue). The first step (nucleation or lag phase) is characterised by the formation of small nucleus that would guide the process; these nuclei incorporate monomeric protein prompting to an exponential growth of the aggregate (elongation or exponential phase); finally, the system enters in an equilibrium in which mature fibrils could be observed (saturation or plateau phase). However, the process could be accelerated (red) as fibrils can fragmentate into smaller aggregates that can be incorporated at the initial stages as nuclei or seeds (seeding).

1.1.3. Amyloids: functional or dangerous?

Amyloid structures have been traditionally considered pathological and toxic, abnormal protein conformations. In humans and several animals, amyloid-forming proteins have been related with the onset and progression of several disorders (**Table 2**). Nevertheless, in the last decades several amyloids have been described to play an important role in multiple functions in living organisms [87-91](#). The vast majority of these functional structures has been found in microorganism as bacteria. One of the best representatives is curli [89](#), extracellular fibrils produced by enterobacteria as *Escherichia coli* or *Salmonella spp* that play a key role in biofilm formation and stabilisation [92](#). Curli system is composed by seven specific genes called *csg* (from A to G) perfectly regulated (**Fig. 4**) [89,93](#), with CsgA being the major component of amyloid fibrils [94,95](#). CsgA contains a small prion-like peptide that lends amyloid properties [96](#). Synthesised intracellularly as a soluble monomer, CsgA is kept soluble in the cell by CsgC inhibitory capacity [97](#). To form fibrils, CsgA is secreted via the CsgF-CsgG complex, interacting with the N-terminal region of CsgG [93,98-100](#). CsgE mediates the translocation by reversibly interacting with CsgA-CsgG thus allowing CsgA release to the extracellular matrix [93,99](#), where CsgB nucleates CsgA fibrillization on the cell surface [94,95](#). Another interesting group of bacterial amyloids is the Fap family of *Pseudomonas spp*, which present an aggregation mechanism

similar to *csg* machinery [101-103](#). In this case FapC contains the amyloidogenic region and constitutes the major component of Fap fibrils [104,105](#). As observed in curli system, FapC extracellular aggregation is driven by a nucleation agent (FapB) [101](#) and its translocation is mediated by a complex secretion mechanism (FapF, FapD and FapE) [106](#). Inside the cells, the solubility of FapC is guaranteed by FapA, an anti-aggregational agent [107](#). Other interesting examples are the phenol-soluble modulins (PSMs), secreted by multiple *Staphylococcus* species [108-110](#). These short peptides (20-40 residues) perform diverse functions in the extracellular matrix, including biofilm formation and cell toxicity against other competitive microorganisms and human cells [110,111](#). Several PSMs have been described to form amyloid fibrils that contribute to biofilm stabilisation, as PSM α 1 and PSM α 4 [112](#), while other amyloid forming PSMs, as PSM α 3, exert a significant antimicrobial or cytotoxic activity [112,113](#).

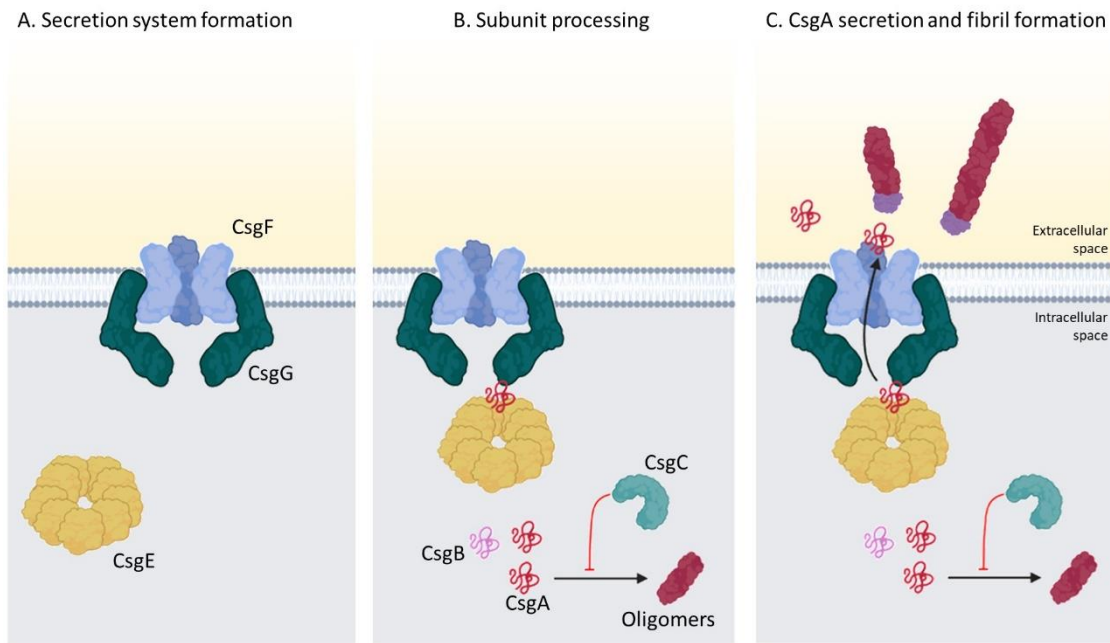


Figure 4. Curli secretion and aggregation system. Schematic representation of curli aggregation pathway where CsgF and CsgG form the secretion system and CsgE induces translocation. CsgB and CsgA are soluble monomers at the intracellular space and interact with CsgC, which avoids the formation of toxic oligomers. When secreted, CsgB nucleates CsgA aggregation in the extracellular matrix. Adapted [114](#).

These functional amyloids have been also observed in eukaryotic organisms such as yeast. Some of the best known functional amyloids are those observed in *Saccharomyces cerevisiae*. Sup35, which regulates translation termination at stop codons [115-118](#), and Ure2p, which modulates nitrogen catabolism, have been reported to form reversible amyloids in yeast [119-123](#). Aggregation of Sup35 importantly increase the elongation rate of multiple proteins, thus altering cell proteome and phenotype [124](#). On the other hand, Ure2p fibril formation induce the activation of the transcription factor Gln3, which induces the expression of Dal5, a transporter of pyrimidine intermediates as allantoate and ueridosuccinate [125](#). In both cases, fibril formation importantly enhances environmental adaptation, with selective growth advantages at certain conditions [124,126,127](#). Importantly, these amyloid structures and their related phenotypes could be transmitted following an epigenetic, non-Mendelian heritage [124,128,129](#). Furthermore, functional amyloids have been uncovered in more complex organisms, as plants. Regardless of several amyloids been described in genetically modified plants, poor evidence of these structures was reported in natural organisms [87](#). One of these cases is the *Pisum sativum* storage protein named vicilin, which exhibits antifungal activity and contains two β -barrel

Cupin-1 domains [130](#). The research developed by Nizhnikov and coworkers demonstrated that this protein is able to form amyloid fibrils *in vitro* and that the Cupin-1.2 domain was sufficient for fibrilization [131](#). These fibrils progressively increase during seed maturation and exert an important cytotoxic effect against yeast, which suggest that fibrils perform a seed-protective role. In contrast, during germination the fibrils rapidly disassembly, releasing monomeric protein [87,130-133](#).

Table 2. Disease-related human amyloid-forming proteins. Brief example of human amyloid proteins related to the development of pathological conditions.

Protein	Disorder
Prion protein	Spongiform encephalopathies
Amyloid β peptide	Alzheimer's disease
α -Synuclein	Synucleinopathies
Tau protein	Tauopathies
Insulin	Injection-localised amyloidosis
Superoxide dismutase 1	Amyotrophic lateral sclerosis
Transthyretin	Senile systemic amyloidosis Familial amyloidotic polyneuropathy
Huntingtin	Huntington's disease
Ataxin	Spinocerebral ataxia
FUS	Amyotrophic lateral sclerosis
TDP-43	Amyotrophic lateral sclerosis
Islet Amyloid Polypeptide	Type II Diabetes
Crystallins	Cataract

In humans, the formation of functional amyloid fibrils has also been an intriguing question due to the close connection of this kind of structures with several diseases. In spite of this relation, the presence of functional amyloid was never dismissed. It was discovered that some proteins, as premelanosome protein (PMEL17), were able to form amyloids with key functions in the organism [134](#). PMEL17 is a transmembrane protein, mainly found at melanocytes, that plays an important role in melanin synthesis [90,135](#). Cleavage of this protein at the melanosome into a fragment named M α , leads to the formation of fibrillar structures that work as template for melanin synthesis enhancing the polymerisation of melanin precursors [90,136,137](#). Interestingly, melanin precursors display an important cytotoxic activity that is attenuated in presence of PMEL17 [90,138](#). Such reduction of their intrinsic toxicity could be explained by PMEL17 fibril-mediated sequestration of these precursors, suggesting that PMEL17 fibrils not only perform structural functions, but also a protective role [90,137](#). Likewise, it has been widely hypothesised that peptide and protein hormones could be stored as reversible amyloids. In a study with 42 randomly selected proteic hormones, including glucagon and corticotropin releasing hormone, Maji and co-workers demonstrated the

presence of amyloid hormones [139](#). In this study, up to 10 of the selected hormones spontaneously aggregated into amyloid fibrils *in vitro* during incubation [139](#). When incubated in presence of heparin, most of these hormones were capable to form amyloid-like structures [139](#). Remarkably, these hormonal amyloid fibrils were able to release functional monomeric protein, supporting, altogether, the role of hormonal storage mechanism of amyloid fibrils [139](#). Direct analysis of different secretory granules of the mouse pituitary demonstrated the existence of amyloid-like structures acting in nature as hormones storage containers [139](#).

Thus, amyloid fibrils are two sides of the same coin. On the one hand, these proteins might perform essential roles for the organism under strict regulation, including structural, storage, signalling or adaptation functions, and might be considered as a singular type of quaternary structure. On the other hand, a myriad of these amyloid structures is responsible of severe pathologies (**Table 2**), including spongiform encephalopathies, AD, PD, amyotrophic lateral sclerosis, Huntington's disease, or type II diabetes, among others [7](#).

1.2. Parkinson's disease

PD is considered the second most prevalent neurodegenerative disorder in the world, only surpassed by AD [140,141](#). This disorder exhibits a global prevalence of 0.3% and affects to 2-3 % of population from 65 years of age, increasing to > 3 % in population older than 80 years [142](#). PD is a complex pathology originally associated only with motor deficiencies as a result of an acute neuronal loss in *substantia nigra pars compacta* (SNc), with a significant dopaminergic (DA) impairment [143](#). Nevertheless, PD is now related also to numerous non-motor symptoms (NMS) that contribute to increase the severity of the pathology [144,145](#). Included in a group of diseases named synucleinopathies [146](#), the cause of PD is still unknown, but its origin seems to result from a combination of environmental and genetic factors [147](#), with the presence of intracellular proteinaceous clusters, mainly composed of α -Synuclein (α -Syn), as the major neuropathological hallmark [11](#). Unfortunately, PD lacks early-diagnosis protocols and efficient therapies, currently focused on alleviating the symptomatology of PD [148,149](#).

1.2.1. Historical overview

The history of PD begins two centuries ago, in England (**Fig. 5**). In 1817 James Parkinson published a book entitled '*An Essay on the shaking palsy*'. In this treatise, Parkinson methodically described the development of a disorder in six patients that exhibited a motor disability, observing resting tremors, paralysis and unnatural posture [150](#). Sixty years later, 1872, the neurologist Jean-Martin Charcot, whose work helped in differentiating between bradykinesia, stiffness and weakness in PD [151](#), baptised the disorder as Parkinson's disease in honour of James Parkinson. Two decades later, in 1893, Blocq and Marinescu analysed a patient exhibiting resting tremor due to a granuloma that affects the SNc [152](#). In 1899 Brissaud finally suggested that SNc is the most affected region in PD suffering patients [153](#). However, it was not until 1919 when the first pathological evidences were obtained by Trétiakoff's description of a significant neuromelanin loss in SNc neurons and the presence of Lewy bodies (LBs) [154](#), cytoplasmatic structures previously reported by Frederic Lewy in PD affected brains [155](#). Altogether, DA cell loss and LBs presence in SNc, constituted the first anatomical evidences of PD and allowed its post-mortem diagnosis [156](#).

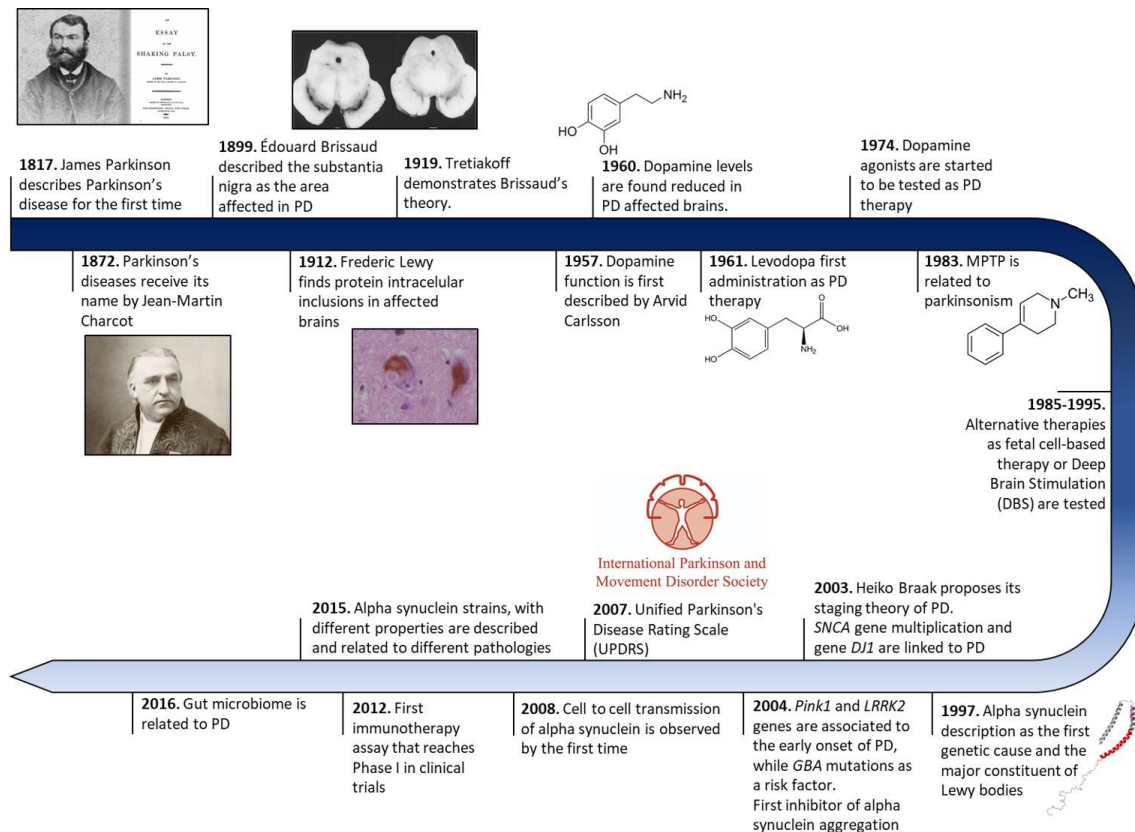


Figure 5. Historical overview of Parkinson's disease research. Schematic representation of the most relevant findings in PD research, from its discovery to treatment development. Adapted [157](#).

Later, in 1957, Arvid Carlsson made a discovery that would play a key role in PD during the following decades. Carlsson described in animals the role of dopamine in motor activity under the control of the basal glial, and whose deficiency could be reverted by L-3,4-dihydroxyphenylalanine (L-DOPA) administration [158](#). Three years later, Ehringer and Hornykiewicz described a dopamine deficiency in the striatum and SNc of PD affected brains [159](#). During the following years, L-DOPA intravenous or oral administrations were profoundly studied [148](#) and many authors reported significant improvements in motor symptoms (MS) [149](#), thus becoming the most effective therapy for PD.

Eighty years after the discovery of LBs, a protein called α -Syn was found out as the major component of these cytoplasmatic structures [11](#). These findings correlated with previous evidence of genetic mutations in *SNCA* gene (that encodes for α -Syn), the first gene described as a genetic cause of PD [160](#). Since then, other numerous genetic alterations in *SNCA* (single-point mutations, duplications and/or triplication) [161-167](#) and other genes (*GBA*, *PINK1*, *LRRK2*, *Parkin* or *DJ1* among others) [168-171](#) gradually appeared as risk factors of PD early onset and progression, opening an avenue to the development of more reliable animal models than 1-methyl-4-phenyl-1,2,3,6-tetrahydropyridine (MPTP) or 6-hydroxydopamine (6-OHDA) neurotoxin based models [172](#). These new cellular and animal models have allowed the study of α -Syn transmission, therapeutic approaches and biomarkers especially for the initial stage of PD (prodromal stage) [173-177](#). Currently, the search of effective treatments for PD has been mainly focused on α -Syn aggregation [178](#), but genetic therapies and microbiota alterations linked to PD are also playing an important role in this area [179,180](#).

1.2.2. Symptomatology

PD has been traditionally considered a neuronal disorder with a symptomatology limited to a several, unilateral and asymmetric motor deficits like rigidity, tremor, bradykinesia and postural instability. Consistently, clinical diagnostic has been based on the presence of bradykinesia together to other cardinal motor deficiency [181,182](#). The onset of these symptoms varies in the range of <40 to >80 years of age, increasing with age [142](#). A young onset of PD is considered at the age of onset <45, which is usually correlated to genetic factors [183-185](#). However, it is currently known that PD involves much severe clinical features with NMS as sleep disorders, cognitive impairment, depression, anxiety, pain or dementia, among others [186-189](#) that significantly impact the quality of life of the patients [190](#). The development of PD importantly affects numerous neurotransmission pathways, which could explain the appearance of these NMS; as an example, depression could be related to the deterioration of cholinergic, noradrenergic, and serotonergic systems while DA and noradrenergic decay would induce anxiety [191-195](#).

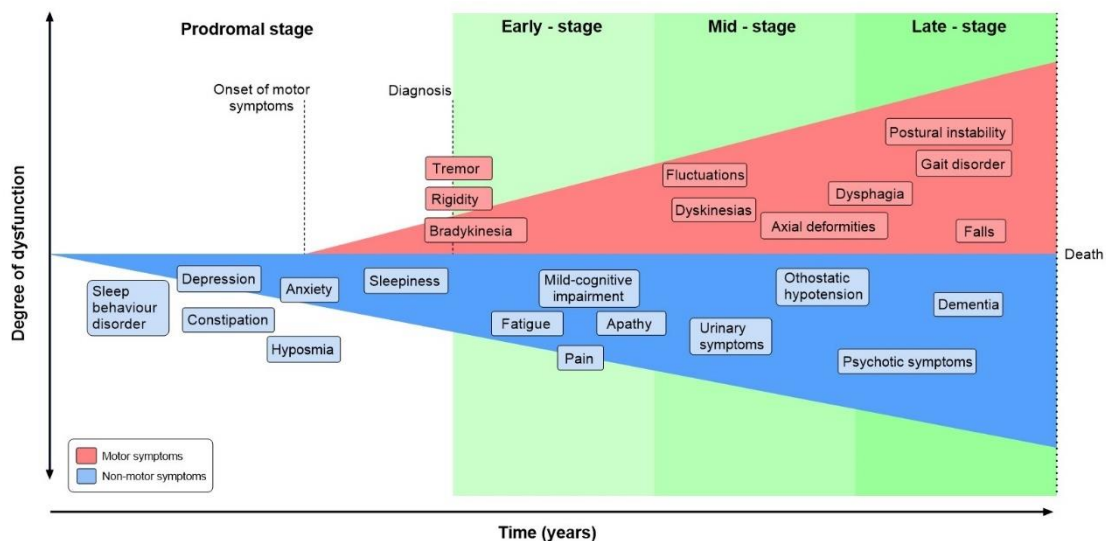


Figure 6. Symptomatic progression of PD. Schematic overview of both, MS and NMS symptoms progression and variability. PD diagnosis is based in MS, but NMS usually appears years before MS could be appreciated during the prodromal stage. The severity of the symptoms results from a combination of NMS, MS and L-DOPA-derived complications. Adapted [183](#).

The absence of MS and the presence of symptoms as olfactory dysfunction, REM sleep behaviour disorder (RBD), constipation and depression are indicators of the prodromal stage of PD [186](#). The development of these NMS during the prodromal phase precedes MS by several years [186,196,197](#) (**Fig. 6**). In early stages of the disorder, patients develop bradykinesia, tremor, and rigidity, and up to a 21 % of them also experience pain, depression or anxiety [198](#). Initially, the disease can be treated with symptomatic therapies, but as it progresses, treatment becomes more complicated [183,199](#). In the latest stages, patients exhibit severe NMS as dementia (83 %), hallucinosis (74 %), orthostatic hypotension (48 %), urinary incontinence (71 %) or constipation (40 %), leading to a pronounced disability [199](#). In addition, these phases are characterised by a progressive physical incapacity and strong resistance to the treatments, inducing freezing gait, postural instability, falls, and choking [200](#).

1.2.3. Risk factors and molecular mechanisms

Neurodegenerative disorders constitute a diverse group of pathologies with many challenges to face. The identification of the main cause behind the disease onset and progression stands as one of the major pending questions, and PD is one of the greatest examples of this paradigm. Despite the intrinsic cause of PD onset and development remains uncertain, numerous factors (from environmental to genetics) have been reported to play a role. In the case of environmental factors, meta-analysis of case-control sets has described environmental factors as both increasing (pesticide exposure, prior head injury, rural living, β -blocker use, agricultural activities, and well-water consumption) and decreasing (tobacco, coffee consumption, non-steroidal anti-inflammatory drug, calcium channel blocker, and alcohol abuse) risk elements for developing PD (**Fig. 7**) [201](#). Tobacco consumption, originally considered a decreasing risk factor of PD, deserves a particular mention as further analysis has demonstrated that this association was most likely due to a lack of nicotine response in PD patients, which translates into a higher probability to quit smoking [202](#).

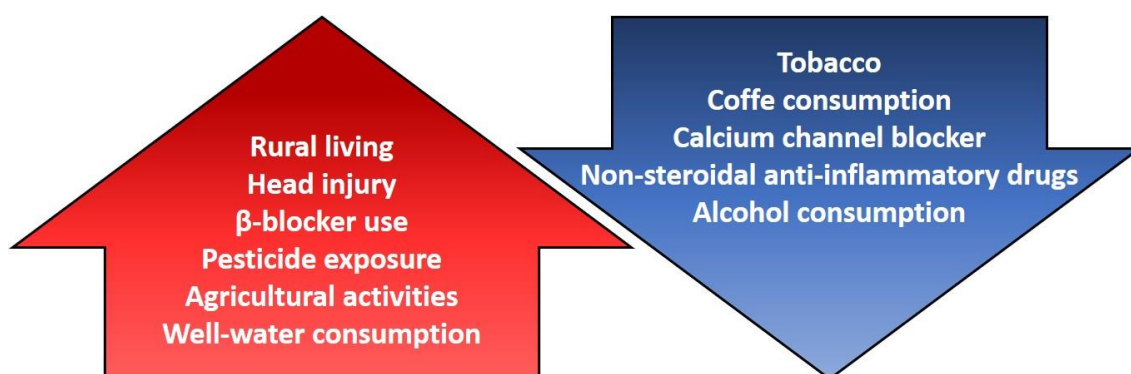


Figure 7. Environmental factors and PD. Schematic summary of the environmental factors that increase (red) or decrease (blue) the risk to develop PD.

Even though aging is still considered the major risk factor, genetics studies have revealed in the last 25 years that defects in numerous genes also play a significant role in the onset and evolution of PD. These genetic alterations are normally associated with familial cases of the pathology (**Table 3**). The first gene linked to PD was *SNCA*, which encodes for α -Syn and includes numerous single points mutations. The first described *SNCA* mutation, A53T [162](#), was initially detected in patients of Greek and Italian descent that presented an accelerated course of the pathology. Patients carrying this mutation presented cognitive impairment developed after 5-7 years of onset and an average onset of 46 years [203,204](#). One year later, in a German family, researchers observed another single point mutation: A30P [161](#), the clinical profile associated to this mutation interestingly revealed a more benign course of the disorder and an onset of 60 years. In the case of E46K mutation, reported in Basque Country [163](#), patients develop severe symptoms at the age of 50- and 65-years including dementia and autonomic failure [163,205](#). Other genetic mutation described in English families was H50Q [165](#). Patients carrying this mutation reported motor symptoms at the age of 60 and a fast development of the pathology [165](#). In the last decade other two genetic mutations, G51D and A53E [166,206](#), have been reported causing dementia and autonomic dysfunction, and early motor symptom progression, respectively [166,207-211](#). In addition, *SNCA* duplications and triplications have been observed in inherited PD. The severity and progression of the disorder in this case is related with the number of gene copies, resulting in a much severe symptomatology and early onset in patients affected by triplications of *SNCA* than those affected by duplications [164](#).

Table 3. The genetics of PD. Summary of the different gene involved in PD and their role in the development of the pathology.

Gene	Role in PD
SNCA (α -Synuclein)	Protein aggregation Prion-like transmission Synaptic function and dopamine transmission
GBA (Glucocerebrosidase)	Lysosome mediated autophagy pathway
LRRK2	Neurite structure Protein and membrane trafficking Lysosome mediated autophagy pathway Synaptic function and dopamine transmission
MAPT (Tau)	Protein aggregation Neurite structure
VPS35	Protein and membrane trafficking Lysosome mediated autophagy pathway
DNAJC13 (REM-8)	Protein and membrane trafficking Lysosome mediated autophagy pathway
GAK	Protein and membrane trafficking
RAB7L1	Protein and membrane trafficking
RAB39B	Protein and membrane trafficking
Parkin	Ubiquitin mediated proteasome Mitochondrial dysfunction and mitophagy
FBX07	Ubiquitin mediated proteasome
SCA3 (Ataxin-3)	Ubiquitin mediated proteasome
PINK1	Mitochondrial dysfunction and mitophagy
DJ-1	Mitochondrial dysfunction and mitophagy
CHCHD2	Mitochondrial dysfunction and mitophagy
POLG1	Mitochondrial dysfunction and mitophagy
SREVF1	Mitochondrial dysfunction and mitophagy
ATP12A2	Lysosome mediated autophagy pathway
SCARB2 (LIMP-2)	Lysosome mediated autophagy pathway
SYNJ1 (Synaptojanin 1)	Synaptic function and dopamine transmission
GCH1	Synaptic function and dopamine transmission
STX1B (Syntaxin-1B)	Synaptic function and dopamine transmission

Other autosomal and dominant mutations described in PD include genes with diverse functions. Missense mutations in *LRRK2* gene (R1441G, R1441C, R1441H, G2019S, Y1699C and I2020T) have been identified in PD patients worldwide [171,212,213](#). This gene encodes for a large kinase (266 KDa) with several domains responsible of various functions, as vesicle trafficking, GTPase activity and protein interactions [214,215](#). Mutant *LRRK2* induces apoptotic neuroblastoma and cortical neurons death probably by altering the autophagy process [216,217](#). Although patients with *LRRK2* mutations exhibited a more benevolent symptomatic progression in terms of MS and maintenance of cognitive capacities, motor complications could easily appear [218-220](#). Nevertheless, the most common genetic alterations, with more than 300 different mutations described, are observed in *GBA* gene [221-223](#), which encodes for a

lysosomal enzyme called glucocerebrosidase that degrades glucosylceramide into glucose and ceramide [224-226](#). The role of *GBA* mutations in PD onset and progression is still under debate. Theories as impaired lysosomal function or endoplasmic reticulum-associated stress have been related to *GBA* mutations in PD, but the accumulation of α -Syn is considered the most plausible hypothesis [227,228](#). *GBA* carrier patients exhibit an early onset of PD with an acute motor deficit, but these mutations notably increase the severity of NMS, enhancing cognition impairment, depression, and anxiety among other symptoms [222](#).

Autosomal dominant mutations, as those above mentioned, are the most common genetic factors of PD. Nevertheless, recessive alterations in autosomal regions have also been related to the disease. *Parkin* gene, which encodes for a E3 protein-ubiquitin ligase, is one of these recessive mutants. This E3 protein-ubiquitin ligase regulates the degradation of misfolded proteins through the ubiquitin-proteasome system [229](#). This enzyme presents two RING fingers that recruit different proteins as the E3 enzyme [229](#), but also interact with LRRK2 [230](#). *Parkin* gene mutations in PD include an altered number of copies and missense and nonsense mutations [231](#). The role of these mutations in the development of the disease seems to be connected with the accumulation of damaged mitochondria [232](#). Patients suffering *Parkin* alterations early develop PD with a more benign symptomatology, despite the complete degeneration in the SNc and *locus coeruleus* without LBs inclusions [233](#). *DJ1* and *PINK1* mutations present similar features to parkin, as they participate in common biochemical pathways [167,232,234-236](#), differing in the presence of diffuse or complete LBs and LNs, respectively. On the one hand, *DJ1* seems to help in gene expression modulation in conditions of cellular stress [237-239](#). Mutations like L166P, E163K or L172Q induce *DJ1* migration to the outer mitochondrial membrane, increasing the sensitivity to stress of the cells [237,238](#). On the other hand, *PINK1* gene alterations include missense, nonsense, splice mutations, or small deletions or insertions [240,241](#). The encoded protein acts as a mitochondrial kinase. Mutations in this protein seems to induce a mitochondrial deficit and alter the mitophagy pathways [169](#).

Altogether, during PD progression, cells suffer numerous interconnected and retroactive alterations (**Fig. 8**) either in presence or absence of these different genetic mutations, which culminate in the death of certain brain regions and cells. Among all these different factors, α -Syn seems to be the key molecular factor around which every molecular and genetic factor converge [242-245](#). In pathogenic conditions, this protein forms neurotoxic oligomeric structures that progressively assemble into insoluble fibrils and accumulate in LBs [11,242,243](#), the major hallmark of PD. Recent studies have demonstrated that these aggregated structures of α -Syn could be transmitted to neighbouring cells, seeding the aggregation in healthy neurons and spreading the disease to different brain regions during PD progression [246-249](#). α -Syn proteostasis is regulated by the ubiquitin–proteasome and the lysosomal autophagy systems [245,250](#), and the inhibition of these processes leads to the accumulation of α -Syn [244,251](#). Accordingly, mutations in genes *LRRK2*, *GBA* and/or *VPS35*, are translated into a pronounced number of LBs and LNs [226,252-254](#). Conversely, pharmacological stimulation of autophagy systems significantly decreased the level of aggregated α -Syn in animal models [255,256](#). At the same time, oligomeric α -Syn and its accumulation alter the function of the ubiquitin-proteasome system, inhibiting macroautophagic processes and the chaperone-mediated autophagy [257](#).

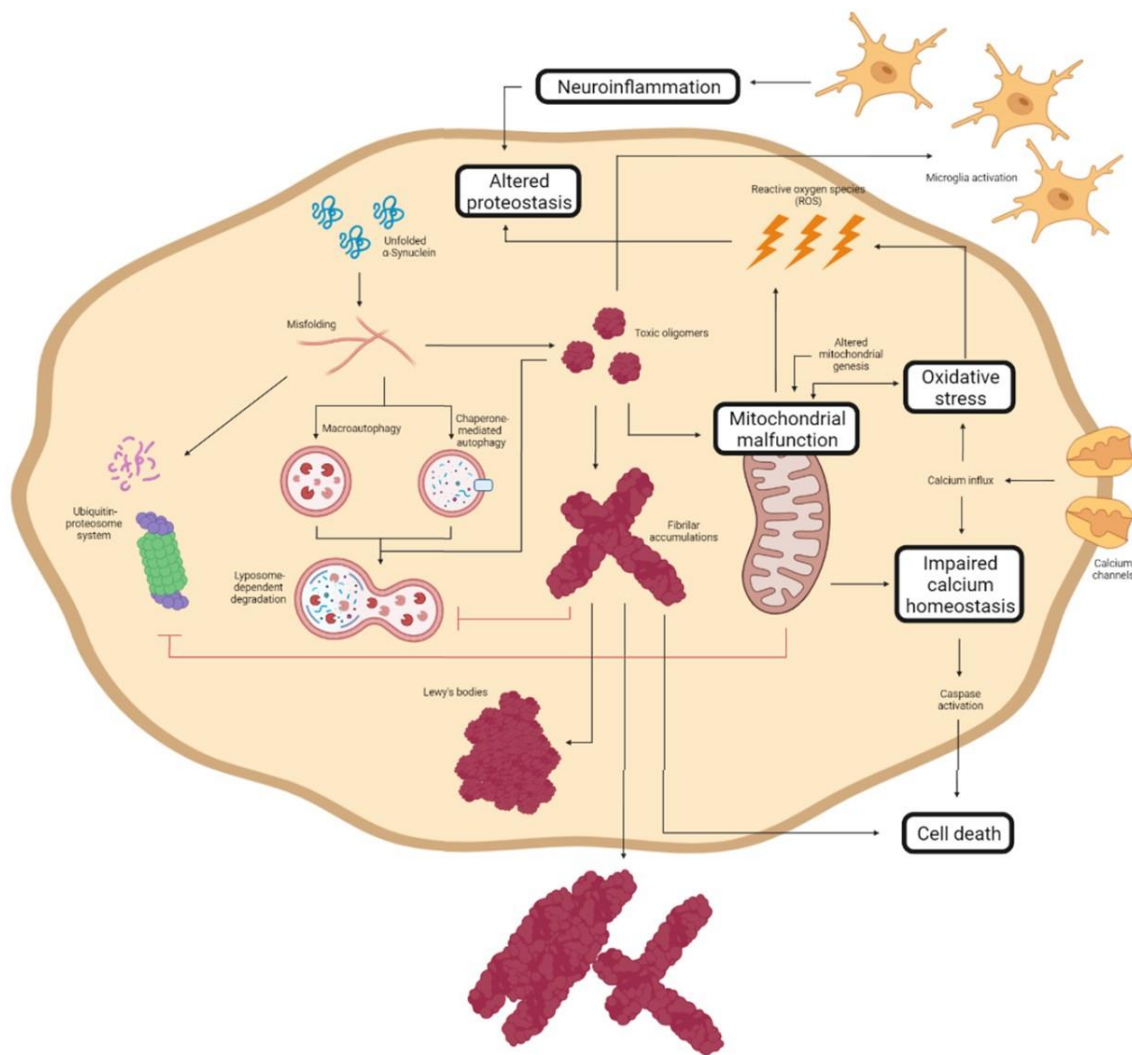


Figure 8. Molecular mechanism of Parkinson's disease cell damage. Schematic representation of the interconnected molecular processes that induce cell death and PD progression. Adapted [183](#).

The aggregation of α -Syn also induces mitochondrial dysfunction that simultaneously stimulates the formation of amyloid structures of α -Syn [184,216](#). α -Syn accumulation decreases the levels of peroxisome proliferator-activated receptor- γ co-activator 1 α (PGC1 α), a mitochondrial regulator of the transcription [258,259](#); when activated, PGC1 α reduces the levels and toxicity of α -Syn oligomers [260](#). This is connected with the relevance of *LRRK2* (that plays a key role in mitochondrial impairment), *Parkin* and *PINK1* (responsible of the degradation of harmed mitochondria) in PD development [216,236](#). As a result of mitochondrial dysfunction there is a significant accumulation of metabolites that produce high oxidative stress [261](#), to which unmyelinated DA neurons are highly sensitive [262,263](#). Mutations in *DJ1* significantly reduce the cellular response to stress [234,237,238](#). Such mitochondrial deficiency also impacts in the energy levels of the neuron, inducing an impaired calcium homeostasis and a rapid axonal degeneration [264,265](#). Another molecular process that plays an important role in PD and that is closely related to α -Syn aggregation and spreading involves the immune system activation [266](#). α -Syn aggregation stimulates adaptive and innate immune response to toxic structures as oligomers, but, at the same time, the generated neuroinflammation enhances protein aggregation [267-269](#) in a retroactive pathway that causes a severe neuroinflammation. In this way, the capacity of the immune system to react to toxic α -Syn species has been widely studied as a therapeutic alternative.

1.2.4. Alpha-synuclein

Due to the close relation between α -Syn and PD onset and progression, this protein has become the preferred target in the search of an effective treatment for PD [178](#). But what is known about this protein? α -Syn is a 140 amino acid protein coded in *SNCA* gene, which is mainly expressed in the synaptic termination of DA neurons in the brain. In normal conditions, α -Syn can be found as a soluble, monomeric and disordered protein or bound to lipidic membranes attaining an alpha-helical conformation (**Fig. 9B**) [270](#). Some studies have also revealed the possibility that α -Syn forms a tetrameric and helical structure in the cytoplasm, but it is still a controversial question [271](#). Although its function remains unclear, it has been related to the vesicle trafficking at the synapsis [272](#), participating in the release and recycling processes. The regulatory potential of vesicle trafficking and recycling by α -Syn might be mediated by its interaction with VAMP2, a synaptobrevin involved in the fusion and binding of synaptic vesicles [273](#). This interaction stabilizes SNARE complexes, which intervene in vesicle fusion and neurotransmitter release [274,275](#). Nevertheless, the disordered nature of this protein allows to perform a large broad of alternative functions. As an example, some studies suggest that α -Syn stabilizes mRNA in P-bodies by binding proteins found at these membrane-less organelles [276](#), while others suggest that α -Syn may modulate DNA repair [277](#).

This multivalent behaviour is connected to its particular sequence, which could be dissected into three different regions (**Fig. 9A**) [278](#). The N-terminal domain is a highly conserved region of the protein that concentrates most of the imperfect KTEGV repeats. These repeats confer a strong amphipathic character, which is responsible for the conformational change to an α -helical configuration and of the protein-lipid interaction that dictates the binding to the membranes [270,279](#). Importantly, this protein-lipid interaction has been described as a risk factor when the concentration of α -Syn increases, as it facilitates local nucleation for amyloid formation [184,280-283](#). Recent studies have also proved that N-terminal region contains two sequences (residues 36-42 and residues 45-57) with an essential role in protein-protein interaction, establishing contacts between monomeric α -Syn that precede cross- β formation [284-286](#). In addition, missense mutations related to the early onset of PD, Multiple System Atrophy (MSA) or Dementia with Lewy Bodies (DLB) are also found in this region [160-163,165,166](#). The central region is also known as Non-Amyloid Component (NAC) as it is an important component of amyloid plaques in AD [287](#). This is a hydrophobic segment often protected by transient interactions, because of the disordered nature of the protein, but that drives the aggregation of α -Syn in pathogenic conditions [288-291](#). In contrast, the C-terminal domain presents a large content of acidic amino acids that provides a rich negative charge density. This net charge seems to reduce the aggregation propensity by electrostatic repulsions [292](#). Accordingly, C-terminal truncations of α -Syn increase the aggregation tendency and toxicity, and form one of the main components of LBs, which suggest that this process could play a relevant role in pathogenesis [293](#).

In normal conditions, α -Syn displays a great solubility but in abnormal and pathogenic situations this protein tends to establish β -sheet interactions that induce the formation of insoluble amyloid-toxic structures, compromising cellular homeostasis and inducing neuronal death [294](#). As outlined previously, amyloid aggregation is a complex process that *in vitro* could be defined by a sigmoidal representation with three different phases, reflecting a nucleation-polymerization process [295](#). During the lag phase, α -Syn monomers interact forming toxic and transmissible structures named oligomers and protofibrils [296](#) that will act as the nuclei of the aggregation. The second step consists in an exponential development of the size of the fibril

that is called elongation phase. Finally, the plateau phase, is characterised by the presence of mature and long amyloid fibrils (**Fig. 3**). However, this is a simplified characterisation of the aggregation process, which in addition comprises alternative steps, due to fibril fragmentation (secondary nucleation) or seeding processes, that contribute to the aggregation and spreading by precluding primary nucleation processes (**Fig. 3**) ²⁹⁷.

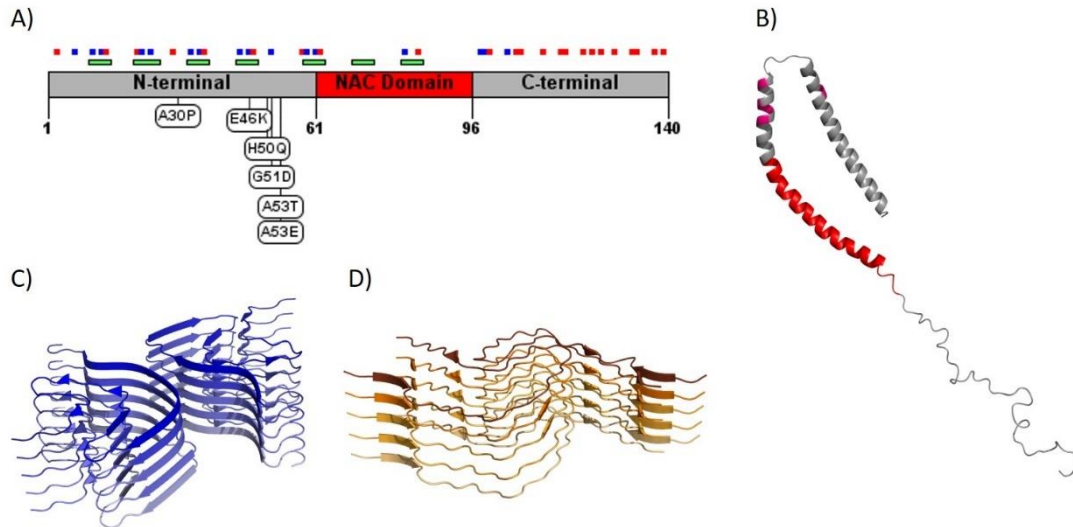


Figure 9. Alpha synuclein architecture. (A) Schematic representation of α -Syn primary sequence indicating positively (blue) and negatively (red) charged amino acid, and KTKEGV repeats (green). Sequential domains and single-point mutations related to familial cases of PD are also shown. (B, C and D) Structure of monomeric (B) and aggregated α -Syn forming different conformations or strains (C and D). PDB files: 1XQ8, 6CU7 and 6CU8 in order.

The complexity of the aggregation process of α -Syn is further increased by genetic and environmental factors. Missense mutations of α -Syn (A30P, E46K, H50Q, G51D, A53E, and A53T), which are located into the membrane-binding region (**Fig. 9A**), are related to early onset of PD and familial cases ^{161-163,165,166,206}. All these mutations impact α -Syn aggregation propensity, inducing either its oligomerization (A30P, H50Q and A53T) or fibril formation (H50Q, A53T and E46K) and, thus, the formation of toxic species of α -Syn ²⁹⁸. In contrast, G51D and A53E variants slow down α -Syn aggregation compared to wild-type (WT) α -Syn, but alter its interaction with membranes ^{206,299}. Despite the exact role of these mutants in PD is still unknown, patients suffering G51D and A53E mutations exhibit a large amount of α -Syn pathological inclusions (in the case of G51D also in oligodendrocytes) ¹⁶⁶ and an earlier onset of PD. Attending to these evidences, it is suggested that these missense mutations could prolong the lifetime or stimulate the generation of toxic α -Syn structures as oligomers ²⁰⁶. Moreover, recent studies have shown that environmental factors, as ionic strength or pH, affect the intermolecular interactions of α -Syn and contribute to the heterogeneity of the aggregation process. As for human prion protein ³⁰⁰, α -Syn fibrils formed under different solution conditions share a common cross- β composition, but exhibit different conformation, seeding activity, neurotoxicity and spreading in cells and when inoculated in rat brains ³⁰¹⁻³⁰⁶. These conformational diverse assemblies are called strains (**Fig. 9C-D**) and could explain the existence of different synucleinopathies with unique clinical features ^{303,307,308} as their different properties would induce particular lesion profiles and brain region dissemination ³⁰⁹.

On top of that, as we learn more about α -Syn, its aggregation becomes more and more complex. Recent studies have suggested that, in addition to aggregation, α -Syn is able to

undergo liquid-liquid phase separation (LLPS) *in vitro* and *in vivo* as a prior step to amyloid formation [310-312](#). LLPS is a recently described aggregation-related phenomena characterised by the formation of multivalent macromolecular interactions, which induce the formation of an alternative phase with particular physicochemical properties and that may be the main responsible for formation of membraneless organelles [313-318](#). The mechanism underlying the transition of LLPS to amyloid is still unclear and very few structural studies have been performed [312](#) but deciphering these contacts could hold the key to prevent the formation of toxic structures. Moreover, environmental conditions, as pH or ionic strength, also condition LLPS and the maturation into aggregates [319](#). This might be the intrinsic mechanism that drives the formation of the different strains. Remarkably, environmental risk factors for PD, like the Ca^{2+} or Mn^{2+} cations have been proved to facilitate LLPS and accelerate the aggregation transition [320,321](#). Thus, even though the functional role of α -Syn in LLPS remains unclear, understanding the interactions that lead to their amyloid formation might become an important strategy to stabilize LLPS and prevent further aggregation [322](#). Moreover, new studies have suggested that α -Syn and other amyloid-like proteins as prion and tau, may be synergistically connected via LLPS contributing to the different amyloidosis [323,324](#).

As regards *in vivo*, the formation of α -Syn fibrillar structures (major components of LNs and LBs in the cytoplasm of the neurons [10,11,325](#)) is preceded by the assembly of the monomeric protein into small and diffusible metastable oligomers and protofibrils, which has been suggested to be the main responsible of neuronal degeneration, rather than the mature fibrils [296,326-331](#). These aggregated structures progressively appear in different brain regions due to their capacity to be transmitted to neighbouring cells in a prion-like manner [332](#). Nevertheless, the heterogenic aggregation process of α -Syn evinces a conformational-dependent transmission pattern, in which the affected cellular and anatomical compartments would depend on the particular aggregates' properties [307-309](#). A recent Cryo-EM comparative study confirms this hypothesis evidencing structural differences between α -Syn fibrils obtained from MSA patients from those obtained from patients with DLB [307](#). Although the affected brain regions may vary, this cell-to-cell transmission capacity of amyloid structures would support Braak's hypothesis, which suggests that PD could be really originated in the peripheral nervous system (PNS), as demonstrated by the presence of LBs in this region, and thus invade the Central Nervous System (CNS) through the vagus nerve (**Fig. 10**) [246,333](#).

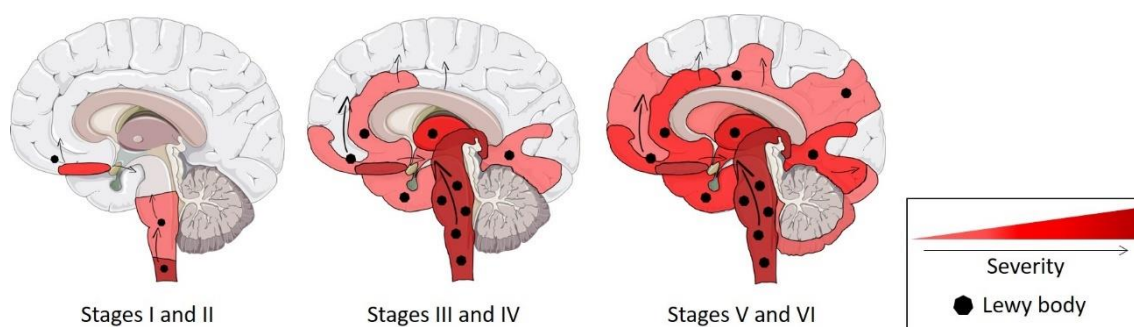


Figure 10. Prion-like progression of Lewy bodies in the brain. Schematic representation of Braak's hypothesis, which correlates the affected regions and symptoms appearance with the spreading of α -Syn aggregates and Lewy bodies. Adapted [334](#).

In PD, the progressive appearance of LBs in the PNS and the CNS, in agreement to Braak's theory, would explain the gradual development of PD symptoms (**Fig. 10**). During the early-stages (stage I and II) α -Syn aggregates originated at PNS enter the CNS impacting the autonomic system and the sense of smell [246,335-338](#). These aggregates affect first the lower

brainstem and the olfactory system (specifically, the dorsal motor nucleus of the vagus nerve and the anterior olfactory nucleus), progressing later through the medulla oblongata and the upper brainstem by travelling to the *locus coeruleus* [246,333,339](#). LNs are more prevalent than LBs during the initial phases. Mid-stage phases (stages III and IV) are characterised by the deterioration of NMS, the appearance of MS and the development of LBs as the disease extends into the SNc [246,333,339](#). At these phases, the basal midbrain and forebrain, the mesocortex and the allocortex start to develop LBs lesions, while the previous early-affected areas are deeply damaged [246,333,339](#). Finally, during the late-stages (stages V and VI) cell death is widely spread in SNc, the basal forebrain, the mesocortex and the allocortex. In these phases the disease progressively invades the neocortex, with severe MS and NMS [246,339](#).

1.2.5. Current diagnosis and treatments

Diagnosis of PD has been traditionally based on the analysis of the symptomatic progression of the patients. The presence of bradykinesia and, at least, one MS as rigidity or resting tremor are the essential criteria for PD diagnosis [147,181,182](#). However, these factors should be accompanied by supportive proofs (such as L-DOPA response) and lack of clinical evidence for alternative pathologies [147,181,182](#). Improved criteria standards as the defined by the UK Parkinson's Disease Society Brain Bank increase the diagnosis accuracy to an 80-90%, according to post-mortem studies [340](#). In 2007 the International Parkinson's and Movement Disorder Society stabilised the Unified Parkinson's Disease Rating Scale (UPDRS), which rapidly became the most used scale to follow and classify the progression of the motor and non-motor deficit of PD patients [341](#). Divided in six parts, UPDRS analyses the mental and motor state and the behaviour of the patients during their daily-life activities, as well as their response to the therapy, but also includes evaluations from Hoehn-Yahr and Schwab-England ADL scales, which assess patients' motor capacities [342,343](#). Importantly, advances in imaging techniques have opened the window to a new generation of detection techniques, such as ¹⁸F-labelled L-DOPA [344](#), positron emission tomography (PET) or single photon emission computed tomography (SPECT), which analyse the decrease of DA nerve terminals and the sympathetic denervation [345-347](#). In addition, genetic factors related to PD (*SNCA*, *Pink1*, *GBA*, *LRRK2*...) are a useful clinical detection tool in particular cases. Regrettably, as these factors correspond to a minority percentage of PD cases, genetic testing has not been included in the diagnostic system. These tests are only considered for patients with suspicions of a possible genetic cause or specific clinical features. Current studies are focused on the detection of pathological biomarkers as α -Syn, DJ-1 or Tau in the cerebrospinal fluid, blood, saliva or urine in order to detect PD during the prodromal stage [348-353](#).

Current available treatments of PD are focused on alleviating the symptomatology but do not modify the course of the disease. First therapy, developed almost 50 years ago, centres its effect in substituting striatal dopamine loss by a systemic administration of L-DOPA [148,354,355](#). This molecule is a Blood-Brain Barrier (BBB) permeant precursor of several neurotransmitters, including dopamine [149](#) by DOPA-decarboxylase activity (**Fig. 11A**). Notwithstanding its capacity to cross the BBB, only ~10% of the administered L-DOPA could be found in the brain due to peripheral metabolism [356](#). Moreover, L-DOPA administration becomes more complex with the evolution of motor complications, including motor response fluctuations (ON/OFF fluctuations) and drug-induced dyskinesias, mostly because of the discontinuous drug delivery due to its short half-life and the variability in its gastrointestinal absorption and BBB transport [199,357-362](#). Progressive L-DOPA failure encouraged to develop new DA and non-DA therapies for the treatment of PD that could be co-administered with L-DOPA (**Fig. 11B**). Initial attempts

help to prevent falls [389,390](#). Nonpharmacological therapies as surgery were initially employed, but levodopa therapy restricted surgery to only a few cases. At the present, deep brain stimulation (DBS) is the most used surgical treatment because it maintains the brain tissue intact, it is reversible, and it can be adapted to each patient [391-393](#). DBS therapy involves the implantation of an electrode in the brain that performs electrical stimulation on a specific region, modulating neural activity and improving MS [378,394-396](#). As it can be seen, unfortunately, available therapies do not really modulate PD molecular processes and just focus on PD symptomatology.

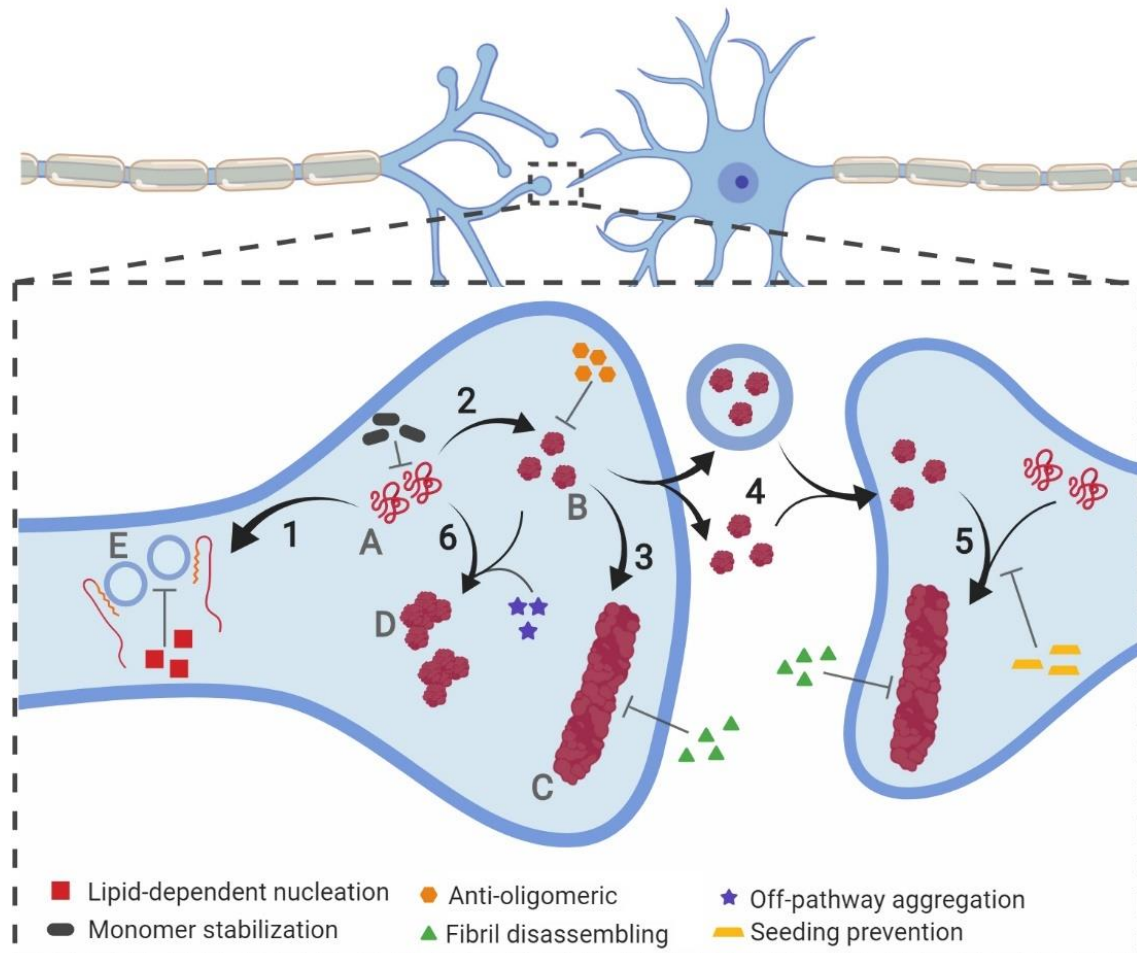


Figure 12. Inhibiting α -Syn aggregation. Schematic representation of the different mechanisms illustrated by coloured symbols and available to prevent the aggregation of α -Syn, which follows a slow process that comprises different assemblies of the protein: monomeric (A), oligomeric (B), and fibrillar (C), or amorphous (D) aggregates. This process comprises different steps during the development of PD: protein–lipid interaction (1), oligomerization (2), fibril elongation (3), transmission (4), seeding (5), and amorphous aggregation (6). Extracted [397](#).

This lack of an effective therapy that targets the molecular basis of PD has led to a continuous search for new treatments. One of these approaches is gene therapy, which has become a relevant strategy in the treatment of numerous diseases. Lentiviral and adenoassociated viral vectors, which have been approved for human use [398-400](#), are the most studied in PD, with different targets been identified for possible gene treatment, including disease modifiers and non-modifiers. Glutamic acid decarboxylase (GAD) overexpression through adenoassociated vectors administration is the first gene therapy studied in PD patients. It improved their symptomatic profile but did not turn out in neuroprotective activity

[401](#). Other studied therapies are based in L-amino acid decarboxylase gene administration, alone or in combination to tyrosine hydroxylase and GTP cyclohydroxylase 1 [402,403](#). L-amino acid decarboxylase gene plays a key role in dopamine metabolism, but genetic therapies based on this gene only resulted in an UPDRS score improvement [402,403](#). Alternative gene therapies are based in the overexpression of growth and/or neuroprotective factors, such as glial cell-line derived neurotrophic factor, neurturin, artemin, persephin, vascular endothelial growth factor or Nurr1 [404-407](#). It has been also suggested that CRISPR/CAS9 technology could be used in order to correct genetic mutations associated with PD [408](#). Other studied approaches were based on cellular transplantation. During the 90's, fetal cell transplantation capacity to restore striatal dopamine transmission and connectivity, and MS improvement was investigated [409,410](#). Despite first results suggested that it could induce side-effects [411](#), advances in stem cells, which can develop DA neurons after grafting in animal models, could provide a new opportunity for cell transplantation as a therapy for PD [411,412](#).

Nonetheless, α -Syn aggregation has become the most interesting target in the search of putative therapies of PD. Accordingly, different strategies have been developed to modulate its aggregation, including *SNCA* gene-silencing to reduce the neuronal levels of α -Syn, strategies to increase the clearance of aggregated α -Syn by stimulating autophagic or proteasomal activities, and agents that prevent the formation and/or spreading of toxic aggregated structures [178,413](#). Antibodies, vaccines, molecular chaperones and small molecules are some of the most representative agents to target the aggregation in CNS and PNS. However, the inability to cross the BBB and the possibility to develop collateral immunological reactions of many of these approaches made of small molecules one of the most promising candidates [414,415](#). Aggregation of α -Syn is a complex process that comprises numerous steps and different structures that could be targeted by small molecules to avoid this process (**Fig. 12**). Accordingly, there are many chemically diverse compounds that were discovered by different methodologies and that exhibit different mechanisms of action to prevent α -Syn aggregation (**Fig. 13**). First analysis of modulators of α -Syn aggregation focused on natural compounds, which have been frequently employed in the development of drugs. A pioneer study of 169 molecules revealed that catecholamines, as dopamine, L-dopa, epinephrine or norepinephrine [416](#), interfered with the aggregation process of α -Syn. Particularly, dopamine oxidized derivatives redirect the aggregation of α -Syn to the formation of off-pathway structures [416](#). The mechanism behind their inhibitory effect is still unclear; covalent interactions with tyrosine or lysine residues, and methionine oxidation of α -Syn by the compounds are some the multiple proposed mechanisms [417-419](#). Non-covalent interactions with the ¹²⁵YEMPS₁₂₉ sequence at the C-terminal region of the protein have also been proposed as the inhibitory basis of polyphenols [420-424](#). Yet, these compounds not only did not prevent the toxicity of α -Syn aggregates, but also stimulated the formation of new toxic species in animal models [425,426](#).

The discovery of the inhibitory capacity of catecholamines was only the beginning and in the following years, many studies assayed new natural compounds as molecular chaperones with anti-aggregational properties. Among them, polyphenols comprised the largest group of candidates with curcumin, baicalein, myricetin, epigallocatechin-3-gallate (EGCG), ferulic acid, caffeic acid, protocatechuic acid, and gallic acid as the most relevant discoveries [427-434](#). The hydroxyl groups present on the phenyl rings of polyphenols interact with α -Syn aggregates and destabilize these structures by disrupting the hydrogen bond network of the β -sheet. In consequence, polyphenols reduced α -Syn self-assembly propensity, interacting preferentially with the charged and disordered C-terminal region, and inducing the formation of non-toxic off-pathway aggregates [432,434,435](#), also rearranging preformed toxic structures or dismantling

preformed fibrils [427](#). Ferulic acid was the first polyphenolic structure described as a fibril-disrupting agent [427](#). These effects are not incompatible and some of the described compounds exhibited a combination of two or more of these activities [432,436-438](#). Structure-Activity Relationship (SAR) analysis of multiple phenolic variants with inhibitory activity revealed that the phenyl group alone does not prevent fibril formation [439](#). The inhibitory potential of polyphenolic structures resides in the number (trihydroxybenzoic acid > dihydroxybenzoic acid > monohydroxybenzoic acid), position, and conjugation of the hydroxyl groups at the benzoic acid scaffold [439](#). The consecutive arrangement of these polar moieties results in a higher inhibitory capacity [439](#). Although several of these compounds have been analysed in animal models of PD showing neuroprotection and a moderation of motor deficits [440-442](#), most of these studies were performed in neurotoxin-induced models of PD [443-445](#). For example, EGCG has been analysed in MPTP mice models of PD in which the compound, as many other polyphenols in similar models [446-452](#), exerted a neuroprotective effect [453](#). These models do not allow to associate the treatment-mediated improvement to an anti-aggregational effect of the compounds, and the antioxidant and anti-inflammatory effects of polyphenols could be the real responsible of preventing the neurotoxin-induced impairments [442,453](#). In this context, curcumin holds a special place, as it is one of the few polyphenols tested in transgenic animal models of PD, resulting in motor and behavioural improvements, but without a clear reduction of protein aggregates [454](#).

The development of new drugs constitutes a complex process that faces high attrition rates, substantial costs and a slow pace. In this context, repositioning or repurposing already approved molecules to develop new treatments for both common and rare diseases has become an attractive strategy. Drug repositioning significantly reduces the risk of failure, the time required for drug development and the cost of the process. Fasudil is a good example of the attempt to reposition a drug for PD based on the inhibition of α -Syn aggregation. This compound is a human Rho kinase inhibitor approved as a therapy in cerebral vasospasm and glaucoma [455](#) with the capacity to cross BBB and exerts neuroprotection in MPTP-treated mice [456](#). This activity was initially considered to derive from its inhibitory capacity of Rho kinase in the brain [456](#). However, further studies demonstrated that fasudil interacts with the aromatic side chains at the C-terminal domain of monomeric α -Syn, preventing the nucleation and elongation processes of α -Syn aggregation, and reducing intracellular accumulations of α -Syn in a cellular model of PD [457,458](#). Remarkably, administration of fasudil in A53T mice models [459](#) and AAV-mediated rat models of PD [460](#) reduced α -Syn deposits and induced a cognitive and behavioural improvement [457,461](#).

Methylthioninium chloride (MTC), also known as methylene blue, and leuco-methylthioninium bis(hydromethanesulfonate) (LMTM), a reduced stable form of methylthioninium (MT) with greater absorption rate than MTC, are other compounds whose repositioning for PD treatment has been studied. Both molecules reported an interesting inhibitory effect in the aggregation of amyloid β (A β) and Tau proteins, which are involved in AD [9,462](#), by disrupting the pre-formed Tau fibril and blocking the Tau-Tau interaction [463](#). Studies with these compounds demonstrated a higher inhibitory effect using MTC *in vitro*, but LMTM presented a greater potential *in vivo* in terms of dosage and bioavailability. Due to these results, MTC and LMTM have been tested in clinical phases II and III for AD, achieving promising results [464-466](#). The inhibitory potential of MTC and LMTM observed in Tau encouraged to test whether these compounds were able to also prevent the aggregation of α -Syn [428](#). Incubation of α -Syn with these phenothiazines was translated into a reduction of the *in vitro* aggregation of α -Syn by increasing its solubility. LMTM treatment in cellular models of PD

resulted in an important decrease in the formation of intracellular aggregates, without any effect in terms of protein expression ⁴⁶⁷. Moreover, oral administration of LMTM in mice models of PD ⁴⁶⁸ demonstrated a reduction in the number of positive α -Syn cells, with a high distribution pattern and without observed side-effects, inducing behavioural improvement. Overall, LMTM treatment induced a normalisation effect in transgenic mice in a dose-dependent manner, correlating with the observed reduction of intra-cellular α -Syn aggregates.

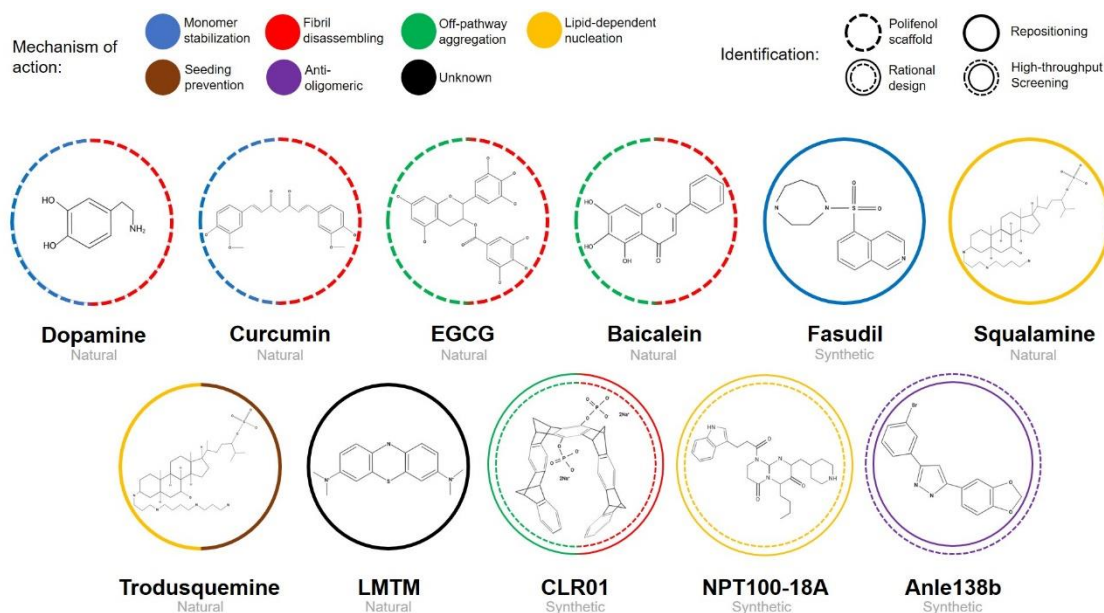


Figure 13. Chemical structures of inhibitors of α -Syn aggregation. Molecular structures of the most relevant modulators grouped by molecular class and mechanism of action Abbreviations: EGCG, epigallocatechin-3-gallate; LMTM, leuco-methylthioninium bis(hydromethanesulphonate). Adapted ³⁹⁷.

Also, squalamine, a steroid-polyamine conjugated compound ⁴⁶⁹ first found in *Squalus acanthias* ⁴⁷⁰ and that presents antimicrobial ^{471,472} and anti-angiogenic properties ⁴⁷³, has been described as an unusual inhibitor of α -Syn aggregation ⁴⁷⁴. Squalamine behaves as a cationic lipid that interacts with the inner leaflet of the plasma membrane and destabilizes protein–lipid contacts ⁴⁷⁵⁻⁴⁷⁷, which could affect to the initialization of α -Syn aggregation ⁴⁷⁸. These properties increased the interest to test whether squalamine could prevent the lipid-mediated aggregation of α -Syn. When α -Syn was incubated in presence of lipid vesicles and squalamine, the typical α -helical content of α -Syn was lost, while the random coil conformation of soluble monomer appeared ⁴⁷⁴. NMR analysis suggested a weak interaction between α -Syn and squalamine at the C-terminal, while the interaction between α -Syn and the lipid vesicle took place at the N-terminal ⁴⁷⁴. However, when squalamine, vesicles and α -Syn were mixed, NMR revealed a reduction in the interaction α -Syn-vesicle, without any evidence of a squalamine- α -Syn binding ⁴⁷⁴. On the basis of these results, squalamine seems to reduce the interaction of α -Syn with the vesicles by competing for binding sites on the surface of the lipid structures ⁴⁷⁴. As a result, squalamine reduces α -Syn aggregation and the oligomeric-mediated toxicity by decreasing the number of oligomers bound to the membranes ^{474,479}. Moreover, the compound significantly decreased the number of intracellular inclusions, without any effect on α -Syn expression, and improved the motility capacity of a *Caenorhabditis elegans* model of PD (as indicated by the trashing, speed and paralysis rate) ⁴⁷⁴.

Structural similarities observed between trodusquemine and squalamine suggested that this compound could also prevent α -Syn lipid-mediated aggregation. Trodusquemine is an aminosterol (a polyamine-steroid) with the potential to cross the BBB and to stimulate the

regeneration of injured tissues in vertebrates by recruiting stem cells, but without affecting the growth of the tissue [480](#). As observed with squalamine, trodusquemine was able to prevent the aggregation of α -Syn in presence of lipid vesicles by displacing α -Syn monomers from the surface of the vesicle where they are bound [481,482](#). The CD measurements confirmed a reduction of α -helix composition accompanied by an increase in the random coil content [481](#). Yet, the obtained data suggested a more complex inhibitory process than squalamine involving both, the displacement of α -Syn monomers from the lipid vesicles and the interaction with aggregation intermediates [481](#). To further determine whether trodusquemine impacts the elongation or the secondary nucleation, the authors incubated monomeric α -Syn with fibrils at different conditions [483-485](#). The assays demonstrated that trodusquemine prevented fibril amplification when the reaction is governed by fibril secondary nucleation, but it did not prevent fibril elongation [481](#). This inhibitory capacity seems to be related with its binding to the surfaces of amyloid fibrils, displacing monomeric α -Syn from fibrils surface [481](#). In addition, trodusquemine also reduced the toxicity of oligomeric structures due to the displacement of these toxic species [327,486](#) from the surface of the cellular membrane [482](#), where they tend to be bound, a phenomenon that correlates with their toxicity [487](#). *In vivo* analysis in a *C. elegans* model of PD demonstrated that the compound reduced the formation of intracellular inclusions, improved the motility up to similar levels to the healthy controls, and increased the longevity, protecting against the aggregation-induced toxicity [481](#).

Rational design is another approach to develop pharmacological therapies, with the idea of targeting specific regions or conformations of a protein. Despite the intrinsically disordered nature of α -Syn complicates exploiting this strategy, targeting residues involved in those intermolecular contacts that induce oligomerization, dimerization or fibrillation has demonstrated to be a successful approach. One of the first rationally designed structures is a molecular tweezer named CLR01, which presents a particular curved structure with a negatively charged cavity. These properties allow non-covalent interactions with Lys10 and Lys12 in the N-terminal domain, which translates into a reduction of α -Syn aggregation and the disassembling of preformed fibrils, presumably stimulating the formation of off-pathway oligomers [488](#). These studies suggested a link between the number of aromatic scaffolds and the inhibitory potential in a given molecular tweezer, as demonstrated by the absence of inhibitory potential of CLR03, a shorter variant of CLR01. Further analysis of the inhibitory mechanism of CLR01, demonstrated that the molecular tweezers bound preferentially to the N-terminal region of monomeric α -Syn but also to oligomers [489](#). This binding alters the hydrophobic and electrostatic interactions that drive protein aggregation and induces an increase in the reconfiguration rate of the protein [489](#). Cellular studies of the inhibitory capacity of CLR01 in two different models suggested that the molecular tweezer was able to reduce the toxicity of endogenously expressed and aggregated α -Syn and to decrease the toxic effect of the administration of exogenous α -Syn oligomers, increasing cell viability in all cases [488](#). *In vivo*, analysis on a zebrafish model of PD [490](#) revealed that CLR01 ameliorates α -Syn-induced damage by reducing the formation of α -Syn neuronal clumps [488](#). Furthermore, intracerebroventricular and peripheral administrations of CLR01 in mice models of PD [491](#) significantly improved the motor behaviour of the mice by inducing the formation of off-pathways oligomers, not directly affecting the α -Syn deposits [492](#). More detailed analysis using α -Syn over-expressing mice models for PD [493](#) and MSA [494](#) revealed that CLR01 administration increased neuronal survival and improved motor behaviour [495,496](#). Interestingly, CLR01 has also shown an inhibitory potential in the aggregation process of different amyloid proteins as A β 40 and A β 42, Tau, TTR or PrP, both *in vitro* [497](#) and *in vivo* [184,498](#).

Another example of rationally designed molecular chaperone was developed by Neuropore and UCB Pharma companies. Based on the assumption that α -Syn dimerization on the membrane surface is crucial for the oligomerization of α -Syn [499,500](#), both companies performed molecular dynamics analysis that revealed a dimerization-responsible pharmacophore region located on residues 96-102 at the C-terminal domain. To target that region, they developed a chemical library with 34 peptidomimetic compounds and identified NPT100-18A as the most promising candidate [501](#). NPT100-18A interaction with the pharmacophore region reduced α -Syn mature aggregates and increased monomeric release *in vitro* by reducing α -Syn interaction with liposomes and thus precluding oligomer formation in lipid membranes [501](#). NPT100-18A reduced aggregation and its associated toxicity in a primary neuronal cell system overexpressing either WT or E83R α -Syn. Moreover, NPT100-18A oral administration in E47K transgenic mice model exerted a significant neuroprotective effect in multiple brain areas, as the neocortex or the hippocampus, by reducing the formation of oligomeric species. The analysis of the substantia nigra of these animals revealed a moderated improvement after NPT100-18A administration [501](#). Unfortunately, pharmacokinetic analysis of the compound revealed poor BBB permeability and very low concentration in the brain [501](#). To overcome such limitation, Neuropore developed NPT200-11, a NPT100-18A derivate with significantly increased BBB permeability. Oral administration of NPT200-11 resulted in brain concentrations of 10 mg/kg, but this increased availability in the brain did not translate into a significant improvement in symptomatology with respect to the original molecule [502](#). Still, NPT200-11 successfully completed a clinical Phase I trial.

High-throughput screening (HTS) of large libraries of compounds stands out as a great alternative for the discovery of new active molecules. These strategies rely on optimized protocols to reduce cost and time. Regardless of the heterogeneity of protein aggregation, several groups have successfully optimised α -Syn aggregation protocols and/or integrated new detection systems to detect new chemical chaperones of α -Syn aggregation [503-506](#). Anle138b is a great example of an anti-aggregational compound identified with this strategy after two rounds of screening [503](#). The first screening step analysed the ability of ~20 000 chemically diverse drug-like structures to prevent the aggregation of prion protein (PrP), with 3,5-diphenyl-pyrazole (DPP) being the one with the highest activity. In a second screening, the authors developed 150 DPP derivatives obtained by SAR analysis with the objective to retain brain permeability and anti-aggregation activity. In this assay, anle138b emerged as the best candidate against PrP and α -Syn aggregation. This molecule did not present a significant interaction with monomeric α -Syn but a high binding affinity with a hydrophobic pocket in oligomeric assemblies. The interaction with oligomeric α -Syn precludes the formation of β -sheet interactions avoiding further amyloid aggregation. Moreover, the interaction of anle138b with aggregated α -Syn modify the fluorescence emission spectrum of the compound, with potential implications in PD diagnosis [507](#). Oral administration of anle138b in three different mice models of PD ameliorated PD-related symptoms as motor activity, gut motility, neuroprotection, and survival [503,508](#). Significantly, A30P transgenic mice model made it possible to demonstrate that the compound can reduce the number of aggregates in the brain, thus associating the observed neuroprotection with the phenotype [503](#). The observed therapeutic effect was also detected in symptomatic late-stage rodents, which opens the possibility that the compound could be effective in advanced stages of the disease [508](#). Moreover, anle138b inhibitory capacity was also observed in animal models of MSA, with a decay of neurodegeneration when administered at early stages [509](#) and motor recovery at the latest

phases [510](#). Preclinical analysis demonstrated that the compound was innocuous and had excellent pharmacological properties, including significant BBB permeability [511](#).

1.3. Other synucleinopathies

PD is a complex neurodegenerative disorder closely related to α -Syn aggregation. Nevertheless, PD is not the only disease associated with α -Syn amyloid formation. In disorders like MSA or DLB, the presence of abnormal protein accumulations in brain cells has been described. As observed in PD, the main component of such protein assemblies are amyloid aggregates of α -Syn [288,293,325](#). Together, these pathologies constitute a heterogeneous group of disorders, known as synucleinopathies, which share common neuropathological features (α -Syn aggregation), but differ in the cellular and anatomical location of α -Syn aggregates [10,325,512](#) and the symptomatic development. Nowadays, there is no effective treatment for these disorders.

1.3.1. Multiple system atrophy (MSA)

MSA is a fatal neurodegenerative disorder considered an orphan disease with an estimated incidence of 0.6 - 0.7 cases per 100000 [513](#). Its similar motor symptomatology usually masquerades MSA as PD, despite its faster development. As in PD, early stages of MSA are characterised by the development of NMS, but in this case affecting the autonomic system and causing sexual and urinary dysfunction, orthostatic hypotension and REM sleep disturbances [514,515](#). As the disease progresses, NMS severity increases, affecting the gastrointestinal system and causing depression, anxiety and pain [516,517](#). In addition, MSA patients develop parkinsonism accompanied by slowness, rigidity and falling tendency, but with a poor response to levodopa [518](#). Cerebellar ataxia and abnormal postures are also observed among the motor characteristics of MSA [516,518,519](#). The fast development of MSA (6-8 years up to bedridden) results in patient death, with a worst prognostic in older age at onset, parkinsonian phenotype and early progression of autonomic failure [520-522](#).

MSA is a sporadic disorder without related environmental factors. Nevertheless, mutations in *COQ2* and *SHC2* genes were observed in Japanese patients [523-525](#). In addition, several mutations, duplications and triplications in *SNCA* gene were detected in familial cases of MSA [166,526,527](#). The major histopathological hallmark of MSA are oligodendroglial cytoplasmic inclusions called Papp-Lantos bodies, mainly composed by amyloid aggregates of α -Syn [325,528](#). α -Syn aggregation is precluded by p25 α delocalization (**Fig. 14**), a protein that stabilizes the myelin sheath [529](#). However, in presence of α -Syn, p25 α promotes its phosphorylation and aggregation [530](#). These aggregates can be released by damaged oligodendrocytes to the extracellular space and assimilated by neighbouring neurons [531](#). Then, these neuronal cells develop cytoplasmic inclusions that could be prion-like transmitted [532-534](#), inducing neuroinflammation, lack of oligodendroglial-mediated protection and neuronal malfunction, a cascade that leads to neuronal death and astrogliosis [531](#).

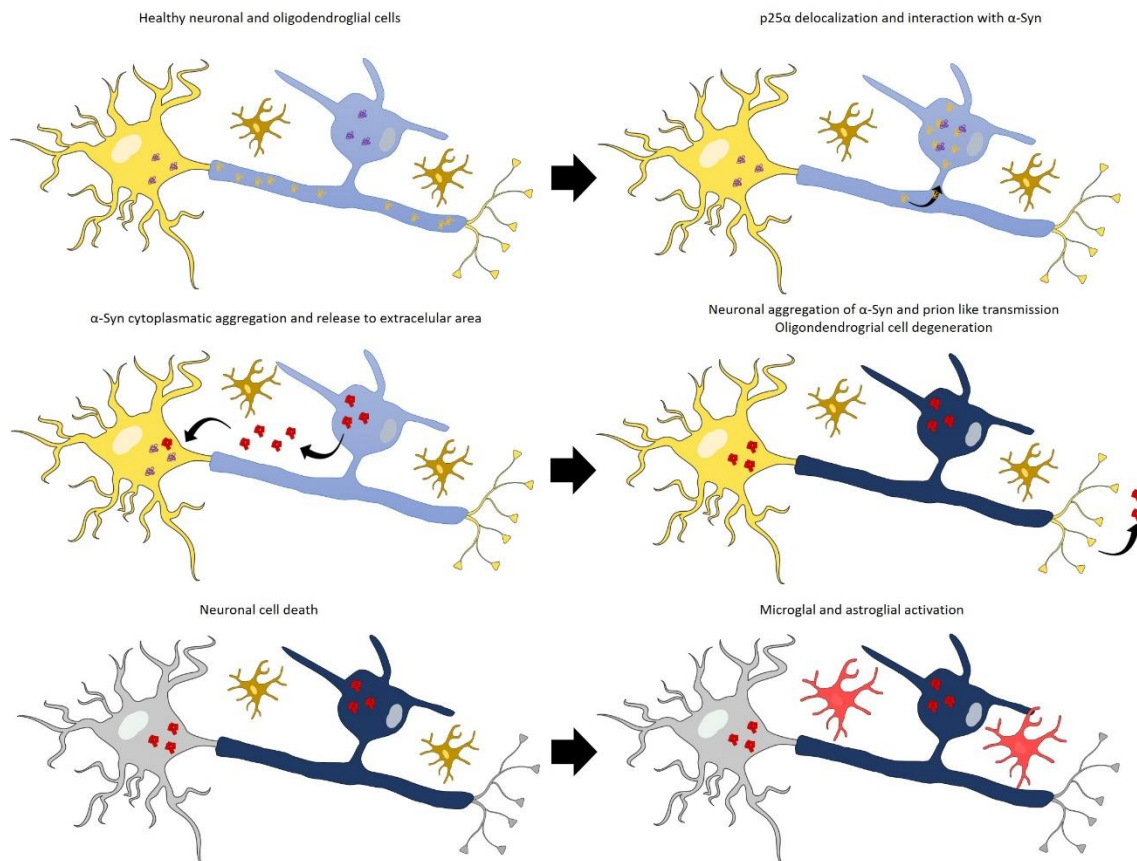


Figure 14. MSA cellular evolution. Schematic representation of MSA neurodegenerative progression from p25 α (yellow) delocalization and interaction with monomeric α -Syn (violet) to the formation and transmission of aggregated species of α -Syn (red), inducing neuronal and oligodendroglial cell death, microglial and astroglia activation and neuroinflammation. Adapted [535](#).

Diagnosis of MSA is a complicated procedure, based on symptomatic analysis of the patient and concludes with post-mortem evidence of α -Syn inclusions. Clinical guidelines define three different levels of MSA evidence. The first level, called possible, defines a disease progression characterised by parkinsonism or cerebellar syndrome with possible autonomic failure. The second level of certainty (probable) includes autonomic failure (as urinary dysfunction or orthostatic blood pressure reduction) with poor levodopa-responding parkinsonism (for parkinsonian subtype) or cerebellar problems (cerebellar subtype). The last level (definite) is based on post-mortem analysis revealing α -Syn inclusions [516,518,536](#).

As in PD, there is a lack of an effective treatment for MSA. However, certain drugs ameliorate the symptomatic severity. Treatment of the parkinsonian subtype is based on levodopa administration, which only induces a transient benefit in a 40% of the patients [518](#), but also (in a lesser extent) therapies based on dopamine agonists, as amantadine, or botulinum toxin locally administered might be used [537,538](#). For cerebellar subtype MSA there is not a specific treatment, but clonazepam, gabapentin and buspirone are often prescribed [539-541](#). In both cases, MS could be additionally treated with neurorehabilitation programs. Regarding NMS, there are as many therapies as the different MSA symptoms, applying a different treatment according to each one. As an example, midodrine and droxidopa are useful in MSA patients with severe orthostatic hypotension [542,543](#).

1.3.2. *Dementia with Lewy's bodies (DLB)*

DLB is a neurodegenerative disorder that progressively affects the CNS. Due to its symptomatology, DLB is usually confused with other neurodegenerative disorders such as PD or AD. This pathology is characterised by an early development of a severe dementia (fluctuating cognition, alertness and attention) that could be accompanied by REM sleep behaviour disorder, visual hallucinations and/or parkinsonism [544](#). In contrast to AD, short-term memory loss is not a prodromal feature of DLB. Compared to other synucleinopathies, DLB exhibits an earlier development of dementia and less severe parkinsonism than PD [545](#), while in MSA, autonomic failure is developed earlier and with higher severity than in DLB [514,515,544](#).

As with other synucleinopathies, the main cause of DLB remains unknown. Nevertheless, mutations in *APOE*, *GBA*, *SNCA* and *LRRK2* genes have been described as genetics risk factors and connect DLB with AD and PD [546-550](#). The main pathological hallmark of DLB is the presence of intracellular inclusions composed by α -Syn amyloid aggregates [10,512](#), which induce the loss of acetylcholinergic and DA neurons [551](#). However, post-mortem analysis of affected brains revealed also the presence of amyloid plaques, common in AD [552-554](#).

Current diagnosis of DLB is still a challenging process as it shares common symptoms with other neurodegenerative diseases. Nonetheless, DLB is diagnosed when an early and severe development of dementia is present with at least two other symptomatic features (parkinsonism, REM sleep behaviour disorder and visual hallucinations) and one suggestive biomarker, as an altered dopamine transport [544,555,556](#). At present, there is no effective treatment and only therapies that slightly alleviate the symptoms, as rivastigmine, donepezil or levodopa, are applied.

2. Research objectives

The main goal of this thesis is to develop small chemical compounds with the capacity to prevent α -Syn aggregation into amyloid fibrils and to prevent the aggregates-mediated neurodegeneration. For this purpose, we have developed a strategy consisting of (i) optimization of a high-throughput screening process to analyse a large library of compounds, (ii) validation and characterisation of the inhibitory capacity of the selected candidates against familial and structural variants of α -Syn, and (iii) confirmation of the observed inhibitory potential in cellular and animal models of PD as well as their putative neuroprotective effect.

2.1. Chapter 1. High-throughput screening methodology to identify alpha-synuclein aggregation inhibitors

The lack of disease-modifying effect of currently available therapies to treat PD is promoting the search for treatments that can address the molecular mechanism causing PD. The presence of α -Syn aggregates in patients' brains has increased the interest in targeting protein aggregation as a therapeutical approach. Nevertheless, the lack of a defined three-dimensional structure of α -Syn and the soaring heterogeneity of the aggregation process hinder the application of rational design. In this situation, HTS strategies appear as one of the best options to identify new anti-aggregational molecules. Still, HTS methods present important limitations, including the long time needed for accomplish protein aggregation, the high amount of protein required or the low robustness of the obtained data. Within this first chapter we attempted to develop a robust protein production and screening method. To this purpose we focused on the following main objectives:

- To establish an expression and purification procedure that returns the largest and purest amount of α -Syn in a short period of time.
- To determine the optimal conditions to follow the aggregation in real time, maximizing the robustness and reproducibility of the kinetics.
- To validate whether the selected conditions allow to detect the inhibitory potential among multiple candidates, differentiating positive and negative hits.
- To test further applications of the aggregation protocol and develop orthogonal techniques to corroborate the obtained results.

2.2. Chapter 2. Small molecule inhibits α -Synuclein aggregation, disrupts amyloid fibrils, and prevents degeneration of dopaminergic neurons

The application of the previously developed protocol allowed the analysis of 14000 different chemical structures as potential inhibitors of α -Syn aggregation. As a result of this arduous and meticulous screening we discovered a small set of putative inhibitors that merit a detailed analysis. One of these candidates was SynuClean-D (SC-D), a small aromatic compound with a moderate, but significant and consistent anti-aggregational capacity. The main goal of this chapter is to decipher the mechanisms of the inhibitory potential of SC-D and prove this effect *in vivo*. This general aim could be divided into different and specific objectives:

- To confirm the inhibitory capacity observed during the HTS analysis, using WT and familial variants of PD and including kinetics and orthogonal techniques as light-scattering or TEM.
- To study the minimal active concentration of SC-D.
- To assess the preferent pathways and structures (monomer or aggregates) targeted by SC-D and to analyse by computational approaches the possible interactions.
- To verify the toxicity of the compound and the inhibitory capacity in a well-established PD cellular model.
- To determine if the anti-aggregation capacity observed *in vitro* is also exerted in *C. elegans* animal models of PD and if this inhibition is translated into a neuroprotective effect.

2.3. Chapter 3. ZPD-2, a Small Compound That Inhibits α -Synuclein Amyloid Aggregation and Its Seeded Polymerization

HTS analysis of the HitFinder Collection chemical library from Maybridge, containing more than 14000 diverse structures, revealed less than 1 % of positive molecules, among them ZPD-2. This small aromatic compound shares similar functional groups with SC-D, although displaying different aromatic content, and also exhibited an important reduction of aggregates during HTS. Such structural coincidences increased the interest to further study the inhibition mechanism of ZPD-2, deciphering the targeted structures and its behaviour, in this chapter. The subsequent study was dissected in different objectives:

- To validate kinetically and orthogonally the capacity of preventing α -Syn aggregation *in vitro*.
- To perform dose- and time-response studies to disclose the minimal effective concentration of ZPD-2 and the specific steps of the kinetics that the compound is mainly targeting.
- To analyse whether ZPD-2 inhibits the aggregation of familial and conformational (strains) variants of α -Syn *in vitro*.
- To complete seeded polymerisation studies in presence and absence of ZPD-2 to study the effect of this molecule under pro-aggregational conditions.
- To assess the effect of ZPD-2 in two different *C. elegans* models of PD, analysing the anti-aggregational and neuroprotective *in vivo* potential of the compound.

2.4. Chapter 4. Inhibition of α -Synuclein Aggregation and Mature Fibril Disassembling With a Minimalistic Compound, ZPDm

Among the less than 1% of positive candidates obtained from the HTS evaluation, we found a potent modulator of α -Syn *in vitro* aggregation. This molecule presented a significant structural similarity to ZPD-2 but contains a single aromatic ring instead of the three aromatics rings of ZPD-2. Thus, this compound, then called ZPDm, seemed a minimalistic variant of ZPD-2 and provided a great opportunity to study the impact of structural variations in the inhibitory mechanisms. Accordingly, we performed a detailed analysis of the inhibitory characteristics of the compound to attain different goals:

- To verify the inhibitory capacity of ZPDm by monitoring Th-T fluorescence variation and performing additional complementary studies as TEM or light-scattering.

- To study the effect of ZPDm in the aggregation of familial variants of α -Syn related with early onset of PD.
- To perform dose-response study and evaluate the effectiveness of ZPDm at substoichiometric conditions.
- To examine conformational dependence on the mechanism of action of ZPDm
- To extrapolate the inhibitory potential of ZPDm *in vivo* using a *C. elegans* model of α -Syn aggregation.

2.5. Chapter 5. The small aromatic compound SynuClean-D inhibits the aggregation and seeded polymerization of multiple α -Synuclein strains

The aggregation of α -Syn is traditionally associated to PD, but we now know that the formation of α -Syn amyloids is related with a set of disorders called synucleinopathies. All these pathologies present related symptoms, yet different progression and brain damage patterns. Comparative studies of the structural conformation of the fibrils of different synucleinopathies seem to shed light on the origin of this diversity, as they revealed that the fibrils differ in their morphology. Further analysis also proved that their chemical and physical properties, including aggregation propensity, transmission and spreading capacity or toxicity, varied among the different strains. Despite this, most of the study of potential anti-aggregational compounds focused on a single strain. In this scenario, we decided to study the conformational dependence of SC-D to determine whether our compound could tackle the aggregation of multiple α -Syn strains. To this purpose we posed experiments to obtain diverse strains and study the effect of SC-D:

- To implement a robust aggregation protocol that allows to monitor the formation of alternative amyloid conformations of α -Syn.
- To demonstrate that the obtained conformation differs on their aggregation, seeding, and physicochemical properties.
- To assess the inhibitory potential of SC-D, deciphering if there is a conformational-dependence.
- To study whether SC-D maintains the previously described disaggregational capacity in the strains.
- To investigate the capacity of SC-D to prevent seeded polymerisation of different strains.
- To evaluate the seeding capacity of the different strains in cellular models and the effect of SC-D treatment on their transmission.

3. Chapters

3.1. Chapter 1. High-throughput screening methodology to identify alpha-synuclein aggregation inhibitors

Published at International Journal of Molecular Sciences on March 2017

Available in: <https://www.mdpi.com/1422-0067/18/3/478>



Article

High-Throughput Screening Methodology to Identify Alpha-Synuclein Aggregation Inhibitors

Jordi Pujols ^{1,†}, Samuel Peña-Díaz ^{1,†}, María Conde-Giménez ², Francisca Pinheiro ¹,
Susanna Navarro ^{1,3}, Javier Sancho ² and Salvador Ventura ^{1,3,*}

¹ Department of Biochemistry and Molecular Biology, Autonomous University of Barcelona, 08193 Bellaterra, Spain; jordi.pujolspujol@gmail.com (J.P.); samuel.pdiaz@gmail.com (S.P.-D.); chicagpinheiro@outlook.pt (F.P.); susanna.navarro.cantero@uab.cat (S.N.)

² Department of Biochemistry and Molecular and Cell Biology, Institute for Biocomputation and Physics of Complex Systems (BIFI), University of Zaragoza, 50018 Zaragoza, Spain; maria.conde@gmail.com (M.C.-G.); jsancho@unizar.es (J.S.)

³ Institute of Biotechnology and Biomedicine, Autonomous University of Barcelona, 08193 Bellaterra, Spain

* Correspondence: salvador.ventura@uab.cat; Tel.: +34-93-586-8956

† These authors contributed equally to this work.

Academic Editor: Irmgard Tegeder

Received: 15 December 2016; Accepted: 20 January 2017; Published: 2 March 2017

Abstract: An increasing number of neurodegenerative diseases are being found to be associated with the abnormal accumulation of aggregated proteins in the brain. In Parkinson's disease, this process involves the aggregation of alpha-synuclein (α -syn) into intraneuronal inclusions. Thus, compounds that inhibit α -syn aggregation represent a promising therapeutic strategy as disease-modifying agents for neurodegeneration. The formation of α -syn amyloid aggregates can be reproduced in vitro by incubation of the recombinant protein. However, the in vitro aggregation of α -syn is exceedingly slow and highly irreproducible, therefore precluding fast high throughput anti-aggregation drug screening. Here, we present a simple and easy-to-implement in-plate method for screening large chemical libraries in the search for α -syn aggregation modulators. It allows us to monitor aggregation kinetics with high reproducibility, while being faster and requiring lower protein amounts than conventional aggregation assays. We illustrate how the approach enables the identification of strong aggregation inhibitors in a library of more than 14,000 compounds.

Keywords: high-throughput screening; α -synuclein; Parkinson disease; amyloid; protein aggregation

1. Introduction

Protein misfolding and amyloid aggregation is behind a growing number of human diseases, including Parkinson's disease (PD) [1]. PD is the second most common neurodegenerative disorder, after Alzheimer's disease (AD) and is still incurable. PD is characterized by protein deposition in intraneuronal inclusions, the so-called Lewy bodies (LB) and Lewy neurites (LN) [2,3], whose major component is α -synuclein (α -syn) [4], a 140 amino acid presynaptic protein encoded by the SNCA gene and normally found in both soluble and membrane-associated fractions of the brain [5,6]. The protein α -syn is a central component in PD pathogenesis and accordingly a privileged target for therapeutic intervention. In vitro, under physiological conditions, α -syn assembles into aggregates that are structurally similar to those found in the inclusions of disease-affected brains [7,8]. The aggregation process is thought to start from soluble monomers that polymerise into ring-shaped and string-like oligomers. These small structures coalesce to form protofibrils that assemble into insoluble fibrils [9,10]. The precise nature of the toxic α -syn species is still unclear, although it is believed that specific oligomeric species play a key role in neuronal toxicity, rather than the mature

aggregates [11,12]. It is thought that the population of these small oligomeric species is also associated with the spread of the disease between different structures in the brain [13,14].

There is strong interest in the discovery of small compounds that can act as chemical chaperones modulating the aggregation of α -syn [15–20]. In the absence of a defined 3D-structure to target, screening of large collections of chemically diverse compounds is a useful approach toward the discovery of novel bioactive molecules exhibiting an α -syn anti-aggregational effect. Chemical kinetics approaches would allow the quantitative detection of the effects of potential therapeutic molecules on aggregation [21]; however, the application of this type of analysis is hampered by the low reproducibility of aggregation reactions, resulting in dissimilar kinetic parameters and/or high errors even within replicates in the same aggregation assay. This is especially true for α -syn, a protein displaying a very slow aggregation reaction, usually taking several days, which is highly influenced by factors like pH, temperature, agitation or the presence of impurities [18–20,22–31]. The lack of reproducibility between aggregation curves is a strong limitation to identify bona fide aggregation inhibitors, since their potency becomes hidden in overlapping errors bars, especially at the beginning of the reaction, where the more toxic oligomeric species are expected to be formed. The slow aggregation kinetics of α -syn is also an important time limitation for large-scale screening, where several thousands of potential inhibitors should be tested. Due to the dependence of the reaction on the initial protein concentration, the aggregation of α -syn can be accelerated by increasing this parameter. However, this means that very large amounts of protein will be necessary for high-throughput screening assays.

The aim of the present work is to provide a detailed aggregation kinetics protocol suitable for the large-scale screening of aggregation modulators that can be used without requiring extensive previous expertise in protein aggregation and/or in the manipulation of α -syn. By ensuring a high purity of the recombinant protein and performing protein aggregation assays in 96-well plates in presence of teflon polyballs, the fibrillation reaction is boosted, requiring times and protein quantities that are compatible with high-throughput screening. After optimizing agitation and temperature, we obtained highly reproducible kinetics that allowed us to derivate accurate aggregation constants. We illustrate how the approach permitted the identification of strong inhibitors after screening a library of more than 14,000 compounds.

2. Results

2.1. Protein Expression and Purification

For protein expression and purification, we adapted a protocol from Volles and Lansbury [32], including an additional sonication step during cell lysis and, more importantly, a final anion exchange chromatography (Figure 1). This purification step is crucial, since not only does it increase homogeneity, but also avoids the co-elution of nucleic acids. α -Syn binds to nucleic acids, the concentrations and identities of which might vary from preparation to preparation. Because most labs monitor the purity of their α -syn preparations using SDS-PAGE (Sodium Dodecyl Sulfate Polyacrylamide Gel Electrophoresis) and protein staining, nucleic acids are not visualized. The use of spectrophotometry to discard nucleic acid contaminations is highly advisable, since, in our hands, their presence results in a large heterogeneity in the kinetics of aggregation reactions.

Following this protocol, we obtained high amounts of nucleic acid free α -syn (35 mg/L culture). Purity of α -syn was checked by SDS-PAGE (Figure 2) and mass spectrometry, obtaining a band and a peak that corresponds to the theoretical weight of α -syn, respectively, without any trace of contaminant proteins.

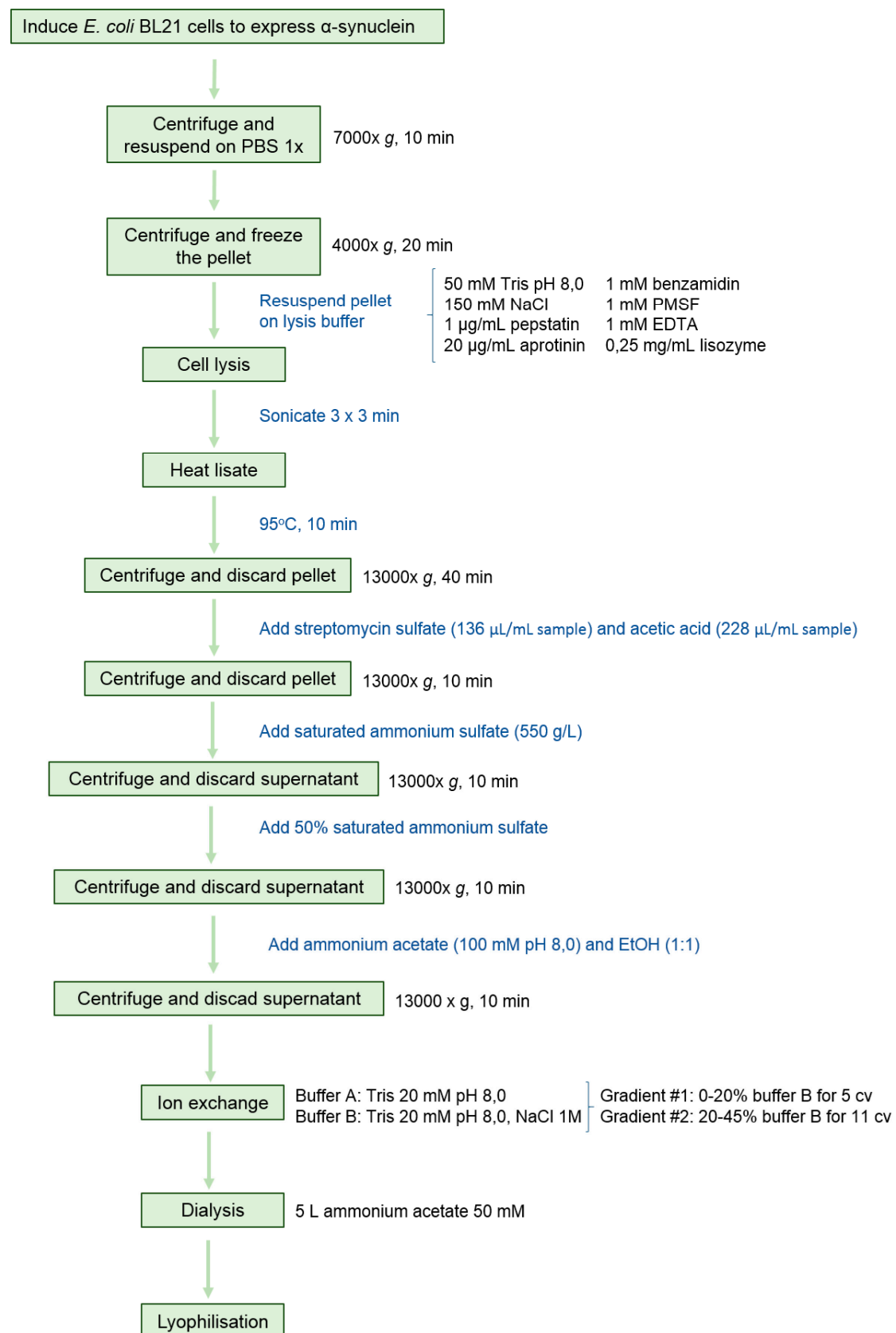


Figure 1. General strategy for the purification of α-synuclein.

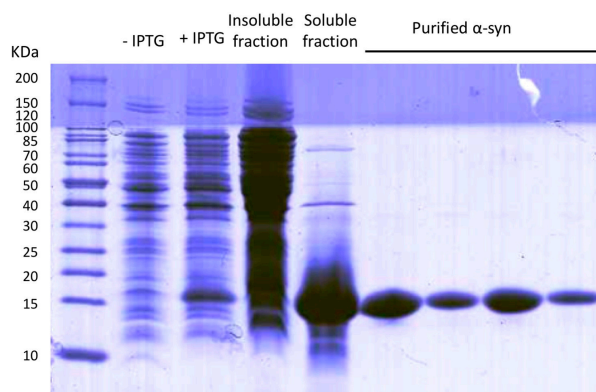


Figure 2. SDS-PAGE of the expression, fractionation and purification process. –IPTG and +IPTG (isopropyl β -D-1-thiogalactopyranoside) lines correspond to non induced and induced cell extracts. The insoluble and soluble fractions of induced cells are shown as well as different fractions eluting from the anion exchange column.

2.2. Aggregation Kinetics

One of the most important hallmarks of α -syn aggregation is the long time it needs to be completed. When compared with other amyloid-forming proteins, the time required for the assembly of detectable mature fibrils is significantly longer, in such a way that at concentrations below 100 μ M, the reaction exhibits a large lag phase, is only completed in one or more weeks and displays low reproducibility [18]. Because the aggregation ratios are extremely dependent on the initial protein concentration, the aggregation of α -syn has usually been accelerated by dramatically increasing its concentration in the assay, up to 400 μ M. High concentration also reduces erratic fibrillation [9]. However, the drawback is that very large amounts of protein are necessary for large-scale screening (0.75 mg of α -syn for a single 150 μ L reaction at 400 μ M) [23,24].

Here we present a protocol, in which, despite the use of concentrations of purified α -syn < 100 μ M, the sigmoidal aggregation reactions are completed in approx. 24 h. To track the aggregation progress, we took advantage of the amyloid specific reporter Th-T (Thioflavin-T), added to each sample at 40 μ M as final concentration. One of the main problems when performing kinetics is the loss of the mixture homogeneity as the reaction progresses. Most of the assays are performed on Eppendorf or glass tubes, from where aliquots are removed at certain times and diluted for fluorescence measurements in a quartz cuvette. Dilutions do not necessarily represent the original species population, and even when samples are sonicated or re-mixed, it is impossible to predict how representative the amount of aggregate is that we are taking out from the solution. To reduce variability, caused by both sample manipulation and aggregates heterogeneity, in our case, measurements were directly recorded in a 96-well plate (black plastic) using a plate reader.

Agitation has been shown to accelerate α -syn aggregation up to 1 order of magnitude. The effect of the agitation is implicitly or explicitly attributed to mass transfer or fibril fragmentation. However, for α -syn, despite agitation with only air resulting in somewhat accelerated kinetics, in our hands, the reactions were inconsistent from well to well and even resulted in different aggregates morphology. The use of glass beads during agitation potentially increases the air–water interface area; however, their effect on the speed and reproducibility of the reaction is controversial [33,34]. Investigations have demonstrated the sensitivity of aggregation reactions to hydrophobic–water interfaces and in particular to teflon–water interfaces [35] and indeed teflon beads have been used in a number of α -syn aggregation studies [36,37]. Therefore, we incorporated a teflon bead (2 mm diameter) in each well and incubated the plates under continuous agitation in an orbital shaker, since it provides more homogeneous ball agitation than a linear one. The presence of these little spheres accelerated dramatically the kinetics of α -syn aggregation, allowing us to work with 70 μ M α -syn in a final sample volume of 150 μ L, thus

reducing the amount of protein needed per reaction (0.145 mg/well). No aggregates were observed to form at the same protein concentration and conditions during the first 24 h in the absence of mixing balls, whereas in their presence, typical long unbranched amyloid fibrils could be observed by TEM (Transmission Electron Microscopy) (Figure 3).

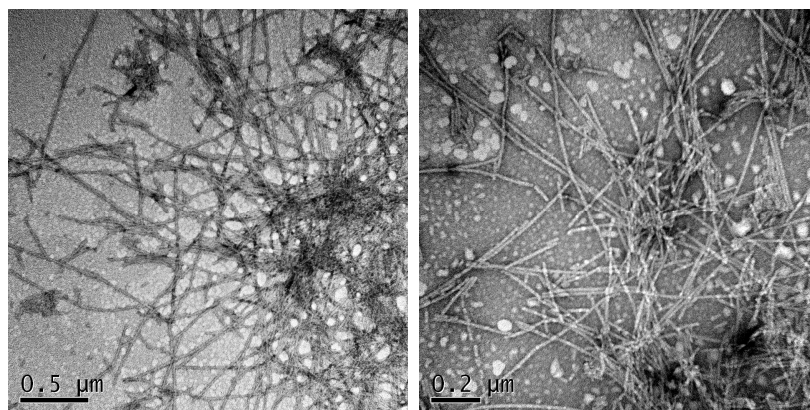


Figure 3. α -Synuclein fibrils formed in the presence of teflon beads. TEM images were collected upon incubation of 70 μ M soluble α -syn for 24 h with agitation in the presence of beads. The samples were briefly sonicated before imaging.

One remarkable advantage of the protocol is the capacity to simultaneously handle a high number of plates by fixing them on a conventional orbital culture incubator, instead of using the plate reader itself to incubate the plates one by one. In this way, we can achieve a smooth, prolonged and continuous agitation, in contrast to the short and intermittent one (commonly only 15 s before each measure) performed by conventional plate readers. Moreover, it is possible to accurately adjust the temperature (37 °C) and agitation conditions (100 rpm), enabling us to acquire well-to-well and plate-to-plate reproducible aggregation curves. Plates are only pulled out from the incubator for fluorescence reads and rapidly returned to their original location. Together, the method reduces both protein concentration and aggregation times, abolishes most sample manipulation, allows for simultaneous assays and maximizes reproducibility (Figure 4A). The accuracy of the protocol can be observed in Figure 4B, where it is shown how plotting Th-T fluorescence signal as a function of time for two different aggregation reactions, recorded in non-consecutive days, results in sigmoidal curves that overlap almost perfectly. In this way, when k_1 (nucleation rate constant) and k_2 (growth rate constant) were calculated using the Finke-Watzky two-step model for the two curves [38] we obtained $k_{11} = 0.00640 \pm 0.0013 \text{ h}^{-1}$, $k_{12} = 0.00645 \pm 0.0016 \text{ h}^{-1}$ and $k_{21} = 0.3623 \pm 0.0264 \text{ h}^{-1}$, $k_{22} = 0.3365 \pm 0.0336 \text{ h}^{-1}$, with correlation coefficients $R > 0.998$, in both cases. As expected, the relative standard error is larger for k_1 than for k_2 , indicating that nucleation is inherently more stochastic than elongation. This is the reason why the use of preformed amyloid seeds usually results in highly reproducible kinetics [39]; however, this precludes the identification of compounds that target the nucleation phase of amyloid formation.

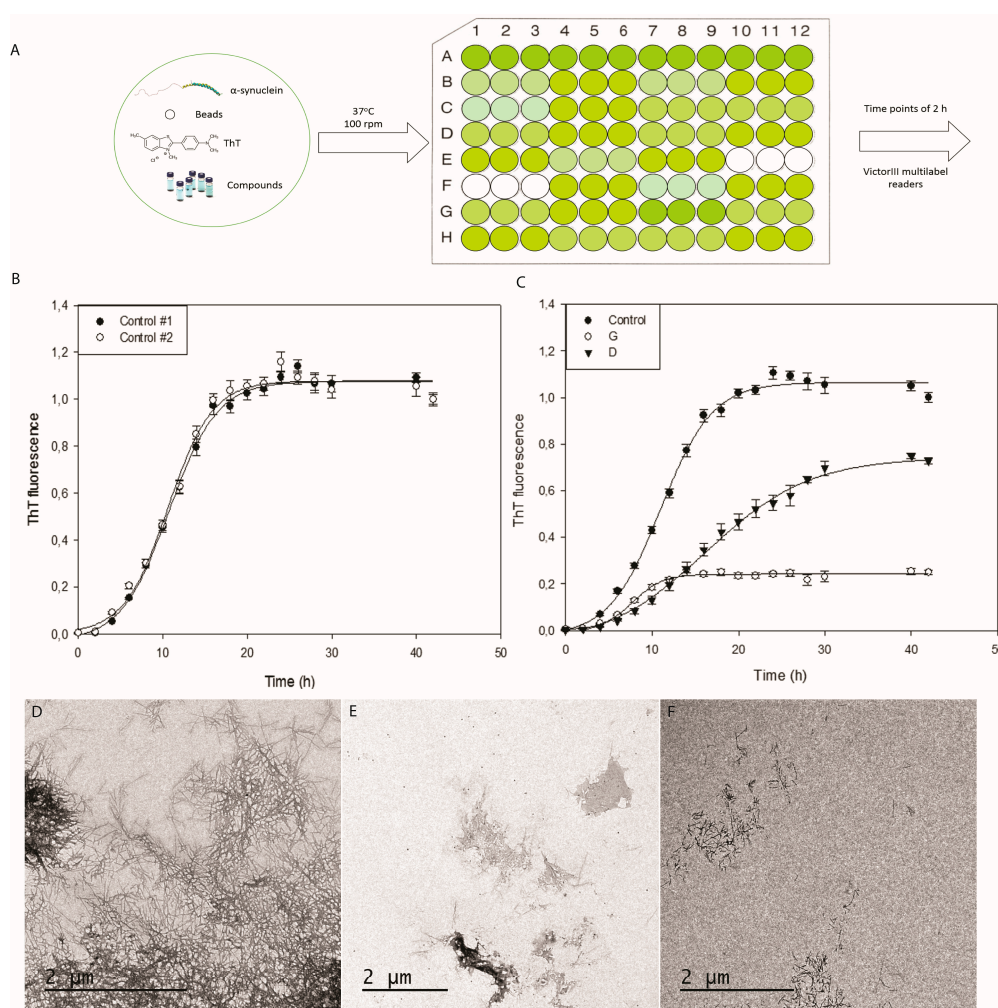
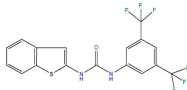
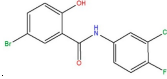
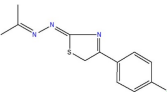
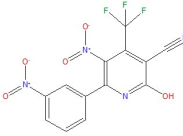
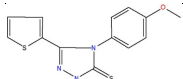
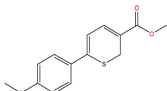
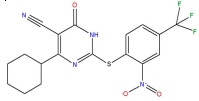
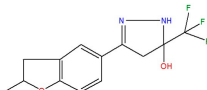
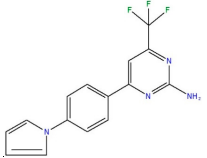
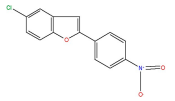
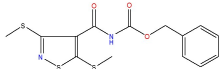


Figure 4. Aggregation kinetics, from plate preparation to putative inhibitors. (A) General scheme for plate preparation and incubation; (B) α -synuclein aggregation kinetics performed on non-consecutive days; (C) α -synuclein aggregation kinetics in presence of putative inhibitors. Measured by Th-T fluorescence emission, represented as normalised means. Error bars are represented as standard error. (D–F) TEM images of α -synuclein fibrils in absence (D) and presence of inhibitors (D–G).

The applicability of this methodology was validated by screening a large chemical library. We used the Maybridge HitFinder Collection, containing 14,400 compounds, in the search for putative inhibitors of α -syn aggregation. Each compound was tested in triplicate and each plate contained a triplicated α -syn control devoid of compound. Discarding false positives caused by Th-T fluorescence quenching during the data collection was essential. For this purpose, we recorded the absorbance spectra from 400 to 600 nm for any putative positive compound, and discarded those absorbing either at the Th-T excitation or emission wavelengths, 450 and 480 nm respectively. The successfulness of the approach is illustrated in Figure 4C, with two compounds (D and G) that exhibit medium and high effect on final Th-T fluorescence. It can be observed the low error bars obtained for all the reactions, which results in high statistical significance when assessing the inhibitory potency of the compounds at any time point. Accordingly, fitting the experimental data to the Finke-Watzky curve resulted in the large majority of cases in correlation coefficients $R > 0.985$. The ability of the method to identify bona fide inhibitors requires an orthogonal validation. In our case it was confirmed by visualizing control and compound-treated reactions end points by TEM. As an example, it can be seen in Figure 4D–F how the presence of compounds D and G results in an important decrease in both number and size of α -syn fibrils. Centrifugation assays indicated higher levels of soluble α -syn at the end of the

reaction in the presence of inhibitors. The screening rendered 47 novel compounds able to efficiently modulate the aggregation and inhibit fibril formation of α -syn. These compounds belong to different chemical families, supporting the versatility of the assay. The chemical structures and the activities of 10 representative molecules are illustrated in Table 1. After fitting their respective aggregation curves, the 47 compounds fall into one of two classes: those that decrease the final Th-T fluorescence without reducing k_1 and k_2 , like compound G, and those that decrease both the fluorescence signal and the kinetic constants, like compound D. They are those last compounds that exhibit pharmacological interest, since they are expected to delay the onset of the aggregation reaction. A convenient way to discriminate between these two types of molecules in large-screening assays is to compare the halftime of aggregation (t_{50}) [40].

Table 1. Representative active compounds identified in the high-throughput screening.

Name	Code	Structure	% Inhibition ^a	t_{50} (h) ^b
<i>N</i> -(1-benzothiophen-2-yl)- <i>N'</i> -[3,5-bis(trifluoromethyl)phenyl]urea	A		79.6	1
5-bromo- <i>N</i> -(3-chloro-4-fluorophenyl)-2-hydroxybenzamide	B		74.4	5
1-[4-(4-chlorophenyl)-2,5-dihydro-1,3-thiazol-2-yliden]-2-(1-methylethylidene)hydrazine	C		76.4	−3
2-hydroxy-5-nitro-6-(3-nitrophenyl)-4-(trifluoromethyl)nicotinonitrile	D		32.4	3
4-(4-methoxyphenyl)-5-(2-thienyl)-2,4-dihydro-3H-1,2,4-triazole-3-thione	E		59.8	3
methyl 6-(4-methoxyphenyl)-2H-thiopyran-3-carboxylate	F		93.0	1
4-cyclohexyl-2-[(2-nitro-4-(trifluoromethyl)phenyl)thio]-6-oxo-1,6-dihydropyrimidine-5-carbonitrile	G		72.7	−2
3-(2-methyl-2,3-dihydro-1-benzofuran-5-yl)-5-(trifluoromethyl)-4,5-dihydro-1H-pyrazol-5-ol	H		31.7	1
4-[4-(1H-pyrrol-1-yl)phenyl]-6-(trifluoromethyl)pyrimidin-2-amine	I		0	11
5-chloro-2-(4-nitrophenyl)benzo[b]furan	J		44.2	1
benzyl <i>N</i> -{[3,5-bis(methylsulfanyl)-4-isothiazolyl]carbonyl}carbamate	K		67.7	5

^a Measured as the change in Th-T fluorescence at the end of the aggregation reaction relative to the control; ^b Δt_{50} corresponds to the difference between the t_{50} of the reaction in the presence and the absence of compound.

The present method not only provides an effective system for screening, but can be used to set up a variety of experiments. For instance, when developing new anti-aggregational drugs, it is essential to titrate their concentration-dependent activity. Many promising potential drugs fail because they are not effective at a concentration compatible with their pharmaceutical application. The high reproducibility of the method allows us to perform accurate titration assays, as illustrated for compound D in Figure 5 where a clear dose-dependent anti-aggregation activity could be tracked for this molecule, which turns out to be active even at sub-stoichiometric protein:compound ratios. However, we should clarify that the method only allows us to detect α -syn species that can be stained with Th-T and thus it fails to monitor the impact of the compounds in the formations of early oligomers.

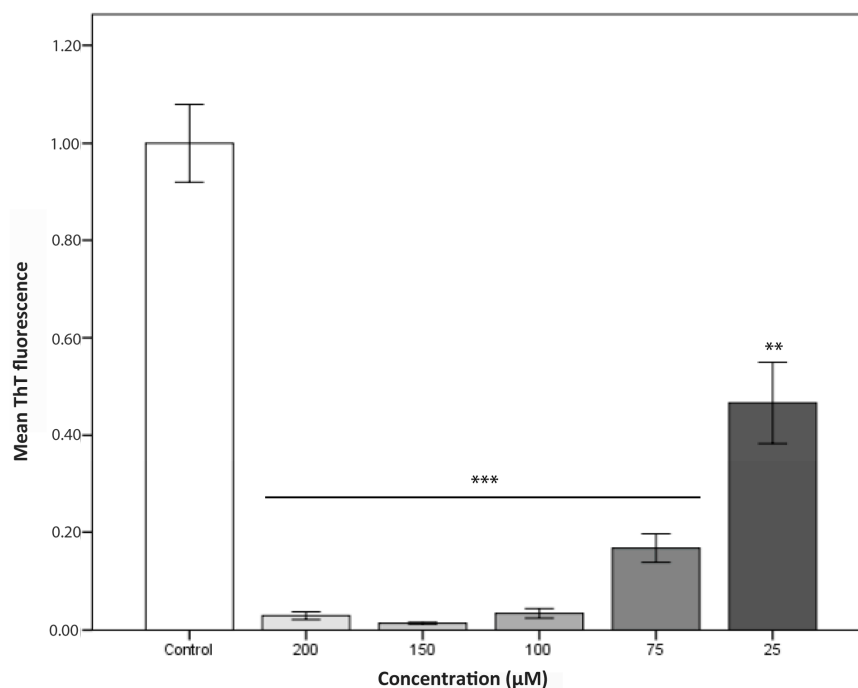


Figure 5. Inhibition of α -synuclein aggregation at different concentrations of the compound D. Error bars are represented as standard error, where $p < 0.005$ and $p < 0.0005$ were indicated by ** and *** respectively.

3. Discussion

The present work provides a simple and accurate method for screening large chemical libraries in the search of lead compounds with the potential to become enrolled in future treatments for PD. It is conceived as a friendly-to-use, easy-to-implement, protocol for non-specialized research labs, with the aim of reducing both time and resources, without losing accuracy. It allows us to monitor aggregation kinetics with high reproducibility and low errors, permitting to identify true positives among large collections of putative candidates and, in addition, assessing specific drug features such as the mechanism of action or the concentration and time dependence of the compound activity. Despite it is true that compounds able to inhibit in vitro α -syn in the presence of teflon polyballs would not necessarily behave in the same manner in vivo and thus that they are still far from being biologically effective therapeutics for synucleinopathies, the possibility to recruit novel labs in the search for such molecules, without the need for an initial large investment in specialized equipment, would likely boost the finding of novel candidates with the potential to halt the onset or the progression of these devastating disorders.

4. Materials and Methods

4.1. Expression and Purification of Human α -Synuclein

Human α -synuclein was expressed and purified adapting a previous protocol from Volles and Lansbury [32]. *Escherichia coli* BL21 (DE3) cells were transformed with a pET21a plasmid (Novagen, EMD-Millipore, Darmstadt, Germany) containing the α -syn cDNA, grown in LB medium containing 100 μ M/mL ampicillin and induced with 1 mM IPTG for 4 h at an optical density at 600 nm of 0.6. After cell centrifugation at $7000\times g$ for 10 min at 4 °C, the pellet was resuspended in 20 mL Phosphate Buffered Saline (PBS) buffer, centrifuged again at $4000\times g$ for 20 min at 4 °C and frozen at -80 °C. When needed, the pellets were defrosted and resuspended in 10 mL lysis buffer (50 mM Tris pH 8, 150 mM NaCl, 1 μ g/mL pepstatin, 20 μ g/mL aprotinin, 1 mM benzamidine, 1mM PMSF, 1 mM EDTA and 0.25 mg/mL lysozyme) prior to sonication using a LabSonic®U sonicator (B. Braun Biotech International, Melsungen, Hessen, Germany) with a power level of 40 W and a repeating duty cycle of 0.7 s for 3 intervals of 3 min. Resultant cell extract was boiled at 95 °C for 10 min and centrifuged at $20,000\times g$ for 40 min at 4 °C. To the obtained supernatant 136 μ L/mL of 10% *w/v* streptomycin sulfate and 228 μ L/mL of pure acid acetic were added and centrifuged at 4 °C ($20,000\times g$, 10 min). The resulting soluble fraction was diluted with saturated ammonium sulfate (550 g/L) 1:1 (*v/v*) and centrifuged at 4 °C ($20,000\times g$, 10 min). Then, the pellet was resuspended in 50% ammonium sulfate and centrifuged at 4 °C ($20,000\times g$, 10 min). The pellet was washed with 100 mM pH 8 ammonium acetate (5 mL per culture litre) and pure EtOH 1:1 (*v/v*), then, the mixture was centrifuged at 4 °C ($20,000\times g$, 10 min). The pellet was resuspended in 20 mM pH 8 Tris and filtered with a 0.45 mm filter. Anion exchange column HiTrap Q HP was coupled to an ÄKTA purifier high performance liquid chromatography system in order to purify α -synuclein. Tris 20 mM pH 8 and Tris 20 mM pH 8, NaCl 1 M were used as buffer A and buffer B respectively. After column equilibration with buffer A, sample was injected by using a Pump Direct Loading P-960 and the weak bonded proteins were washed with 5 column volumes (cv) of Buffer A. To properly isolate α -syn, a step gradient was applied as follows: (i) 0%–20% buffer B, 5 cv; (ii) 20%–45% buffer B, 11 cv; (iii) 100% buffer B, 5 cv, obtaining pure α -syn between 25% and 35% buffer B concentration. The collected peaks were dialyzed in 5 L ammonium sulfate 50 mM overnight. α -Syn concentration was determined measuring the absorbance at 280 nm and using the extinction coefficient $5960\text{ M}^{-1}\cdot\text{cm}^{-1}$. Purity was checked using 15% SDS-PAGE and unstained Protein Standard markers from Thermo Fisher Scientific. The gel was stained with comassie brilliant blue. Identity was checked by mass spectrometry. 2 μ L of protein were dialyzed for 30 min at room temperature using 20 mL of 50 mM ammonic bicarbonate and a 0.025 μ m pore membrane (EMD-Millipore, Darmstadt, Germany). After that, MALDI-TOF was analysis was performed with a ground steel plate and 2,6-dihydroxiacetophenone acid as a matrix, in a MALDI-TOF UltrafleXtreme (Bruker Daltonics, Billerica, MA, USA). A 1:1 sample:matrix mixture was used, adding just 1 μ L of these sample to the plate. For the analysis, a lineal mode was used with an accelerated voltage of 25 kV. Finally, after lyophilisation, the protein was kept at -80 °C.

4.2. Quenching Analysis of Compounds

The different compounds were dissolved at 50 mM in pure 100% DMSO solution. In order to check the interference of the compounds with thioflavin-T (Th-T) excitation or emission, the absorption spectra for each compound at 100 μ M was measured from 400 to 600 nm in a spectrophotometer Cary100.

4.3. α -Synuclein Aggregation and Thioflavin-T Assays

Previously lyophilised α -synuclein was carefully dissolved in PBS buffer to a final concentration of 210 μ M and filtered through a Millipore s 0.22- μ m filters. α -syn aggregation assay was performed in a 96 wells plate (non-treated, black plastic) containing in each well a teflon polyball (1/8" diameter), 40 μ M thiofalvin-T, 70 μ M α -synuclein, 100 μ M of the tested compounds and PBS up to a final

volume of 150 µL. Plates were fixed into an orbital culture shaker Max-Q 4000 Thermo Scientific (Waltham, MA, USA) to keep the incubation at 37 °C, 100 rpm. Every 2 h, the fluorescence intensity was measured using a Victor3.0 Multilabel Reader, PerkinElmer (Waltham, MA, USA) by exciting the mixtures with 430–450 filter and collecting the emission intensity with 480–510 filter (triplicates for each measurement). Each plate contained 3 α -syn controls in the absence of any compound. The averaged Th-T fluorescence obtained for these wells at the end of the experiment was normalized to 1 and the kinetic curves in the different wells re-scaled accordingly. Re-scaled curves were used to compare the controls with the effect of compounds and to ensure that the controls were reproducible between different experiments.

For the titration assay the following concentrations for all selected compounds (200, 150, 100, 75 and 25 µM) were used.

4.4. Transmission Electron Microscopy (TEM)

α -Synuclein fibers from final point reaction (either in absence or presence of the final concentration inhibitors) were collected and after diluting the aggregated α -syn to a concentration of 10 µM α -synuclein, each sample was sonicated for 10 min. A volume of 5 µL of these samples were placed on carbon-coated copper grids and allowed them to stand for 5 min. Then, samples were carefully dried with filter paper to remove the excess of sample. Grids were washed twice with MiliQ water by immersion and stained by incubating grids with 5 µL 2% (*w/v*) uranyl acetate for 2 min for the negative staining. After removal of the uranyl acetate excess with filter paper, grids were left to air-dry for 10 min. The samples were imaged using a Transmission Electron Microscopy Jeol 1400, JEOL (Peabody, MA, USA) operating at an accelerating voltage of 120 kV. At least 30 fields were screened, to obtain representative images.

4.5. Statistical Analysis

Data were analysed by ANOVA Tukey test using SPSS software version 20.0 (IBM Analytics, Armonk, NY, USA). All data are shown as means and standard error. $p < 0.05$ was considered statistically significant and indicated by ** and *** if $p < 0.005$ and $p < 0.0005$, respectively.

Acknowledgments: Salvador Ventura has been granted an ICREA ACADEMIA award. Salvador Ventura is supported by a grant from Fundación La Marató de TV3 (Ref. 20144330) and by the Spanish Ministry of Economy and Competitiveness (MINECO) BFU2013-44763-P. Javier Sancho is supported by MINECO grant BFU2013-47064-P and Protein Targets group from Diputación General de Aragón (Spain). Salvador Ventura and Javier Sancho are supported by SOE4/P1/E831 grant from SUDOE. INTERREG IV B. EUROPEAN UNION.

Author Contributions: Jordi Pujols, Samuel Peña-Díaz, Javier Sancho and Salvador Ventura conceived and designed the experiments; Jordi Pujols, Samuel Peña-Díaz, María Conde-Giménez, Francisca Pinheiro and Susanna Navarro, performed the experiments; Jordi Pujols, Samuel Peña-Díaz, Javier Sancho and Salvador Ventura analyzed the data; and Jordi Pujols, Samuel Peña-Díaz and Salvador Ventura wrote the manuscript.

Conflicts of Interest: The authors declare no conflict of interest.

Abbreviations

α -syn	α -synuclein
PD	Parkinson Disease
AD	Alzheimer's disease
Th-T	Thioflavin T
TEM	Transmission Electron Microscopy
cv	column volumes

References

1. Invernizzi, G.; Papaleo, E.; Sabate, R.; Ventura, S. Protein aggregation: Mechanisms and functional consequences. *Int. J. Biochem. Cell Biol.* **2012**, *44*, 1541–1554. [[CrossRef](#)] [[PubMed](#)]

2. Houlden, H.; Singleton, A.B. The genetics and neuropathology of parkinson's disease. *Acta Neuropathol.* **2012**, *124*, 325–338. [[CrossRef](#)] [[PubMed](#)]
3. Bendor, J.T.; Logan, T.P.; Edwards, R.H. The function of α -synuclein. *Neuron* **2013**, *79*, 1044–1066. [[CrossRef](#)] [[PubMed](#)]
4. Spillantini, M.G.; Schmidt, M.L.; Lee, V.M.; Trojanowski, J.Q.; Jakes, R.; Goedert, M. α -Synuclein in lewy bodies. *Nature* **1997**, *388*, 839–840. [[CrossRef](#)] [[PubMed](#)]
5. Maroteaux, L.; Campanelli, J.T.; Scheller, R.H. Synuclein: A neuron-specific protein localized to the nucleus and presynaptic nerve terminal. *J. Neurosci.* **1988**, *8*, 2804–2815. [[PubMed](#)]
6. Goedert, M. α -Synuclein and neurodegenerative diseases. *Nat. Rev. Neurosci.* **2001**, *2*, 492–501. [[CrossRef](#)] [[PubMed](#)]
7. Peelaerts, W.; Bousset, L.; van der Perren, A.; Moskalyuk, A.; Pulizzi, R.; Giugliano, M.; van den Haute, C.; Melki, R.; Baekelandt, V. α -Synuclein strains cause distinct synucleinopathies after local and systemic administration. *Nature* **2015**, *522*, 340–344. [[CrossRef](#)] [[PubMed](#)]
8. Serpell, L.C.; Berriman, J.; Jakes, R.; Goedert, M.; Crowther, R.A. Fiber diffraction of synthetic α -synuclein filaments shows amyloid-like cross- β conformation. *Proc. Natl. Acad. Sci. USA* **2000**, *97*, 4897–4902. [[CrossRef](#)] [[PubMed](#)]
9. Conway, K.A.; Harper, J.D.; Lansbury, P.T., Jr. Fibrils formed in vitro from α -synuclein and two mutant forms linked to Parkinson's disease are typical amyloid. *Biochemistry* **2000**, *39*, 2552–2563. [[CrossRef](#)] [[PubMed](#)]
10. Conway, K.A.; Lee, S.J.; Rochet, J.C.; Ding, T.T.; Williamson, R.E.; Lansbury, P.T., Jr. Acceleration of oligomerization, not fibrillization, is a shared property of both α -synuclein mutations linked to early-onset Parkinson's disease: Implications for pathogenesis and therapy. *Proc. Natl. Acad. Sci. USA* **2000**, *97*, 571–576. [[CrossRef](#)] [[PubMed](#)]
11. Winner, B.; Jappelli, R.; Maji, S.K.; Desplats, P.A.; Boyer, L.; Aigner, S.; Hetzer, C.; Loher, T.; Vilar, M.; Campioni, S.; et al. In vivo demonstration that α -synuclein oligomers are toxic. *Proc. Natl. Acad. Sci. USA* **2011**, *108*, 4194–4199. [[CrossRef](#)] [[PubMed](#)]
12. Karpinar, D.P.; Balija, M.B.; Kugler, S.; Opazo, F.; Rezaei-Ghaleh, N.; Wender, N.; Kim, H.Y.; Taschenberger, G.; Falkenburger, B.H.; Heise, H.; et al. Pre-fibrillar α -synuclein variants with impaired β -structure increase neurotoxicity in Parkinson's disease models. *EMBO J.* **2009**, *28*, 3256–3268. [[CrossRef](#)] [[PubMed](#)]
13. Hansen, C.; Angot, E.; Bergstrom, A.L.; Steiner, J.A.; Pieri, L.; Paul, G.; Outeiro, T.F.; Melki, R.; Kallunki, P.; Fog, K.; et al. α -synuclein propagates from mouse brain to grafted dopaminergic neurons and seeds aggregation in cultured human cells. *J. Clin. Investig.* **2011**, *121*, 715–725. [[CrossRef](#)] [[PubMed](#)]
14. Luk, K.C.; Kehm, V.; Carroll, J.; Zhang, B.; O'Brien, P.; Trojanowski, J.Q.; Lee, V.M. Pathological α -synuclein transmission initiates parkinson-like neurodegeneration in nontransgenic mice. *Science* **2012**, *338*, 949–953. [[CrossRef](#)] [[PubMed](#)]
15. Ibrahim, T.; McLaurin, J. α -Synuclein aggregation, seeding and inhibition by scyllo-inositol. *Biochem. Biophys. Res. Commun.* **2016**, *469*, 529–534. [[CrossRef](#)] [[PubMed](#)]
16. Deeg, A.A.; Reiner, A.M.; Schmidt, F.; Schueder, F.; Ryazanov, S.; Ruf, V.C.; Giller, K.; Becker, S.; Leonov, A.; Griesinger, C.; et al. Anle138b and related compounds are aggregation specific fluorescence markers and reveal high affinity binding to α -synuclein aggregates. *Biochim. Biophys. Acta* **2015**, *1850*, 1884–1890. [[CrossRef](#)] [[PubMed](#)]
17. Wang, W.; Zheng, L.L.; Wang, F.; Hu, Z.L.; Wu, W.N.; Gu, J.; Chen, J.G. Tanshinone iia attenuates neuronal damage and the impairment of long-term potentiation induced by hydrogen peroxide. *J. Ethnopharmacol.* **2011**, *134*, 147–155. [[CrossRef](#)] [[PubMed](#)]
18. Jiang, M.; Porat-Shliom, Y.; Pei, Z.; Cheng, Y.; Xiang, L.; Sommers, K.; Li, Q.; Gillardon, F.; Hengerer, B.; Berlinicke, C.; et al. Baicalein reduces E46K α -synuclein aggregation in vitro and protects cells against E46K α -synuclein toxicity in cell models of familial parkinsonism. *J. Neurochem.* **2010**, *114*, 419–429. [[CrossRef](#)] [[PubMed](#)]
19. Ji, K.; Zhao, Y.; Yu, T.; Wang, Z.; Gong, H.; Yang, X.; Liu, Y.; Huang, K. Inhibition effects of tanshinone on the aggregation of α -synuclein. *Food Funct.* **2016**, *7*, 409–416. [[CrossRef](#)] [[PubMed](#)]
20. Ahsan, N.; Mishra, S.; Jain, M.K.; Surolia, A.; Gupta, S. Curcumin pyrazole and its derivative (N-(3-nitrophenyl)pyrazole) curcumin inhibit aggregation, disrupt fibrils and modulate toxicity of wild type and mutant α -synuclein. *Sci. Rep.* **2015**, *5*, 9862. [[CrossRef](#)] [[PubMed](#)]

21. Vazquez, J.A. Modeling of chemical inhibition from amyloid protein aggregation kinetics. *BMC Pharmacol. Toxicol.* **2014**, *15*, 9. [[CrossRef](#)] [[PubMed](#)]
22. Lam, H.T.; Graber, M.C.; Gentry, K.A.; Bieschke, J. Stabilization of α -synuclein fibril clusters prevents fragmentation and reduces seeding activity and toxicity. *Biochemistry* **2016**, *55*, 675–685. [[CrossRef](#)] [[PubMed](#)]
23. Celej, M.S.; Sarroukh, R.; Goormaghtigh, E.; Fidelio, G.D.; Ruysschaert, J.M.; Raussens, V. Toxic prefibrillar α -synuclein amyloid oligomers adopt a distinctive antiparallel β -sheet structure. *Biochem. J.* **2012**, *443*, 719–726. [[CrossRef](#)] [[PubMed](#)]
24. Zhang, H.; Griggs, A.; Rochet, J.C.; Stanciu, L.A. In vitro study of α -synuclein protofibrils by cryo-EM suggests a Cu^{2+} -dependent aggregation pathway. *Biophys. J.* **2013**, *104*, 2706–2713. [[CrossRef](#)] [[PubMed](#)]
25. Planchard, M.S.; Exley, S.E.; Morgan, S.E.; Rangachari, V. Dopamine-induced α -synuclein oligomers show self- and cross-propagation properties. *Protein Sci.* **2014**, *23*, 1369–1379. [[CrossRef](#)]
26. Ghosh, D.; Singh, P.K.; Sahay, S.; Jha, N.N.; Jacob, R.S.; Sen, S.; Kumar, A.; Riek, R.; Maji, S.K. Structure based aggregation studies reveal the presence of helix-rich intermediate during α -synuclein aggregation. *Sci. Rep.* **2015**, *5*, 9228. [[CrossRef](#)] [[PubMed](#)]
27. Lorenzen, N.; Nielsen, S.B.; Buell, A.K.; Kaspersen, J.D.; Arosio, P.; Vad, B.S.; Paslawski, W.; Christiansen, G.; Valnickova-Hansen, Z.; Andreasen, M.; et al. The role of stable α -synuclein oligomers in the molecular events underlying amyloid formation. *J. Am. Chem. Soc.* **2014**, *136*, 3859–3868. [[CrossRef](#)] [[PubMed](#)]
28. Bai, J.; Zhang, Z.; Liu, M.; Li, C. α -Synuclein-lanthanide metal ions interaction: Binding sites, conformation and fibrillation. *BMC Biophys.* **2015**, *9*, 1. [[CrossRef](#)] [[PubMed](#)]
29. Kardani, J.; Roy, I. Understanding caffeine's role in attenuating the toxicity of α -synuclein aggregates: Implications for risk of Parkinson's disease. *ACS Chem. Neurosci.* **2015**, *6*, 1613–1625. [[CrossRef](#)] [[PubMed](#)]
30. Shaykhalishahi, H.; Gauhar, A.; Wordehoff, M.M.; Gruning, C.S.; Klein, A.N.; Bannach, O.; Stoldt, M.; Willbold, D.; Hard, T.; Hoyer, W. Contact between the $\beta 1$ and $\beta 2$ segments of α -synuclein that inhibits amyloid formation. *Angew. Chem. Int. Ed. Engl.* **2015**, *54*, 8837–8840. [[CrossRef](#)] [[PubMed](#)]
31. Shvadchak, V.V.; Claessens, M.M.; Subramaniam, V. Fibril breaking accelerates α -synuclein fibrillization. *J. Phys. Chem. B* **2015**, *119*, 1912–1918. [[CrossRef](#)] [[PubMed](#)]
32. Volles, M.J.; Lansbury, P.T., Jr. Relationships between the sequence of α -synuclein and its membrane affinity, fibrillization propensity, and yeast toxicity. *J. Mol. Biol.* **2007**, *366*, 1510–1522. [[CrossRef](#)] [[PubMed](#)]
33. Giehm, L.; Otzen, D.E. Strategies to increase the reproducibility of protein fibrillization in plate reader assays. *Anal. Biochem.* **2010**, *400*, 270–281. [[CrossRef](#)] [[PubMed](#)]
34. Pronchik, J.; He, X.; Giurleo, J.T.; Talaga, D.S. In vitro formation of amyloid from α -synuclein is dominated by reactions at hydrophobic interfaces. *J. Am. Chem. Soc.* **2010**, *132*, 9797–9803. [[CrossRef](#)] [[PubMed](#)]
35. Sluzky, V.; Tamada, J.A.; Klibanov, A.M.; Langer, R. Kinetics of insulin aggregation in aqueous solutions upon agitation in the presence of hydrophobic surfaces. *Proc. Natl. Acad. Sci. USA* **1991**, *88*, 9377–9381. [[CrossRef](#)] [[PubMed](#)]
36. Ulrih, N.P.; Barry, C.H.; Fink, A.L. Impact of Tyr to Ala mutations on α -synuclein fibrillation and structural properties. *Biochim. Biophys. Acta* **2008**, *1782*, 581–585. [[CrossRef](#)] [[PubMed](#)]
37. Janowska, M.K.; Wu, K.P.; Baum, J. Unveiling transient protein-protein interactions that modulate inhibition of α -synuclein aggregation by β -synuclein, a pre-synaptic protein that co-localizes with α -synuclein. *Sci. Rep.* **2015**, *5*, 15164. [[CrossRef](#)] [[PubMed](#)]
38. Morris, A.M.; Watzky, M.A.; Agar, J.N.; Finke, R.G. Fitting neurological protein aggregation kinetic data via a 2-step, minimal/"Ockham's Razor" model: The Finke-Watzky mechanism of nucleation followed by autocatalytic surface growth. *Biochemistry* **2008**, *47*, 2413–2427. [[CrossRef](#)] [[PubMed](#)]
39. Kim, H.J.; Chatani, E.; Goto, Y.; Paik, S.R. Seed-dependent accelerated fibrillation of α -synuclein induced by periodic ultrasonication treatment. *J. Microbiol. Biotechnol.* **2007**, *17*, 2027–2032. [[PubMed](#)]
40. Malisauskas, R.; Botyriute, A.; Cannon, J.G.; Smirnovas, V. Flavone derivatives as inhibitors of insulin amyloid-like fibril formation. *PLoS ONE* **2015**, *10*, e0121231. [[CrossRef](#)] [[PubMed](#)]



3.2. Chapter 2. Small molecule inhibits α -Synuclein aggregation, disrupts amyloid fibrils, and prevents degeneration of dopaminergic neurons

Published at Proceedings of the National Academy of Sciences on October 2018

Available in: <https://www.pnas.org/content/115/41/10481.long>

Small molecule inhibits α -synuclein aggregation, disrupts amyloid fibrils, and prevents degeneration of dopaminergic neurons

Jordi Pujols^{a,b,1}, Samuel Peña-Díaz^{a,b,1}, Diana F. Lázaro^{c,d,e}, Francesca Peccati^{f,g}, Francisca Pinheiro^{a,b}, Danilo González^f, Anita Carija^{a,b}, Susanna Navarro^{a,b}, María Conde-Giménez^{h,i}, Jesús García^j, Salvador Guardiola^j, Ernest Giralt^{k,l}, Xavier Salvatella^{j,l}, Javier Sancho^{h,i}, Mariona Sodupe^{f,l}, Tiago Fleming Outeiro^{c,d,e,m,n}, Esther Dalfó^{b,o,p}, and Salvador Ventura^{a,b,l,2}

^aInstitut de Biotecnologia i Biomedicina, Universitat Autònoma de Barcelona, 08193 Bellaterra, Spain; ^bDepartament de Bioquímica i Biologia Molecular, Universitat Autònoma de Barcelona, 08193 Bellaterra, Spain; ^cDepartment of Experimental Neurodegeneration, University Medical Center Göttingen, 37073 Göttingen, Germany; ^dCenter for Biostructural Imaging of Neurodegeneration, University Medical Center Göttingen, 37073 Göttingen, Germany; ^eCenter for Nanoscale Microscopy and Molecular Physiology of the Brain, University Medical Center Göttingen, 37073 Göttingen, Germany; ^fDepartament de Química, Universitat Autònoma de Barcelona, 08193 Bellaterra, Spain; ^gLaboratoire de Chimie Théorique, Sorbonne Universités, CNRS, F-75005 Paris, France; ^hDepartment of Biochemistry and Molecular and Cell Biology, University of Zaragoza, 50018 Zaragoza, Spain; ⁱInstitute for Biocomputation and Physics of Complex Systems (BIFI), University of Zaragoza, 50018 Zaragoza, Spain; ^jInstitute for Research in Biomedicine (IRB Barcelona), The Barcelona Institute of Science and Technology (BIST), 08028 Barcelona, Spain; ^kDepartment of Inorganic and Organic Chemistry, University of Barcelona, 08028 Spain; ^lInstitució Catalana de Recerca i Estudis Avançats (ICREA), 08010 Barcelona, Spain; ^mMax Planck Institute for Experimental Medicine, 37075 Göttingen, Germany; ⁿInstitute of Neuroscience, The Medical School, Newcastle University, Newcastle upon Tyne NE2 4HH, United Kingdom; ^oFaculty of Medicine, University of Vic-Central University of Catalonia (UVic-UCC), 08500 Vic, Spain; and ^pInstitut de Neurociències, Universitat Autònoma de Barcelona, 08193 Bellaterra, Spain

Edited by Gregory A. Petsko, Weill Cornell Medical College, New York, NY, and approved August 16, 2018 (received for review April 3, 2018)

Parkinson's disease (PD) is characterized by a progressive loss of dopaminergic neurons, a process that current therapeutic approaches cannot prevent. In PD, the typical pathological hallmark is the accumulation of intracellular protein inclusions, known as Lewy bodies and Lewy neurites, which are mainly composed of α -synuclein. Here, we exploited a high-throughput screening methodology to identify a small molecule (SynuClean-D) able to inhibit α -synuclein aggregation. SynuClean-D significantly reduces the in vitro aggregation of wild-type α -synuclein and the familial A30P and H50Q variants in a substoichiometric molar ratio. This compound prevents fibril propagation in protein-misfolding cyclic amplification assays and decreases the number of α -synuclein inclusions in human neuroglioma cells. Computational analysis suggests that SynuClean-D can bind to cavities in mature α -synuclein fibrils and, indeed, it displays a strong fibril disaggregation activity. The treatment with SynuClean-D of two PD *Caenorhabditis elegans* models, expressing α -synuclein either in muscle or in dopaminergic neurons, significantly reduces the toxicity exerted by α -synuclein. SynuClean-D-treated worms show decreased α -synuclein aggregation in muscle and a concomitant motility recovery. More importantly, this compound is able to rescue dopaminergic neurons from α -synuclein-induced degeneration. Overall, SynuClean-D appears to be a promising molecule for therapeutic intervention in Parkinson's disease.

Parkinson's disease | α -synuclein | protein aggregation | aggregation inhibition | dopaminergic degeneration

Parkinson's disease (PD) is the second most prevalent neurodegenerative disorder after Alzheimer's disease (AD) and is still incurable (1). PD is the most common synucleinopathy, a group of neurodegenerative disorders that includes dementia with Lewy bodies and multiple system atrophy (MSA), among others (2, 3). Although the synucleinopathies are multifactorial disorders, the molecular events triggering the pathogenic breakthrough of the disease converge to the abnormal aggregation of α -synuclein (α -Syn) in dopaminergic neurons (4, 5). α -Syn aggregation also occurs in oligodendrocytes in patients with MSA (6). α -Syn is an intrinsically disordered protein, which is expressed at high levels in the brain. α -Syn function is thought to be related to vesicle trafficking (7). This wild-type protein is the main component of cytoplasmic Lewy bodies (LB) and Lewy neurites (LN) in sporadic PD (8). In addition, dominantly inherited mutations in α -Syn, as well as multiplications of the gene encoding for α -Syn (*SNC4*), cause familial forms of PD (9).

Interfering with α -Syn aggregation has been envisioned as a promising disease-modifying approach for the treatment of PD (1). However, the disordered nature of α -Syn precludes the use of structure-based drug design for the discovery of novel molecules able to modulate α -Syn aggregation. Therefore, many efforts have focused on the analysis of large collections of chemically diverse molecules to identify lead compounds (10). Recently, we have developed an accurate and robust high-throughput screening methodology to identify α -Syn aggregation inhibitors (11). Here, we describe the properties of SynuClean-D (SC-D), a small molecule identified with this approach (*SI Appendix, Fig. S1*). We first performed a detailed in vitro biophysical characterization of the inhibitory and disaggregation activities of SC-D and tested its performance in human neural cells. Finally, we validated the effects in vivo in two well-established *Caenorhabditis elegans* models of PD, which express α -Syn either in muscle cells or in dopaminergic

Significance

Parkinson's disease is characterized by the accumulation of amyloid deposits in dopaminergic neurons, mainly composed of the protein α -synuclein. The disordered nature of α -synuclein and its complex aggregation reaction complicate the identification of molecules able to prevent or revert the formation of these inclusions and the subsequent neurodegeneration. By exploiting a recently developed high-throughput screening assay, we identified SynuClean-D, a small compound that inhibits α -synuclein aggregation, disrupts mature amyloid fibrils, prevents fibril propagation, and abolishes the degeneration of dopaminergic neurons in an animal model of Parkinson's disease.

Author contributions: S.V. designed research; J.P., S.P.-D., D.F.L., F. Peccati, F. Pinheiro, D.G., A.C., S.N., M.C.-G., J.G., S.G., and E.D. performed research; J.P., S.P.-D., D.F.L., E.G., X.S., J.S., M.S., T.F.O., E.D., and S.V. analyzed data; and M.S., E.D., and S.V. wrote the paper.

Conflict of interest statement: J.P., S.P.-D., M.C.-G., J.S., E.D., and S.V. are inventors on a patent application (PCT/EP2018/054540) related to the compound in this study.

This article is a PNAS Direct Submission.

Published under the PNAS license.

¹J.P. and S.P.-D. contributed equally to this work.

²To whom correspondence should be addressed. Email: salvador.ventura@uab.es.

This article contains supporting information online at www.pnas.org/lookup/suppl/doi:10.1073/pnas.1804198115/-DCSupplemental.

Published online September 24, 2018.

neurons. The inhibitor reduced α -Syn aggregation, improved motility, and protected against neuronal degeneration.

Results

SynuClean-D Inhibits α -Syn Aggregation in Vitro. The formation of α -Syn amyloid fibrils can be reproduced in vitro by incubating the recombinant protein. However, fibril growth is very slow and highly variable, complicating drug screening (12). We have implemented a robust high-throughput kinetic assay to screen large chemical libraries in the search for α -Syn aggregation inhibitors (11). The assay uses thioflavin-T (Th-T) as readout of amyloid formation, completing highly reproducible reactions in 30 h. Approximately 14,400 chemically diverse compounds of the HitFinder Collection from Maybridge were screened with this approach. SC-D [2-hydroxy-5-nitro-6-(3-nitrophenyl)-4-(trifluoromethyl)nicotinonitrile], a small aromatic compound, was identified as one of the molecules of potential interest (SI Appendix, Fig. S1). Many compounds with promising pharmacological characteristics never become drugs because they are rapidly metabolized in the liver and therefore have low oral bioavailability. SC-D was metabolically stable in the presence of human hepatic microsomes, with an intrinsic clearance of $<5 \mu\text{L}\cdot\text{min}^{-1}\cdot\text{mg}^{-1}$ (SI Appendix, Fig. S2).

Incubation of $70 \mu\text{M}$ α -Syn with $100 \mu\text{M}$ SC-D impacted α -Syn aggregation, as monitored by Th-T fluorescence (Fig. 1A). The analysis of the aggregation curves indicated that the autocatalytic rate constant in the presence of the compound (k_a 0.25 h^{-1}) was 25% lower than in its absence (k_a 0.33 h^{-1}). SC-D increases t_{50} by 1.5 h and reduces by 53% the amount of Th-T-positive material at the end of the reaction. By measuring light scattering, we confirmed that the observed changes in Th-T fluorescence reflected an effective decrease in the levels of α -Syn aggregates, with a reduction of 48 and 58% in the scattering signal at the end of the reaction in the presence of SC-D when exciting at 300 and 340 nm, respectively (Fig. 1B). Nanoparticle tracking analysis indicated that the presence of SC-D increased the number of

particles of $<100 \text{ nm}$ and decreased the formation of large aggregates (150 to 500 nm) (SI Appendix, Fig. S3). Finally, transmission electron microscopy (TEM) images confirmed that samples incubated with SC-D contained smaller and much fewer fibrils per field than untreated samples (Fig. 1C and D). The inhibitory activity of SC-D was dose-dependent and still statistically significant at $10 \mu\text{M}$ (1:7 compound: α -Syn ratio), where it reduces the final Th-T signal by 34% (Fig. 1E).

We further investigated whether SC-D was active against the aggregation of α -Syn variants associated with PD (1). SC-D was able to reduce by 45 and 73% the amount of Th-T-positive aggregates at the end of the reaction for the H50Q and A30P α -Syn familial variants, respectively (Fig. 1F).

The inhibitory activity of SC-D was also assessed using protein-misfolding cyclic amplification (PMCA) (13). Conceptually based on the nucleation-dependent polymerization model for prion replication, PMCA has been recently adapted to amplify α -Syn amyloid fibrils (14). The PMCA technique combines cycles of incubation at 37°C , to grow fibrils, and sonication, to break fibrils into smaller seeds. In our conditions, a single cycle of amplification was sufficient to generate amyloid-like protease K (PK)-resistant α -Syn assemblies, but the highest levels of protection were attained after four rounds (Fig. 1G). When the same experiment was performed in the presence of SC-D, we observed a substantial decrease in the amount of PK-resistant material (Fig. 1H), indicating that the molecule was interfering with α -Syn template seeding amyloid formation.

SynuClean-D Disrupts Preformed α -Syn Fibrils. The progress of α -Syn PMCA reactions can also be monitored by using the Th-T signal as the readout for fibril assembly (15). Consistent with PK resistance analysis, Th-T fluorescence of α -Syn increased significantly after four cycles of PMCA (Fig. 2A). Surprisingly, in the presence of SC-D, the Th-T signal not only did not increase, but

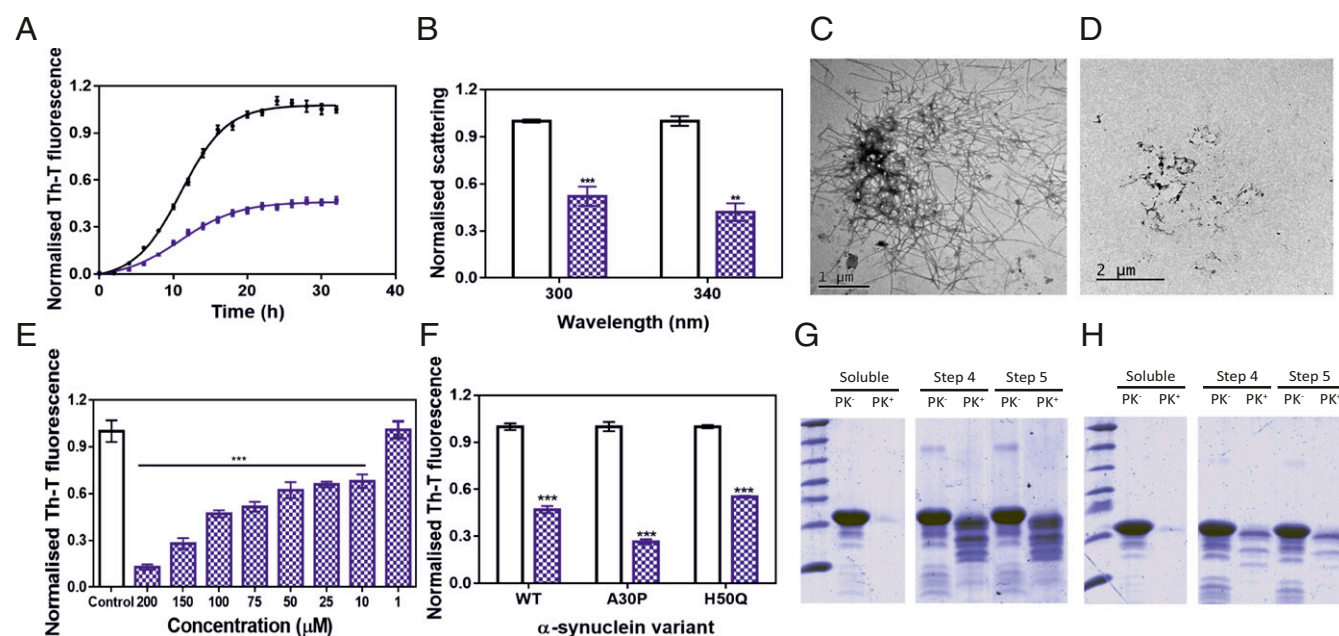


Fig. 1. Effect of SynuClean-D on the aggregation of α -Syn in vitro. (A) α -Syn aggregation kinetics in the absence (black) and presence (blue) of SC-D followed by Th-T-derived fluorescence. (B) Light-scattering signal at 300 and 340 nm, both in the absence (white) and presence (blue) of SC-D. (C and D) Representative TEM images in the absence (C) and presence (D) of SC-D. (E) Inhibition of α -Syn aggregation in the presence of different concentrations of SC-D. (F) H50Q and A30P α -Syn variant aggregation in the absence (white) and presence (blue) of SC-D. (G and H) Bis/Tris gels of PMCA samples in the absence (G) and presence (H) of SC-D, both analyzed after PK digestion. Soluble α -Syn and PMCA steps 4 and 5 are shown. Th-T fluorescence is plotted as normalized means. Final points were obtained at 48 h. Error bars are represented as SE of mean values; ** $P < 0.01$ and *** $P < 0.001$.

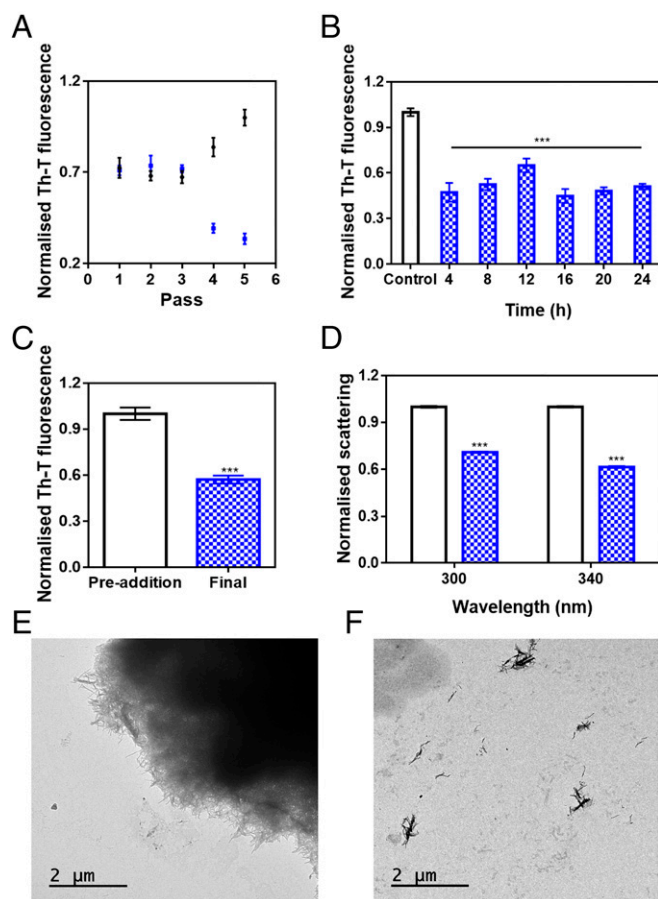


Fig. 2. Disaggregational capacity of SynuClean-D. (A) Th-T fluorescence of the different PMCA passes of both treated (blue) and untreated (black) samples with SC-D. (B) Aggregation kinetics of α -Syn after the addition of SC-D at different time points. (C and D) Th-T-derived fluorescence (C) and light-scattering (D) assays before and after the addition of SC-D to preformed α -Syn fibrils. (E and F) Representative TEM images in the absence (E) and presence (F) of SC-D. Th-T fluorescence is plotted as normalized means. Error bars are represented as SE of mean values; *** $P < 0.001$.

began to decrease after the third cycle. This suggested that SC-D might disrupt newly formed amyloid fibrils.

To address the time window in which SC-D is active, we set up aggregation reactions with a constant amount of SC-D at different time intervals. As presented in Fig. 2B, the effect of SC-D on the final amount of amyloid structures was independent of whether it was added at the beginning (4 h), in the middle (12 h), or at the end (18 h) of the exponential phase, or even when the reaction had already attained a plateau (24 h). These results suggested again ability to disrupt/destabilize fibrils.

To confirm the fibril-disrupting activity of SC-D, 4-d mature α -Syn fibrils were incubated in the absence or presence of the compound for 24 h. Incubation with SC-D promoted a 43% reduction in Th-T fluorescence emission (Fig. 2C). Moreover, light-scattering measurements indicated a reduction in the amount of detectable aggregates by 29 and 39% at 300 and 340 nm, respectively (Fig. 2D). Consistently, TEM images illustrated how 4-d-incubated α -Syn tended to form big fibrillary clusters (Fig. 2E), which became completely disrupted in the presence of SC-D (Fig. 2F).

α -Syn Fibrils Can Accommodate SynuClean-D. To assess if SC-D can bind monomeric and soluble α -Syn, the recombinant protein was isotopically labeled and NMR ^1H - ^{15}N -HSQC spectra of 70 μM [^{15}N] α -Syn were recorded in the absence and presence of SC-D.

We did not detect any perturbations in chemical shifts or peak intensities with respect to the original α -Syn spectrum in the presence of 100 μM concentration of the molecule (SI Appendix, Fig. S4), indicating that SC-D does not bind α -Syn monomers.

Induced-fit docking simulations of α -Syn-SC-D revealed four major poses for its interaction with α -Syn fibrils (16): two internal, with SC-D fully inserted in the fibril (poses 1 and 2), and two external, with SC-D partially exposed (poses 3 and 4) (SI Appendix, Fig. S5). In the internal poses, the ligand is sandwiched between two parallel β -sheets of the Greek-key motif and interacts with the side chains of ALA53, VAL55, THR59, GLU61, THR72, and GLY73. The only difference between pose 1 and 2 lies in the orientation of the compound in the binding pocket. PELE (17) interaction energies are stronger for the internal poses, where SC-D binds essentially through dispersion interactions into a solvent-excluded cavity, than for external ones, where SC-D inserts into a surface groove of the fibril. In light of these calculations, we predict that SC-D binds into the core of α -Syn fibrils.

MM/GBSA calculations (SI Appendix, Table S1) (18, 19) show that internal binding pose 1 (Fig. 3) exhibits the largest binding energy with the fibril, the computed ΔG_{bind} being -18.4 ± 4.1 kcal·mol $^{-1}$. The main contribution comes from the van der Waals term, representing roughly 80% of the interaction. This is not surprising given the nature of SC-D, a planar aromatic molecule. Plots of the reduced density gradient versus the density (SI Appendix, Fig. S6A) provide information on the nature of the noncovalent interactions in the system (20). Peaks in the negative and positive regions of the x axis are indicative of attractive and repulsive interactions, respectively. The region around zero corresponds to the weakest noncovalent van der Waals contacts. Though weak, these interactions are present in large number and involve the whole body of the molecule, being the largest contribution to the binding energy. Their spatial extension is shown in SI Appendix, Fig. S6B. For pose 1, the noncovalent interaction plot shows that

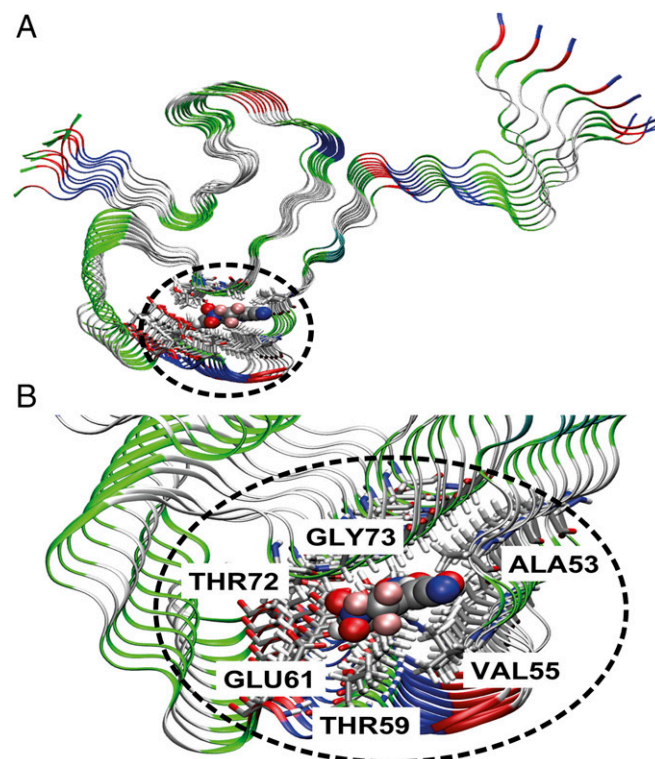


Fig. 3. Characterization of SynuClean-D-fibril interaction. General view (A) and zoom (B) of the most stable binding pose of SC-D on the α -Syn fibril model.

besides van der Waals, an H-bond contact is responsible for the binding of SC-D (*SI Appendix, Fig. S64*).

SynuClea-D Inhibits the Formation of Intracellular α -Syn Aggregates in Cultured Cells. We tested the potential toxicity of SC-D for human neuroglioma (H4) and human neuroblastoma (SH-SY5Y) cells. For both cell lines, the molecule was innocuous at concentrations as high as 50 μ M (Fig. 4*A* and *SI Appendix, Fig. S7*). We used a well-established cell model that enabled us to assess α -Syn inclusion formation. H4 cells were transiently transfected with C-terminally modified α -Syn (synT) and synphilin-1, which results in the formation of LB-like inclusions, as we previously described (9). The formation of α -Syn inclusions was assessed 24 h after treatment by immunofluorescence (Fig. 4*D*). Upon treatment with 1 and 10 μ M SC-D, we observed a significant increase in the number of transfected cells devoid of α -Syn inclusions (SC-D, 1 μ M: $42.4 \pm 1.0\%$; SC-D, 10 μ M: $49.5 \pm 4.5\%$) relative to untreated samples (control: $28.7 \pm 2.0\%$) (Fig. 4*B*). SC-D treatment also promoted a significant decrease in the number of transfected cells displaying more than five aggregates (SC-D, 1 μ M: $35.5 \pm 5.0\%$; SC-D, 10 μ M: $32.5 \pm 6.6\%$) relative to control cells (control: $49.6 \pm 5.6\%$) (Fig. 4*C*).

SynuClea-D Inhibits α -Syn Aggregation in a *C. elegans* Model of PD. Next, we tested SC-D in a living system. We used a well-studied nematode model of PD, the strain NL5901, in which human α -Syn fused to the yellow fluorescent protein (YFP) is under control of the muscular *unc-54* promoter, transgene *p_{unc-54}::YFP:: α -SYN* (21). Muscle expression has been used successfully to model protein-misfolding diseases and to identify modifier genes without considering neuronal effects (21, 22). To determine the effects of SC-D in α -Syn accumulations, animals at the fourth larval stage (L4) (23) were incubated with and without the compound, to analyze the inhibitor efficiency in aged worms at 9 d posthatching

(L4 + 7), which mimics aged human PD (24). We avoided a compound burst at L1 (25) because this treatment mimics a preventive rather than a disease-modifying intervention. Quantification of the number of α -Syn aggregates revealed that, in treated animals, the number of visible α -Syn aggregates decreased by 13.2 units, relative to untreated worms (18.3 ± 2.8 vs. 31.5 ± 1.1 , respectively) (Fig. 5*A* and *D*). In some animals, treatment resulted in a near-complete loss of protein aggregates (*SI Appendix, Fig. S8*). In this assay, SC-D is as effective as epigallocatechin gallate (EGCG), a polyphenol able to inhibit α -Syn aggregation and to disentangle preformed α -Syn aggregates (26, 27). EGCG has also been shown to reduce the deposits of the amyloid β -peptide in a *C. elegans* muscular model of AD (28). In our PD model, EGCG treatment reduced the number of visible aggregates by 13.4 units (18.1 ± 0.7) (Fig. 5*A*).

Major defects in regular bending have been used to identify modifiers of protein aggregation (21). Indeed, *C. elegans* thrashing can be measured in liquid media by counting the number of body bends per unit of time (29). By using this method, we confirmed an improved motility in SC-D-treated animals in comparison with nontreated worms (Fig. 5*B* and *E*). We observed a decrease of bending of 72.2% in YFP:: α -SYN animals compared with the N2 wild-type strain (18.1 ± 2.5 vs. 90.3 ± 6.7 , respectively). This motility decrease was reverted in YFP:: α -SYN animals treated with SC-D. In these animals, the average bending increased by 2.7-fold, compared with nontreated animals (18.1 ± 2.5 vs. 49.1 ± 4.4) (*Movies S1* and *S2*).

SynuClea-D Prevents Degeneration of Dopaminergic Neurons in a *C. elegans* Model of PD. PD is characterized by the degeneration of dopaminergic (DA) neurons. There exist four pairs of DA neurons in *C. elegans* hermaphrodites, three of them (CEPD, CEPV, and ADE) located in the anterior part, and one pair, the PDE, in the posterior part of the nematode (30). To investigate the neuroprotective role of SC-D in dopaminergic cell death, we sought to analyze its effect in a *C. elegans* model of PD in which DA neurons undergo age-dependent neurodegeneration (31). In this model (strain UA196), animals express both human α -Syn and GFP in DA neurons, according to the simplified genotype *Pdat-1::GFP; Pdat-1:: α -SYN* (the full genotype is detailed in *SI Appendix*). This strain has been successfully used for the investigation of human PD-related mechanisms (24). When human α -Syn is expressed in these animals' DA neurons, the six DA neurons within the anterior region of the worm display progressive degenerative characteristics (32). To model the aging contribution to PD, we determined the inhibitor capacity of SC-D in dealing with DA cell death induced by human α -Syn at 9 d (L4 + 7) posthatching. Cell bodies and neuronal processes were assessed to determine whether these structures displayed morphology changes. At 9 d posthatching, only $14.0 \pm 1.5\%$ of nontreated animals showed six wild-type DA neurons. In contrast, $44.4 \pm 2.8\%$ of treated animals showed the six intact DA neurons (Fig. 5*C* and *F*), which evidenced the ability of SC-D to protect against α -Syn-induced DA neuron degeneration. In contrast to SC-D, the administration of EGCG did not have any beneficial impact on neurodegeneration, since only $12.0 \pm 0.8\%$ of EGCG-treated animals exhibited six intact DA neurons, a proportion that is fairly similar to that in untreated worms ($14.0 \pm 1.5\%$) (Fig. 5*C*).

Discussion

α -Syn aggregation plays a major pathophysiological role in the development of PD. Since its discovery and subsequent identification as the most abundant protein in Lewy bodies (3), α -Syn was shown to be important for a number of cellular processes (7). Therapeutic strategies targeting the aggregation of α -Syn thus hold the promise to result in disease modification and mitigate pathology in PD (33).

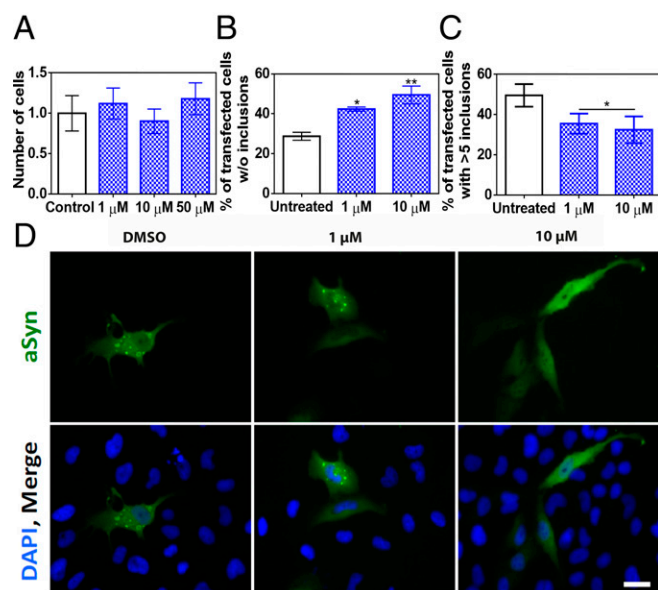


Fig. 4. Inhibition of α -Syn aggregate formation in cultured cells. (A) Human neuroglioma cell (H4) survival when incubated with different concentrations of compound (blue) and without (white) the compound. (B and C) Reduction of α -Syn inclusion formation in human cultured cells in the presence of different concentrations of SC-D. (B) Percentage of transfected cells devoid of α -Syn aggregates. (C) Percentage of transfected cells bearing >5 α -Syn aggregates. (D) Representative epifluorescent images from cells treated with SC-D. $n = 3$. (Scale bar, 30 μ m.) Error bars are represented as SE of means; * $P < 0.05$ and ** $P < 0.01$.

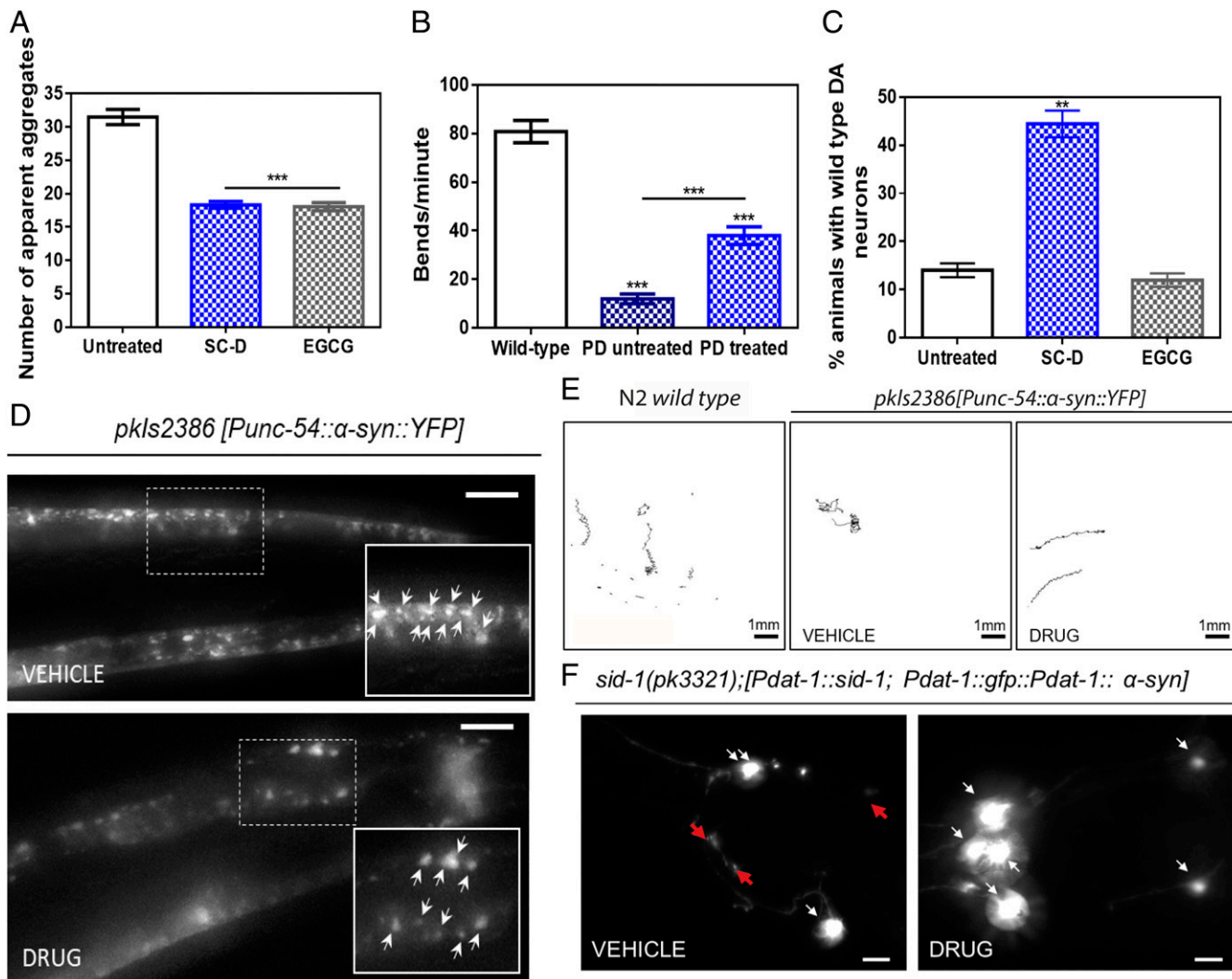


Fig. 5. Inhibition effect of the compound in the formation of α -Syn inclusions and protection from the α -Syn-induced dopaminergic cell death in *C. elegans* models of PD. (A) Quantification of α -Syn muscle inclusions per area of NL5901 worms in the absence (white) and presence of SC-D (blue) or EGCG (gray). (B) Worm-thrashing representation as the number of bends per minute of N2 wild-type and NL5901 worms treated without (white) and with SC-D (blue). (C) Percentage of UA196 worms that maintain a complete set of dopaminergic neurons (four pairs located in the head) after treatment without (white) and with SC-D (blue) or EGCG (gray) for 7 d after the L4 stage. (D) Representative images of α -Syn muscle aggregates obtained by epifluorescence microscopy of NL5901 worms treated without (*Top*, vehicle) and with SC-D (*Bottom*, drug). (Scale bars, 10 μ m.) Between 40 and 50 animals were analyzed per condition. Aggregates are indicated by white arrows. (E) Path representation of the mobility of N2 wild-type (*Left*, vehicle) and NL5901 worms grown without (*Middle*, vehicle) and with SC-D (*Right*, drug). (Scale bars, 1 mm.) (F) Representative worms expressing GFP- α -Syn specifically in DA neurons without (*Left*, vehicle) and with SC-D (*Right*, drug) for 7 d after L4. Healthy neurons are labeled with white arrows, whereas neurodegenerated or missing neurons are labeled with red arrows. (Scale bars, 30 μ m.) Between 40 and 50 animals were analyzed per condition in each experiment. Data are shown as means, and error bars are shown as the SE of means; ** P < 0.01 and *** P < 0.001.

(12). However, our *in vivo* experiments demonstrate that this is not the case for SC-D.

The ability of SC-D to target preformed fibrils might have important implications for the prion-like pathological spreading of α -Syn aggregates in the brain (4). By disentangling transmissible fibrillary assemblies, SC-D might reduce templated seeding and thus aggregate-catalyzed conversion of soluble α -Syn molecules into their insoluble forms. It has been suggested that to attain a sustainable spreading and prevent dilution of aggregates as they propagate from cell to cell, a process of aggregate amplification is required, in addition to templated seeding (36). PMCA emulates these particular conditions *in vitro*. The potency of SC-D in blocking PMCA-induced amplification of α -Syn fibrils is thus promising.

SC-D displayed low toxicity for neural cells and displayed cellular permeability. Indeed, SC-D treatment at concentrations as low as 1 μ M significantly reduced the number of α -Syn inclusions and the number of inclusions per cell. These data prompted us to assess the effects of SC-D treatment in *in vivo* models of α -Syn aggregation. First, we selected a well-validated *C. elegans* model of PD that expresses human α -Syn in muscular cells (21). When worms were treated with SC-D at preadult stages, we observed an important decrease in the number of α -Syn inclusions and a significant recovery of motility in adult PD worms. However, independent of whether a compound targets the early stages of aggregation or disrupts mature protein inclusions, or both, the final aim of a PD-oriented therapy is not to interfere with α -Syn aggregation *per se* but instead to prevent the neuronal degeneration associated with this phenomenon. It is in this therapeutic context where SC-D stands out, since it is able to increase by more than threefold the number of animals with intact DA neurons in a *C. elegans* model in which the

expression of human α -Syn is directly connected to dopaminergic degeneration (31).

Conclusions

In the present study, we describe how drug-screening efforts have crystallized in the discovery of a molecule able to inhibit α -Syn aggregation, both *in vitro* and *in vivo*, without interacting significantly with functional, monomeric, and soluble α -Syn. SC-D is a nontoxic molecule that exhibits a unique capability to interact with and disassemble amyloid fibrils, a property that is likely connected to its ability to prevent the α -Syn-promoted degeneration of dopaminergic neurons. Taken together, SC-D constitutes a very promising lead compound for the development of a novel therapeutic molecule for disease modification in PD and other synucleinopathies.

Materials and Methods

Protein purification, metabolic stability assays, *in vitro* aggregation studies, protein-misfolding cyclic amplification, molecular dynamics simulations, NMR studies, cytotoxicity assays, in-cell aggregation studies, and the *C. elegans* models of PD are described in detail in [SI Appendix](#).

ACKNOWLEDGMENTS. We thank the Infraestructura Científica y Técnica Singular NMR facility at Centres Científics i Tecnològics de la Universitat de Barcelona for help with NMR, Amable Bernabé at Institut de Ciència de Materials de Barcelona–Consejo Superior de Investigaciones Científicas for help with nanoparticle tracking analysis, and Anna Villar-Pique for help with plasmid construction. The worm strain UA196 used for neurodegeneration assays was a generous gift of Dr. Guy A. Caldwell. S.V. and T.F.O. are supported by Fundación La Marató de TV3 (Ref. 20144330). T.F.O. is supported by the Deutschen Forschungsgemeinschaft Center for Nanoscale Microscopy and Molecular Physiology of the Brain and by SFB1286. S.V. is supported by Ministerio de Economía y Competitividad (MINECO) (BIO2016-78310-R). J.S. is supported by MINECO (BFU2016-78232-P) and Gobierno de Aragón (E45_17R). E.D. is supported by Instituto de Salud Carlos III (PH613883/ERDF/ESF). J.G. and X.S. are supported by MINECO (BIO2015-70092-R) and the European Research Council (Contract 648201).

- Kalia LV, Lang AE (2015) Parkinson's disease. *Lancet* 386:896–912.
- Fanciulli A, Wenning GK (2015) Multiple-system atrophy. *N Engl J Med* 372:1375–1376.
- Spillantini MG, Crowther RA, Jakes R, Hasegawa M, Goedert M (1998) Alpha-synuclein in filamentous inclusions of Lewy bodies from Parkinson's disease and dementia with Lewy bodies. *Proc Natl Acad Sci USA* 95:6469–6473.
- Luk KC, et al. (2012) Pathological α -synuclein transmission initiates Parkinson-like neurodegeneration in nontransgenic mice. *Science* 338:949–953.
- Winner B, et al. (2011) *In vivo* demonstration that alpha-synuclein oligomers are toxic. *Proc Natl Acad Sci USA* 108:4194–4199.
- Fellner L, Jellinger KA, Wenning GK, Stefanova N (2011) Glial dysfunction in the pathogenesis of α -synucleinopathies: Emerging concepts. *Acta Neuropathol* 121:675–693.
- Bendor JT, Logan TP, Edwards RH (2013) The function of α -synuclein. *Neuron* 79:1044–1066.
- Spillantini MG, et al. (1997) Alpha-synuclein in Lewy bodies. *Nature* 388:839–840.
- Lázaro DF, et al. (2014) Systematic comparison of the effects of alpha-synuclein mutations on its oligomerization and aggregation. *PLoS Genet* 10:e1004741.
- Silva BE, Einarsson O, Fink AL, Uversky VN (2011) Modulating α -synuclein misfolding and fibrillation *in vitro* by agrochemicals. *Res Rep Biol* 2:43–56.
- Pujols J, et al. (2017) High-throughput screening methodology to identify alpha-synuclein aggregation inhibitors. *Int J Mol Sci* 18:E478.
- Ahsan N, Mishra S, Jain MK, Suroliya A, Gupta S (2015) Curcumin pyrazole and its derivative (N-(3-nitrophenyl)pyrazole) purcumin inhibit aggregation, disrupt fibrils and modulate toxicity of wild type and mutant α -synuclein. *Sci Rep* 5:9862.
- Barria MA, Gonzalez-Romero D, Soto C (2012) Cyclic amplification of prion protein misfolding. *Methods Mol Biol* 849:199–212.
- Jung BC, et al. (2017) Amplification of distinct α -synuclein fibril conformers through protein misfolding cyclic amplification. *Exp Mol Med* 49:e314.
- Herva ME, et al. (2014) Anti-amyloid compounds inhibit α -synuclein aggregation induced by protein misfolding cyclic amplification (PMCA). *J Biol Chem* 289:11897–11905.
- Tuttle MD, et al. (2016) Solid-state NMR structure of a pathogenic fibril of full-length human α -synuclein. *Nat Struct Mol Biol* 23:409–415.
- Madadkar-Sobhani A, Guallar V (2013) PELE web server: Atomistic study of biomolecular systems at your fingertips. *Nucleic Acids Res* 41:W322–W328.
- Salomon-Ferrer R, Case DA, Walker RC (2013) An overview of the Amber biomolecular simulation package. *Wiley Interdiscip Rev Comput Mol Sci* 3:198–210.
- Genheden S, Ryde U (2015) The MM/PBSA and MM/GBSA methods to estimate ligand-binding affinities. *Expert Opin Drug Discov* 10:449–461.
- Johnson ER, et al. (2010) Revealing noncovalent interactions. *J Am Chem Soc* 132:6498–6506.
- van Ham TJ, et al. (2008) *C. elegans* model identifies genetic modifiers of alpha-synuclein inclusion formation during aging. *PLoS Genet* 4:e1000027.
- Hamamichi S, et al. (2008) Hypothesis-based RNAi screening identifies neuroprotective genes in a Parkinson's disease model. *Proc Natl Acad Sci USA* 105:728–733.
- Brenner S (1974) The genetics of *Caenorhabditis elegans*. *Genetics* 77:71–94.
- Kim H, et al. (2018) The small GTPase RAC1/CED-10 is essential in maintaining dopaminergic neuron function and survival against alpha-synuclein-induced toxicity. *Mol Neurobiol* 55:7533–7552, and erratum (2018) 55:7553–7554.
- Perni M, et al. (2017) A natural product inhibits the initiation of α -synuclein aggregation and suppresses its toxicity. *Proc Natl Acad Sci USA* 114:E1009–E1017, and erratum (2017) 114:E2543.
- Ehrnhoefer DE, et al. (2008) EGCG redirects amyloidogenic polypeptides into unstructured, off-pathway oligomers. *Nat Struct Mol Biol* 15:558–566.
- Bieschke J, et al. (2010) EGCG remodels mature alpha-synuclein and amyloid-beta fibrils and reduces cellular toxicity. *Proc Natl Acad Sci USA* 107:7710–7715.
- Abbas S, Wink M (2010) Epigallocatechin gallate inhibits beta amyloid oligomerization in *Caenorhabditis elegans* and affects the *daf-2*/insulin-like signaling pathway. *Phytomedicine* 17:902–909.
- Gidalevitz T, Krupinski T, Garcia S, Morimoto RI (2009) Destabilizing protein polymorphisms in the genetic background direct phenotypic expression of mutant SOD1 toxicity. *PLoS Genet* 5:e1000399.
- Sulston J, Dew M, Brenner S (1975) Dopaminergic neurons in the nematode *Caenorhabditis elegans*. *J Comp Neurol* 163:215–226.
- Harrington AJ, Yacoubian TA, Slone SR, Caldwell KA, Caldwell GA (2012) Functional analysis of VPS41-mediated neuroprotection in *Caenorhabditis elegans* and mammalian models of Parkinson's disease. *J Neurosci* 32:2142–2153.
- Cao S, Gelwix CC, Caldwell KA, Caldwell GA (2005) Torsin-mediated protection from cellular stress in the dopaminergic neurons of *Caenorhabditis elegans*. *J Neurosci* 25:3801–3812.
- Tatenhorst L, et al. (2016) Fasudil attenuates aggregation of α -synuclein in models of Parkinson's disease. *Acta Neuropathol Commun* 4:39.
- Moree B, et al. (2015) Small molecules detected by second-harmonic generation modulate the conformation of monomeric α -synuclein and reduce its aggregation in cells. *J Biol Chem* 290:27582–27593.
- Wagner J, et al. (2013) Anle138b: A novel oligomer modulator for disease-modifying therapy of neurodegenerative diseases such as prion and Parkinson's disease. *Acta Neuropathol* 125:795–813.
- Ilijina M, et al. (2016) Kinetic model of the aggregation of alpha-synuclein provides insights into prion-like spreading. *Proc Natl Acad Sci USA* 113:E1206–E1215.

3.3. Chapter 3. ZPD-2, a Small Compound That Inhibits α -Synuclein Amyloid Aggregation and Its Seeded Polymerization

Published at Frontiers in Molecular Neurosciences on December 2019

Available in: <https://www.frontiersin.org/articles/10.3389/fnmol.2019.00306/full>



ZPD-2, a Small Compound That Inhibits α -Synuclein Amyloid Aggregation and Its Seeded Polymerization

Samuel Peña-Díaz^{1,2†}, Jordi Pujols^{1,2†}, María Conde-Giménez³, Anita Čarija^{1,2}, Esther Dalfo^{4,5†}, Jesús García⁶, Susanna Navarro^{1,2}, Francisca Pinheiro^{1,2}, Jaime Santos^{1,2}, Xavier Salvatella^{6,7}, Javier Sancho³ and Salvador Ventura^{1,2,7*}

¹ Institut de Biotecnologia i Biomedicina, Universitat Autònoma de Barcelona, Barcelona, Spain, ² Departament de Bioquímica i Biologia Molecular, Universitat Autònoma de Barcelona, Barcelona, Spain, ³ Department of Biochemistry and Molecular and Cell Biology, Institute for Biocomputation and Physics of Complex Systems (BIFI), University of Zaragoza, Zaragoza, Spain, ⁴ Faculty of Medicine, M2, Universitat Autònoma de Barcelona, Barcelona, Spain, ⁵ Faculty of Medicine, University of Vic – Central University of Catalonia, Vic, Spain, ⁶ Institute for Research in Biomedicine, The Barcelona Institute of Science and Technology, Barcelona, Spain, ⁷ Catalan Institute for Research and Advance Studies, Barcelona, Spain

OPEN ACCESS

Edited by:

Sandra Macedo-Ribeiro,
University of Porto, Portugal

Reviewed by:

Yoshitaka Nagai,
Osaka University, Japan
Daniel E. Otzen,
Aarhus University, Denmark

*Correspondence:

Salvador Ventura
salvador.ventura@uab.es

[†] These authors have contributed
equally to this work

*ORCID:

Esther Dalfo
orcid.org/0000-0003-4677-8515

Received: 10 September 2019

Accepted: 28 November 2019

Published: 17 December 2019

Citation:

Peña-Díaz S, Pujols J, Conde-Giménez M, Čarija A, Dalfo E, García J, Navarro S, Pinheiro F, Santos J, Salvatella X, Sancho J and Ventura S (2019) ZPD-2, a Small Compound That Inhibits α -Synuclein Amyloid Aggregation and Its Seeded Polymerization. *Front. Mol. Neurosci.* 12:306. doi: 10.3389/fnmol.2019.00306

α -Synuclein (α -Syn) forms toxic intracellular protein inclusions and transmissible amyloid structures in Parkinson's disease (PD). Preventing α -Syn self-assembly has become one of the most promising approaches in the search for disease-modifying treatments for this neurodegenerative disorder. Here, we describe the capacity of a small molecule (ZPD-2), identified after a high-throughput screening, to inhibit α -Syn aggregation. ZPD-2 inhibits the aggregation of *wild-type* α -Syn and the A30P and H50Q familial variants *in vitro* at substoichiometric compound:protein ratios. In addition, the molecule prevents the spreading of α -Syn seeds in protein misfolding cyclic amplification assays. ZPD-2 is active against different α -Syn strains and blocks their seeded polymerization. Treating with ZPD-2 two different PD *Caenorhabditis elegans* models that express α -Syn either in muscle or in dopaminergic (DA) neurons substantially reduces the number of α -Syn inclusions and decreases synuclein-induced DA neurons degeneration. Overall, ZPD-2 is a hit compound worth to be explored in order to develop lead molecules for therapeutic intervention in PD.

Keywords: Parkinson's disease, α -synuclein, amyloid, protein aggregation, aggregation inhibitor, *Caenorhabditis elegans*, neurodegeneration

INTRODUCTION

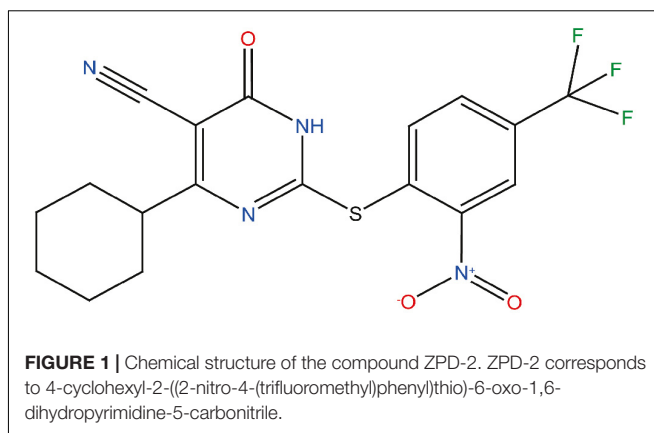
Parkinson's disease (PD) is a neurodegenerative disorder that affects about 0.3% of the population and >1% of people over 60 years of age (4% over 80 years) (Nussbaum and Ellis, 2003; Dexter and Jenner, 2013). It is characterized by the loss of dopaminergic (DA) neurons in *substantia nigra pars compacta*, which compromises the motor capacity of PD-suffering patients, producing tremor, rigidity, and bradykinesia (Marti et al., 2003). Additionally, since the disease spreads to the cerebral cortex (Braak et al., 2003), symptoms could include emotional and cognitive impairment (Marti et al., 2003). Nowadays, treatments are focused on alleviating the above mentioned motor

symptoms, mostly using dopamine replacement by administration of dopamine precursor (L-DOPA), combined with carbidopa, a L-DOPA decarboxylase inhibitor, and/or catechol-O-methyl transferase inhibitors and monoamine oxidase-B inhibitors (Dexter and Jenner, 2013). However, these treatments do not prevent the progression of PD and they lose efficacy as the disease advances.

Parkinson's disease is pathologically characterized by the accumulation of protein aggregates in the neuronal body, Lewy's bodies (LB), and/or fibrils deposited in neuronal processes, Lewy's neurites (LN), of affected neurons (Spillantini et al., 1997). These inclusions are mainly composed of α -synuclein (α -Syn), a protein predominantly expressed in the synaptic termination of DA neurons (Bendor et al., 2013). This evidence, together with the identification of mutations in the gene that encodes for this protein (SNCA) as the cause behind familial cases of PD (Polymeropoulos et al., 1997) and the observation that duplications and triplications of the SNCA gene lead to highly penetrant forms of the disease (Singleton et al., 2003; Ibanez et al., 2004) directly connect PD and α -Syn. In fact, the presence of aggregated α -Syn in the brain is a common feature of a group of diseases named synucleinopathies, which, in addition to PD, include Dementia with Lewy's bodies (DLB) and multiple system atrophy (MSA), among others (Marti et al., 2003).

In solution, α -Syn is a 140 amino acid intrinsically disordered protein whose function seems to be related with vesicle trafficking (Bendor et al., 2013). *In vitro* it forms thermodynamically stable amyloid aggregates (Serpell et al., 2000) that can display different conformational features (Li et al., 2018). The formation of amyloids by α -Syn follows the typical sigmoidal kinetics, reflecting a nucleation-polymerization process (Sabate et al., 2003); although secondary nucleation reactions might also occur (Xue et al., 2010). *In vivo*, α -Syn assemblies exert a toxic effect (Winner et al., 2011) and could be transmitted from cell to cell in a prion-like manner by seeding native α -Syn aggregation in previously unaffected neurons (Hansen et al., 2011).

Preventing α -Syn aggregation seems to hold the potential to achieve significant therapeutic impact. Several strategies have been developed toward this objective: SNCA gene-silencing approaches to decrease the protein levels (McCormack et al., 2010), methods to increase the clearance of aggregated α -Syn by autophagic and proteasomal machineries (Gao et al., 2019), and molecules intended to avoid the formation and/or propagation of aggregated α -Syn (Dehay et al., 2015; Hauser, 2015). One of the main limitations of this last strategy is the absence of a well-defined structure of monomeric α -Syn in solution, due to its intrinsically disordered nature, which hampers the rational design of inhibitors. High-throughput screening protocols have been developed to circumvent this problem (Silva et al., 2011; Levin et al., 2014). A number of promising small molecules have been discovered with this approach, including anle138b (Levin et al., 2014), BIOD303 (Moree et al., 2015), fasudil (Tatenhorst et al., 2016), squalamine (Perni et al., 2017), or SynuClean-D (SCD) (Pujols et al., 2018). In this context, we have developed a robust screening and validation protocol to analyze large chemical libraries in the search for effective inhibitors of α -Syn aggregation (Pujols et al., 2017). The *in vitro* pipeline



integrates thioflavin-T (Th-T) fluorescence and light scattering measurements, transmission electron microscopy (TEM), and protein misfolding cyclic amplification assays (PMCA). This approach allowed us to identify ZPD-2 (**Figure 1**) as a novel small molecule able to inhibit the aggregation of *wild-type* (WT) α -Syn, as well as that of the A30P (Kruger et al., 1998) and H50Q (Appel-Cresswell et al., 2013) familial mutants, being active against the seeded polymerization of different α -Syn strains. The compound displayed low toxicity for neuronal human cells and demonstrated significant inhibitory capacity in two well-established *Caenorhabditis elegans* models of PD (van Ham et al., 2008; Harrington et al., 2012).

MATERIALS AND METHODS

Protein Purification

Protein expression and purification of WT α -Syn and its variants (H50Q and A30P) were carried out as previously described (Pujols et al., 2017) and the resulting purified protein was lyophilized and kept at -80°C until its use.

In vitro Aggregation of α -Syn

α -Syn was resuspended in sterile PBS and filtered through 0.22 μm membranes to remove small aggregates. Aggregation was performed in a sealed 96-well plate, containing 70 μM α -Syn (WT, A30P or H50Q), 40 μM Th-T in PBS 1 \times , a 1/8" diameter Teflon polyball (Polysciences Europe GmbH, Eppenheim, Germany) and 100 μM ZPD-2 or DMSO (in control samples) in a total volume of 150 μL per well. The plate was incubated at 100 rpm and 37°C after having been fixed in an orbital culture shaker Max-Q 4000 (ThermoScientific, Waltham, MA, United States). Measurements of Th-T fluorescence were done every 2 h in a Victor3.0 Multilabel Reader (PerkinElmer, Waltham, MA, United States), exciting through a 430–450 nm filter and collecting the emission signal with a 480–510 filter. Each assay was done in triplicate. The values of the aggregation kinetics were fitted to the following Eq. 1 (Crespo et al., 2016):

$$\alpha = 1 - \frac{1}{k_b(e^{k_a t} - 1) + 1} \quad (1)$$

where k_b and k_a constitute the homogeneous nucleation rate constant and the secondary rate constant (fibril elongation and secondary nucleation), respectively (Crespo et al., 2016).

Titration assays were done by applying different ZPD-2 concentrations (200, 150, 100, 75, 50, 25, and 10 μ M). Time-dependent assays were developed by adding 100 μ M of ZPD-2 at different time points after the beginning of the reaction (4, 8, 12, 16, 20, and 24 h). In all cases a fixed concentration of α -Syn at 70 μ M was maintained.

Strains were generated as previously described (Bousset et al., 2013; Peelaerts et al., 2015; Carija et al., 2019). Briefly, lyophilized α -Syn was resuspended in PBS 1 \times and dialyzed for 24 h in a 1:1000 (v/v) ratio with buffer B (50 mM Tris-HCl pH 7.0), or buffer C (50 mM Tris-HCl pH 7.0 supplemented with 150 mM NaCl). Then, the protein was filtered through 0.22 μ m membrane and incubated at 70 μ M in presence or absence of 100 μ M ZPD-2 in a 96-well plate as described above. For the seeding assays, α -Syn pre-formed fibrils were sonicated for 5 min and then added to the aggregation reaction at ratios of 1% (v/v) for each condition. The plate was then incubated, and Th-T fluorescence measured as previously indicated.

The soluble fraction was obtained for subsequent quantification by centrifuging 300 μ L of aggregated sample at 16,900 $\times g$ for 90 min. The supernatant was then recovered and loaded into a Tricine-SDS-PAGE gel. Gels were stained with Blue safe. Finally, the density of the α -Syn bands was calculated using Quantity One software (Bio-Rad, Hercules, CA, United States). Experiments were done at least in triplicate.

Transmission Electron Microscopy

End-point α -Syn aggregates incubated for 32 h were collected, diluted 1:10 with PBS 1 \times and sonicated for 5 min. Five microliters of these sonicated samples was placed rapidly on a carbon-coated copper grid and incubated for 5 min. The grids were dried with a filter paper to withdraw the excess of sample and immediately washed twice with miliQ water. Finally, 5 μ L of 2% (w/v) uranyl acetate was added to the top of the grid and incubated for 2 min. The excess of uranyl acetate was removed with a filter paper and grids were left to air-dry for 10 min. Images were obtained using a TEM Jeol 1400 (Peabody, MA, United States) operating at an accelerating voltage of 120 kV. A minimum of 30 fields were screened per sample, in order to collect representative images.

Light Scattering

End-point α -Syn aggregates were collected, placed into a quartz cuvette, and analyzed in a Cary Eclipse Fluorescence Spectrophotometer (Agilent, Santa Clara, CA, United States). The sample was excited at 300 nm and the subsequent scattering at 90° monitored between 280 and 320 nm.

Protein Misfolding Cyclic Amplification

The PMCA assay was carried out as previously described (Herva et al., 2014). Briefly, α -Syn was resuspended to a final concentration of 90 μ M in Conversion Buffer (PBS 1 \times , 1% Triton X-100, 150 mM NaCl), supplemented with Complete Protease Inhibitor Mixture (Roche Applied Science, Penzberg, Germany).

Sixty microliters of this α -Syn solution was added into 200- μ L PCR tubes containing 1.0 mm silica beads (Biospec Products, Bartlesville, OK, United States). Samples were exposed to 24-h cycles of 30 s sonication and 30 min incubation at 37°C, using a Misonix 4000 sonicator, at 70% power. After every 24 h-cycle, 1 μ L of the incubated sample was added to a new PCR-tube containing fresh α -Syn. This process was repeated for 5 days. In the case of treated samples, ZPD-2 was added in each cycle to the fresh non-sonicated sample to a final concentration of 128 μ M, which corresponds to the 0.7:1 α -Syn:ZPD-2 ratio of the previous set of aggregation kinetics assays. Untreated samples were prepared adding the same concentration of DMSO (0.26%) present in the treated mixtures. All the reactions were made in triplicate.

At the end of each cycle, 10 μ L of the incubated samples were diluted 1:10 with 90 μ L of PBS 1 \times , 40 μ M Th-T. Th-T fluorescence was measured in a Cary Eclipse Fluorescence Spectrophotometer (Agilent, Santa Clara, CA, United States), exciting at 445 nm and collecting the emission signal between 460 and 600 nm.

Proteinase K Digestion

For protein digestion, 6 μ L of Proteinase K (5 μ g/mL final concentration) was added to 18 μ L of PMCA aggregated samples and incubated for 30 min at 37°C. After the incubation, 8 μ L of loading buffer containing 1% β -mercaptoethanol was added and the enzyme was thermally inactivated at 95°C for 10 min. Finally, 7 μ L of the incubated and stained samples was loaded into a Tricine-SDS-PAGE gel together with unstained Protein Standard markers (ThermoFisher Scientific, Waltham, MA, United States). Gels were stained with Blue safe.

Nuclear Magnetic Resonance

Expression of 15 N-labeled human WT α -Syn was carried out in *Escherichia coli* BL21 DE3 strain. First, cells were grown in LB medium until an OD₆₀₀ of 0.6. The culture was then centrifuged at 3000 rpm for 15 min and the pellets collected and resuspended in 1 L minimal medium, composed of: 768 mL of miliQ water with 1 mL of ampicillin 100 mg/mL, 100 μ L CaCl₂ 1 M, 2 mL MgSO₄ 2 M, 20 mL glucose 20%, 10 mL vitamins 100 \times (Sigma-Aldrich, Darmstadt, Germany), 200 mL salts M9, and 1 g 15 NH₄ (Cambridge Isotope Laboratories, Inc., Tewksbury, MA, United States). Cells were incubated for 1 h at 37°C and 250 rpm. After that, protein expression was induced for 4 h with 1 mM IPTG. Protein was purified as previously described (Pujols et al., 2017).

^1H - ^{15}N HSQC spectra were obtained at 20°C on a Bruker 600 MHz NMR spectrometer equipped with a cryoprobe in a mixture containing 70 μ M 15 N-labeled α -Syn, PBS buffer (pH 7.4), 2.5% d₆-DMSO, and 10% D₂O in the absence or in the presence of 100 μ M ZPD-2.

Toxicity Assays

Neuroblastoma cells were incubated 24 h in DMEM medium in a 96-well plate before the addition of different concentrations of ZPD-2 (from 1 μ M to 1 mM). Cells were incubated for 48 h at 37°C and PrestoBlue® reagent

(ThermoFisher Scientific, Waltham, MA, United States) was added to analyze cell death. Treated and untreated cells were incubated with PrestoBlue® for 10 min at 37°C. Finally, fluorescence emission was measured by exciting at 560 nm and collecting at 590 nm.

Caenorhabditis elegans Assays

Maintenance

Animals synchronization was carried out by bleaching and overnight hatching in M9 (3 g/L KH_2PO_4 , 6 g/L Na_2HPO_4 , 5 g/L NaCl, 1 M MgSO_4) buffer. Thus, nematodes were cultured at 20°C on growth media plates (NGM) containing 1 mM CaCl_2 , 1 mM MgSO_4 , 5 $\mu\text{g/mL}$ cholesterol, 250 M KH_2PO_4 pH 6.0, 17 g/L Agar, and 3 g/L NaCl. Plates were previously seeded with *E. coli OP50* strain. Nematodes were maintained using standard protocols (Brenner, 1974).

Strains

Strain NL5901, *unc-119(ed3) III; pkIs2386 [Punc-54: α -SYN:YFP; unc-119(+)]* was obtained from the *C. elegans* Genetic Center (CGC). For the α -Syn-induced DA degeneration analysis, strain UA196 (Harrington et al., 2012), gifted generously by the laboratory of Dr. Guy Caldwell (Department of Biological Science, The University of Alabama, Tuscaloosa, AL, United States), was used; [*sid-1(pk3321); baIn33 (Pdat-1:sid-1, Pmyo-2:mCherry); baIn11 (Pdat-1: α -SYN; Pdat-1:GFP)*]. In the main text, this strain was named *Pdat-1:GFP; Pdat-1: α -SYN*.

ZPD-2 Administration

After cooled, the autoclaved NGM agar medium (1 mM CaCl_2 , 1 mM MgSO_4 , 5 $\mu\text{g/mL}$ cholesterol, 250 M KH_2PO_4 pH 6.0, 17 g/L Agar, and 3 g/L NaCl) was enriched with 100 μM of a stock of ZPD-2 in 0.2% DMSO to a final concentration of 10 μM . After 2 days, plates were seeded with 250 μL of *E. coli OP50* with 10 μM of ZPD-2. Nematodes were placed on the plates at larval stages L4 and exposed either to ZPD-2 or DMSO (controls) for 7 days. Daily transfer was done to avoid cross progeny.

Aggregate Quantification

The number of cellular inclusions was quantified as previously described (van Ham et al., 2008; Munoz-Lobato et al., 2014). Briefly, NL5901 (*Punc-54: α -SYN:YFP*) worms were age-synchronized and left overnight to hatch. Nematodes in phase L1 were cultured and grown into individual NGM plates seeded with *E. coli OP50*. When animals reached L4 developmental stage, they were transferred onto either ZPD-2-treated plates or DMSO-treated plates (negative control). Every day, animals were transferred into a new plate to avoid cross contamination. At stage L4 + 7, the aggregates in the anterior part of every single animal were counted. For each experiment, 30 7-day-old nematodes per treatment were analyzed using a Nikon Eclipse E800 epifluorescence microscope equipped with an Endow GFP HYQ filter cube (Chroma Technology Corp., Bellows Falls, VT, United States) and each experiment was carried out in triplicate. Inclusions could be described as discrete bright structures, with edges

distinguishable from surrounding fluorescence. ImageJ software was used for measuring the number of cellular aggregates considering the area dimensions. For the quantification of α -syn aggregates in *C. elegans* one single image was taken from each animal. Every image contained among 30–45 stacks (1 μm) that allowed to detect aggregates at different animal positions. At least 30 animals were imaged for each assayed condition.

C. elegans Lifespan Analysis

L4-stage synchronized *C. elegans* were exposed to 10 μM of ZPD-2 or DMSO (controls) during lifespan analysis. The worms were classified as alive, dead, or censored every 2 days by determining their movement and response to nose and tail tap. The numbers of alive and dead worms were recorded until all worms perished. The data were plotted as a Kaplan–Meier survival curve and groups compared using a Wilcoxon-test.

C. elegans Neurodegeneration Assays

Worms were analyzed for α -Syn-induced DA neurodegeneration as described previously (Harrington et al., 2012). Briefly, 20–30 L4-staged animals were transferred to ZPD-2 – NGM plates and make them grow up to 7 days (L4 + 7 days of development) after which the DA cell death induced by the over-expression of α -Syn was analyzed by fluorescence. Plates containing only 0.2% DMSO, without ZPD-2, were used as control. Worms were transferred daily to avoid cross contamination.

The six anterior DA neurons (four CEP and two ADE DA neurons) were scored for neurodegeneration according to previously described criteria (Sulston et al., 1975; Harrington et al., 2012). Worms were considered normal when all six anterior DA neurons (four CEP, cephalic, and two ADE, anterior deirid) were present without any visible signs of degeneration. If a worm displayed degeneration in at least one of the six neurons, it was scored as exhibiting degeneration. For each independent experiment, 30 worms of each treatment were examined under a Nikon Eclipse E800 epifluorescence microscope equipped with an Endow GFP HYQ filter cube (Chroma Technology Corp., Bellows Falls, VT, United States).

Microscopy and Imaging

Animals were placed in a 1 mM solution of sodium azide and mounted with a coverslip on a 4% agarose pad. Animals were visualized with a Nikon Eclipse E800 epifluorescence microscope. The system acquires a series of frames at specific Z-axis position (focal plane) using a Z-axis motor device. Animals were examined at 100 \times magnification to examine α -Syn-induced DA cell death and at 40 \times to examine α -Syn apparent aggregate.

Statistical Analysis

All graphs were generated with GraphPad Prism 6.0 software (GraphPad Software Inc., La Jolla, CA, United States). Data were analyzed by two-way ANOVA Tukey's HSD test using SPSS software version 20.0 (IBM Analytics, Armonk, NY, United States) and *t*-test using GraphPad software version 6.0 (GraphPad Software Inc., La Jolla, CA, United States).

All data are shown as means and standard error of mean (SEM). $p < 0.05$ was considered statistically significant. In the graphs *, **, and *** indicate $p < 0.05$, $p < 0.01$, and $p < 0.001$, respectively.

RESULTS

ZPD-2 Reduces and Delays the Aggregation of Human α -Synuclein *in vitro*

We designed and optimized a screening protocol that allows to follow the aggregation kinetics of α -Syn by monitoring Th-T fluorescence emission for 32 h. This approach permitted us to study the inhibitory potential of more than 14,000 compounds (Pujols et al., 2017, 2018). The activity of molecules able to reduce significantly the final amount of Th-positive material and/or impact the nucleation or elongation rates of the reaction was further confirmed using light scattering and TEM measurements at the end of the reaction. This allowed us to identify 30 active compounds, most of which seem not to be connected in terms of structure, precluding QSAR studies. We have previously described the properties of SCD a molecule that acts preferentially on top of α -Syn proto-fibrillar or fibrillar assemblies (Pujols et al., 2018). Here, we describe the properties of ZPD-2 (Figure 1), a compound that differs in its mechanism of action. SCD and ZPD-2 share a benzotrifluoride group, which suggested that it could constitute the minimal inhibitory unit; however, this group is devoid of any anti-aggregation activity by itself (unpublished), indicating that, most likely, it only acts as a framework for the different active groups in the two molecules.

The incubation of 70 μ M of α -Syn in the presence and absence of 100 μ M of ZPD-2 revealed that the compound modulated the protein aggregation, reducing the formation of Th-T positive structures at the end of the reaction by an 80%, while extending t_{50} by 8 h (Figure 2A). The analysis of the kinetics revealed a reduction in the nucleation rate constant in presence of ZPD-2 ($k_b = 0.008833$) by threefold, when compared to the control reaction ($k_b = 0.02754$). The autocatalytic rate constant was also lower in the treated sample ($k_a = 0.2432 \text{ h}^{-1}$) than in the control ($k_a = 0.3230 \text{ h}^{-1}$). Light scattering measurements at 300 nm confirmed that the observed reduction in Th-T fluorescence corresponds to an effective decrease in the levels of α -Syn aggregates, with a 67% decrease in the dispersion of light in the presence of ZPD-2 (Figure 2B). TEM images corroborated that the samples incubated with ZPD-2 (Figure 2D) contained less fibrils per field than the non-treated ones (Figure 2C). In good agreement with these data, quantification of soluble α -Syn at the end of the aggregation reaction indicated that its level was threefold higher in ZPD-2-treated samples (Supplementary Figure S1A).

Further analysis of the inhibition capacity of ZPD-2 indicated that it exhibited a dose-dependent effect, displaying a statistically significant effect even at 10 μ M (1:7 compound:protein ratio) (Figure 3A), where the final Th-T signal was reduced by 49%.

To address the time window in which ZPD-2 is active, we set up aggregation reactions with a constant amount of ZPD-2 added at different time points after the reaction begins. A time-dependent response was observed (Figure 3B), with a very significant inhibition when ZPD-2 was added at early (4–8 h) and intermediate (12–16 h) times, and a less pronounced effect when it was added at the plateau phase (20–24 h). This indicates that ZPD-2 is mostly active against the species formed early in the aggregation reaction, consistent with its highest impact on the nucleation rate constant k_b . Importantly, NMR studies using isotopically labeled monomeric and soluble α -Syn indicated that ZPD-2 does not interact with its native form, since we could not detect any perturbations in chemical shifts or peak intensities in α -Syn in the presence of a molar excess of the molecule (Supplementary Figure S2).

Several α -Syn single point mutations are connected with the onset of familial cases of PD (Kruger et al., 1998; Appel-Cresswell et al., 2013). We studied the ability of ZPD-2 to prevent the aggregation of two of the most frequent and aggressive variants, H50Q and A30P. The molecule was also active against these α -Syn forms in kinetic assays (Figure 4A). According to the relative Th-T signal at the end of the reaction in ZPD-2-treated and non-treated samples, the molecule inhibited the aggregation of A30P and H50Q by 96 and 94%, respectively (Figure 4B).

ZPD-2 Prevents α -Syn Seeded Aggregation in Protein Misfolding Cyclic Amplification Assays

Protein misfolding cyclic amplification assays, initially developed to study the polymerization and propagation process of the prion protein (Barria et al., 2012; Morales et al., 2012), has been recently adapted for α -Syn amyloid aggregation (Herva et al., 2014). Essentially, cycles of incubation at 37°C are followed by vigorous sonication in order to allow fibril growth and subsequent fibrillar rupture, thus producing α -Syn seeds. These preformed seeds are used to trigger the aggregation of fresh protein in the following cycle, amplifying the fibrillar content. At 90 μ M of α -Syn, PMCA produced amyloid structures resistant to protease K (PK) digestion, as observed by SDS-PAGE, with the maximum protection arising after four rounds (Figure 5A, middle). Th-T fluorescence measurements of the same samples indicated that this protection correlates with an increasing presence of amyloid-like assemblies (Figure 5B). In sharp contrast, in the presence of ZPD-2, the amount of PK-resistant protein after four rounds is negligible (Figure 5A, right), Th-T fluorescence signal being also significantly low relative to control samples at this stage (Figure 5B). These results suggested that ZPD-2 was strongly interfering with the PMCA-promoted seeding of α -Syn amyloids. The fact that Th-T decrease becomes significant only at pass 4, likely indicates that the aggregated non PK-resistant species generated at early steps still retain certain Th-T binding ability, since SDS-PAGE analysis indicates that the levels of PK-resistant

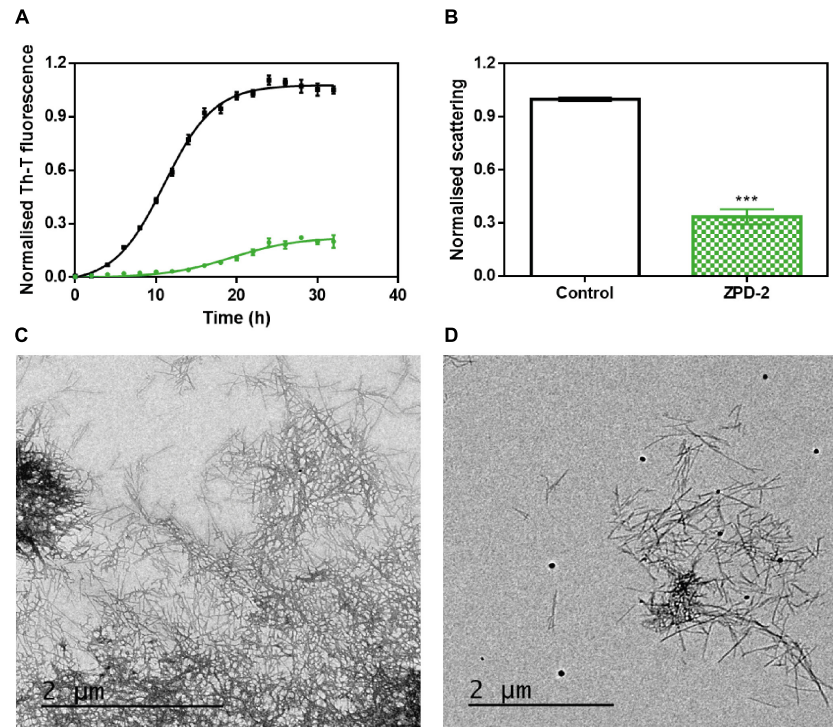


FIGURE 2 | ZPD-2 inhibits the aggregation of wild-type α -synuclein *in vitro*. **(A)** Aggregation kinetics of α -Syn in absence (black) and presence (green) of ZPD-2. Intensity of Th-T fluorescence is plotted as a function of time. **(B)** Light scattering of end-point aggregates is measured at 300 nm for untreated (white) and ZPD-2-treated samples (green). **(C,D)** Representative TEM images of untreated **(C)** and ZPD-2-treated **(D)** samples. Th-T fluorescence is expressed as normalized means. Final points were obtained at 48 h after the aggregation reaction begin. Error bars are shown as standard errors of mean values, *** $p < 0.001$.

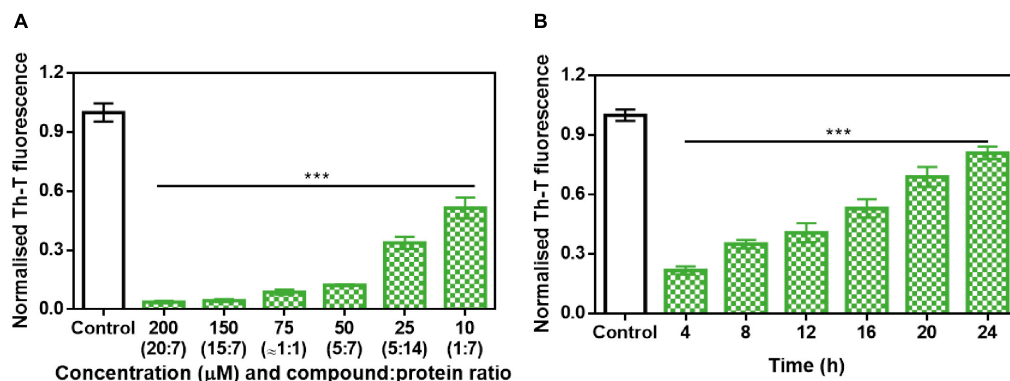


FIGURE 3 | Analysis of the inhibitory capacity of ZPD-2. **(A)** Titration of the effect of different concentrations of ZPD-2 on 70 μM α -Syn aggregation. **(B)** Th-T fluorescence of α -Syn end-point aggregates after the addition of ZPD-2 at different time points during the aggregation kinetics. Th-T fluorescence is plotted as normalized means. End-points were obtained at 48 h of α -Syn incubation. Error bars are shown as standard errors of mean values, *** $p < 0.001$.

protein is already decreased in treated samples at passes 1–3 (Supplementary Figure S3).

ZPD-2 Prevents the Aggregation of Different α -Synuclein Amyloid Conformations

The aggregation of α -Syn has been described to lead to the formation of different amyloid conformations, or strains,

depending on the environmental conditions (Li et al., 2018); a property that has been linked with its spreading in the brain and the manifestation of different synucleinopathies (Peelaerts et al., 2015). We analyzed the capacity of ZPD-2 to prevent the aggregation of α -Syn into different previously described amyloid conformations (Bousset et al., 2013; Carija et al., 2019). We refer them as strain B (buffer B, 50 mM Tris-HCl pH 7.0) and strain C (buffer C, 50 mM Tris-HCl pH 7.0 supplemented with 150 mM NaCl), to keep the original strain nomenclature. ZPD-2 was

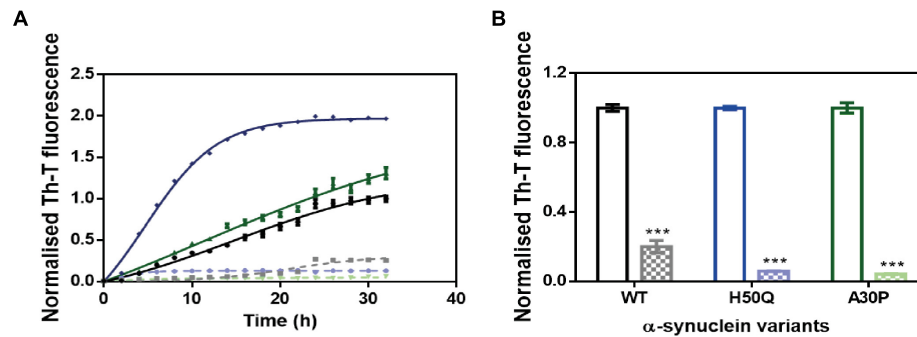


FIGURE 4 | ZPD-2 inhibits the aggregation of α -synuclein familial variants. **(A)** Aggregation kinetics of WT (black), H50Q (blue), and A30P (green) variants of α -Syn in presence (dotted) and absence (continuous) of ZPD-2, using Th-T as reporter. **(B)** End-point measurements of the aggregation of WT, H50Q, and A30P variants of α -Syn in presence (dotted) or absence (continuous) of ZPD-2 Th-T fluorescence are expressed as normalized means. Error bars are shown as standard errors of mean values.

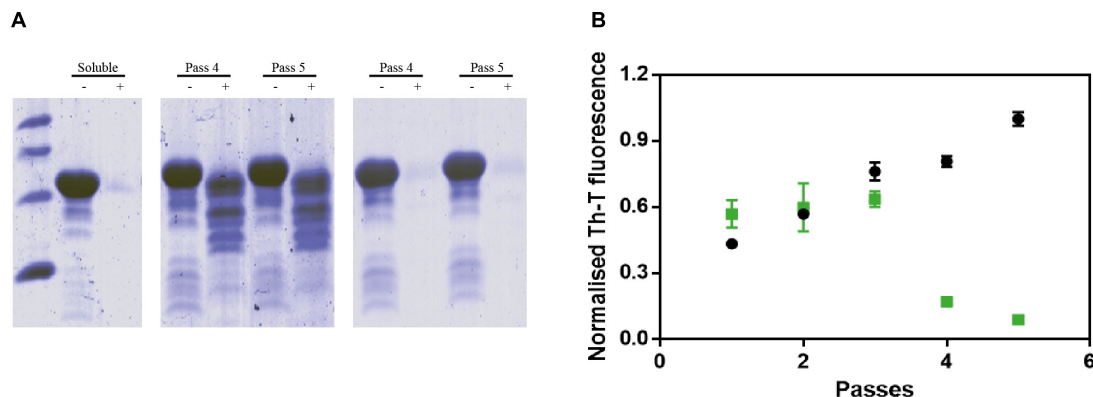


FIGURE 5 | PMCA of α -synuclein in presence of ZPD-2. **(A)** Tricine-SDS-PAGE gels of untreated (middle) and ZPD-2-treated (right) PMCA samples before (–) and after (+) being digested with proteinase K. **(B)** Th-T fluorescence of different PMCA cycles of treated (green) and untreated (black) samples. Soluble α -Syn and PMCA steps 4 and 5 are shown. Th-T fluorescence is plotted as normalized means. Error bars are shown as standard errors of mean values.

active in both cases (**Figures 6A,E**), inhibiting by up to 90% the formation of the amyloid strains B and C, as monitored by Th-T fluorescence. Light scattering measurements (**Figures 6B,F**) and TEM imaging (**Figures 6C,D,G,H**) and soluble protein quantification at the end of the reaction (**Supplementary Figure S1B**) of the different samples confirmed the inhibitory activity of ZPD-2 against the two strains. Non-fibrillar aggregates might be necessary for fibril formation (obligate), able to convert into fibrils, but not indispensable for fibril formation (on-pathway), or unable of converting directly to fibrils (off-pathway). The difference between the large reduction in Th-T fluorescence promoted by ZPD-2 in strain C aggregation kinetics and the moderate impact the molecule has in light scattering and soluble protein levels might indicate the formation of Th-T negative off-pathway aggregates in these conditions, since they do not evolve into fibrils. However, their size should be rather small, since we did not observe any large amorphous aggregate in ZPD-2-treated samples (**Figure 6H**).

We addressed whether the strong inhibitory capability of ZPD-2 at neutral pH can be overridden by the presence of preformed fibrils able to seed the aggregation reaction. The

addition of 1% (v/v) of seeds effectively accelerated the formation of both B and C strains (**Figures 7A,B**). However, the presence of ZPD-2 abrogates this effect, reducing the final amount of amyloid-like structures in seeded reactions by an 87% for strain B (**Figure 7A**) and a 90% for strain C (**Figure 7B**), according to Th-T fluorescence. Again, light dispersion measured at 300 nm revealed a significant decrease of aggregates by 57 and 70% in the case of strains B and C, respectively (**Figures 7C,D**).

ZPD-2 Reduces the Formation of α -Synuclein Inclusions in a *C. elegans* Model of PD

We assessed the toxicity of ZPD-2 for human neuroblastoma cells. No significant toxicity was observed when the molecule was added to the cell culture up to 80 μ M (**Supplementary Figure S4**). We skipped efficacy studies on neuroblastoma cells, because, with more than 20 different compounds analyzed, we could not find a straightforward connection between the potency of the molecules in cell cultures and that in our *C. elegans* models of PD. We first analyzed the effect of ZPD-2 in the *C. elegans*

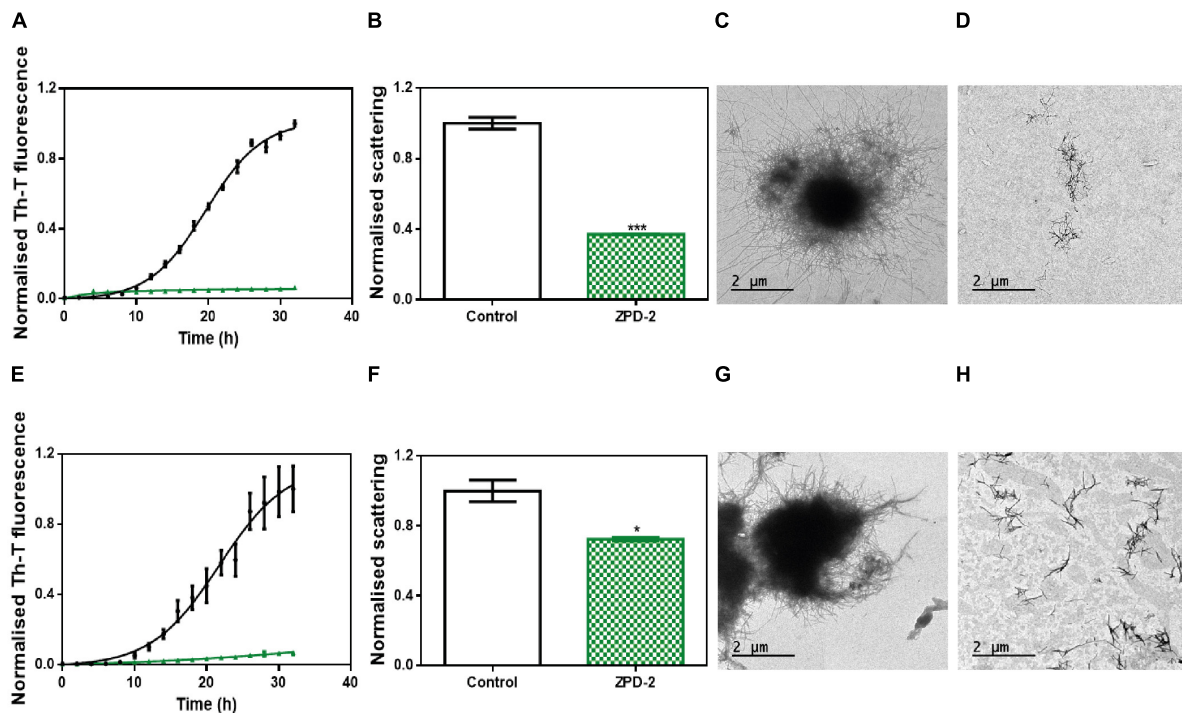


FIGURE 6 | ZPD-2 blocks the aggregation of two different α -synuclein strains. **(A,E)** Aggregation kinetics of α -Syn strains B **(A)** and C **(E)** in absence (black) and presence (green) of ZPD-2. **(B,F)** Light scattering final point measurements at 300 nm of untreated (white) and ZPD-2-treated samples (green) of strains B **(B)** and C **(F)**. **(C,D,G,H)** Representative TEM images of untreated α -Syn aggregates **(C,G)** and treated **(D,H)** samples for strains B and C, respectively. Th-T fluorescence is expressed as normalized means. Final points were obtained at 48 h after the aggregation reaction begins. Error bars are shown as standard errors of mean values, where $p < 0.05$ and $p < 0.001$ were indicated by * and ***, respectively.

strain NL5901. This strain over-expresses human α -Syn fused to the yellow fluorescent protein (YFP), under the control of the muscular *unc-54* promoter, transgene *phIs2386* (*Punc-54: α -SYN:YFP*). The expression of human α -Syn in the muscle of this nematode has been successfully used to identify modifier genes (Hamamichi et al., 2008; van Ham et al., 2008). Animals at the fourth larval stage (L4) were incubated in the presence or absence of 10 μ M ZPD-2 and analyzed at 9 days post-hatching (L4 + 7). These aged worms, which mimic aged PD patients, were then analyzed by epifluorescent microscopy and the number of visible α -Syn inclusions was quantified (**Figures 8A,B**). In these assays, ZPD-2 moderately, but significantly, reduced the number of apparent aggregates (25.7 ± 1.3) when compared to untreated worms (31.8 ± 1.7) (**Figure 8C**). In addition, worms treated with ZPD-2 showed an increase in their mean lifespan of 14.2%, relative to untreated animals (p -value = 0.015, Wilcoxon unpaired test) (**Supplementary Figure S5**).

Neuroprotective Role of ZPD-2 in a *C. elegans* Model of PD

The loss of DA neurons is one of the most important characteristics of PD and an important target in the search for a future treatment for this disorder. *C. elegans* presents a total of four pairs of DA neurons, three of them in the anterior part (CEPD, CEPV, and ADE) and one pair in the posterior part (PDE)

(Sulston et al., 1975). The existence of six anterior DA neurons has been recently used to analyze PD-related processes in a model (strain UA196) that expresses both human α -Syn and GFP under the control of the dopamine transporter promoter (*Pdat-1:GFP; Pdat-1: α -SYN*) (Kim et al., 2018). Human α -Syn expression in these DA neurons induces a progressive degeneration process (Cao et al., 2005). At 9 days post-hatching, the number of remaining functional neurons of untreated (**Figure 9A**) and ZPD-2-treated (**Figure 9B**) worms was analyzed. As an average, in control worms 48.1% of DA neurons are non-functional, whereas in treated animals this value decreases to 40.4% (p -value = 0.038, Wilcoxon unpaired test). Despite the difference between both means is rather low, the distribution of the data indicated a displacement in the DA neurons survival profile (**Figure 9C** and **Supplementary Figure S6**) in the presence of ZPD-2 when compared to the control worms. As a result, there is a significant increase in the number of worms containing more than three functional neurons in the anterior region in the presence of ZPD-2 ($51.0 \pm 4.8\%$) when compared to the controls ($29.1 \pm 3.1\%$) (**Figure 9D**).

DISCUSSION

Protein aggregation is tightly connected with neurodegenerative disorders such as Alzheimer's and PDs. Immediately after the

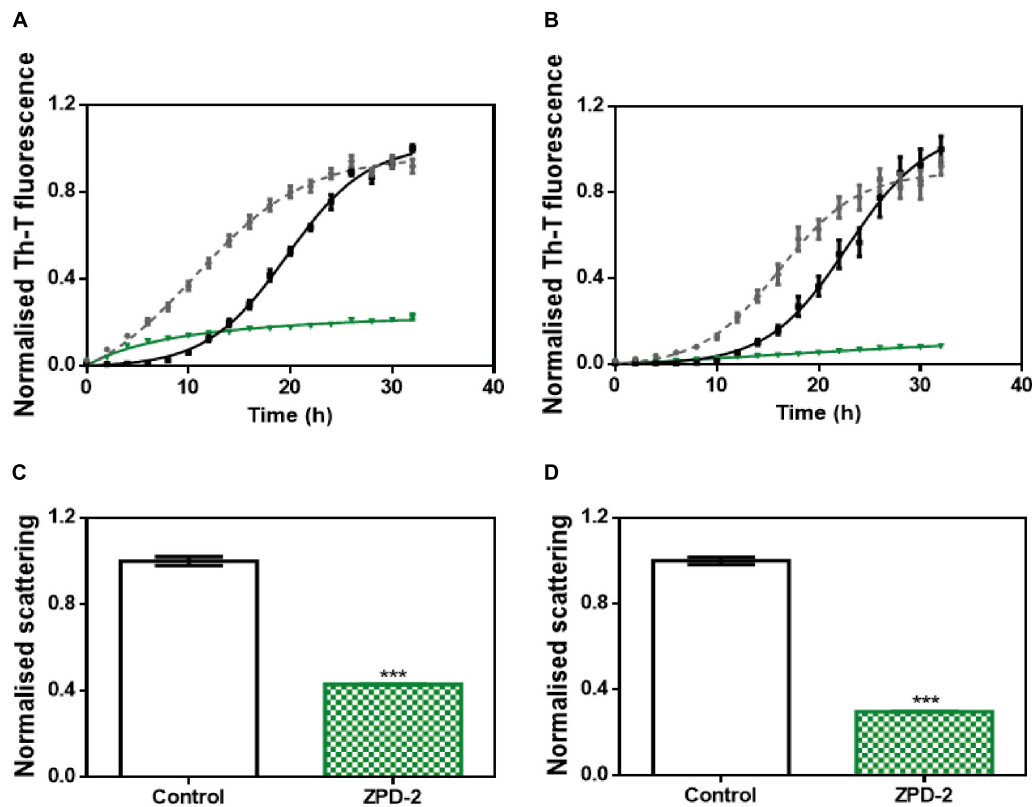


FIGURE 7 | Seeding assays with three different strains. (A,B) Aggregation kinetics of α -Syn, buffer B (50 mM Tris-HCl pH 7.0) (A), or buffer C (50 mM Tris-HCl pH 7.0 supplemented with 150 mM NaCl) (B), reported by Th-T fluorescence, in absence of compounds and seeds (black), in presence of 1% (v/v) of preformed seeds at the specific condition (gray dotted line) and in presence of seeds and 100 μ M of ZPD-2 (green). Light dispersion of treated (green) and untreated (white) seeded samples at final point of strain B (C) and strain C (D). Error bars are shown as standard errors of mean values, *** p < 0.001.

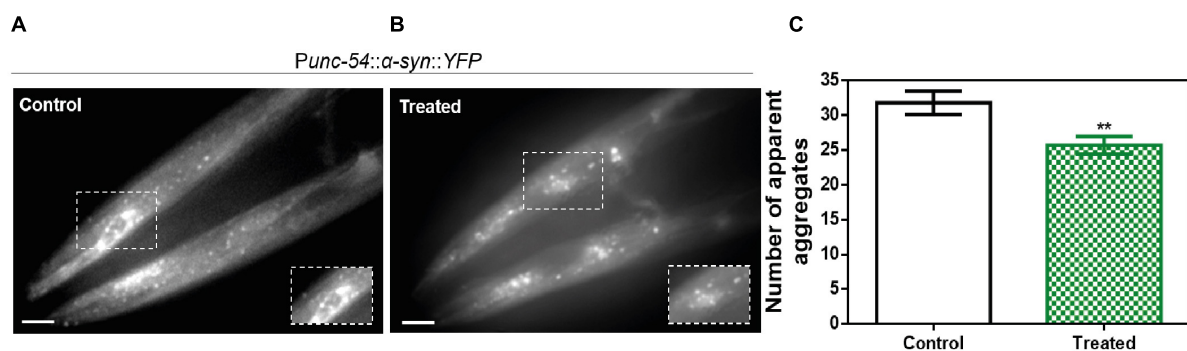


FIGURE 8 | *In vivo* anti-aggregational assays in *Caenorhabditis elegans*. Representative images of apparent α -Syn aggregates in *C. elegans* body wall muscle cells obtained by epifluorescence microscopy of NL5901 worms treated without (A) and with ZPD-2 (B). (C) Quantification of α -Syn muscle inclusions in the absence (white) and presence of ZPD-2 (green). ** p < 0.01.

identification of α -Syn as the main fibrillar component in LBs and LNs (Spillantini et al., 1997, 1998) it became evident that targeting the aggregation of this protein might hold therapeutic potential (Tatenhorst et al., 2016).

Nevertheless, the absence of a defined three-dimensional structure for the functional state of α -Syn due to its intrinsically disordered nature makes the rational design of effective inhibitors

that stabilize α -Syn and thus prevent or delay its aggregation, as it has been successfully done for globular proteins like transthyretin (Bulawa et al., 2012; Sant'Anna et al., 2016), difficult. In this scenario, evaluation of large chemical libraries appears as one of the few strategies we have to discover an effective inhibitor of α -Syn deposition and, indeed, this approach has already rendered promising molecules (Levin et al., 2014; Moree et al., 2015;

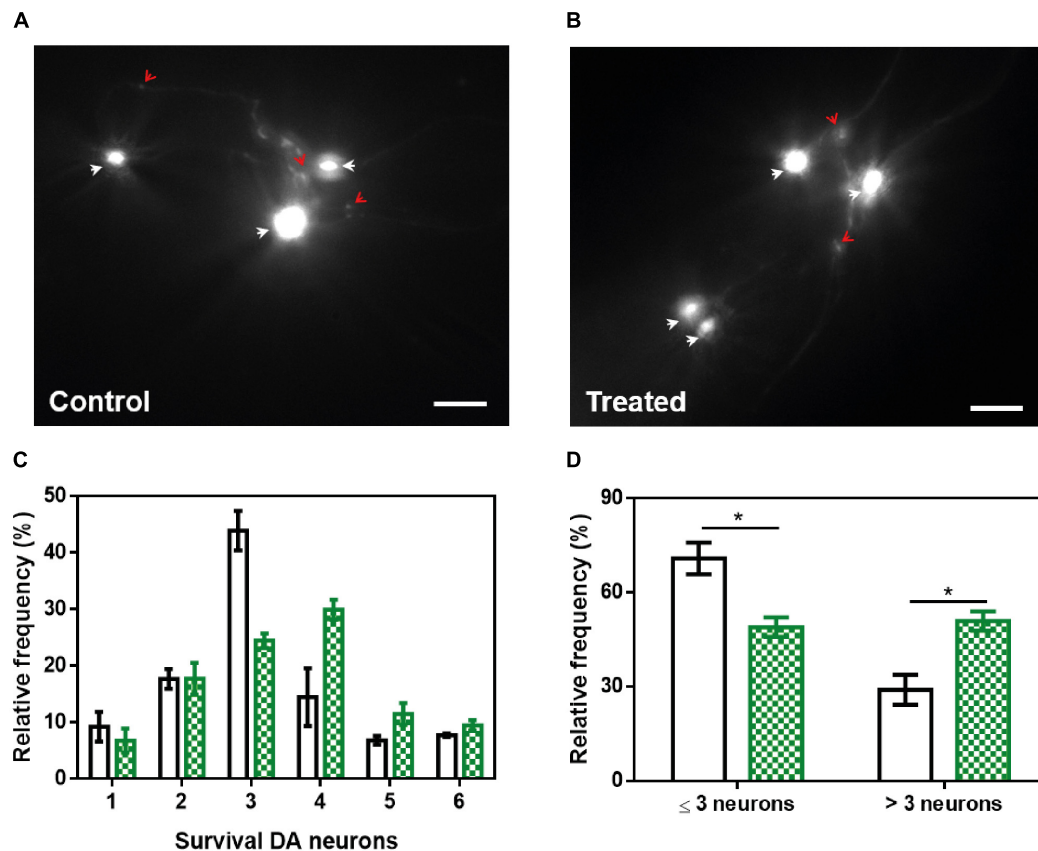


FIGURE 9 | Neuroprotective activity of ZPD-2 in a *Caenorhabditis elegans* model of PD. Representative images of GFP and α -Syn expressing anterior DA neurons in worms treated without (A) and with ZPD-2 (B) for 7 days after L4. Healthy neurons are labeled with white arrows. (C) Distribution of DA surviving neurons in the anterior region of worms. (D) Percentage of worms containing three neurons functional or less and more than three functional neurons after 7 days post-hatching. White bars indicate control samples while the green ones correspond to treated samples. * $p < 0.05$.

Tatenhorst et al., 2016; Perni et al., 2017; Pujols et al., 2018). In the present work, we describe the discovery of ZPD-2, a small molecule able to prevent up to 90% the *in vitro* aggregation of WT α -Syn and of familial mutants of the protein when used in a 0.7:1 (protein:ZPD-2) ratio, delaying also significantly the completion of the reaction. Its inhibitory capacity was confirmed by orthogonal techniques such as light scattering and TEM.

Further analysis demonstrated that ZPD-2 was able to prevent the aggregation in a concentration-dependent manner, with $\sim 50\%$ inhibition at a 7:1 protein:compound ratio. This, together with solution NMR measurements indicate that ZPD-2 does not interact significantly with soluble monomeric α -Syn, which suggests that it will not interfere with the functional state of the protein. In addition, the inhibitory potential of ZPD is time-dependent, being more significant at early (0–8 h) stages, in fair contrast with SC-D, a compound we identified in the same screening campaign, whose activity was time-independent, being able to target late species (Pujols et al., 2018). The largest affinity of ZPD-2 for early aggregating species is also inferred from the fact that it mainly impacts the nucleation constant, reducing it by threefold. This might also explain why, at a 0.7:1 ratio, the molecule works well for the A30P (96% inhibition)

and H50Q (94% inhibition) familial variants, provided that both mutations facilitate oligomerization, H50Q favoring also fibrillation (Marvian et al., 2019).

ZPD-2 is able to inhibit the aggregation of α -Syn under different solution conditions. This ability opens a possibility for its use in different synucleinopathies, where different α -Syn strains might occur (Bousset et al., 2013; Peelaerts et al., 2015). Importantly, ZPD-2 is one of a few small molecules shown to inhibit efficiently α -Syn seeded aggregation, where the lag phase of the reaction is shortened or abrogated because the soluble protein can be directly incorporated on top of the preformed fibrillar fragments. This seeding-blocking activity explains why ZPD-2 is so effective preventing the formation of PK-resistant/Th-T-positive species in PMCA assays, which promote both templated seeding and aggregates amplification. This effect might respond to the ability of the compound to either destabilize small aggregates or to prevent their elongation, a property that can be very relevant to prevent the cell-to-cell spreading of misfolded α -Syn.

ZPD-2 had not detectable toxic effect for neuronal cells at 10 μ M, a concentration at which it reduces the presence of α -Syn inclusions in a *C. elegans* model of PD expressing human α -Syn

in body wall muscle cells and extends lifespan. Not surprisingly, this anti-aggregational activity translates in reduced DA neurons degeneration in a *C. elegans* model that over-expresses human α -Syn exclusively in these cells, increasing significantly the proportion of animals that keep > 50% of their anterior part DA neurons intact.

CONCLUSION

In conclusion, ZPD-2 properties make this molecule a promising hit for the sake of developing leads able to tackle α -Syn aggregation and seeds propagation in PD and, potentially, other synucleinopathies.

DATA AVAILABILITY STATEMENT

All datasets generated for this study are included in the article/**Supplementary Material**.

AUTHOR CONTRIBUTIONS

SP-D, JP, XS, JavS, ED, and SV conceived and designed the experiments, and analyzed the results. SP-D, JP, FP, JaiS, and MC-G performed the aggregation assays. AC expressed and purified the H50Q and A30P variants. SP-D and SN performed the PMCA assays. SN performed the toxicity assays. JG and XS performed the NMR assays. SP-D and ED performed the *C. elegans* tests. SP-D, JP, and SV wrote the manuscript.

FUNDING

SV was supported by the Ministerio de Economía y Competitividad (MINECO) (BIO2016-78310-R), the ICREA (ICREA-Academia 2015) and the Fundación La Marató de TV3 (Ref. 20144330). JavS was supported by the MINECO (BFU2016-78232-P) and the Gobierno de Aragón (E45_17R). ED was supported by the Instituto de Salud Carlos III (PH613883/ERDF/ESF). JG and XS were supported by the

MINECO (BIO2015-70092-R) and the European Research Council (Contract 648201).

ACKNOWLEDGMENTS

We thank the Infraestructura Científica y Técnica Singular NMR facility at Centres Científics i Tecnològics de la Universitat de Barcelona for help with NMR, the Servei de Microscòpia at Universitat Autònoma de Barcelona for their help with TEM, and Anna Villar-Pique for help with plasmid construction. The worm strain UA196 used for neurodegeneration assays was a generous gift of Dr. Guy A. Caldwell.

SUPPLEMENTARY MATERIAL

The Supplementary Material for this article can be found online at: <https://www.frontiersin.org/articles/10.3389/fnmol.2019.00306/full#supplementary-material>

FIGURE S1 | α -Synuclein soluble fraction at the end of the aggregation. **(A)** Soluble fraction of α -Syn when incubated in absence (black) or presence (green) of ZPD-2 in PBS solution. **(B)** Soluble fraction of strains B and C at final point of the aggregation when incubated in presence (green) or absence (black) of ZPD-2.

FIGURE S2 | Lack of interaction between monomeric α -synuclein and ZPD-2 assessed by NMR. Superposition of the 1H-15N HSQC NMR spectra of 15N-labeled α -Syn (70 μ M) in absence (black) and presence (green) of 100 μ M of ZPD-2.

FIGURE S3 | PMCA assay at early stages. Tricine-SDS-PAGE gels of untreated **(middle)** and ZPD-2-treated **(right)** PMCA samples before (–) and after (+) being digested with proteinase K. Soluble α -Syn and PMCA steps 1–3 are shown.

FIGURE S4 | Toxicity assays. Analysis of neuronal cells culture survival in presence of different concentration of ZPD-2. Survival is potted as normalized means. Error bars are shown as standard error of means values, where $p < 0.001$ was indicated by ***.

FIGURE S5 | *C. elegans* lifespan analysis. Effect of ZPD-2 treatment (green) on the survival of PD model animals, in comparison with untreated PD worms (black). The data represent the survival ratio (approximately 60–80 animals per group).

FIGURE S6 | Distribution of functional neurons in the *C. elegans* dopaminergic model. Normal distribution of the remaining functional dopaminergic (DA) neurons in transgenic animals when treated with ZPD-2 (green) or vehicle (gray). The dashed line delimits animals having four or more functional DA neurons.

REFERENCES

- Appel-Cresswell, S., Vilarino-Guell, C., Encarnacion, M., Sherman, H., Yu, I., Shah, B., et al. (2013). Alpha-synuclein p.H50Q, a novel pathogenic mutation for Parkinson's disease. *Mov. Disord.* 28, 811–813. doi: 10.1002/mds.25421
- Barria, M. A., Gonzalez-Romero, D., and Soto, C. (2012). Cyclic amplification of prion protein misfolding. *Methods Mol. Biol.* 849, 199–212. doi: 10.1007/978-1-61779-551-0_14
- Bendor, J. T., Logan, T. P., and Edwards, R. H. (2013). The function of alpha-synuclein. *Neuron* 79, 1044–1066. doi: 10.1016/j.neuron.2013.09.004
- Bousset, L., Pieri, L., Ruiz-Arlandis, G., Gath, J., Jensen, P. H., Habenstein, B., et al. (2013). Structural and functional characterization of two alpha-synuclein strains. *Nat. Commun.* 4:2575. doi: 10.1038/ncomms3575
- Braak, H., Del Tredici, K., Rub, U., de Vos, R. A., Jansen Steur, E. N., and Braak, E. (2003). Staging of brain pathology related to sporadic Parkinson's disease. *Neurobiol. Aging* 24, 197–211. doi: 10.1016/s0197-4580(02)00065-9
- Brenner, S. (1974). The genetics of *Caenorhabditis elegans*. *Genetics* 77, 71–94.
- Bulawa, C. E., Connelly, S., Devit, M., Wang, L., Weigel, C., Fleming, J. A., et al. (2012). Tafamidis, a potent and selective transthyretin kinetic stabilizer that inhibits the amyloid cascade. *Proc. Natl. Acad. Sci. U.S.A.* 109, 9629–9634. doi: 10.1073/pnas.1121005109
- Cao, S., Gelwix, C. C., Caldwell, K. A., and Caldwell, G. A. (2005). Torsin-mediated protection from cellular stress in the dopaminergic neurons of *Caenorhabditis elegans*. *J. Neurosci.* 25, 3801–3812. doi: 10.1523/jneurosci.5157-04.2005
- Carija, A., Pinheiro, F., Pujols, J., Bras, I. C., Lazaro, D. F., Santambrogio, C., et al. (2019). Biasing the native alpha-synuclein conformational ensemble towards compact states abolishes aggregation and neurotoxicity. *Redox Biol.* 22:101135. doi: 10.1016/j.redox.2019.101135
- Crespo, R., Villar-Alvarez, E., Taboada, P., Rocha, F. A., Damas, A. M., and Martins, P. M. (2016). What can the kinetics of amyloid fibril formation tell about off-pathway aggregation? *J. Biol. Chem.* 291, 2018–2032. doi: 10.1074/jbc.M115.699348

- Dehay, B., Bourdenx, M., Gorry, P., Przedborski, S., Vila, M., Hunot, S., et al. (2015). Targeting alpha-synuclein for treatment of Parkinson's disease: mechanistic and therapeutic considerations. *Lancet. Neurol.* 14, 855–866. doi: 10.1016/S1474-4422(15)00006-X
- Dexter, D. T., and Jenner, P. (2013). Parkinson disease: from pathology to molecular disease mechanisms. *Free Radic. Biol. Med.* 62, 132–144. doi: 10.1016/j.freeradbiomed.2013.01.018
- Gao, J., Perera, G., Bhadbhade, M., Halliday, G. M., and Dзамко, N. (2019). Autophagy activation promotes clearance of alpha-synuclein inclusions in fibril-seeded human neural cells. *J. Biol. Chem.* 294, 14241–14256. doi: 10.1074/jbc.RA119.008733
- Hamamichi, S., Rivas, R. N., Knight, A. L., Cao, S., Caldwell, K. A., and Caldwell, G. A. (2008). Hypothesis-based RNAi screening identifies neuroprotective genes in a Parkinson's disease model. *Proc. Natl. Acad. Sci. U.S.A.* 105, 728–733. doi: 10.1073/pnas.0711018105
- Hansen, C., Angot, E., Bergstrom, A. L., Steiner, J. A., Pieri, L., Paul, G., et al. (2011). alpha-Synuclein propagates from mouse brain to grafted dopaminergic neurons and seeds aggregation in cultured human cells. *J. Clin. Invest.* 121, 715–725. doi: 10.1172/JCI43366
- Harrington, A. J., Yacoubian, T. A., Slone, S. R., Caldwell, K. A., and Caldwell, G. A. (2012). Functional analysis of VPS41-mediated neuroprotection in *Caenorhabditis elegans* and mammalian models of Parkinson's disease. *J. Neurosci.* 32, 2142–2153. doi: 10.1523/jneurosci.2606-11.2012
- Hauser, R. A. (2015). alpha-Synuclein in Parkinson's disease: getting to the core of the matter. *Lancet. Neurol.* 14, 785–786. doi: 10.1016/S1474-4422(15)00136-2
- Herva, M. E., Zibae, S., Fraser, G., Barker, R. A., Goedert, M., and Spillantini, M. G. (2014). Anti-amyloid compounds inhibit alpha-synuclein aggregation induced by protein misfolding cyclic amplification (PMCA). *J. Biol. Chem.* 289, 11897–11905. doi: 10.1074/jbc.M113.542340
- Ibanez, P., Bonnet, A. M., Debarges, B., Lohmann, E., Tison, F., Pollak, P., et al. (2004). Causal relation between alpha-synuclein gene duplication and familial Parkinson's disease. *Lancet* 364, 1169–1171. doi: 10.1016/S0140-6736(04)17104-3
- Kim, H., Calatayud, C., Guha, S., Fernandez-Carasa, I., Berkowitz, L., Carballo-Carbajal, I., et al. (2018). The small GTPase RAC1/CED-10 is essential in maintaining dopaminergic neuron function and survival against alpha-synuclein-induced toxicity. *Mol. Neurobiol.* 55, 7533–7552. doi: 10.1007/s12035-018-0881-7
- Kruger, R., Kuhn, W., Muller, T., Woitalla, D., Graeber, M., Kosel, S., et al. (1998). Ala30Pro mutation in the gene encoding alpha-synuclein in Parkinson's disease. *Nat. Genet.* 18, 106–108.
- Levin, J., Schmidt, F., Boehm, C., Prix, C., Botzel, K., Ryazanov, S., et al. (2014). The oligomer modulator anle138b inhibits disease progression in a Parkinson mouse model even with treatment started after disease onset. *Acta Neuropathol.* 127, 779–780. doi: 10.1007/s00401-014-1265-3
- Li, B., Ge, P., Murray, K. A., Sheth, P., Zhang, M., Nair, G., et al. (2018). Cryo-EM of full-length alpha-synuclein reveals fibril polymorphs with a common structural kernel. *Nat. Commun.* 9:3609. doi: 10.1038/s41467-018-05971-2
- Marti, M. J., Tolosa, E., and Campdelacreu, J. (2003). Clinical overview of the synucleinopathies. *Mov. Disord.* 18(Suppl. 6), S21–S27.
- Marvin, A. T., Koss, D. J., Aliakbari, F., Morshedi, D., and Outeiro, T. F. (2019). In vitro models of synucleinopathies: informing on molecular mechanisms and protective strategies. *J. Neurochem.* 150, 535–565. doi: 10.1111/jnc.14707
- McCormack, A. L., Mak, S. K., Henderson, J. M., Bumcrot, D., Farrer, M. J., and Di Monte, D. A. (2010). Alpha-synuclein suppression by targeted small interfering RNA in the primate substantia nigra. *PLoS One* 5:e12122. doi: 10.1371/journal.pone.0012122
- Morales, R., Duran-Aniotz, C., Diaz-Espinoza, R., Camacho, M. V., and Soto, C. (2012). Protein misfolding cyclic amplification of infectious prions. *Nat. Protoc.* 7, 1397–1409. doi: 10.1038/nprot.2012.067
- Moree, B., Yin, G., Lazaro, D. F., Munari, F., Strohaker, T., Giller, K., et al. (2015). Small molecules detected by second-harmonic generation modulate the conformation of monomeric alpha-synuclein and reduce its aggregation in cells. *J. Biol. Chem.* 290, 27582–27593. doi: 10.1074/jbc.M114.636027
- Munoz-Lobato, F., Rodriguez-Palero, M. J., Naranjo-Galindo, F. J., Shephard, F., Gaffney, C. J., Szewczyk, N. J., et al. (2014). Protective role of DJN-27/ERdj5 in *Caenorhabditis elegans* models of human neurodegenerative diseases. *Antioxid. Redox Signal.* 20, 217–235. doi: 10.1089/ars.2012.5051
- Nussbaum, R. L., and Ellis, C. E. (2003). Alzheimer's disease and Parkinson's disease. *N. Engl. J. Med.* 348, 1356–1364.
- Peelaerts, W., Bousset, L., Van der Perren, A., Moskalyuk, A., Pulizzi, R., Giugliano, M., et al. (2015). alpha-Synuclein strains cause distinct synucleinopathies after local and systemic administration. *Nature* 522, 340–344. doi: 10.1038/nature14547
- Perni, M., Galvagnion, C., Maltsev, A., Meisl, G., Muller, M. B., Challa, P. K., et al. (2017). A natural product inhibits the initiation of alpha-synuclein aggregation and suppresses its toxicity. *Proc. Natl. Acad. Sci. U.S.A.* 114, E1009–E1017.
- Polymeropoulos, M. H., Lavedan, C., Leroy, E., Ide, S. E., Dehejia, A., Dutra, A., et al. (1997). Mutation in the alpha-synuclein gene identified in families with Parkinson's disease. *Science* 276, 2045–2047. doi: 10.1126/science.276.5321.2045
- Pujols, J., Pena-Díaz, S., Conde-Gimenez, M., Pinheiro, F., Navarro, S., Sancho, J., et al. (2017). High-throughput screening methodology to identify alpha-synuclein aggregation inhibitors. *Int. J. Mol. Sci.* 18:E478. doi: 10.3390/ijms18030478
- Pujols, J., Pena-Díaz, S., Lazaro, D. F., Peccati, F., Pinheiro, F., Gonzalez, D., et al. (2018). Small molecule inhibits alpha-synuclein aggregation, disrupts amyloid fibrils, and prevents degeneration of dopaminergic neurons. *Proc. Natl. Acad. Sci. U.S.A.* 115, 10481–10486. doi: 10.1073/pnas.1804198115
- Sabate, R., Gallardo, M., and Estelrich, J. (2003). An autocatalytic reaction as a model for the kinetics of the aggregation of beta-amyloid. *Biopolymers* 71, 190–195. doi: 10.1002/bip.10441
- Sant'Anna, R., Gallego, P., Robinson, L. Z., Pereira-Henriques, A., Ferreira, N., Pinheiro, F., et al. (2016). Repositioning tolcapone as a potent inhibitor of transthyretin amyloidogenesis and associated cellular toxicity. *Nat. Commun.* 7:10787. doi: 10.1038/ncomms10787
- Serpell, L. C., Berriman, J., Jakes, R., Goedert, M., and Crowther, R. A. (2000). Fiber diffraction of synthetic alpha-synuclein filaments shows amyloid-like cross-beta conformation. *Proc. Natl. Acad. Sci. U.S.A.* 97, 4897–4902. doi: 10.1073/pnas.97.9.4897
- Silva, B., Einarsson, O., Fink, and Uversky, V. (2011). Modulating α -synuclein misfolding and fibrillation in vitro by agrochemicals. *Res. Rep. Biol.* 2, 43–56.
- Singleton, A. B., Farrer, M., Johnson, J., Singleton, A., Hague, S., Kachergus, J., et al. (2003). alpha-Synuclein locus triplication causes Parkinson's disease. *Science* 302:841. doi: 10.1126/science.1090278
- Spillantini, M. G., Crowther, R. A., Jakes, R., Cairns, N. J., Lantos, P. L., and Goedert, M. (1998). Filamentous alpha-synuclein inclusions link multiple system atrophy with Parkinson's disease and dementia with Lewy bodies. *Neurosci. Lett.* 251, 205–208. doi: 10.1016/S0304-3940(98)00504-7
- Spillantini, M. G., Schmidt, M. L., Lee, V. M., Trojanowski, J. Q., Jakes, R., and Goedert, M. (1997). Alpha-synuclein in lewy bodies. *Nature* 388, 839–840.
- Sulston, J., Dew, M., and Brenner, S. (1975). Dopaminergic neurons in the nematode *Caenorhabditis elegans*. *J. Comp. Neurol.* 163, 215–226.
- Tatenhorst, L., Eckermann, K., Dambeck, V., Fonseca-Ornelas, L., Walle, H., Lopes da Fonseca, T., et al. (2016). Fasudil attenuates aggregation of alpha-synuclein in models of Parkinson's disease. *Acta Neuropathol. Commun.* 4:39. doi: 10.1186/s40478-016-0310-y
- van Ham, T. J., Thijssen, K. L., Breitling, R., Hofstra, R. M., Plasterk, R. H., and Nollen, C. (2008). *elegans* model identifies genetic modifiers of alpha-synuclein inclusion formation during aging. *PLoS Genet.* 4:e1000027. doi: 10.1371/journal.pgen.1000027
- Winner, B., Jappelli, R., Maji, S. K., Desplats, P. A., Boyer, L., Aigner, S., et al. (2011). In vivo demonstration that alpha-synuclein oligomers are toxic. *Proc. Natl. Acad. Sci. U.S.A.* 108, 4194–4199. doi: 10.1073/pnas.1100976108
- Xue, W. F., Hellewell, A. L., Hewitt, E. W., and Radford, S. E. (2010). Fibril fragmentation in amyloid assembly and cytotoxicity: when size matters. *Prion* 4, 20–25. doi: 10.4161/pri.4.1.11378

Conflict of Interest: The authors declare that the research was conducted in the absence of any commercial or financial relationships that could be construed as a potential conflict of interest.

Copyright © 2019 Peña-Díaz, Pujols, Conde-Giménez, Čarija, Dalfo, García, Navarro, Pinheiro, Santos, Salvatella, Sancho and Ventura. This is an open-access article distributed under the terms of the Creative Commons Attribution License (CC BY). The use, distribution or reproduction in other forums is permitted, provided the original author(s) and the copyright owner(s) are credited and that the original publication in this journal is cited, in accordance with accepted academic practice. No use, distribution or reproduction is permitted which does not comply with these terms.

3.4. Chapter 4. Inhibition of α -Synuclein Aggregation and Mature Fibril Disassembling With a Minimalistic Compound, ZPDm

Published at Frontiers in Bioengineering and Biotechnology on October 2020

Available in: <https://www.frontiersin.org/articles/10.3389/fbioe.2020.588947/full>



Inhibition of α -Synuclein Aggregation and Mature Fibril Disassembling With a Minimalistic Compound, ZPDm

Samuel Peña-Díaz^{1,2†}, Jordi Pujols^{1,2†}, Francisca Pinheiro^{1,2}, Jaime Santos^{1,2}, Irantzu Pallarés^{1,2}, Susanna Navarro^{1,2}, María Conde-Gimenez³, Jesús García⁴, Xavier Salvatella^{4,5}, Esther Dalfó^{6,7}, Javier Sancho³ and Salvador Ventura^{1,2,5*}

¹ Institut de Biotecnologia i Biomedicina, Universitat Autònoma de Barcelona, Barcelona, Spain, ² Departament de Bioquímica i Biologia Molecular, Universitat Autònoma de Barcelona, Barcelona, Spain, ³ Department of Biochemistry and Molecular and Cell Biology, Institute for Biocomputation and Physics of Complex Systems (BIFI), University of Zaragoza, and Aragon Institute for Health Research (IIS Aragon), Zaragoza, Spain, ⁴ Institute for Research in Biomedicine (IRB Barcelona), The Barcelona Institute of Science and Technology, Barcelona, Spain, ⁵ ICREA, Barcelona, Spain, ⁶ Medicine, M2, Universitat Autònoma de Barcelona (UAB), Barcelona, Spain, ⁷ Faculty of Medicine, University of Vic-Central University of Catalonia (UVic-UCC), Barcelona, Spain

OPEN ACCESS

Edited by:

Jesus R. Requena,
University of Santiago
de Compostela, Spain

Reviewed by:

Eva Zerovnik,
Institut Jožef Stefan (IJS), Slovenia
Joaquín Castilla,
CIC bioGUNE, Spain

*Correspondence:

Salvador Ventura
Salvador.Ventura@uab.cat;
salvador.ventura@uab.es

[†] These authors have contributed
equally to this work

Specialty section:

This article was submitted to
Biosafety and Biosecurity,
a section of the journal
Frontiers in Bioengineering and
Biotechnology

Received: 29 July 2020

Accepted: 22 September 2020

Published: 16 October 2020

Citation:

Peña-Díaz S, Pujols J, Pinheiro F,
Santos J, Pallarés I, Navarro S,
Conde-Gimenez M, García J,
Salvatella X, Dalfó E, Sancho J and
Ventura S (2020) Inhibition
of α -Synuclein Aggregation
and Mature Fibril Disassembling With
a Minimalistic Compound, ZPDm.
Front. Bioeng. Biotechnol. 8:588947.
doi: 10.3389/fbioe.2020.588947

Synucleinopathies are a group of disorders characterized by the accumulation of α -Synuclein amyloid inclusions in the brain. Preventing α -Synuclein aggregation is challenging because of the disordered nature of the protein and the stochastic nature of fibrillogenesis, but, at the same time, it is a promising approach for therapeutic intervention in these pathologies. A high-throughput screening initiative allowed us to discover ZPDm, the smallest active molecule in a library of more than 14.000 compounds. Although the ZPDm structure is highly related to that of the previously described ZPD-2 aggregation inhibitor, we show here that their mechanisms of action are entirely different. ZPDm inhibits the aggregation of wild-type, A30P, and H50Q α -Synuclein variants *in vitro* and interferes with α -Synuclein seeded aggregation in protein misfolding cyclic amplification assays. However, ZPDm distinctive feature is its strong potency to dismantle preformed α -Synuclein amyloid fibrils. Studies in a *Caenorhabditis elegans* model of Parkinson's Disease, prove that these *in vitro* properties are translated into a significant reduction in the accumulation of α -Synuclein inclusions in ZPDm treated animals. Together with previous data, the present work illustrates how different chemical groups on top of a common molecular scaffold can result in divergent but complementary anti-amyloid activities.

Keywords: α -synuclein, protein aggregation, amyloid inhibitor, Parkinson's disease, synucleinopathies, small molecules

INTRODUCTION

Parkinson's disease (PD) is an incurable disorder that affects around 0.3% of the population and more than 1% of people over 60 years of age (4% over 80 years), being the second most prevalent neurodegenerative disease worldwide (Nussbaum and Ellis, 2003; Dexter and Jenner, 2013; Kalia and Lang, 2015). Together with Dementia with Lewy Bodies (DLB) and Multiple System Atrophy (MSA), PD is part of a group of human disorders known

as synucleinopathies (Spillantini et al., 1998a,b; Fanciulli and Wenning, 2015). Intracellular proteinaceous inclusions constitute the main culprit of neuronal damage and disease progression in the synucleinopathies, although the aggregates accumulate in different cell types and affect distinct brain regions depending on the disease (Fellner et al., 2011; Luk et al., 2012). These abnormal protein deposits are mostly composed of aggregated α -synuclein (α -Syn). In the particular case of PD, α -Syn aggregation occurs in the dopaminergic neurons of *substantia nigra pars compacta*. As a consequence, PD suffering patients display reduced dopamine levels, which results in the archetypic motor and non-motor symptoms of the disease (Spillantini et al., 1997). Indeed, single-point mutations and multiplications of the gene that encodes for α -Syn (SNCA) (Singleton et al., 2003; Ibanez et al., 2004) have been related to familial cases of PD with early-onset (Polymeropoulos et al., 1997), thus reinforcing the connection between α -Syn and PD.

α -Syn is an intrinsically disordered protein highly expressed in the brain and associated with vesicle trafficking in healthy conditions (Bendor et al., 2013). In pathological situations, α -Syn aggregates into oligomers and amyloid fibrils that compromise cellular homeostasis, exert toxicity and ultimately lead to neuronal death (Serpell et al., 2000). Remarkably, diffusible aggregated species can be internalized by healthy neighboring neurons, where they seed the aggregation of soluble α -Syn molecules, a mechanism that has been compared with the templated conformational conversion occurring in prion diseases (Hansen et al., 2011). As it occurs in prions, α -Syn assemblies can present diverse structural arrangements, forming strains (Li et al., 2018) that differ in their aggregation properties (Bousset et al., 2013), and target distinct brain regions and cell types (Lau et al., 2020).

Many of the current therapeutic approaches for PD aim to reduce the neuronal load of aggregated α -Syn, either by targeting the α -Syn polypeptide directly or through indirect approaches such as the stimulation of degradation pathways (Spencer et al., 2009; Decressac et al., 2013; Xilouri et al., 2013) and gene silencing (Faustini et al., 2018; Kantor et al., 2018; Lassot et al., 2018; Zharikov et al., 2019). Among them, the identification of small compounds that might act as chemical chaperones blocking the aggregation and propagation of α -Syn or, in the best-case scenario, dismantling α -Syn mature aggregates into non-toxic species is receiving increasing attention. However, the disordered nature of α -Syn, together with the multiplicity of conformationally different species that populate the aggregation process, imposes significant difficulties for the rational design of effective α -Syn binders. For this reason, high-throughput screening (HTS) of large chemical libraries has become a significant focus of research in the hunt for disease-modifying lead compounds (Silva et al., 2011).

To analyze the inhibitory potential of a chemical library with more than 14,000 chemically diverse structures, we optimized a robust HTS screening protocol (Pujols et al., 2017) based on Thioflavin-T (Th-T) fluorescence, light-scattering measurements and Transmission Electron Microscopy (TEM). This pipeline was used to discover and characterize small molecules that act as potent inhibitors of α -Syn amyloid formation, such as

SynuClean-D (SC-D) (Pujols et al., 2018) and ZPD-2 (Pena-Díaz et al., 2019). In the present work, we present and characterize ZPDm (Figure 1), a novel molecule identified in the primary HTS screen. ZPDm was the smallest compound in the library displaying a significant inhibitory potency at a substoichiometric concentration. ZPDm prevents the aggregation of *wild type* α -Syn and the familial A30P and H50Q variants. The molecule acts preferentially at the late stages of the polymerization reaction, suggesting that it targets preferentially ordered aggregates. Indeed, ZPDm is highly effective at disaggregating the mature α -Syn fibrils of different strains. To the best of our knowledge, it constitutes the minimal synthetic molecule that conjugates inhibitory and α -Syn fibril disrupting activity in the same chemical scaffold. These *in vitro* activities are translated into the ability to reduce significantly α -Syn aggregation in a well-established *Caenorhabditis elegans* (*C. elegans*) model of PD.

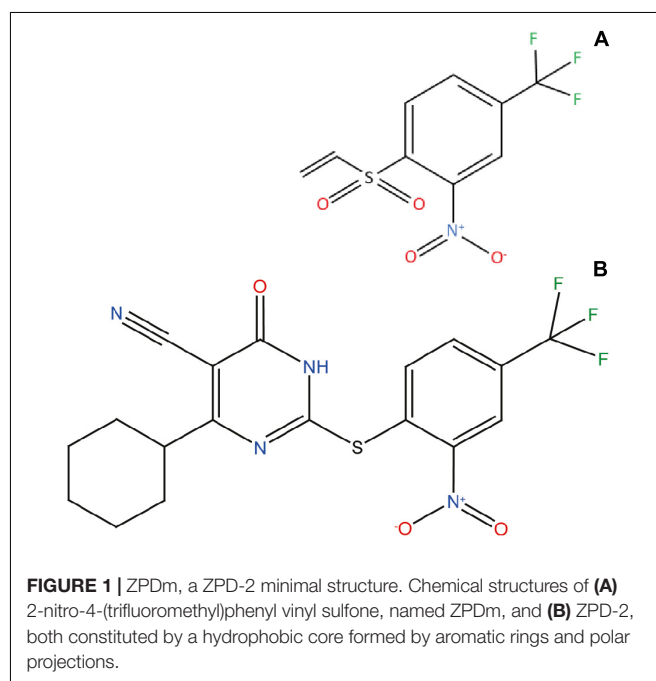
MATERIALS AND METHODS

Protein Expression and Purification

WT α -Syn and its variants (H50Q and A30P) were expressed and purified as previously described (Pujols et al., 2017); the obtained protein was lyophilized and kept at -80°C until its use.

In vitro Aggregation of α -Syn

Lyophilized α -Syn was carefully resuspended in sterile PBS 1X and filtered through $0.22\ \mu\text{m}$ membrane to discard small aggregates. Aggregation was performed at $70\ \mu\text{M}$ of α -Syn (WT, H50Q or A30P) in a sealed 96-well plate, in a total volume of $150\ \mu\text{L}$. $40\ \mu\text{M}$ Th-T in PBS 1X, a $1/8''$ diameter Teflon polyball (Polysciences Europe GmbH, Eppelheim, Germany) and $100\ \mu\text{M}$ ZPDm, (trifluoromethyl)benzene or DMSO (in control samples)



were also added to each well. The plate was incubated at 37°C and 100 rpm fixed in an orbital shaker Max-Q 4000 (Thermo Fisher Scientific, Waltham, Massachusetts, United States). Every 2 h, Th-T fluorescence was measured in a Victor3.0 Multilabel Reader (PerkinElmer, Waltham, Massachusetts, United States), exciting through a 430–450 nm filter and collecting emission signal with a 480–510 filter. Each assay was done in triplicate and the values of the kinetic fitted according to the following equation:

$$\alpha = 1 - \frac{1}{k_b(e^{k_a t} - 1) + 1} \quad (1)$$

where k_b and k_a constitute the homogeneous nucleation rate constant and the autocatalytic rate constant, respectively (Crespo et al., 2016).

ZPDm was added at different concentrations in the titration assays (200, 150, 100, 75, and 50 μ M). In time-dependent assays, 7 independent aggregation reactions were prepared simultaneously and incubated as aforementioned in a 96-well plate as triplicates. 100 μ M of ZPDm were added at different time points after the reaction had begun (4, 8, 12, 16, 20, and 24 h). In all cases α -Syn concentration was constant at 70 μ M. An equivalent volume of DMSO was added to the control sample at the beginning of the reaction.

For the study of the disaggregation assays, α -Syn 70 μ M was incubated in a 96-well plate as previously described for 2 days and Th-T fluorescence measured. Then, ZPDm was added to a final concentration of 100 μ M. The plate was incubated for an additional 24 h and Th-T fluorescence was measured.

Strains were generated as previously described (Bousset et al., 2013; Peelaerts et al., 2015; Li et al., 2018; Carija et al., 2019). Briefly, α -Syn was resuspended in PBS 1X and dialysed for 24 h in a 1:1,000 (v/v) ratio with either buffer B (50 mM Tris-HCl pH 7.0) or buffer C (50 mM Tris-HCl pH 7.0, 150 mM NaCl). Dialysed samples were filtered through 0.22 μ m membranes and incubated at 70 μ M for 2 days as described above. ZPDm was added to a final concentration of 100 μ M and plates incubated for additional 24 h. Then, Th-T fluorescence was measured.

Light-Scattering

80 μ L of end-point aggregates were collected, placed into a quartz cuvette and analyzed in a Cary Eclipse Fluorescence Spectrophotometer (Agilent, Santa Clara, CA, United States) by exciting at 300 and 340 nm and 90° collecting between 280 and 360 nm.

Transmission Electron Microscopy (TEM)

End-point α -Syn aggregates were collected and Diluted 1/10 (v/v) in PBS 1X. Diluted samples were gently sonicated for 5 min and 5 μ L of the resultant sample were placed on a carbon-coated copper grid for 5 min. Using a filter paper, the grids were dried to remove the excess of sample and washed twice with miliQ water. Finally, 5 μ L of 2% (w/v) uranyl acetate were added and left incubate for 2 min. As previously indicated, the excess of uranyl acetate was removed, and grids were left to air-dry for 10 min. Images were obtained using a Transmission Electron Microscopy Jeol 1400

(Peabody, MA, United States) operating at an accelerating voltage of 120 kV. A minimum of 30 fields were screened per sample, in order to collect representative images.

Protein Misfolding Cyclic Amplification (PMCA)

PMCA protocol was performed as previously described (Herva et al., 2014). Briefly, α -Syn was resuspended in Conversion Buffer (PBS 1X, 1% Triton X-100, 150 mM NaCl) to a final concentration of 90 μ M and supplemented with Complete Protease Inhibitor Mixture (Roche Applied Science, Penzberg, Germany). 60 μ L of this solution were loaded into 200 μ L PCR tubes containing 1.0 mm silica beads (Biospec Products, Bartlesville, OK, United States). α -Syn was then exposed to 24 h cycles of 30 s sonication and 30 min of incubation at 37°C, using a Misonix 4000 sonicator, at 70% power. The incubated sample was recovered after each 24 h cycle and 1 μ L was added to a new PCR tube containing fresh α -Syn at 90 μ M. In the case of ZPDm treated samples, the compound was added to the fresh sample in each step to a final concentration of 128 μ M, which corresponds to the 0.7:1 α -Syn:ZPDm ratio of the previous aggregation assays. Untreated samples were prepared adding the same concentration of DMSO (0.26%) present in the treated mixtures. This process was repeated for 5 days. All the reactions were made in triplicate.

Ten microliter of aggregated samples at the end of each cycle were diluted 1:10 with 90 μ L of PBS 1X, 40 μ M Th-T. Th-T fluorescence emission was measured in a Cary Eclipse Fluorescence Spectrophotometer (Agilent, Santa Clara, CA, United States), by exciting the samples at 445 nm and collecting the emission signal between 460 and 600 nm.

Proteinase K Digestion

18 μ L of PMCA-aggregated α -Syn were incubated with 6 μ L of Proteinase K (5 μ g/mL as final concentration) for 30 min at 37°C. Then, 8 μ L of loading buffer containing 1% β -mercaptoethanol was added and the sample was incubated 10 min at 95°C for PK inactivation. Finally, 7 μ L of the samples were loaded into a Tricine-SDS-PAGE gel. Unstained Protein Standard markers (Thermo Fisher Scientific, Waltham, MA, United States) were used as a reference. Gels were stained with Blue safe.

Nuclear Magnetic Resonance (NMR)

¹⁵N-labeled human WT α -Syn was expressed in *E. coli* BL21 DE3 strains. Cells were grown in LB medium until the optical density (OD) at 600 nm reached a level of 0.6. Cultures were then centrifuged at 3,000 rpm for 15 min and the obtained pellets resuspended in 1 L of minimal medium: 768 mL of miliQ water with 1 mL of ampicillin 100 mg/mL, 100 μ L CaCl₂ 1M, 2 mL MgSO₄ 2 M, 20 mL glucose 20%, 10 mL vitamins 100x (Sigma-Aldrich, Darmstadt, Germany), 200 mL salts M9 and 1 g ¹⁵NH₄ (Cambridge Isotope Laboratories, Inc., Tewksbury, MA, United States). Cells were incubated for 1 h at 250 rpm and 37°C. Finally, 1 mM IPTG was added to induce protein expression for 4 h. Protein was purified as previously described (Pujols et al., 2017).

Caenorhabditis Elegans Assays

Maintenance

Animals synchronization was carried out by bleaching and overnight hatching in M9 (3 g/L KH_2PO_4 , 6 g/L Na_2HPO_4 , 5 g/L NaCl, 1 M MgSO_4) buffer. Thus, nematodes were cultured at 20°C on growth media plates (NGM) containing 1 mM CaCl_2 , 1 mM MgSO_4 , 5 $\mu\text{g/mL}$ cholesterol, 250 M KH_2PO_4 pH 6.0, 17 g/L Agar, 3 g/L NaCl. Plates were previously seeded with *E. coli* OP50 strain. Nematodes were maintained using standard protocols (Brenner, 1974).

Strains

Strain NL5901, *unc-119(ed3) III; pkIs2386 [Punc-54:: α -SYN::YFP; unc-119(+)]* was obtained from the *C. elegans* Genetic Center (CGC). For the α -Syn induced dopaminergic degeneration analysis, strain UA196 (Harrington et al., 2012), gifted generously by the laboratory of Dr. Guy Caldwell (Department of Biological Science, The University of Alabama, Tuscaloosa, United States), was used; [*sid-1(pk3321); baln33 [Pdat-1::sid-1, Pmyo-2::mCherry]; baln11 [Pdat-1:: α -SYN; Pdat-1::GFP]*]. In the main text, this strain was named *Pdat-1::GFP; Pdat-1:: α -SYN*.

ZPDm Administration

After cooling, the autoclaved NGM agar medium (1 mM CaCl_2 , 1 mM MgSO_4 , 5 $\mu\text{g/mL}$ cholesterol, 250 M KH_2PO_4 pH 6.0, 17 g/L Agar, 3 g/L NaCl) was enriched with 100 μM of a stock solution of 4 mM ZPDm in 0.2% DMSO to a final concentration of 10 μM . After 2 days, plates were seeded with 250 μL of *E. coli* OP50 with 10 μM of ZPDm. Nematodes were placed on the plates at larval stages L4 and exposed either to ZPDm or DMSO (controls) for 7 days. Daily transfer was done to avoid cross progeny.

Aggregate Quantification

The number of cellular inclusions was quantified as previously described (van Ham et al., 2008; Munoz-Lobato et al., 2014). Briefly, NL5901 (*Punc-54:: α -SYN::YFP*) worms were age-synchronized and left overnight to hatch. Nematodes in phase L1 were cultured and grown into individual NGM plates seeded with *E. coli* OP50. When animals reached L4 developmental stage, they were transferred onto either ZPDm treated plates or DMSO treated plates (negative control). Every day, animals were transferred into a new plate to avoid cross contamination. At stage L4+7, the aggregates in the anterior part of every single animal were counted. For each experiment, thirty 7-days old nematodes per treatment were analyzed using a Nikon Eclipse E800 epifluorescence microscope equipped with an Endow GFP HYQ filter cube (Chroma Technology Corp., Bellows Falls, Vermont United States) and each experiment was carried out in triplicate. Inclusions could be described as discrete bright structures, with edges distinguishable from surrounding fluorescence. ImageJ software was used for measuring the number of cellular aggregates considering the area dimensions. For the quantification of α -syn aggregates in *C. elegans* one single image was taken from each animal. However, every image contained among 30–45 stacks (1 μm) that allowed to detect aggregates that are at different positions.

Microscopy and Imaging

Animals were placed in a 1 mM solution of sodium azide and mounted with a coverslip on a 4% agarose pad. Animals were visualized with a Nikon Eclipse E800 epifluorescence microscope. The system acquires a series of frames at specific Z-axis position (focal plane) using a Z-axis motor device. Animals were examined at 100 \times magnification to examine α -Syn induced DA cell death and at 40 \times to examine α -Syn apparent aggregate.

Statistical Analysis

All graphs were generated with GraphPad Prism 6.0 software (GraphPad Software Inc., La Jolla, CA, United States). Data were analyzed by two-way ANOVA Tukey test using SPSS software version 20.0 (IBM Analytics, Armonk, NY, United States) and *t*-test using GraphPad software version 6.0 (GraphPad Software Inc., La Jolla, CA, United States). All data are shown as means and standard error of mean (SEM). $P < 0.05$ was considered statistically significant. In the graphs *, **, and *** indicate $p < 0.05$, $p < 0.01$, and $p < 0.001$, respectively.

RESULTS

ZPDm Inhibits α -Synuclein Aggregation *in vitro*

ZPDm is a molecule that was initially identified as a positive hit in the HTS performed by our lab back in 2017 on top of the HitFinderTM chemical library from Maybridge (Pujols et al., 2017). Although they were found independently, structurally, ZPDm is a minimalistic version of ZPD-2 (Pena-Díaz et al., 2019) with a reduced MW, LogP, and TPSA, which, in principle, would increase its drug-likeness (Figure 1 and Table 1). Still, ZPDm implements the generic physicochemical properties common to most of the published inhibitors of α -Syn aggregation, namely, a planar hydrophobic core formed by aromatic rings that interact with apolar exposed regions in α -syn assemblies. This core is frequently coated with polar projections that interfere with hydrophobic packing and disrupt intermolecular hydrogen

TABLE 1 | SwissADME predicted properties of ZPDm and ZPD-2.

	ZPDm	ZPD-2
Molecular weight (g/mol)	281.21	424.4
Heavy atoms	18	29
Aromatic heavy atoms	6	12
H-bond acceptors	7	8
H-bond donors	0	1
TPSA (\AA^2)	88.34	140.66
Log $P_{O/W}$	2.42	3.9
Solubility (mg/mL)	9.28E-02	1.94E-03
GI absorption	High	Low
Drug-like (Lipinski)	0 violations	0 violations
Drug-like (Veber)	0 violations	1 violations
Drug-like (Egan)	0 violations	2 violations
Leadlikeness	0 violations	2 violations

bonds; they difficult elongation and, eventually, might promote fibril disassembly (Pujols et al., 2020). A benzene ring constitutes the hydrophobic moiety of ZPDm, connected to three polar groups—vinyl sulfone, nitro, and trifluoromethyl—in carbon positions 1, 2, and 4, respectively. Remarkably, the ZPD-2 chemical structure displays the same functional groups in carbons 1, 2, and 4 of the primary phenyl ring. However, the vinyl sulfone is substituted by a sulfide group that extends the molecule to incorporate additional aromatic moieties, which we previously assumed to be critical for its activity (Pena-Díaz et al., 2020). Thus, ZPDm can be considered as a building block for

the synthesis of the more complex ZPD-2 molecule. Considering these structural differences, we performed a set of orthogonal experiments to contrast if, as ZPD-2, ZPDm might turn to be a lead compound with significant α -Syn anti-aggregational activity.

The incubation of 70 μ M α -Syn with 100 μ M ZPDm inhibited the protein aggregation, decreasing the final Th-T fluorescence signal by 60% compared to control untreated samples (Figure 2A). Fitting of the kinetic data to a typical sigmoidal nucleation-polymerization reaction revealed that ZPDm diminishes the primary nucleation rate constant by eightfold ($k_b = 0.0034$), relative to the control reaction

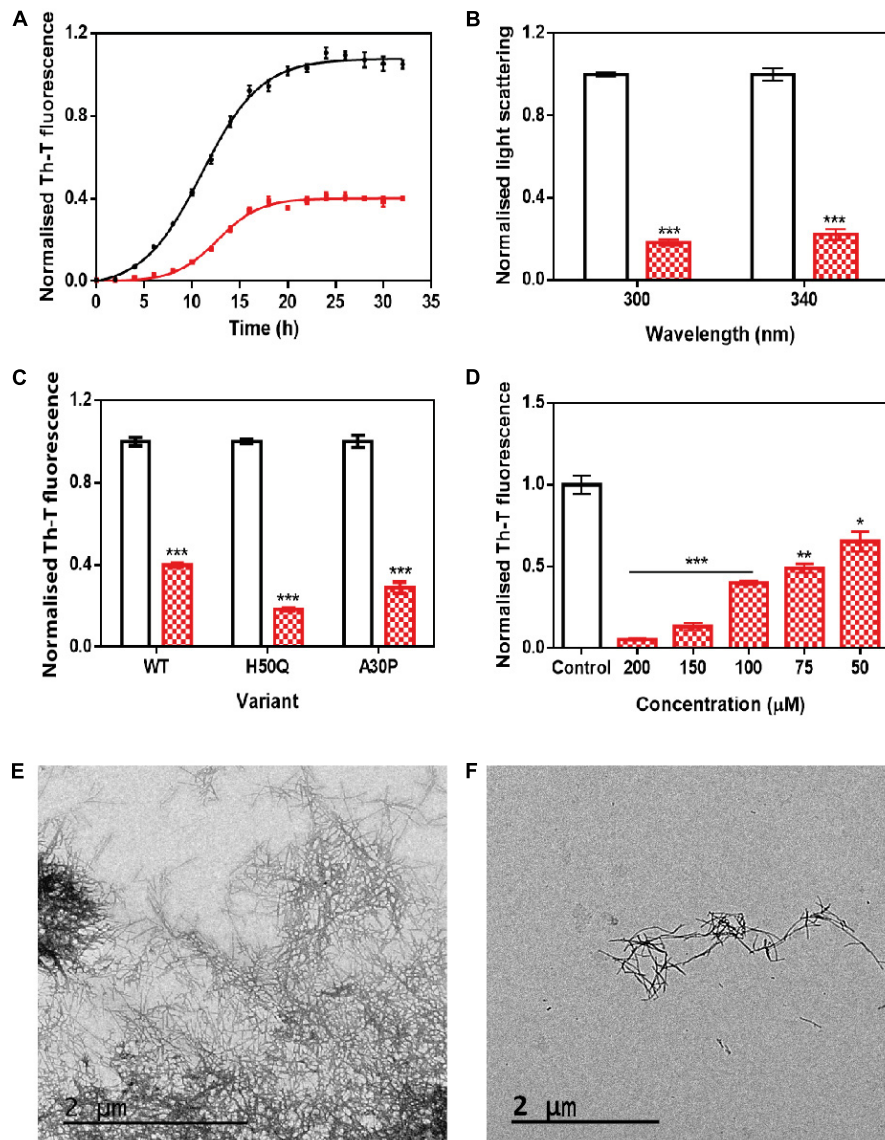


FIGURE 2 | *In vitro* analysis of the capacity of ZPDm to inhibit α -Syn aggregation. **(A)** α -Syn aggregation kinetics in the absence (black) and presence (red) of 100 μ M of ZPDm followed by Th-T fluorescence. **(B)** Light-scattering measurements at 300 and 340 nm, in the absence (white) and presence (red) of ZPDm. **(C)** H50Q and A30P α -Syn variants aggregation in the absence (white) and presence (blue) of ZPDm. **(D)** Inhibition of α -Syn aggregation with different concentrations of ZPDm. **(E,F)** Representative TEM images in the absence **(E)** and presence **(F)** of ZPDm. Th-T fluorescence is plotted as normalized means. Final points were obtained at 48 h. Error bars are represented as SE of mean values; * $p < 0.05$, ** $p < 0.01$, and *** $p < 0.001$. ZPDm prevents the aggregation of WT, A30P, and H50Q α -Syn variants *in vitro*, even at substoichiometric ratios.

($k_b = 0.0275$), at the expenses of a slightly higher autocatalytic rate constant, with k_a of 0.449 and 0.323 h^{-1} for ZPDm treated and untreated samples, respectively. This results in t_0 and $t_{1/2}$ being increased by 4 and 2 h, respectively, in the compound's presence. Light-scattering measurements at 300 and 340 nm at the end of the reaction reported a decrease of 81 and 78% in the dispersed light (**Figure 2B**) in the presence of ZPDm, respectively, consistent with a reduction of the total aggregated material. The visual inspection of α -Syn samples by TEM corroborated a reduction in the number of amyloid fibrils per field in the presence of ZPDm (**Figure 2F**), compared to untreated samples (**Figure 2E**). A titration assay in which we incubated 70 μM α -Syn in the presence of decreasing amounts of ZPDm indicated a dose-dependent inhibition, with a statistically significant activity at a substoichiometric concentration of 50 μM , at which ZPDm still reduces the Th-T signal at the end of the reaction by 35% (**Figure 2D**).

We further examined if ZPDm was able to prevent the aggregation of two mutants of α -Syn, H50Q, and A30P, which have been associated with familial PD (Kruger et al., 1998; Appel-Cresswell et al., 2013). The incubation of these α -Syn variants with ZPDm reduced Th-T fluorescence at the end of the reaction by 81 and 71% for H50Q and A30P, respectively (**Figure 2C**).

ZPDm, ZPD-2, and SC-D and other positive hits in the library, share a common property, the presence of a trifluoromethyl group connected to an aromatic ring. We hypothesized that perhaps we were in front of the minimal inhibitory unit, which might be very useful for future Structure Activity Relationship (SAR) studies. Therefore, we synthesized the (trifluoromethyl)benzene moiety and assessed its anti-aggregational potential (**Supplementary Figure S1**). Both kinetic data using Th-T and light scattering measurements converged to indicate that this molecule is devoid of any activity, suggesting that it might be necessary, but not sufficient to endorse ZPDm with the above-described anti-aggregation properties.

ZPDm Prevents α -Syn Aggregation in Protein Misfolding Cyclic Amplification Assays

We used protein-misfolding cyclic amplification (PMCA) to test the inhibitory capacity of ZPDm under continuous seeding conditions. Based on the nucleation-dependent polymerization model for prion replication, PMCA is a technique that forces aggregation to happen by seeding soluble α -Syn with preformed fibrils (Jung et al., 2017). After the first round of fibril elongation, aggregates are sonicated and used as seeds for the second cycle of PMCA. A representative sample from each cycle is then treated with proteinase K (PK) and analyzed by SDS-PAGE, to evidence fibril formation, since in contrast to soluble α -Syn, the fibrils are significantly resistant to proteolysis. Using this protocol, PK-resistant species could be observed already in the 1st cycle of PMCA in untreated samples, with a maximum of PK resistance at the 4th cycle (**Figure 3A**). Th-T fluorescence measurements of the same samples indicated that this protection correlates with the presence of amyloid-like assemblies (**Figure 3C**). In contrast, in the presence of ZPDm, PK-resistant species are

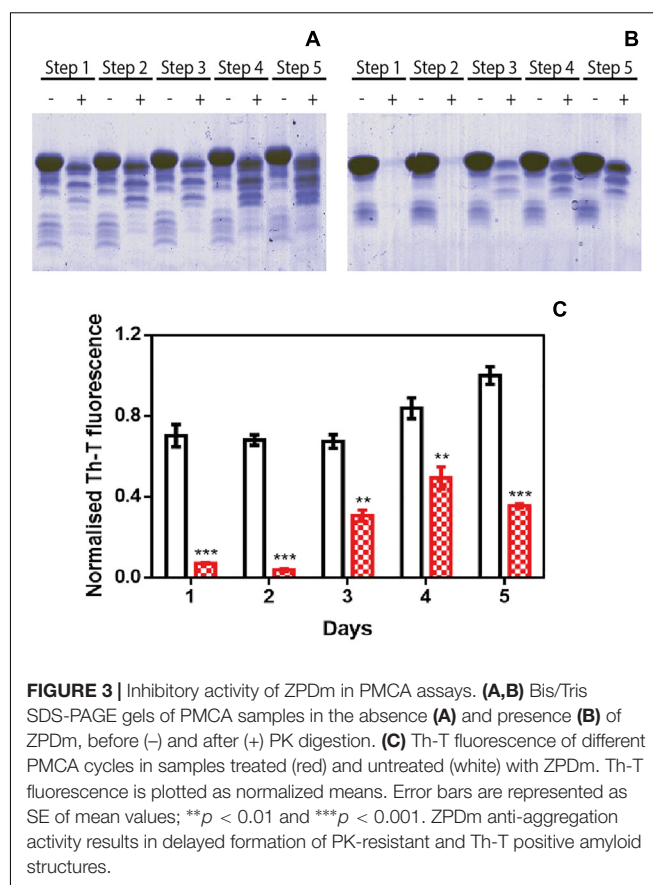


FIGURE 3 | Inhibitory activity of ZPDm in PMCA assays. **(A,B)** Bis/Tris SDS-PAGE gels of PMCA samples in the absence **(A)** and presence **(B)** of ZPDm, before (–) and after (+) PK digestion. **(C)** Th-T fluorescence of different PMCA cycles in samples treated (red) and untreated (white) with ZPDm. Th-T fluorescence is plotted as normalized means. Error bars are represented as SE of mean values; ** $p < 0.01$ and *** $p < 0.001$. ZPDm anti-aggregation activity results in delayed formation of PK-resistant and Th-T positive amyloid structures.

absent until the 3rd cycle, and they never reach the levels of the control samples, although certain adaptation of misfolded α -Syn to ZPDm seems to occur in cycles 4th and 5th (**Figure 3B**). The Th-T fluorescence signal is negligible in the two first PMCA cycles and significantly lower than that of control samples at any considered cycle (**Figure 3C**).

ZPDm Exhibits Amyloid Disaggregation Activity *in vitro*

ZPD-2 does not interact with soluble and monomeric α -Syn and, therefore, is not expected to interfere with the protein's functional state. Nuclear Magnetic Resonance ^1H - ^{15}N HSQC spectra of N^{15} labeled α -Syn in the presence and absence of ZPDm, indicates that this is also the case for this smaller molecule since we could not identify any perturbations in chemical shifts or peak intensities in the spectra (**Supplementary Figure S2**).

To address the time window in which ZPDm remains active, we set up an experiment in which a constant amount of ZPDm was added to different aggregation reactions at different time intervals after the reaction has begun (**Figure 4A**). To our surprise, the respective Th-T signals indicated that the anti-amyloid activity increased as the reaction progressed, which is in stark contrast with the behavior of ZPD-2, which was mostly active when added at the early stages of the reaction and inactive when added at the plateau phase (Pena-Díaz et al., 2019). The time-dependent activity profile of ZPDm can only be explained

if this compound recognizes the Th-T positive aggregated species and exerts an intense fibril disruption activity. To confirm this extent, α -Syn mature fibrils were incubated for 24 h with ZPDm. The Th-T fluorescence analysis revealed that treated samples suffered a signal reduction of 74% (**Figure 4B**). This data was supported by TEM images, which illustrated the disruption of large fibrillar clusters into shorter fibrils or amorphous aggregates (**Figures 4C,D**).

We assessed if this amyloid-disrupting activity was independent of the conformational properties of the mature fibrils, by aggregating α -Syn in 50 mM Tris-HCl pH 7.0 in the absence or presence of 150 mM NaCl, which generates two different strains, known as strain B and C, respectively (Bousset et al., 2013; Carija et al., 2019). As shown in **Figure 4**, the addition of ZPDm to the mature fibrils of these strains promoted a significant decrease in the amount of amyloid-like material as monitored both by Th-T fluorescence and TEM 24 h after the addition of the molecule (**Figure 5**). These data suggest that in contrast to ZPD-2, insensitive to preformed amyloid fibrils, ZPDm is endorsed with a generic and potent disaggregation activity.

ZPDm Decreases the Formation of α -Syn Aggregates in a *C. elegans* Model of PD

We decided to test if the ZPDm *in vitro* activity can be translated *in vivo* to a simple animal model of PD. To do so, we employed the well-described strain NL5901 of *C. elegans*. In this strain, α -Syn is fused to Yellow Fluorescence Protein (YFP) and expressed under the control of the *unc-54* promoter, transgene *pkIs2386 [Punc-54:: α -SYN::YFP]* (Hamamichi et al., 2008; van Ham et al., 2008), generating protein inclusions in body wall muscle cells. ZPDm was administered in the food at 10 μ M final concentration to animals at the L4 stage, and they were examined 7 days later, 9 days after hatching (L4+7). These aged worms are intended to mimic aged PD patients. We used epifluorescence microscopy to visualize the fluorescent aggregates. The images demonstrated that ZPDm reduced the formation of muscular inclusions by 43% (**Figure 6A**), with an average of 20.2 ± 2.13 apparent α -Syn aggregates in treated worms (**Figure 6C**) compared with the 35.2 ± 3.04 observed in control samples (**Figure 6B**).

DISCUSSION

The identification of small compounds that may abrogate the process of protein aggregation in neurodegenerative disorders is attracting increasing interest, both in academia and industry (Pujols et al., 2020).

The lack of structural information about the intermediate species that populate the reaction, and the intrinsically disordered nature of many of the proteins behind these diseases, has made it challenging to use of structure-guided drug design for amyloid inhibitors. Only recently, the high-resolution structures of the fibrils formed by proteins connected to different amyloidosis have allowed the rational design of peptides that interfere with the growth or seeding of the fibrils (Seidler et al., 2018; Saelices et al., 2019; Sangwan et al., 2020). However, because peptides usually

display poor pharmacokinetics, which should be significantly optimized before they become drugs, small molecules are still the preferred option for the treatment of the diseases caused by the aggregation of proteins within the brain.

The screening of large chemical libraries in the search for α -Syn aggregation inhibitors has provided potent molecules like anle138b (Wagner et al., 2013), BIOD303 (Moree et al., 2015), SynuClean-D (Pujols et al., 2018), 582032 (Toth et al., 2019) or the collection of compounds recently reported by Kurnik et al. (2018). All these molecules display two or more aromatic rings in their structures, a property that is shared by active polyphenols like curcumin (Pandey et al., 2008), EGCG (Bieschke et al., 2010), and baicalein (Jiang et al., 2010), repurposed inhibitors like Fasudil (Tatenhorst et al., 2016), and LMTM (Schwab et al., 2017) or compounds generated by rational design like NPT100-18A (Wrasidlo et al., 2016). Usually, the aromatic rings form a planar hydrophobic core that is thought to interact with apolar exposed regions in α -Syn or its assemblies. However, despite the presence of multiple aromatic groups is recurrent in natural α -Syn aggregation inhibitors and many of the reported screening efforts result in the identification of this kind of molecules, several natural compounds exhibiting a single aromatic ring have been shown to act as α -Syn aggregation modulators (**Supplementary Figure S3**), including scyllo-inositol, gallic acid, dopamine, safranal and caffeic acid (Herrera et al., 2008; Di Giovanni et al., 2010; Liu et al., 2014; Ibrahim and McLaurin, 2016; Save et al., 2019).

We recently used a robust high-throughput screening pipeline to uncover molecules able to modulate α -Syn fibrillation (Pujols et al., 2017). Among the active compounds, we searched for a small compound bearing a single aromatic ring. We identified ZPDm, which, interestingly enough, is a minimal version of ZPD-2, a potent inhibitor identified in the same library (Peña-Díaz et al., 2019), with half of its heavy aromatic atoms. This opened an opportunity to approach a comparative SAR for these molecules.

ZPDm reduces the *in vitro* aggregation of WT α -Syn and the protein's A30P and H50Q familial variants in a 60%, or higher, at a 0.7:1 (protein: ZPDm) ratio. This activity was orthogonally confirmed by light-scattering and TEM. Moreover, the inhibitory activity of ZPDm reduced the number of PK-resistant and Th-T positive species in PMCA assays, thus interfering with α -Syn templated seeding and/or aggregates amplification (Herva et al., 2014). It should be explored whether adaptation of α -Syn to ZPDm at late PMCA stages might translate in some resistance to the molecule during aggregates propagation.

Solution NMR measurements indicated that ZPDm was not interacting with soluble α -Syn monomers, and, therefore, it is not expected to impact the physiological function of the protein. Moreover, the addition of ZPDm at different time points of the aggregation reaction suggested that ZPDm is mainly active at the latest stages of the aggregation and indeed, further analysis demonstrated that the molecule is capable of disassembling mature α -Syn amyloid fibrils generated under different solution conditions, conceptually similar to the α -Syn strains observed in different synucleinopathies (Bousset et al., 2013; Peelaerts et al., 2015). Importantly, these features translate into a significant reduction in the number of

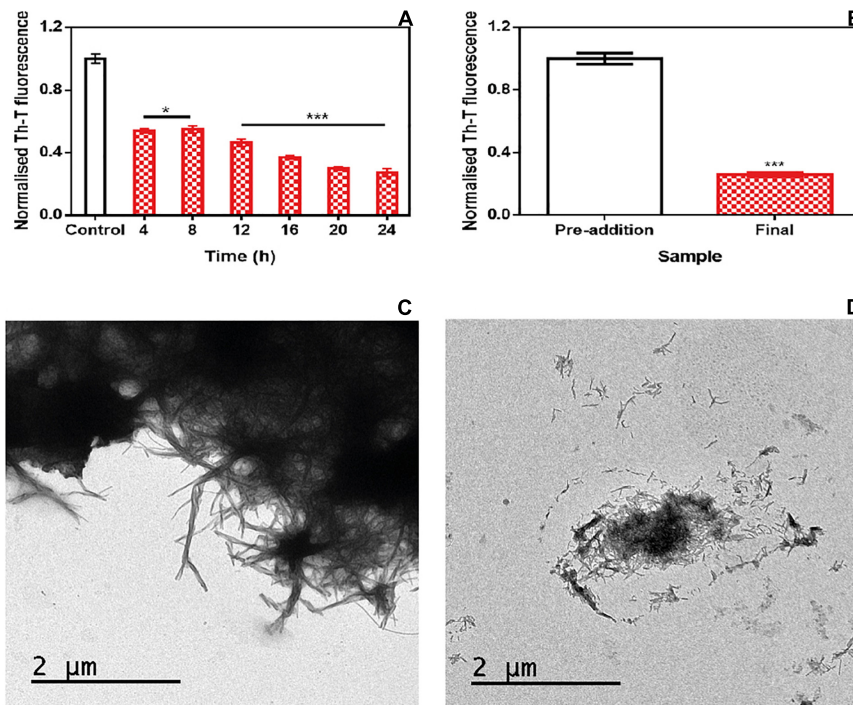


FIGURE 4 | Disaggregational activity of ZPDm. **(A)** Th-T fluorescence of α -Syn end-point aggregates after the addition of ZPDm at different time points during the aggregation kinetics. **(B)** Th-T fluorescence assay before and 24 h after the addition of ZPDm to mature α -Syn fibrils. **(C,D)** Representative TEM images in the absence **(C)** and presence **(D)** of ZPDm. Th-T fluorescence is plotted as normalized means. Error bars are represented as SE of mean values; * $p < 0.05$ and *** $p < 0.001$. ZPDm inhibitory capacity increases with the reaction progress, indicating that the compound may interact with aggregated structures and disentangle them.

apparent aggregates in the muscular cell wall of a *C. elegans* model of PD when the compound is added in the food at a concentration of 10 μ M; whether this *in vivo* anti-aggregational effect results in animal phenotypic benefits should be further explored.

The above-described results illustrate how despite ZPD-2 and ZPDm share a significant part of their chemical structure and both are effective α -Syn aggregation inhibitors, their mechanism of action differs significantly, with ZPD-2 acting preferentially at the early stages of the fibrillation and becoming inactive once the polymerization has advanced significantly, being devoid of detectable fibril disrupting activity.

In contrast, ZPDm is more effective at later stages and behaves as a robust disaggregating agent. The fact that (trifluoromethyl)benzene is an inactive molecule indicates that the bulk of the structure shared by ZPD-2 and ZPDm acts as a building block and that the particular chemistry and spatial disposition of the groups that decorate this moiety are responsible for the different mode of action of these compounds. For instance, the (trifluoromethyl)benzene contains the aromatic ring common to the vast majority of small active compounds. However, it lacks a strong hydrogen bond donor/acceptor, which is another characteristic common to many of these molecules (**Supplementary Figure S3**). Therefore, our data suggest that these are the minimum requirements for an active α -Syn aggregation inhibitor. The aromatic rings

would allow interactions with hydrophobic regions, and the polar groups might disrupt the abundant short inter-strand hydrogen bonds that contribute to the amyloid structure's sustainment. Indeed, despite their different size, the number of hydrogen bonds acceptors in ZPD-2 and ZPDm is fairly similar (**Table 1**). Despite speculative, the preferential affinity for early-stage aggregates exhibited by ZPD-2 could be explained by its extended aromatic core and higher Log $P_{O/W}$, which might facilitate interactions with exposed hydrophobic patches in oligomers and small aggregates. In contrast, the compact structure of ZPDm might allow targeting defined binding pockets at the ends of amyloid fibrils, interfering with fibril elongation, and eventually disrupting pre-formed non-covalent interactions.

From a pharmacokinetic point of view, ZPDm is predicted to be more soluble than ZPD-2, to exhibit a higher gastrointestinal absorption and better drug-likeness (**Table 1**). ZPDm is also predicted to be a better lead compound from a medicinal chemistry perspective than ZPD-2 (**Table 1**).

To the best of our knowledge, the only other active molecule with a single aromatic ring derived from the screening of a large chemical library is the compound 576755 (Toth et al., 2019), which in addition to a benzene ring, displays the expected hydrogen bonds acceptors/donors (**Supplementary Figure S3**). 576755 is a potent aggregation inhibitor that acts at the oligomerization stage both *in vitro* and *in cells*. However,

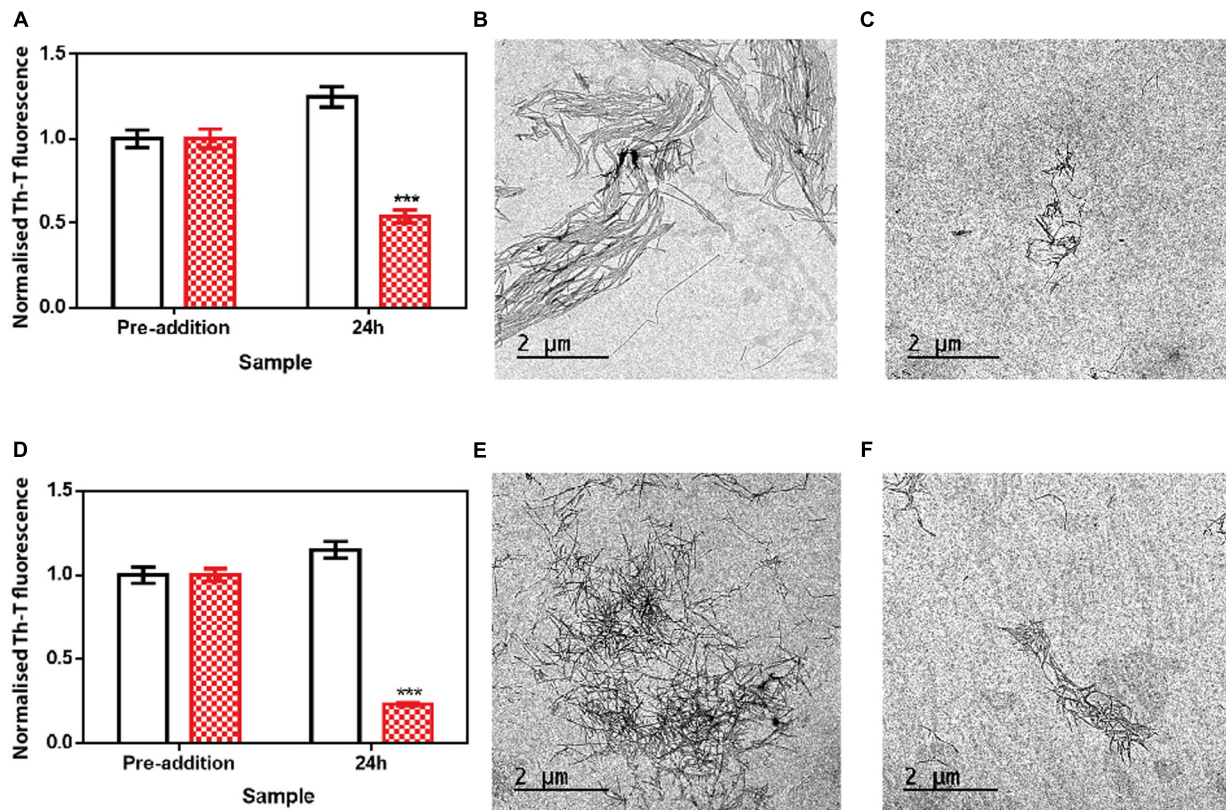


FIGURE 5 | Disaggregational effect of ZPDm in preformed fibrils of two different strains. **(A)** Strain B aggregates disaggregation in the presence (red) and absence (white) of ZPDm as monitored by Th-T fluorescence. **(B,C)** Representative TEM images of untreated **(B)** and ZPDm treated **(C)** samples. **(D)** Strain C aggregates disaggregation in presence (red) and absence (white) of ZPDm as monitored by Th-T fluorescence. **(E,F)** Representative TEM images of untreated **(E)** and ZPDm treated **(F)** samples. Data are shown as means, and error bars are shown as the SE of means; *** $p < 0.001$. The disaggregational ability of ZPDm is also observed in two morphologically different α -Syn strains.

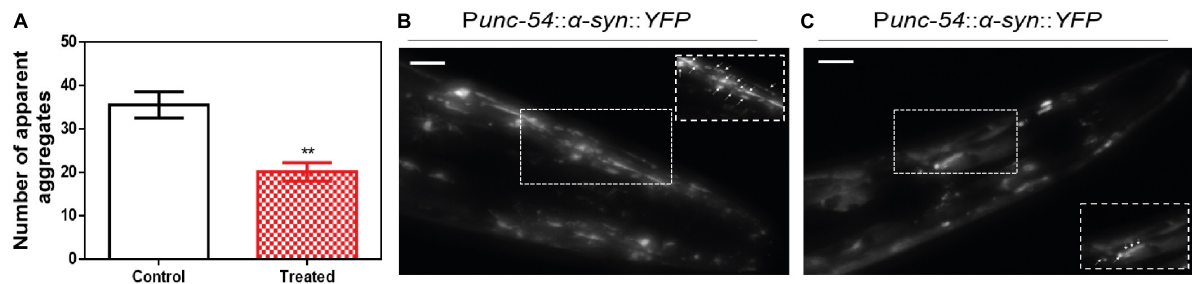


FIGURE 6 | Inhibition of α -Syn inclusions formation in a *C. elegans* model. **(A)** Quantification of α -Syn muscle inclusions per area in NL5901 worms in the absence (white) and presence of ZPDm (red). **(B,C)** Representative images of apparent α -Syn muscle aggregates obtained by epifluorescence microscopy of NL5901 worms treated without **(B)** and with ZPDm **(C)**. (Scale bars, 10 μ m). Between 40 and 50 animals were analyzed per condition. Aggregates are indicated by white arrows. Data are shown as means, and error bars are shown as the SE of means; ** $p < 0.01$. NL5901 *C. elegans* strain forms visible accumulations of aggregated α -Syn that are reduced when ZPDm is administered.

it was identified in a screening for compounds that interact with monomeric α -Syn, and therefore, is not expected to have fibril disrupting activity. Indeed, it did not impact fibril transmission (Toth et al., 2019), consistent with its activity and being complementary to that of ZPDm, a fibril anti-propagating agent in PMCA assays.

Overall, here we describe a new small molecule with the potential to be converted into a lead compound and, perhaps more importantly, together with previous data, envision a way to design minimal aromatic molecules with different α -Syn anti-aggregational activities rationally. Because ZPD-2 and ZPDm function on the same target but have complementary activity, it

will be interesting to test if a combination of them can have a synergic effect that overpasses the individual molecules' potential.

DATA AVAILABILITY STATEMENT

All datasets presented in this study are included in the article/**Supplementary Material**.

AUTHOR CONTRIBUTIONS

SV designed the research. SP-D, JP, FP, JST, SN, MC-G, JSC, JG, and ED performed the research. SP-D, JP, IP, XS, JSC, ED, and SV analyzed the data. SP-D, JP, and SV wrote the manuscript. All authors contributed to the article and approved the submitted version.

FUNDING

SV was supported by the Ministerio de Economía y Competitividad (MINECO) (BIO2016-78310-R), the ICREA (ICREA-Academia 2015), and the Fundación La Marató de TV3 (Ref. 20144330). JSC was supported by the MINECO (BFU2016-78232-P) and the Gobierno de Aragón (E45_17R). ED was supported by the Instituto de Salud Carlos III (PH613883/ERDF/ESF). JG and XS were supported by the MINECO (BIO2015-70092-R) and the European Research Council (Contract 648201).

REFERENCES

- Appel-Cresswell, S., Vilarino-Guell, C., Encarnacion, M., Sherman, H., Yu, I., Shah, B., et al. (2013). Alpha-synuclein p.H50Q, a novel pathogenic mutation for Parkinson's disease. *Mov Disord.* 28, 811–813. doi: 10.1002/mds.25421
- Bendor, J. T., Logan, T. P., and Edwards, R. H. (2013). The function of alpha-synuclein. *Neuron* 79, 1044–1066. doi: 10.1016/j.neuron.2013.09.004
- Bieschke, J., Russ, J., Friedrich, R. P., Ehrnhoefer, D. E., Wobst, H., Neugebauer, K., et al. (2010). EGCG remodels mature alpha-synuclein and amyloid-beta fibrils and reduces cellular toxicity. *Proc. Natl. Acad. Sci. U.S.A.* 107, 7710–7715. doi: 10.1073/pnas.0910723107
- Brenner, S. (1974). The genetics of *Caenorhabditis elegans*. *Genetics* 77, 71–94.
- Bousset, L., Pieri, L., Ruiz-Arlandis, G., Gath, J., Jensen, P. H., Habenstein, B., et al. (2013). Structural and functional characterization of two alpha-synuclein strains. *Nat. Commun.* 4:2575. doi: 10.1038/ncomms3575
- Carija, A., Pinheiro, F., Pujols, J., Bras, I. C., Lazaro, D. F., Santambrogio, C., et al. (2019). Biasing the native alpha-synuclein conformational ensemble towards compact states abolishes aggregation and neurotoxicity. *Redox Biol.* 22:101135. doi: 10.1016/j.redox.2019.101135
- Crespo, R., Villar-Alvarez, E., Taboada, P., Rocha, F. A., Damas, A. M., and Martins, P. M. (2016). What Can the Kinetics of Amyloid Fibril Formation Tell about Off-pathway Aggregation? *J. Biol. Chem.* 291, 2018–2032. doi: 10.1074/jbc.M115.699348
- Decressac, M., Mattsson, B., Weikop, P., Lundblad, M., Jakobsson, J., and Bjorklund, A. (2013). TFEB-mediated autophagy rescues midbrain dopamine neurons from alpha-synuclein toxicity. *Proc.*

ACKNOWLEDGMENTS

We thank the Infraestructura Científica y Técnica Singular NMR facility at Centres Científics i Tecnològics de la Universitat de Barcelona for help with NMR, the Servei de Microscòpia at Universitat Autònoma de Barcelona for their help with TEM, and Anna Villar-Pique for help with plasmid construction.

SUPPLEMENTARY MATERIAL

The Supplementary Material for this article can be found online at: <https://www.frontiersin.org/articles/10.3389/fbioe.2020.588947/full#supplementary-material>

Supplementary Figure 1 | Inhibitory capacity of (trifluoromethyl)benzene. **(A)** Chemical structures of (trifluoromethyl)benzene, (left) and ZPDm (right). **(B)** α -Syn aggregation kinetics in the absence (black) and presence (green) of 100 μ M of (trifluoromethyl)benzene followed by Th-T fluorescence. **(C)** Light-scattering measurements at 300 and 340 nm, in the absence (white) and presence (green) of (trifluoromethyl)benzene.

Supplementary Figure 2 | NMR analysis of ZPDm lack of interaction with monomeric α -Syn. ^1H - ^{15}N HSQC NMR spectra of ^{15}N -labeled α -Syn (70 μ M) in the presence **(A)** and in the absence **(B)** of ZPDm (100 μ M). The superposition of the two NMR spectra is shown in **(C)**.

Supplementary Figure 3 | Chemical structures of different α -Syn aggregation inhibitors with a single aromatic ring. Chemical structures of **(A)** scyllo-inositol, **(B)** gallic acid, **(C)** dopamine, **(D)** epinephrine, **(E)** norepinephrine, **(F)** thymoquinone, **(G)** safranal, **(H)** caffeic acid, **(I)** ferulic acid, **(J)** protocatechuic acid, **(K)** tyrosol, and **(L)** 576755.

Natl. Acad. Sci. U.S.A. 110, E1817–E1826. doi: 10.1073/pnas.1305623110

- Dexter, D. T., and Jenner, P. (2013). Parkinson disease: from pathology to molecular disease mechanisms. *Free Radic. Biol. Med.* 62, 132–144. doi: 10.1016/j.freeradbiomed.2013.01.018
- Di Giovanni, S., Eleuteri, S., Paleologou, K. E., Yin, G., Zweckstetter, M., Carrupt, P. A., et al. (2010). Entacapone and tolcapone, two catechol O-methyltransferase inhibitors, block fibril formation of alpha-synuclein and beta-amyloid and protect against amyloid-induced toxicity. *J. Biol. Chem.* 285, 14941–14954. doi: 10.1074/jbc.M109.080390
- Fanciulli, A., and Wenning, G. K. (2015). Multiple-system atrophy. *N. Engl. J. Med.* 372, 249–263. doi: 10.1056/NEJMra1311488
- Faustini, G., Longhena, F., Varanita, T., Bubacco, L., Pizzi, M., Missale, C., et al. (2018). Synapsin III deficiency hampers alpha-synuclein aggregation, striatal synaptic damage and nigral cell loss in an AAV-based mouse model of Parkinson's disease. *Acta Neuropathol.* 136, 621–639. doi: 10.1007/s00401-018-1892-1
- Fellner, L., Jellinger, K. A., Wenning, G. K., and Stefanova, N. (2011). Glial dysfunction in the pathogenesis of alpha-synucleinopathies: emerging concepts. *Acta Neuropathol.* 121, 675–693. doi: 10.1007/s00401-011-0833-z
- Hamamichi, S., Rivas, R. N., Knight, A. L., Cao, S., Caldwell, K. A., and Caldwell, G. A. (2008). Hypothesis-based RNAi screening identifies neuroprotective genes in a Parkinson's disease model. *Proc. Natl. Acad. Sci. U.S.A.* 105, 728–733. doi: 10.1073/pnas.0711018105
- Harrington, A. J., Yacoubian, T. A., Slone, S. R., Caldwell, K. A., and Caldwell, G. A. (2012). Functional analysis of VPS41-mediated neuroprotection in *Caenorhabditis elegans* and mammalian models of Parkinson's disease. *J. Neurosci.* 32, 2142–2153. doi: 10.1523/jneurosci.2606-11.2012

- Hansen, C., Angot, E., Bergstrom, A. L., Steiner, J. A., Pieri, L., Paul, G., et al. (2011). α -Synuclein propagates from mouse brain to grafted dopaminergic neurons and seeds aggregation in cultured human cells. *J. Clin. Invest.* 121, 715–725. doi: 10.1172/JCI43366
- Herrera, F. E., Chesi, A., Paleologou, K. E., Schmid, A., Munoz, A., Vendruscolo, M., et al. (2008). Inhibition of α -synuclein fibrillization by dopamine is mediated by interactions with five C-terminal residues and with E83 in the NAC region. *PLoS One* 3:e3394. doi: 10.1371/journal.pone.0003394
- Herva, M. E., Zibae, S., Fraser, G., Barker, R. A., Goedert, M., and Spillantini, M. G. (2014). Anti-amyloid compounds inhibit α -synuclein aggregation induced by protein misfolding cyclic amplification (PMCA). *J. Biol. Chem.* 289, 11897–11905. doi: 10.1074/jbc.M113.542340
- Ibanez, P., Bonnet, A. M., Debarges, B., Lohmann, E., Tison, F., Pollak, P., et al. (2004). Causal relation between α -synuclein gene duplication and familial Parkinson's disease. *Lancet* 364, 1169–1171. doi: 10.1016/S0140-6736(04)17104-3
- Ibrahim, T., and McLaurin, J. (2016). α -Synuclein aggregation, seeding and inhibition by scyllo-inositol. *Biochem. Biophys. Res. Commun.* 469, 529–534. doi: 10.1016/j.bbrc.2015.12.043
- Jiang, M., Porat-Shliom, Y., Pei, Z., Cheng, Y., Xiang, L., Sommers, K., et al. (2010). Baicalein reduces E46K α -synuclein aggregation in vitro and protects cells against E46K α -synuclein toxicity in cell models of familial Parkinsonism. *J. Neurochem.* 114, 419–429. doi: 10.1111/j.1471-4159.2010.06752.x
- Jung, B. C., Lim, Y. J., Bae, E. J., Lee, J. S., Choi, M. S., Lee, M. K., et al. (2017). Amplification of distinct α -synuclein fibril conformers through protein misfolding cyclic amplification. *Exp. Mol. Med.* 49:e314. doi: 10.1038/emmm.2017.1
- Kalia, L. V., and Lang, A. E. (2015). Parkinson's disease. *Lancet* 386, 896–912. doi: 10.1016/S0140-6736(14)61393-3
- Kantor, B., Tagliafierro, L., Gu, J., Zamora, M. E., Ilich, E., Grenier, C., et al. (2018). Downregulation of SNCA expression by targeted editing of DNA methylation: a potential strategy for precision therapy in PD. *Mol. Ther.* 26, 2638–2649. doi: 10.1016/j.ymthe.2018.08.019
- Kruger, R., Kuhn, W., Muller, T., Woitalla, D., Graeber, M., Kosel, S., et al. (1998). Ala30Pro mutation in the gene encoding α -synuclein in Parkinson's disease. *Nat. Genet.* 18, 106–108. doi: 10.1038/ng0298-106
- Kurnik, M., Sahin, C., Andersen, C. B., Lorenzen, N., Giehm, L., Mohammad-Beigi, H., et al. (2018). Potent α -synuclein aggregation inhibitors, identified by high-throughput screening, mainly target the monomeric state. *Cell Chem. Biol.* 25, 1389.e9–1402.e9. doi: 10.1016/j.chembiol.2018.08.005
- Lassot, I., Mora, S., Lesage, S., Zieba, B. A., Coque, E., Condroyer, C., et al. (2018). The E3 Ubiquitin Ligases TRIM17 and TRIM41 Modulate α -Synuclein Expression by Regulating ZSCAN21. *Cell Rep.* 25, 2484.e9–2496.e9. doi: 10.1016/j.celrep.2018.11.002
- Lau, A., So, R. W. L., Lau, H. H. C., Sang, J. C., Ruiz-Riquelme, A., Fleck, S. C., et al. (2020). α -Synuclein strains target distinct brain regions and cell types. *Nat. Neurosci.* 23, 21–31. doi: 10.1038/s41593-019-0541-x
- Li, B., Ge, P., Murray, K. A., Sheth, P., Zhang, M., Nair, G., et al. (2018). Cryo-EM of full-length α -synuclein reveals fibril polymorphs with a common structural kernel. *Nat. Commun.* 9:3609. doi: 10.1038/s41467-018-05971-2
- Liu, Y., Carver, J. A., Calabrese, A. N., and Pukala, T. L. (2014). Gallic acid interacts with α -synuclein to prevent the structural collapse necessary for its aggregation. *Biochim. Biophys. Acta* 1844, 1481–1485. doi: 10.1016/j.bbapap.2014.04.013
- Luk, K. C., Kehm, V., Carroll, J., Zhang, B., O'Brien, P., Trojanowski, J. Q., et al. (2012). Pathological α -synuclein transmission initiates Parkinson-like neurodegeneration in nontransgenic mice. *Science* 338, 949–953. doi: 10.1126/science.1227157
- More, B., Yin, G., Lazaro, D. F., Munari, F., Strohaker, T., Giller, K., et al. (2015). Small molecules detected by second-harmonic generation modulate the conformation of monomeric α -synuclein and reduce its aggregation in cells. *J. Biol. Chem.* 290, 27582–27593. doi: 10.1074/jbc.M114.636027
- Munoz-Lobato, F., Rodriguez-Palero, M. J., Naranjo-Galindo, F. J., Shephard, F., Gaffney, C. J., Szewczyk, N. J., et al. (2014). Protective role of DJN-27/ERdj5 in *Caenorhabditis elegans* models of human neurodegenerative diseases. *Antioxid. Redox Signal.* 20, 217–235. doi: 10.1089/ars.2012.5051
- Nussbaum, R. L., and Ellis, C. E. (2003). Alzheimer's disease and Parkinson's disease. *N. Engl. J. Med.* 348, 1356–1364. doi: 10.1056/NEJM2003ra020003
- Pandey, N., Strider, J., Nolan, W. C., Yan, S. X., and Galvin, J. E. (2008). Curcumin inhibits aggregation of α -synuclein. *Acta Neuropathol.* 115, 479–489. doi: 10.1007/s00401-007-0332-4
- Peelaerts, W., Bousset, L., Van der Perren, A., Moskalyuk, A., Pulizzi, R., Giugliano, M., et al. (2015). α -Synuclein strains cause distinct synucleinopathies after local and systemic administration. *Nature* 522, 340–344. doi: 10.1038/nature14547
- Pena-Díaz, S., Pujols, J., Conde-Gimenez, M., Carija, A., Dalfó, E., García, J., et al. (2019). ZPD-2, a small compound that inhibits α -synuclein amyloid aggregation and its seeded polymerization. *Front. Mol. Neurosci.* 12:306. doi: 10.3389/fnmol.2019.00306
- Pena-Díaz, S., Pujols, J., and Ventura, S. (2020). Small molecules to prevent the neurodegeneration caused by α -synuclein aggregation. *Neural Regen. Res.* 15, 2260–2261. doi: 10.4103/1673-5374.284993
- Polymeropoulos, M. H., Lavedan, C., Leroy, E., Ide, S. E., Dehejia, A., Dutra, A., et al. (1997). Mutation in the α -synuclein gene identified in families with Parkinson's disease. *Science* 276, 2045–2047. doi: 10.1126/science.276.5321.2045
- Pujols, J., Pena-Díaz, S., Conde-Gimenez, M., Pinheiro, F., Navarro, S., Sancho, J., et al. (2017). High-throughput screening methodology to identify α -synuclein aggregation inhibitors. *Int. J. Mol. Sci.* 18:478. doi: 10.3390/ijms18030478
- Pujols, J., Pena-Díaz, S., Lazaro, D. F., Peccati, F., Pinheiro, F., Gonzalez, D., et al. (2018). Small molecule inhibits α -synuclein aggregation, disrupts amyloid fibrils, and prevents degeneration of dopaminergic neurons. *Proc. Natl. Acad. Sci. U.S.A.* 115, 10481–10486. doi: 10.1073/pnas.1804198115
- Pujols, J., Pena-Díaz, S., Pallares, I., and Ventura, S. (2020). Chemical chaperones as novel drugs for Parkinson's Disease. *Trends Mol. Med.* 26, 408–421. doi: 10.1016/j.molmed.2020.01.005
- Saelices, L., Nguyen, B. A., Chung, K., Wang, Y., Ortega, A., Lee, J. H., et al. (2019). A pair of peptides inhibits seeding of the hormone transporter transthyretin into amyloid fibrils. *J. Biol. Chem.* 294, 6130–6141. doi: 10.1074/jbc.RA118.005257
- Sangwan, S., Sahay, S., Murray, K. A., Morgan, S., Guenther, E. L., Jiang, L., et al. (2020). Inhibition of synucleinopathic seeding by rationally designed inhibitors. *eLife* 9:e46775. doi: 10.7554/eLife.46775
- Save, S. S., Rachineni, K., Hosur, R. V., and Choudhary, S. (2019). Natural compound safranal driven inhibition and dis-aggregation of α -synuclein fibrils. *Int. J. Biol. Macromol.* 141, 585–595. doi: 10.1016/j.ijbiomac.2019.09.053
- Schwab, K., Frahm, S., Horsley, D., Rickard, J. E., Melis, V., Goatman, E. A., et al. (2017). A protein aggregation inhibitor, leuco-methylthionium Bis(Hydromethanesulfonate), decreases α -synuclein inclusions in a transgenic mouse model of synucleinopathy. *Front. Mol. Neurosci.* 10:447. doi: 10.3389/fnmol.2017.00447
- Seidler, P. M., Boyer, D. R., Rodriguez, J. A., Sawaya, M. R., Cascio, D., Murray, K., et al. (2018). Structure-based inhibitors of tau aggregation. *Nat. Chem.* 10, 170–176. doi: 10.1038/nchem.2889
- Serpell, L. C., Berriman, J., Jakes, R., Goedert, M., and Crowther, R. A. (2000). Fiber diffraction of synthetic α -synuclein filaments shows amyloid-like cross-beta conformation. *Proc. Natl. Acad. Sci. U.S.A.* 97, 4897–4902. doi: 10.1073/pnas.97.9.4897
- Silva, B., Einarsdóttir, O., Fink, A. L., and Uversky, V. (2011). Modulating α -synuclein misfolding and fibrillation in vitro by agrochemicals. *Res. Rep. Biol.* 2011, 43–56. doi: 10.2147/RRB.S16448
- Singleton, A. B., Farrer, M., Johnson, J., Singleton, A., Hague, S., Kachergus, J., et al. (2003). α -Synuclein locus triplication causes Parkinson's disease. *Science* 302:841. doi: 10.1126/science.1090278
- Spencer, B., Potkar, R., Trejo, M., Rockenstein, E., Patrick, C., Gindi, R., et al. (2009). Beclin 1 gene transfer activates autophagy and ameliorates the neurodegenerative pathology in α -synuclein models of Parkinson's and Lewy body diseases. *J. Neurosci.* 29, 13578–13588. doi: 10.1523/JNEUROSCI.4390-09.2009

- Spillantini, M. G., Crowther, R. A., Jakes, R., Cairns, N. J., Lantos, P. L., and Goedert, M. (1998a). Filamentous alpha-synuclein inclusions link multiple system atrophy with Parkinson's disease and dementia with Lewy bodies. *Neurosci. Lett.* 251, 205–208. doi: 10.1016/s0304-3940(98)00504-7
- Spillantini, M. G., Crowther, R. A., Jakes, R., Hasegawa, M., and Goedert, M. (1998b). alpha-Synuclein in filamentous inclusions of Lewy bodies from Parkinson's disease and dementia with lewy bodies. *Proc. Natl. Acad. Sci. U.S.A.* 95, 6469–6473. doi: 10.1073/pnas.95.11.6469
- Spillantini, M. G., Schmidt, M. L., Lee, V. M., Trojanowski, J. Q., Jakes, R., and Goedert, M. (1997). Alpha-synuclein in Lewy bodies. *Nature* 388, 839–840. doi: 10.1038/42166
- Tatenhorst, L., Eckermann, K., Dambeck, V., Fonseca-Ornelas, L., Walle, H., Lopes da Fonseca, T., et al. (2016). Fasudil attenuates aggregation of alpha-synuclein in models of Parkinson's disease. *Acta Neuropathol. Commun.* 4:39. doi: 10.1186/s40478-016-0310-y
- Toth, G., Neumann, T., Berthet, A., Masliah, E., Spencer, B., Tao, J., et al. (2019). Novel Small molecules targeting the intrinsically disordered structural ensemble of alpha-synuclein protect against diverse alpha-synuclein mediated dysfunctions. *Sci. Rep.* 9:16947. doi: 10.1038/s41598-019-52598-4
- van Ham, T. J., Thijssen, K. L., Breitling, R., Hofstra, R. M., Plasterk, R. H., and Nollen, E. A. (2008). *C. elegans* model identifies genetic modifiers of alpha-synuclein inclusion formation during aging. *PLoS Genet.* 4:e1000027. doi: 10.1371/journal.pgen.1000027
- Wagner, J., Ryazanov, S., Leonov, A., Levin, J., Shi, S., Schmidt, F., et al. (2013). Anle138b: a novel oligomer modulator for disease-modifying therapy of neurodegenerative diseases such as prion and Parkinson's disease. *Acta Neuropathol.* 125, 795–813. doi: 10.1007/s00401-013-1114-9
- Wrasidlo, W., Tsigelny, I. F., Price, D. L., Dutta, G., Rockenstein, E., Schwarz, T. C., et al. (2016). A de novo compound targeting alpha-synuclein improves deficits in models of Parkinson's disease. *Brain* 139(Pt 12), 3217–3236. doi: 10.1093/brain/aww238
- Xilouri, M., Brekk, O. R., Landeck, N., Pitychoutis, P. M., Papasilekas, T., Papadopoulou-Daifoti, Z., et al. (2013). Boosting chaperone-mediated autophagy in vivo mitigates alpha-synuclein-induced neurodegeneration. *Brain* 136(Pt 7), 2130–2146. doi: 10.1093/brain/awt131
- Zharikov, A., Bai, Q., De Miranda, B. R., Van Laar, A., Greenamyre, J. T., and Burton, E. A. (2019). Long-term RNAi knockdown of alpha-synuclein in the adult rat substantia nigra without neurodegeneration. *Neurobiol. Dis.* 125, 146–153. doi: 10.1016/j.nbd.2019.01.004

Conflict of Interest: The authors declare that the research was conducted in the absence of any commercial or financial relationships that could be construed as a potential conflict of interest.

Copyright © 2020 Peña-Díaz, Pujols, Pinheiro, Santos, Pallarés, Navarro, Conde-Gimenez, García, Salvatella, Dalfó, Sancho and Ventura. This is an open-access article distributed under the terms of the Creative Commons Attribution License (CC BY). The use, distribution or reproduction in other forums is permitted, provided the original author(s) and the copyright owner(s) are credited and that the original publication in this journal is cited, in accordance with accepted academic practice. No use, distribution or reproduction is permitted which does not comply with these terms.

3.5. Chapter 5. The small aromatic compound SynuClean-D inhibits the aggregation and seeded polymerization of multiple α -Synuclein strains

Published at Journal of Biological Chemistry on April 2022

Available in: [https://www.jbc.org/article/S0021-9258\(22\)00342-8/fulltext](https://www.jbc.org/article/S0021-9258(22)00342-8/fulltext)

The small aromatic compound SynuClean-D inhibits the aggregation and seeded polymerization of multiple α -synuclein strains

Received for publication, January 12, 2022, and in revised form, March 25, 2022. Published, Papers in Press, April 4, 2022,

<https://doi.org/10.1016/j.jbc.2022.101902>

Samuel Peña-Díaz^{1,2,‡}, Jordi Pujols^{1,2,‡}, Eftychia Vasili^{3,4} , Francisca Pinheiro^{1,2}, Jaime Santos^{1,2} ,
Zoe Manglano-Artuñedo^{1,2}, Tiago F. Outeiro^{3,4,5,6}, and Salvador Ventura^{1,2,7,*}

From the ¹Institut de Biotecnologia i Biomedicina, Universitat Autònoma de Barcelona, Bellaterra, Spain; ²Departament de Bioquímica i Biologia Molecular, Universitat Autònoma de Barcelona, Bellaterra, Spain; ³Department of Experimental Neurodegeneration, Center for Biostructural Imaging of Neurodegeneration, University Medical Center Göttingen, Göttingen, Germany; ⁴Max Planck Institute for Experimental Medicine, Göttingen, Germany; ⁵Translational and Clinical Research Institute, Faculty of Medical Sciences, Newcastle University, Framlington Place, Newcastle Upon Tyne, Newcastle, United Kingdom; ⁶Scientific Employee With a Honorary Contract at Deutsches Zentrum für Neurodegenerative Erkrankungen (DZNE), Göttingen, Germany; ⁷ICREA, Passeig Lluís Companys 23, Barcelona, Spain

Edited by Wolfgang Peti

Parkinson's disease is a neurodegenerative disorder characterized by the loss of dopaminergic neurons in the substantia nigra, as well as the accumulation of intraneuronal proteinaceous inclusions known as Lewy bodies and Lewy neurites. The major protein component of Lewy inclusions is the intrinsically disordered protein α -synuclein (α -Syn), which can adopt diverse amyloid structures. Different conformational strains of α -Syn have been proposed to be related to the onset of distinct synucleinopathies; however, how specific amyloid fibrils cause distinctive pathological traits is not clear. Here, we generated three different α -Syn amyloid conformations at different pH and salt concentrations and analyzed the activity of SynuClean-D (SC-D), a small aromatic molecule, on these strains. We show that incubation of α -Syn with SC-D reduced the formation of aggregates and the seeded polymerization of α -Syn in all cases. Moreover, we found that SC-D exhibited a general fibril disaggregation activity. Finally, we demonstrate that treatment with SC-D also reduced strain-specific intracellular accumulation of phosphorylated α -Syn inclusions. Taken together, we conclude that SC-D may be a promising hit compound to inhibit polymorphic α -Syn aggregation.

Parkinson's disease (PD) is the second most prevalent neurodegenerative disorder associated with protein misfolding and aggregation after Alzheimer's disease and affects 0.5 to 1% of the population aged between 65 and 69 years, increasing to 1 to 3% of people aged over 80 years (1, 2). PD is characterized by the loss of dopaminergic neurons in the substantia nigra pars compacta, resulting in motor symptoms such as rigidity, tremor, and bradykinesia and nonmotor symptoms such as dementia (3). A major histopathological hallmark of PD is the formation of proteinaceous assemblies in the neuronal body

and processes, known as Lewy bodies and Lewy neurites, respectively (4), whose primary protein component consists of aggregated forms of α -synuclein (α -Syn) (5, 6). This intrinsically disordered protein is a soluble monomer with diverse functions, like regulating synaptic vesicle release and trafficking, fatty acid binding, and neuronal survival (7). However, under pathological conditions, α -Syn misfolds and readily aggregates. The presence of altered α -Syn in the brain is a common feature of the synucleinopathies that, aside from PD, include PD with dementia, multiple system atrophy (MSA), and dementia with Lewy bodies (8).

The synucleinopathies differ in their symptomatology, progression, and affected cellular and anatomical compartments. It has been hypothesized that these differences might ultimately rely on the conformational heterogeneity of α -Syn amyloid structures (9–11), in analogy with the human prion protein, where distinct polymorphs, or strains, cause different histopathological lesion profiles, with divergent brain region distributions and clinical manifestations (12). This view is supported by a recent cryo-EM study showing that the structure of α -Syn amyloid filaments from the brains of individuals with MSA differs from those of individuals with dementia with Lewy bodies (10). The therapeutic implications of this conformational diversity are huge since molecules that efficiently block the aggregation of one α -Syn strain may not necessarily recognize another polymorph.

Recombinant soluble α -Syn forms amyloid fibrils *in vitro* that, despite differing at the atomic level from those observed in patients' brains (10), can seed the aggregation of endogenous α -Syn in cultured neuronal cells, primary cultured neurons, and animal brains (13–15). Moreover, synthetic α -Syn fibrils formed under different solution conditions exhibit different conformation, seeding activity, and neurotoxicity in cells and when inoculated in rat brains (11, 16–22). Surprisingly, despite compounds like anle138b (23, 24), squalamine (25), trodusquemine (26), BIOD303 (27), or fasudil (28) have

[‡] These authors contributed equally to this work.

* For correspondence: Salvador Ventura, salvador.ventura@uab.es.

SC-D inhibits α -synuclein strains aggregation

been shown to modulate α -Syn aggregation *in vitro* effectively, studies addressing the activity of small molecules on distinct α -Syn strains are still scarce (29).

In the present study, we prepared three assemblies from α -Syn monomer under different conditions. After confirming that they differ in their conformation and in their capacity to convert endogenous α -Syn into phosphorylated aggregates in a cellular model, we characterized how SynuClean-D (SC-D), a potent inhibitor of α -Syn aggregation (30), performs on top of the three polymorphs. We demonstrate that SC-D reduces amyloid formation in all the experimental conditions and disrupts the different fibrils. In addition, it reduces the seeding capacity of preformed aggregates *in vitro* and in cells. Altogether, the data converge to indicate that SC-D is active against different α -Syn fibrillar conformations, thus becoming a promising hit compound for developing a generic molecule to treat the synucleinopathies.

Results

α -Syn amyloid fibrils characterization

SC-D, (5-nitro-6-(3-nitrophenyl)-2-oxo-4-(trifluoromethyl)-1H-pyridine-3-carbonitrile) (Fig. S1A), has been previously described as an inhibitor of α -Syn aggregation, which can reduce protein misfolding cyclic amplification-induced aggregates propagation and disrupt fibrils, displaying anti-aggregation and neuroprotective activity in animal models of PD (30). However, whether the activity of this small molecule is restricted to the assemblies formed in the conditions in which we performed the screening or it can target alternative α -Syn aggregated conformations was unknown. To decipher this, we generated three distinct α -Syn assemblies in conditions that differ from those of previous assays, where we used phosphate-buffered saline (PBS). Both pH and salt concentration have been shown to influence α -Syn fibril formation (16, 31); therefore, we incubated recombinant α -Syn (70 μ M) in buffer A (50 mM sodium acetate pH 5.0) and buffer B (50 mM Tris-HCl pH 7.5) to assess the effect of the pH and in buffer B and buffer C (50 mM Tris-HCl pH 7.5/150 mM KCl) to test the impact of physiological salt concentration.

Kinetic analysis indicated that in the three conditions, α -Syn assembled into thioflavin-T (Th-T)-positive structures. Noticeably, α -Syn exhibited a high Th-T binding in buffer C, whereas the lowest levels of Th-T fluorescence corresponded to those attained in buffer A (Fig. 1A). Thus, both the pH and the salt of the solution significantly conditioned the kinetics of α -Syn amyloid formation. In contrast, the highest levels of light scattering were observed in buffer A, with buffers B and C rendering much lower and almost identical signals (Fig. 1B). This indicated the formation of aggregated species with poor Th-T staining in buffer A.

Proteinase K (PK) digestion of the aggregates indicated differential susceptibility to proteolysis. The species formed in buffer B were completely cut into two smaller fragments, whereas those in buffers A and C were significantly more resistant, while exhibiting different degradation profiles (Fig. 1C).

Low-magnification transmission electron microscopy (TEM) images of negatively stained samples evidenced that fibrillar sheet-like structures with many parallel protofilaments and rod-like assemblies coexisted with large and abundant, apparently amorphous, aggregates in buffer A. In contrast, isolated fibrils were apparent in buffer B, whereas fibrils tend to cluster into a mesh in buffer C (Fig. S2). High-magnification images revealed that the fibrillar material in the three solutions displayed different morphology, with fibrils in buffer A being mostly sheet-like, those in buffer B and C having a more canonical fibrillar appearance, those in buffer B appearing as straight, and the ones in buffer C twisted (Fig. 1, D–F). The width of the fibrils formed in buffers A, B, and C were 8.6 ± 1.9 nm, 14.6 ± 2.7 nm, and 11.9 ± 1.8 nm, respectively.

The secondary structure content of the samples was analyzed using attenuated total reflection Fourier-transform infrared (ATR-FTIR) spectroscopy (Fig. 1, G–I and Table S1). In all cases, the spectra were dominated by a band at 1624 to 1628 cm^{-1} attributed to the presence of intermolecular β -sheet structure. When comparing only the structures formed at physiological pH, buffer B favors a higher content of disorder (28%) than buffer C (23%), which might account for a higher sensitivity to proteolysis. Indeed, when we compared the resistance to chemical denaturation with 4 M urea of the two species in a kinetic assay, we observed that the fibrils formed in buffer C were clearly more stable and could not be denatured entirely in this harsh condition (Fig. S3). Overall, these results indicated that we had successfully prepared three distinct types of α -Syn fibrils from the same monomer, named here strains A, B, and C.

SC-D inhibits the aggregation of α -Syn into different strains

Once the generation of different conformations was confirmed, we examined the impact of SC-D (100 μ M) in their aggregation processes. First, we confirmed that the SC-D does not exhibit absorbance in buffers A, B, and C at the excitation (450 nm) and emission (480 nm) wavelengths used to monitor Th-T fluorescence in our assays (Fig. S1B). Kinetic analysis indicated that SC-D exhibited a moderate impact on the formation of Th-T-positive species of strain A, reducing the fluorescence at the endpoint of the reaction by 32% (Fig. 2A). In contrast, the impact in light scattering was large, with 45% reduction at 340 nm (Fig. 2A inset). Thus, SC-D effectively inhibits the aggregation of α -Syn in buffer A. Its reduced effect on Th-T fluorescence can be explained by the low dye binding of the final solution, likely because of the presence of amorphous aggregates coexisting with fibrils. TEM images confirmed a reduction in the number and size of the aggregates in the presence of SC-D (Fig. 2G) when compared with the control samples (Fig. 2D).

SC-D was very effective at inhibiting the formation of α -Syn amyloid fibrils at physiological pH, both in the absence (Fig. 2B) and presence of salt (Fig. 2C), resulting in a 73% and 72% reduction of the Th-T fluorescence signal at the end of the reaction for strains B and C, respectively. In addition, light scattering measurements indicated that SC-D effectively

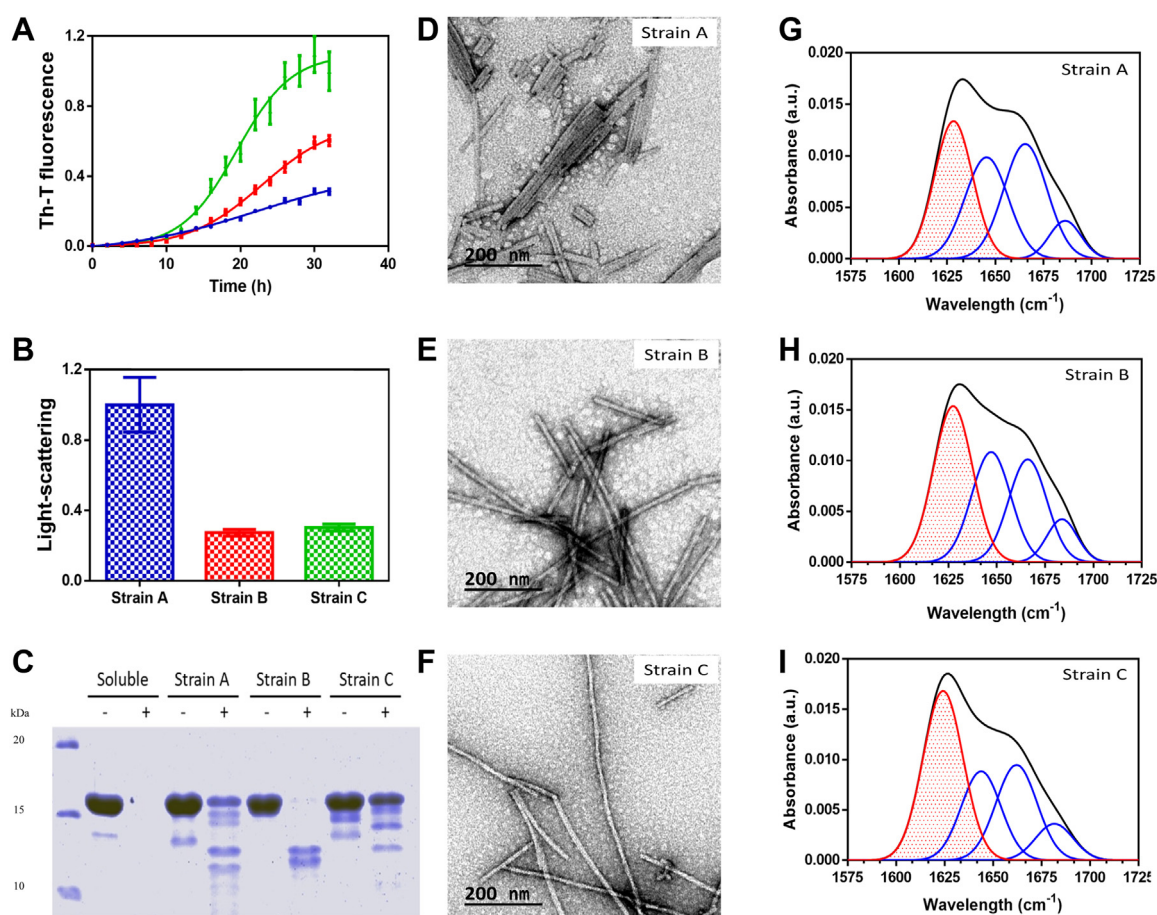


Figure 1. Strain characterization. A, aggregation kinetics of strain A (blue), strain B (red), and strain C (green). Intensity of Th-T fluorescence is plotted as normalized means in function of time and error bars as standard errors of mean. B, normalized light scattering measurements of final point aggregates of strain A (blue), strain B (red), and strain C (green). Error bars are shown as standard errors of mean values. C, Tricine-SDS-PAGE gels of soluble α -Syn and aggregated strains A, B, and C before (–) and after (+) PK digestion. D–F, representative TEM images of strain A (D), strain B (E), and C (F) end point aggregates. Scale bars correspond to 200 nm. G–I, ATR-FTIR absorbance spectra in the amide I region of final point aggregates of strain A (G), B (H), and C (I). α -Syn, α -synuclein; ATR, attenuated total reflectance; PK, Proteinase K; TEM, transmission electron microscopy; Th-T; thioflavin-T.

reduced the amount of aggregated material for both strains, with a decrease in the signals at 340 nm of 44% in buffer B (Fig. 2B inset) and 45% in buffer C (Fig. 2C inset). Not surprisingly, TEM images corroborated that, in both cases, the population of amyloid fibrils was significantly reduced upon SC-D treatment (Fig. 2, H and I), relative to untreated control reactions (Fig. 2, E and F). Overall, SC-D appears to act as a general inhibitor of spontaneous α -Syn aggregation.

SC-D hampers α -Syn seeded polymerization

Preformed amyloid structures, or seeds, have been shown to induce and accelerate the aggregation of the soluble protein counterpart (32). We studied the seeding capacity of the three polymorphs by adding 1% (v/v) of preformed and sonicated α -Syn fibrils formed in the same conditions followed for the correspondent assay.

No seeding capacity was observed for fibrils formed in buffer A. Nonetheless, SC-D still reduced Th-T fluorescence in 66% (Fig. 3A) and light scattering in 45% at 340 nm, in the presence of seeds (Fig. 3A inset). The highest activity of SC-D in the seeded reaction, relative to the spontaneous one, is

puzzling and might indicate that despite the two processes are kinetically similar, they might involve different species for which SC-D has a distinct affinity.

Strain B seeds were very effective, abrogating the lag phase of the aggregation process and inducing a faster reaction. SC-D did restore the sigmoidal shape of the unseeded reaction but significantly reduced its speed and the final amount of Th-T-positive species by 40% (Fig. 3B). In addition, light scattering in the presence of the molecule was reduced in 38% at 340 nm (Fig. 3B inset) and thus to a lower extent than in the spontaneous reaction.

Strain C fibrils effectively seeded the soluble protein aggregation, shortening the lag phase and promoting a significantly faster reaction, which still displayed a sigmoidal shape. SC-D is exceptionally active in this condition, abrogating almost entirely α -Syn aggregation, with an 86% reduction in the final Th-T fluorescence (Fig. 3C). Consistently, the impact in light scattering in the seeded reaction was also very high, with a reduction of 63% at 340 nm (Fig. 3C inset).

These data indicate that SC-D is a very effective inhibitor of α -Syn seeded polymerization for all the strains and in all assayed conditions. The high activity on the fibrils formed in

SC-D inhibits α -synuclein strains aggregation

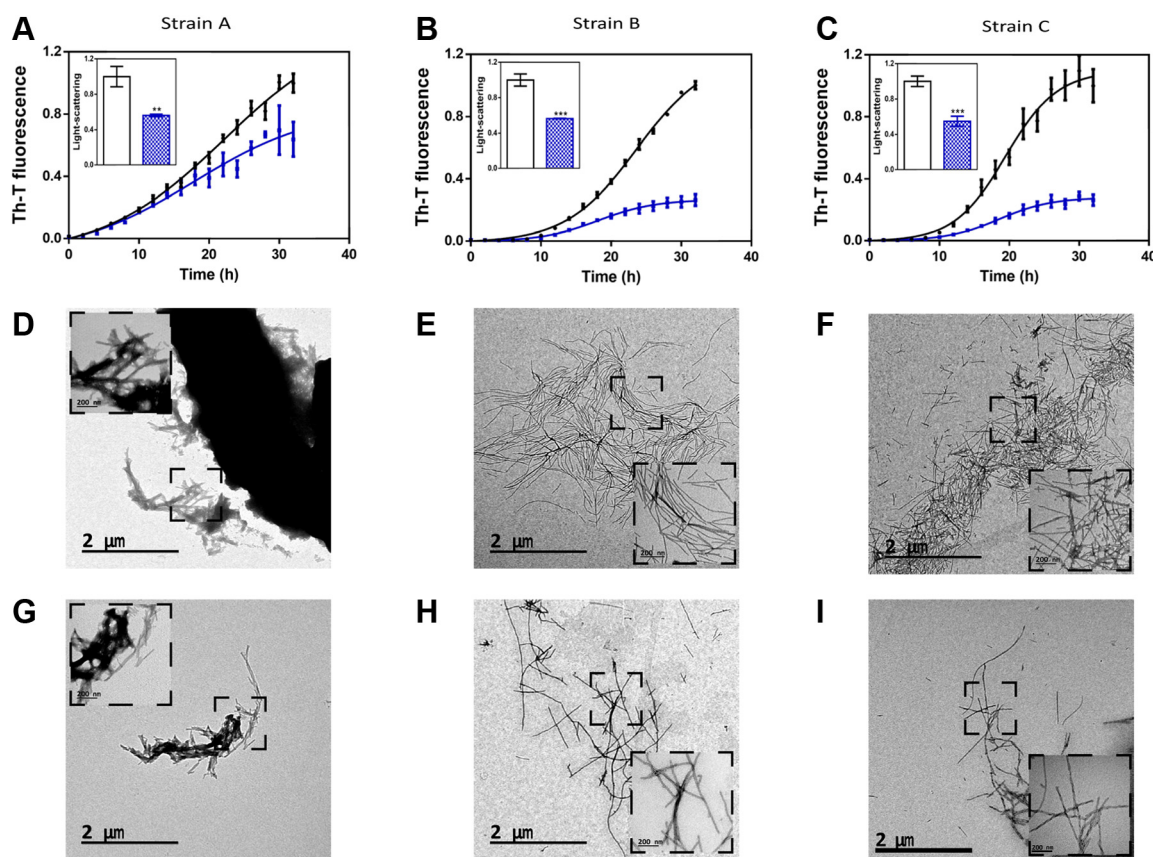


Figure 2. SynuClean-D (SC-D) effects on strain A, strain B, and strain C aggregation. A–C, aggregation kinetics and final point light scattering measurements (insets) of α -Syn in the presence (blue) or absence (black) of SC-D for strain A (A), strain B (B), and strain C (C). Th-T fluorescence and light scattering are plotted as normalized means. Error bars are shown as standard errors of mean values. $**p < 0.01$ and $***p < 0.001$. D–I, representative TEM images of α -Syn aggregates of strain A (D and G), strain B (E and H), and strain C (F and I), obtained in the presence (G–I) or absence (D–F) of SC-D. Scale bars correspond to 2 μ m and 200 nm for main images and insets, respectively. TEM, transmission electron microscopy; Th-T; thioflavin-T.

buffer C might be related to the fact that it is the buffer that resembles more in ionic strength to the one in which we performed the initial screening, and SC-D was shown to bind preferentially to fibrillar structures in this condition.

SC-D disrupts preformed aggregates of different strains

In a previous study, SC-D evidenced fibril disaggregation capacity (30). Importantly, the compound could partially

disassemble the preformed mature fibrils of the different strains formed after 48 h of incubation (Fig. 4). Strain A exhibited the highest levels of Th-T reduction after 24 h of incubation with 100 μ M of SC-D (Fig. 4A), with a decrease of 71%. Light scattering was also reduced in 53% at 340 nm (Fig. 4B). This indicated that SC-D was active against both the fibrillar and nonfibrillar assemblies formed at acidic pH, which was corroborated by TEM images of SC-D-incubated samples (Fig. 4, C and D). Strain C Th-T signal decreased by 57% upon

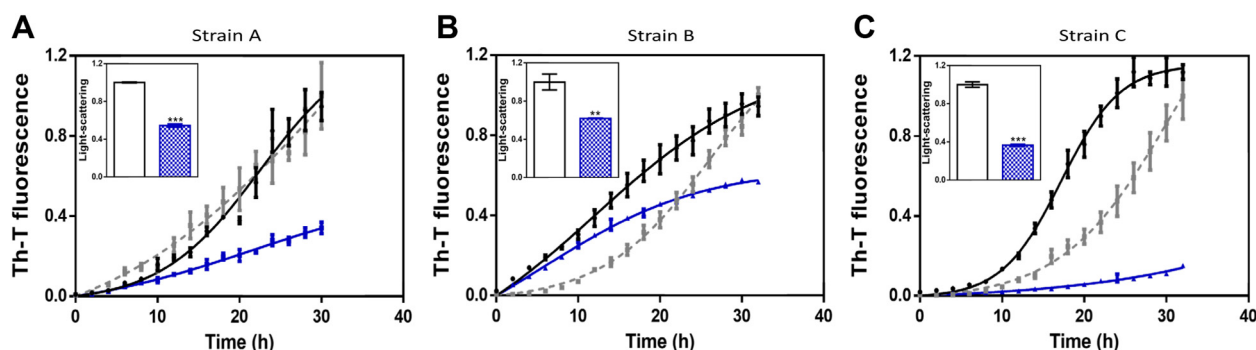


Figure 3. Seeding assays with three different strains. A–C, aggregation kinetics and final point light scattering measurements (insets) of α -Syn in buffer A (A), buffer B (B), or buffer C (C) in the absence of compounds and seeds (gray dotted line), in the presence of 1% (v/v) of preformed seeds at the specific condition (black), or in the presence of seeds and 100 μ M of SC-D (blue). Th-T fluorescence is plotted as normalized means. Normalized light scattering of treated (blue) and untreated (white) seeded samples at final point for each strain is shown as inset. Error bars are shown as standard errors of mean values; $**p < 0.01$ and $***p < 0.001$. α -Syn, α -synuclein; SC-D, SynuClean-D.

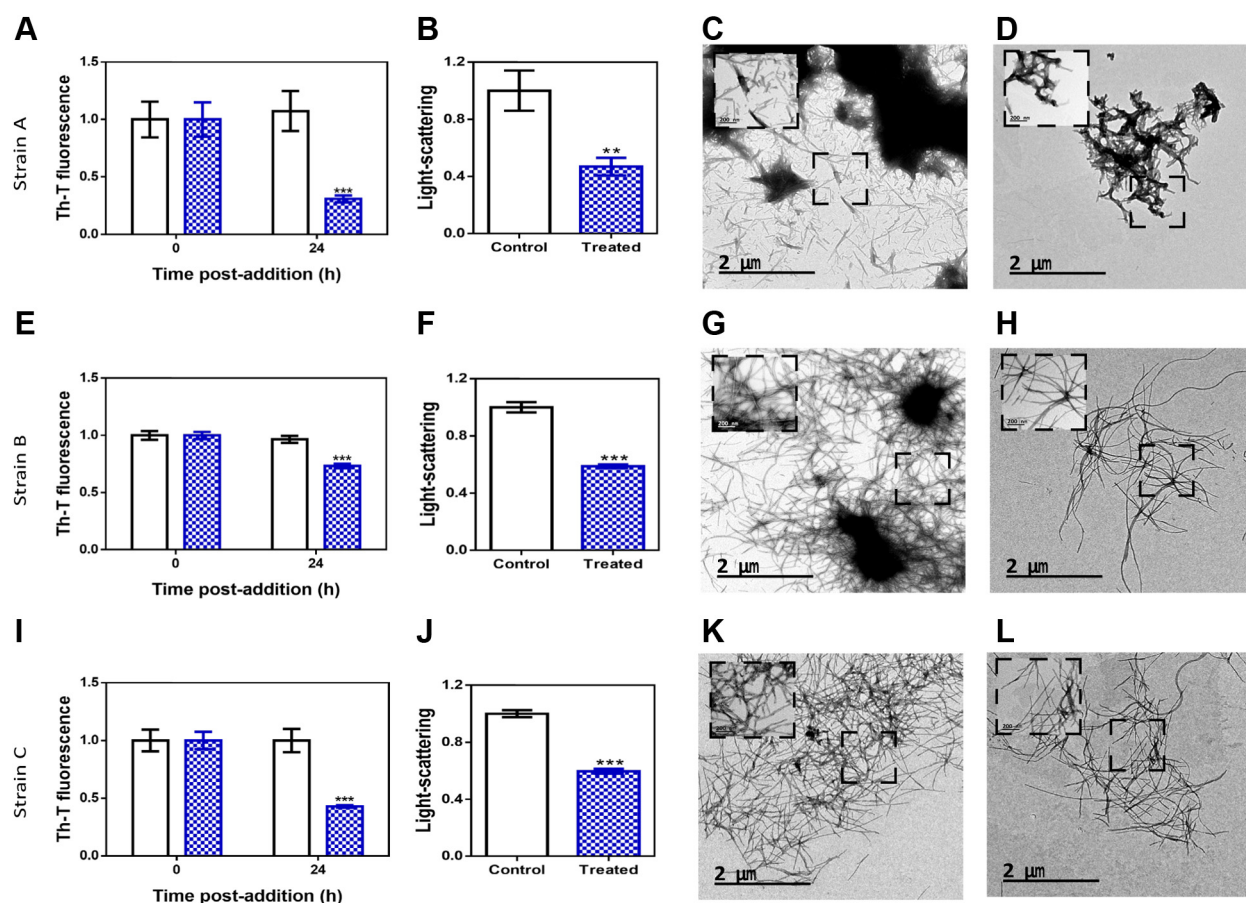


Figure 4. Disaggregational effect of SynuClean-D (SC-D). A, E, and I, Th-T-derived fluorescence assays before (black) and after (blue) the addition of SC-D to strain A (A), strain B (E), and strain C (I) preformed α -Syn fibrils. B, F, and J, final point light-scattering measurements in absence (black) and after (blue) the addition of SC-D to strain A (B), strain B (F), and strain C (J) mature α -Syn fibrils. Th-T fluorescence and light scattering are plotted as normalized means. Error bars are shown as standard errors of mean values. C–D, G–H, and K–L, representative TEM images of strain A (C–D), B (G–H), and C (K–L) aggregates in the absence (C, G, and K) or presence of SC-D (D, H, and L). Scale bars correspond to 2 μ m and 200 nm for main images and insets, respectively; ** p < 0.01 and *** p < 0.001. α -Syn, α -synuclein; TEM, transmission electron microscopy; Th-T; thioflavin-T.

incubation with the molecule (Fig. 4I), whereas the impact on strain B was more moderate with a 27% reduction (Fig. 4E). Overall, the disrupting activity of SC-D on top of the different strains seems to correlate with its ability to interfere with the formation of Th-T-positive species in seeded polymerization reactions.

For both strains formed at pH 7.5, the reduction in light scattering upon SC-D addition was similar, ranging between 30 and 40% (Fig. 4, F and J). Consistently, with Th-T and light scattering data, TEM analysis of strains B and C demonstrated a significant reduction in the number of fibrils and fibril clusters for samples incubated with the molecule (Fig. 4, H and L), relative to the respective controls (Fig. 4, G and K). Overall, SC-D demonstrated significant and strain-dependent fibril dismantling activity.

α -Syn aggregates formed in the presence of SC-D show reduced seeding activity in cell culture models

We next investigated the effect of the different α -Syn fibril strains on the aggregation of endogenous α -Syn, using a stable human embryonic kidney cells 293 (HEK293) cell line that

expresses α -Syn fused with enhanced green fluorescence protein (EGFP), called HEK293- α -Syn-EGFP (33, 34). In this cellular model, endogenous aggregation of α -Syn can be induced by the administration of exogenous seeds. In addition, endogenous α -Syn aggregation is accompanied by an increase in phosphorylation at serine 129 (S129), recapitulating what is observed in animal models and in the brain of patients with PD (35–38). Here, we incubated HEK293- α -Syn-EGFP cells with the different aggregated α -Syn strains, A, B, and C (100 nM), and performed immunocytochemistry (ICC) experiments with an antibody against phosphorylated α -Syn at S129 (pS129) to identify seed-promoted endogenous intracellular inclusions. The α -Syn strains were pelleted and washed with Milli Q water four times under sterile conditions; this process did not alter their physicochemical and morphological properties (Fig. S4). Then, they were diluted in PBS, sonicated, and diluted in the cell culture media and further incubated for 4 days. The same volume of PBS, buffers A, B, and C, was added to control cells.

The percentage of cells with intracellular accumulation of α -Syn-EGFP was first determined. Importantly, we did not observe any α -Syn-EGFP or pS129-positive inclusions after treatment only with PBS and buffers A, B, and C (Fig. S5). In

SC-D inhibits α -synuclein strains aggregation

contrast, we found that treatment with seeds of the strain B led to a statistically significant increase of the α -Syn-EGFP inclusions compared to the cells treated with seeds of the strains A and C (Fig. 5A). Likewise, quantification of the pS129-positive inclusions revealed a significant increase upon treatment with strain B, whereas strains A and C did not affect the percentage of cells with pS129 inclusions (Fig. 5A).

These data indicate that strain B is the only one able to propagate effectively in this cell model. When the α -Syn aggregation reaction in buffer B was done in the presence of SC-D and the sample sonicated and added to the cell culture, the number of α -Syn-EGFP aggregates and especially of pS129-positive inclusions decreased significantly (Fig. 5, A and B), with respect to untreated fibrils, indicating that the molecule interfered with the exogenous seeding of intracellular α -Syn.

Discussion

Prion-like proteins can aggregate into multiple fibrillar structures. This conformational heterogeneity might explain why a single amyloidogenic protein is behind the development of disorders with diverse phenotypic traits (19, 39). As for what refers to α -Syn, evidence on structural fibrillar plasticity and its linkage to diverse synucleinopathies is progressively accumulating (13–15, 17–22). The administration of brain extracts from patients with PD or MSA into mice brains resulted in a different lesion pattern and symptomatology (40). In addition, when different recombinant α -Syn polymorphs are administered to cells and animals, the damage caused and the area of the brain that is affected vary; the different conformations, aggregation, and transmission propensity of these multiple fibrillar structures are thought to be the ultimate cause of such differential effect (9, 20). This has important implications for treating synucleinopathies since each of these disorders might need specific drugs.

Different small molecules have been described to modulate α -Syn amyloidogenesis. These include compounds that, as SC-D, interact with aggregated forms of α -Syn like anle138b, a molecule that targets oligomeric but not monomeric α -Syn (23, 24), reducing aggregation and eliciting neuroprotection in

animal models of PD (41). Another class of compounds target monomeric α -Syn, such as fasudil and BIOD303, which stabilize the native protein conformation and reduce aggregation in cellular and animal models of PD (27, 28). Finally, molecules like squalamine and trodusquemine act on destabilizing α -Syn-membrane contacts and interact with the protein's negatively charged C-terminal domain (25, 26), displacing oligomeric species from cellular membranes and thus reducing their toxicity (42, 43). Furthermore, as SC-D, trodusquemine can prevent seeding-mediated aggregation of α -Syn and has shown to be effective in the same *Caenorhabditis elegans* model of PD (26). Thus, different conformations of α -Syn can now be targeted effectively, but we lack information on how the activity of these molecules depends on the aggregation conditions. In this study, we analyzed the different properties, aggregation propensities, and seeding capacity of three alternative polymorphs of α -Syn *in vitro* and in a cellular model to decipher how the activity of SC-D responds in front of different α -Syn amyloid formation scenarios.

Our study confirms a clear pH and salt dependence of the *in vitro* aggregation of α -Syn, indicating a critical role of the chemical conditions of the microenvironment surrounding the nascent aggregate. In agreement with previous data, aggregation at acidic pH is fast (44–47). This comes at the expense of the formation of abundant aggregates of lower amyloid content than at neutral pH, as deduced from Th-T, scattering, and FTIR analysis (Fig. 1 and Table S1). TEM images confirmed that short amyloid fibrils coexist with large amorphous aggregates (Figs. 1 and S2). These aggregates are significantly resistant to proteolysis but display low seeding capability *in vitro* (Fig. 3), likely due to the low proportion of ordered fibrils that can act as fibrillization nuclei. Accordingly, when exogenously applied to cells, strain A has a negligible impact on the formation of endogenous aggregated and phosphorylated α -Syn (Fig. 5). The C-terminal region of α -Syn (residues 96–140) is very acidic (10 Glu + 5 Asp), and it regulates aggregation since C-terminally truncated α -Syn aggregates faster than the full-length protein (48, 49). It is likely the impact of acidic pH in the protonation state of this region that accounts for the aggregation properties of strain A (47). SC-D

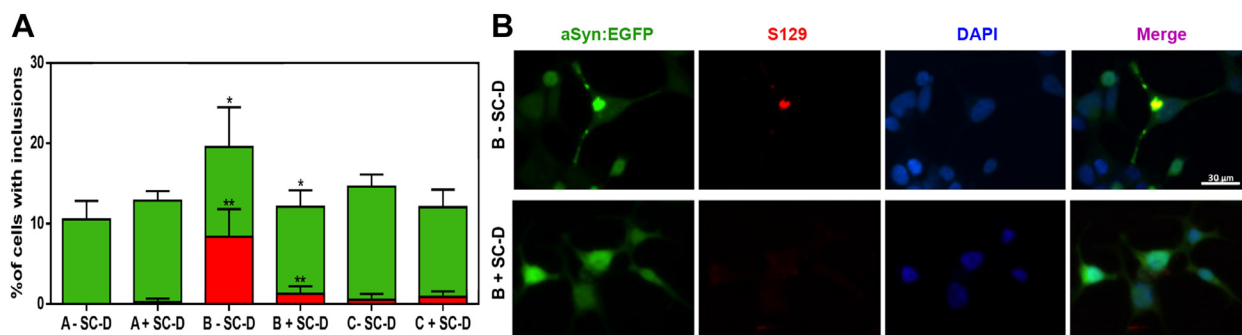


Figure 5. Effect of α -Syn strains in aggregation of endogenously expressed α -Syn-EGFP. A, quantification of the percentage of cells with inclusions shows that α -Syn-EGFP (green) and pS129 positive (red) inclusions are increased under treatment with strain B. Treatment α -Syn strain B with SC-D leads to a decrease in phosphorylated α -Syn inclusions (red) and the total level of inclusions (green). B, representative images from strain B \pm SC-D buffer. Treatment with the α -Syn strain B-SC-D at the concentration of 100 nM for 4 days revealed the formation of α -Syn inclusions phosphorylated in S129. Representative images of cells under the treatment with B strain \pm SC-D buffer (Scale bar 30 μ m). DAPI was used for nuclear staining. Data are shown as mean \pm SD (>100 cells counted per condition, four independent experiments); * $p < 0.05$ and ** $p < 0.01$. α -Syn, α -synuclein; DAPI, 4',6'-diamidino-2-phenylindol; EGFP, enhanced GFP; pS129, phosphorylated S129; SC-D, SynuClean-D.

can inhibit the aggregation of α -Syn into strain A amyloid-like structures, as measured by Th-T, but it is especially active in inhibiting the formation of the predominant, amorphous, β -sheet-containing α -Syn aggregates formed at low pH as reported by light scattering and TEM data (Fig. 2). It also effectively disaggregates the mature ordered and nonordered α -Syn aggregates formed in this condition (Fig. 4). Surprisingly, SC-D is very good at inhibiting the seeded aggregation of strain A, which suggests that the species formed at pH 5.0 in the absence and presence of seeds differ conformationally and that SC-D recognizes the later ones preferentially (Fig. 3).

In contrast to pH 5.0, α -Syn aggregation at pH 7.5 results in the formation of regular amyloid fibrils with significantly higher Th-T binding and lower scattering relative to aggregates formed under acidic conditions (Fig. 1). However, the properties of these assemblies are strongly dependent on the salt content of the solution. Fibrils formed in the presence of physiological salt concentrations (strain C) display a higher β -sheet content and bind Th-T with higher affinity than those formed in its absence (strain B) (Fig. 1 and Table S1). Accordingly, strain C is significantly more resistant to proteolysis and chemical denaturation than strain B (Figs. 1 and S3). Previous studies suggested that the presence of salt induces high-level compaction of mature fibrils by hiding the C-terminal acidic domain of α -Syn (31, 50), which might account for the observed conformational and stability differences between strains B and C. The fibrils formed in both conditions seeded the *in vitro* aggregation of soluble α -Syn, but the seeding effect is more substantial for strain B, where the seeds completely abrogate the lag phase of the polymerization reaction (Fig. 3). This differential seeding capability is translated to the cellular model, with strain B significantly stimulating the aggregation of endogenous α -Syn and the accumulation of pS129 α -Syn (Fig. 5). In contrast, strain C had a lower effect on aggregation and a negligible impact on pS129 inclusion formation (Fig. 5). These properties fairly correlated with those observed when injecting α -Syn fibrils formed under the same solution conditions as our study into the striatum of mice, with the fibrils formed in the absence of KCl inducing abnormal phosphorylated α -Syn deposits through the mouse brain, whereas few pS129-positive deposits were induced by the fibrils formed in the presence of KCl (31). Salt-induced compaction and masking of the C-terminal region in strain C might explain these differences since recent studies indicate that cell surface receptors that bind α -Syn in the amyloid state to initiate cell-to-cell transmission recognize this acidic region when it is exposed at the surface of the fibrils, as it would be in strain B due to uncompensated electrostatic repulsion in the absence of salts (51). SC-D is very effective at inhibiting the aggregation of strains B and C both in the absence and the presence of seeds (Figs. 2 and 3) and acts as a fibril-disaggregating molecule for both polymorphs (Fig. 4). However, as a general trend, SC-D performs better with strain C, especially in seeded aggregation (Fig. 3), likely because the conditions in which these assemblies form resemble more in terms of salt content than those in which we performed the assay in which SC-D was initially identified. Irrespective of

that, SC-D blocks the *in cell* seeding potential of strain B, decreasing the number of intracellular aggregates and, especially, of phosphorylated α -Syn inclusions (Fig. 5).

Overall, the results confirm the sensitivity of α -Syn aggregation to the solution conditions and converge to indicate that SC-D acts as a pan-inhibitor of the spontaneous and seeded formation of different α -Syn amyloid polymorphs, being able to partially disentangle them and eventually prevent the induction of intracellular aggregates by exogenous seeds. This generic property might be related to the fact that, according to previous molecular dynamic simulations (30), SC-D preferentially targets residues within (Glu61, Thr72, and Gly73) or close to (Ala53, Val55, and Thr59) the non-amyloid component domain (Fig. S6), which are expected to be relevant for α -Syn aggregation in all the assayed conditions. However, it is also clear that the activity of this molecule differs between strains, suggesting the establishment of conformation-dependent interactions with the different intermediate species. It is worth remarking that the highest SC-D activity occurs in solution conditions that resemble most those of the initial screening study, which suggests that, in principle, one can set up drug discovery assays to identify molecules that target preferentially a specific, biologically relevant, α -Syn polymorph. Meanwhile, the generic activity of SC-D positions this aromatic molecule as a hit compound from which evolve potentially active drugs for the different synucleinopathies.

Experimental procedures

Protein expression and purification

The expression and purification of α -Syn was carried out in *Escherichia coli* BL21 DE3 strain as previously described (52). Briefly, *E. coli* BL21 (DE3) containing a pET21a plasmid encoding for the α -Syn complementary DNA were grown in LB medium containing 100 μ M/ml ampicillin and induced with 1 mM IPTG for 4 h at an absorbance of 600 nm of 0.6. Cells were recovered by centrifugation and washed up by resuspension and centrifugation in PBS, pH 7.4. Pellets were stored at -80°C until used, when pellets were resuspended in 50 ml per culture liter in lysis buffer (50 mM Tris pH 8, 150 mM NaCl, 1 μ g/ml pepstatin, 20 μ g/ml aprotinin, 1 mM benzamidine, 1 mM PMSF, 1 mM EDTA, and 0.25 mg/ml lysozyme) and sonicated using a LABSONICU sonicator (B. Braun Biotech International). Then, sonicated samples were boiled for 10 min at 95°C and centrifuged at 20,000g at 4°C for 40 min. The soluble fraction was treated with 136 μ l/ml of 10% w/v streptomycin sulfate and 228 μ l/ml of pure acetic acid and centrifuged at 20,000g at 4°C for 10 min. Upon centrifugation, soluble extracts were fractionated by adding 1:1 of saturated ammonium sulfate. Samples were centrifuged for 10 min at 20,000g and 4°C , and the resultant pellets resuspended with 50% ammonium sulfate. After centrifugation (at 20,000g and 4°C for 10 min), the pellet was resuspended in 100 mM, pH 8, ammonium acetate (5 ml per culture liter) and pure EtOH 1:1 (v/v) and harvested by centrifugation for 10 min at 20,000g at 4°C . The insoluble fraction was resuspended in Tris 20 mM pH 8, filtered with a 0.22- μ m filter, and

SC-D inhibits α -synuclein strains aggregation

loaded into an anion exchange column HiTrap Q HP (GE Healthcare) coupled to an ÄKTA purifier high-performance liquid chromatography system (GE Healthcare). Tris 20 mM, pH 8, and NaCl 1 M were used as buffer A and buffer B. α S was eluted using a step gradient: step 1, 0 to 20% buffer B, 5 cv; step 2, 20 to 45% buffer B, 11 cv; step 3, 100% buffer B, 5 cv. Purified α S was dialyzed against 5 L of ammonium acetate 50 mM in two steps: 4 h and overnight. The obtained protein was lyophilized and stored at -80°C until used in the experiments.

Sample preparation

Lyophilized α -Syn was resuspended in PBS 1X to a final concentration of 210 μM and dialyzed in a 1:1000 (v/v) ratio in the presence of buffer A (50 mM sodium acetate pH 5.0), buffer B (50 mM Tris-HCl pH 7.5), or buffer C (50 mM Tris-HCl pH 7.5 supplemented with 150 mM KCl) for 24 h. Protein was filtered through a 22- μm membrane to eliminate small aggregates of α -Syn, and sample concentration was measured at 280 nm in a spectrophotometer Cary100 (Agilent) using the extinction coefficient $5960\text{ M}^{-1}\text{ cm}^{-1}$. SC-D (5-nitro-6-(3-nitrophenyl)-2-oxo-4-(trifluoromethyl)-1H-pyridine-3-carbonitrile) was resuspended in 100% dimethyl sulfoxide (DMSO) to a final concentration of 50 mM as preservation stock and kept stored at -20°C . Working solutions of 4 mM SC-D in 100% were prepared for the different experiments just before use.

Protein aggregation assays

The aggregation was performed on a 96-well sealed plate, containing in each well 70 μM α -Syn (in buffer A, B, or C), 40 μM Th-T, a 1/8" diameter Teflon polyball (Polysciences Europe GmbH), and SC-D at 100 μM . Briefly, 3.75 μL of 4 mM SC-D stock was added to each well; 3.75 μL of 100% DMSO was added instead to control samples. The final volume was 150 μL (2.5% DMSO in the assay solution). The plate was fixed into an orbital Max-Q 4000 (ThermoScientific) and constantly agitated at 100 rpm and 37°C . Th-T fluorescence was measured every 2 h by exciting through a 430- to 450-nm filter and collecting the emission signal with a 480- to 510-nm filter, using a Victor3.0 Multilabel Reader (PerkinElmer). All the assays were done in triplicate. Data were normalized and represented as mean and SEM and fitted with GraphPad Prism 6.0 software (GraphPad Software Inc) using the following equation:

$$\propto 1 - \frac{1}{k_b(e^{k_b t} - 1) + 1}$$

accounting k_b and k_a for the homogeneous nucleation rate constant and the secondary rate constant (fibril elongation and secondary nucleation), respectively (53).

For the seeding assays, 1% (v/v) of preformed α -Syn fibrils were added to their corresponding condition after a sonication process of 5 min at intensity 9 with a Ultrasonic Cleaner sonicator (VWR International). As previously mentioned,

aggregation was performed in a 96-well sealed plate, containing in each well 70 μM α -Syn (in buffer A, B, or C), 40 μM Th-T, a 1/8" diameter Teflon polyball, and SC-D at 100 μM in a total volume of 150 μL (2.5% DMSO final concentration). Control samples contained the corresponding amount of DMSO (2.5% final concentration). The plate was fixed into an orbital Max-Q 4000 (ThermoScientific) and constantly agitated at 100 rpm and 37°C , and Th-T fluorescence measured every 2 h as previously indicated.

In the disaggregation assays, 70 μM α -Syn was incubated for 48 h at 100 rpm and 37°C in a 96-well sealed plate, which also contains in each well 40 μM Th-T and a 1/8" diameter Teflon polyball. After 48 h, aggregated samples were exposed to 100 μM of SC-D or 2.5% of DMSO in controls. The plate was incubated for an additional period of 24 h at 100 rpm and 37°C in an orbital Max-Q 4000, and Th-T fluorescence measured at final point as before.

TEM

Aggregated samples were diluted 1:10 in PBS 1X and softly sonicated for 5 min at intensity 2 with a Ultrasonic Cleaner sonicator (VWR International) to avoid large accumulations of fibrils. Immediately, 5 μL of the samples was placed on a carbon-coated copper grid. Grids were carefully dried 5 min later with a filter paper to remove the excess of sample and washed in Mili-Q water twice. Finally, 5 μL of 2% (w/v) uranyl acetate was added on the top of the grid for 2 min and then removed with a filter paper. Grids were left to air-dry for 10 min. Representative images were obtained screening a minimum of 30 fields per sample and using a Transmission Electron Microscopy Jeol 1400 (Peabody) operating at an accelerating voltage of 120 kV.

Light scattering

In all the assays, final-point-aggregated protein samples were carefully resuspended and recovered to measure the total aggregate formation. To a quartz cuvette, 80 μL of aggregated samples were added and excited at 340 nm to collect 90° scattering from 320 to 360 nm in a Cary Eclipse Fluorescence Spectrophotometer (Agilent).

Secondary structure determination

ATR-FTIR spectroscopy analysis of amyloid fibrils was performed using a Bruker Tensor 27 FTIR Spectrometer (Bruker Optics Inc) with a Golden Gate MKII ATR accessory. Each spectrum consists of 16 independent scans, measured at a spectral resolution of 4 cm^{-1} , within the 1800- to 1500-cm^{-1} range. Second derivatives of the spectra were used to determine the frequencies at which the different spectral components were located. Fourier-deconvolution and determination of band position of the original amide I band were performed using PeakFit software (Systat Software).

PK digestion

Eighteen microliters of aggregated α -Syn at final point was mixed with 6 μL of PK, rendering a final concentration of

5 μ g/ml, and incubated for 5 min at 37 °C. Then, 8 μ l of loading buffer containing 1% β -mercaptoethanol was added and the enzyme thermally inactivated for 10 min at 95 °C in a ThermoCell cooling & heating block (BIOER). Finally, 7 μ l of the samples was loaded into a 12% SDS-PAGE, later stained with Blue Safe.

Mature fibril denaturation

For denaturation assays of strains B and C, 70 μ M α -Syn was incubated for 48 h in the presence of DMSO and Th-T as described previously. The resultant aggregates were carefully resuspended and recovered. For chemical denaturation, 500 μ l of aggregated α -Syn fibrils was mixed with 4 M urea (final concentration) in a quartz cuvette (1 ml final volume) and incubated for 2000 s at 37 °C under constant agitation (150 rpm). Meanwhile, Th-T fluorescence was recorded in a Cary Eclipse Fluorescence Spectrophotometer (Agilent) with a data pitch of 1 s using an excitation wavelength of 445 nm and recorded at 485 nm with an excitation and emission bandwidth of 2.5 and 5 nm, respectively (54). Denaturing curves were fitted to a one-step reaction using GraphPad Prism 5 (GraphPad Software).

Cell culture, cell treatment, and ICC

HEK293 stably expressing WT α -Syn fused to EGFP (HEK293- α -Syn-EGFP), under the cytomegalovirus promoter, was used for the seeding experiments (34). Cells were maintained in Dulbecco's modified Eagle's medium supplemented with 10% fetal bovine serum Gold (PAA) and 1% penicillin-streptomycin (PAN). Cells were grown at 37 °C in an atmosphere of 5% CO₂. For the seeding experiments, cells were plated on 13-mm glass coverslips in 24-well plates and incubated in 5% fetal bovine serum media. The following day, α -Syn strains were diluted in PBS, fragmented by sonication (55) and then added to cells at a final concentration of 100 nM. The fibrils were prepared in an aggregation reaction starting from 70 μ M of monomeric α -Syn, in the absence or presence of 100 μ M of SC-D and the corresponding proportion of DMSO for 48 h at 100 rpm and 37 °C. Preformed fibrils (PFFs) were then recovered and centrifuged at 14,000 rpm for 30 min. The supernatant was discarded, and the pellet resuspended in Milli-Q water under sterile conditions. PFFs were then centrifuged again at 14,000 rpm for 30 min, and the pellet was resuspended in Milli-Q water under sterile conditions. This step was repeated three additional times. We performed the imaging in 24-well dishes (with volume media 0.5 ml/well) and calculated to add 50 μ l of PBS or PFFs (dilution 1:10). We prepared seeds by adding PFFs to sterile PBS to a final concentration of 1 μ M. The minimal volume that can be used for sonication is 200 μ l. We diluted 50 μ l of sonicated PFFs or an equivalent volume of PBS as a control, into prewarmed cell media (1:10 dilution). We checked our PFF preparations, and we did not detect amorphous aggregates during the preparation. Control cells were exposed to vehicle only (PBS). Cells were further incubated for 4 days. ICC was carried out using standard protocols. Briefly, after treatment, the cells were

washed first with PBS and then with diluted 1:10 trypsin, fixed with 4% paraformaldehyde for 20 min at room temperature (RT), permeabilized with 0.5% Triton X-100 (Sigma-Aldrich) for 20 min at RT, and blocked in 1.5% bovine serum albumin/Dulbecco's PBS for 1 h. Cells were incubated with primary antibody overnight (1:1000; anti-pS129- α -syn Rabbit Ab51253 Abcam) and secondary antibody Alexa Fluor 555 goat anti-rabbit immunoglobulin G (Life Technologies-Invitrogen) for 2 h at RT, followed by nuclei staining with 4',6'-diamidino-2-phenylindol (Sigma-Aldrich, D8417) (1:5000 in Dulbecco's PBS) for 10 min. After a final wash, coverslips were mounted by using Mowiol (Sigma-Aldrich) and subjected to fluorescence microscopy.

The proportion of cells with α -Syn inclusions within the population was then determined by counting. Each experiment was reproduced at least three independent times. Data were analyzed using a *t* test. For quantification of aggregation, at least 100 cells were counted per variant and per experiment. Images were acquired using a 63 \times objective lens and analyzed using LAS AF, version 2.2.1 (Leica Microsystems) software.

Statistical analysis

All graphs were generated with GraphPad Prism 6.0 software (GraphPad Software Inc). Data were analyzed by two-way ANOVA and Tukey's Honestly Significant Difference test using SPSS software, version 20.0 (IBM Analytics). All data are shown as means and SEM. *p* < 0.05 was considered statistically significant. In the graphs, *, **, and *** indicate *p* < 0.05, *p* < 0.01, and *p* < 0.001, respectively. For cellular assays, statistical analysis was done using the Student's *t* test for independent variables and the data were presented as mean \pm standard deviations and represent results from at least four independent experiments.

Data availability

All data are contained within the manuscript.

Supporting information—This article contains supporting information (30).

Acknowledgments—We thank the Servei de Microscòpia at Universitat Autònoma de Barcelona for their help with TEM.

Author contributions—S. P.-D., J. P., and S. V. conceptualization; S. P.-D., J. P., E. V., F. P., J. S., and Z. M.-A. methodology; S. P.-D., J. P., E. V., S. V., and T. F. O. validation; S. P.-D. and S. V., formal analysis; S. P.-D., J. P., E. V., F. P., J. S., and Z. M.-A. investigation; S. P.-D. and S. V., writing—original draft; Z. M.-A. and S. V. supervision; T. F. O. and S. V. project administration; T. F. O. and S. V. funding acquisition.

Funding and additional information—S. V. was supported by the Spanish Ministry of Science and Innovation (PID2019-105017RB-I00), ICREA (ICREA-Academia 2015 and 2020), and the Fundación La Marató de TV3 (Ref. 20144330). T. F. O. was supported by the Deutsche Forschungsgemeinschaft (DFG, German Research Foundation) under Germany's Excellence Strategy (EXC 2067/1-390729940) and by SFB1286 (Project B8).

SC-D inhibits α -synuclein strains aggregation

Conflict of interest—The authors declare that they have no conflicts of interest with the contents of this article.

Abbreviations—The abbreviations used are: α -Syn, α -synuclein; AD, Alzheimer's disease; ATR, attenuated total reflectance; DMSO, dimethyl sulfoxide; EGFP, enhanced GFP; HEK293, human embryonic kidney cells 293; ICC, immunocytochemistry; MSA, multiple system atrophy; PFF, preformed fibril; PK, proteinase K; pS129, phosphorylated S129; RT, room temperature; S129, serine 129; SC-D, SynuClean-D; TEM, transmission electron microscopy; Th-T, thioflavin-T.

References

1. Kalia, L. V., and Lang, A. E. (2015) Parkinson's disease. *Lancet* **386**, 896–912
2. Dexter, D. T., and Jenner, P. (2013) Parkinson disease: From pathology to molecular disease mechanisms. *Free Radic. Biol. Med.* **62**, 132–144
3. Marti, M. J., Tolosa, E., and Campdelacreu, J. (2003) Clinical overview of the synucleinopathies. *Mov. Disord.* **18**, S21–S27
4. Bethlem, J., and Den Hartog Jager, W. A. (1960) The incidence and characteristics of Lewy bodies in idiopathic paralysis agitans (Parkinson's disease). *J. Neurol. Neurosurg. Psychiatry* **23**, 74–80
5. Spillantini, M. G., Schmidt, M. L., Lee, V. M., Trojanowski, J. Q., Jakes, R., and Goedert, M. (1997) Alpha-synuclein in Lewy bodies. *Nature* **388**, 839–840
6. Serpell, L. C., Berriman, J., Jakes, R., Goedert, M., and Crowther, R. A. (2000) Fiber diffraction of synthetic alpha-synuclein filaments shows amyloid-like cross-beta conformation. *Proc. Natl. Acad. Sci. U. S. A.* **97**, 4897–4902
7. Bendor, J. T., Logan, T. P., and Edwards, R. H. (2013) The function of alpha-synuclein. *Neuron* **79**, 1044–1066
8. Alafuzoff, I., and Hartikainen, P. (2017) Alpha-synucleinopathies. *Handbook Clin. Neurol.* **145**, 339–353
9. Lau, A., So, R. W. L., Lau, H. H. C., Sang, J. C., Ruiz-Riquelme, A., Fleck, S. C., Stuart, E., Menon, S., Visanji, N. P., Meisl, G., Faidi, R., Marano, M. M., Schmitt-Ulms, C., Wang, Z., Fraser, P. E., et al. (2019) alpha-Synuclein strains target distinct brain regions and cell types. *Nat. Neurosci.* **23**, 21–31
10. Schweighauser, M., Shi, Y., Tarutani, A., Kametani, F., Murzin, A. G., Ghetti, B., Matsubara, T., Tomita, T., Ando, T., Hasegawa, K., Murayama, S., Yoshida, M., Hasegawa, M., Scheres, S. H. W., and Goedert, M. (2020) Structures of alpha-synuclein filaments from multiple system atrophy. *Nature* **585**, 464–469
11. Shah Nawaz, M., Mukherjee, A., Pritzkow, S., Mendez, N., Rabadia, P., Liu, X., Hu, B., Schmeichel, A., Singer, W., Wu, G., Tsai, A. L., Shirani, H., Nilsson, K. P. R., Low, P. A., and Soto, C. (2020) Discriminating alpha-synuclein strains in Parkinson's disease and multiple system atrophy. *Nature* **578**, 273–277
12. Aguzzi, A., Heikenwalder, M., and Polymenidou, M. (2007) Insights into prion strains and neurotoxicity. *Nat. Rev. Mol. Cell Biol.* **8**, 552–561
13. Luk, K. C., Kehm, V., Carroll, J., Zhang, B., O'Brien, P., Trojanowski, J. Q., and Lee, V. M. (2012) Pathological alpha-synuclein transmission initiates Parkinson-like neurodegeneration in nontransgenic mice. *Science* **338**, 949–953
14. Luk, K. C., Kehm, V. M., Zhang, B., O'Brien, P., Trojanowski, J. Q., and Lee, V. M. (2012) Intracerebral inoculation of pathological alpha-synuclein initiates a rapidly progressive neurodegenerative alpha-synucleinopathy in mice. *J. Exp. Med.* **209**, 975–986
15. Masuda-Suzukake, M., Nonaka, T., Hosokawa, M., Oikawa, T., Arai, T., Akiyama, H., Mann, D. M., and Hasegawa, M. (2013) Prion-like spreading of pathological alpha-synuclein in brain. *Brain* **136**, 1128–1138
16. Bousset, L., Pieri, L., Ruiz-Arlandis, G., Gath, J., Jensen, P. H., Habenstein, B., Madiona, K., Olieric, V., Bockmann, A., Meier, B. H., and Melki, R. (2013) Structural and functional characterization of two alpha-synuclein strains. *Nat. Commun.* **4**, 2575
17. Gribaud, S., Tixador, P., Bousset, L., Fenyi, A., Lino, P., Melki, R., Peyrin, J. M., and Perrier, A. L. (2019) Propagation of alpha-synuclein strains within human reconstructed neuronal network. *Stem Cell Rep.* **12**, 230–244
18. Guerrero-Ferreira, R., Taylor, N. M., Arteni, A. A., Kumari, P., Mona, D., Ringler, P., Britschgi, M., Lauer, M. E., Makky, A., Verasdonck, J., Riek, R., Melki, R., Meier, B. H., Bockmann, A., Bousset, L., et al. (2019) Two new polymorphic structures of human full-length alpha-synuclein fibrils solved by cryo-electron microscopy. *Elife* **8**, e56825
19. Peelaerts, W., and Baekelandt, V. (2016) α -Synuclein strains and the variable pathologies of synucleinopathies. *J. Neurochem.* **139**, 256–274
20. Peelaerts, W., Bousset, L., Van der Perren, A., Moskalyuk, A., Pulizzi, R., Giugliano, M., Van den Haute, C., Melki, R., and Baekelandt, V. (2015) alpha-Synuclein strains cause distinct synucleinopathies after local and systemic administration. *Nature* **522**, 340–344
21. Woerman, A. L., Oehler, A., Kazmi, S. A., Lee, J., Halliday, G. M., Middleton, L. T., Gentleman, S. M., Mordes, D. A., Spina, S., Grinberg, L. T., Olson, S. H., and Prusiner, S. B. (2019) Multiple system atrophy prions retain strain specificity after serial propagation in two different Tg(SNCA^{A53T}) mouse lines. *Acta Neuropathol.* **137**, 437–454
22. Froula, J. M., Castellana-Cruz, M., Anabtawi, N. M., Camino, J. D., Chen, S. W., Thrasher, D. R., Freire, J., Yazdi, A. A., Fleming, S., Dobson, C. M., Kumita, J. R., Cremades, N., and Volpicelli-Daley, L. A. (2019) Defining alpha-synuclein species responsible for Parkinson's disease phenotypes in mice. *J. Biol. Chem.* **294**, 10392–10406
23. Wagner, J., Ryazanov, S., Leonov, A., Levin, J., Shi, S., Schmidt, F., Prix, C., Pan-Montojo, F., Bertsch, U., Mitteregger-Kretzschmar, G., Geissen, M., Eiden, M., Leidel, F., Hirschberger, T., Deeg, A. A., et al. (2013) Anle138b: A novel oligomer modulator for disease-modifying therapy of neurodegenerative diseases such as prion and Parkinson's disease. *Acta Neuropathol.* **125**, 795–813
24. Dominguez-Mejide, A., Vasili, E., Konig, A., Cima-Omori, M. S., Ibanez de Opakua, A., Leonov, A., Ryazanov, S., Zweckstetter, M., Griesinger, C., and Outeiro, T. F. (2020) Effects of pharmacological modulators of alpha-synuclein and tau aggregation and internalization. *Sci. Rep.* **10**, 12827
25. Perni, M., Galvagnion, C., Maltsev, A., Meisl, G., Muller, M. B., Challa, P. K., Kirkegaard, J. B., Flagmeier, P., Cohen, S. I., Cascella, R., Chen, S. W., Limbicker, R., Sormanni, P., Heller, G. T., Aprile, F. A., et al. (2017) A natural product inhibits the initiation of alpha-synuclein aggregation and suppresses its toxicity. *Proc. Natl. Acad. Sci. U. S. A.* **114**, E1009–E1017
26. Perni, M., Flagmeier, P., Limbicker, R., Cascella, R., Aprile, F. A., Galvagnion, C., Heller, G. T., Meisl, G., Chen, S. W., Kumita, J. R., Challa, P. K., Kirkegaard, J. B., Cohen, S. I. A., Mannini, B., Barbut, D., et al. (2018) Multistep inhibition of alpha-synuclein aggregation and toxicity *in vitro* and *in vivo* by trodusquemine. *ACS Chem. Biol.* **13**, 2308–2319
27. Moree, B., Yin, G., Lazaro, D. F., Munari, F., Strohaber, T., Giller, K., Becker, S., Outeiro, T. F., Zweckstetter, M., and Salafsky, J. (2015) Small molecules detected by second-harmonic generation modulate the conformation of monomeric alpha-synuclein and reduce its aggregation in cells. *J. Biol. Chem.* **290**, 27582–27593
28. Tatenhorst, L., Eckermann, K., Dambeck, V., Fonseca-Ornelas, L., Walle, H., Lopes da Fonseca, T., Koch, J. C., Becker, S., Tonges, L., Bahr, M., Outeiro, T. F., Zweckstetter, M., and Lingor, P. (2016) Fasudil attenuates aggregation of alpha-synuclein in models of Parkinson's disease. *Acta Neuropathol. Commun.* **4**, 39
29. Peña-Díaz, S., Pujols, J., Conde-Giménez, M., Čarija, A., Dalfo, E., García, J., Navarro, S., Pinheiro, F., Santos, J., Salvatella, X., Sancho, J., and Ventura, S. (2019) ZPD-2, a small compound that inhibits α -synuclein amyloid aggregation and its seeded polymerization. *Front. Mol. Neurosci.* **12**, 306
30. Pujols, J., Pena-Diaz, S., Lazaro, D. F., Peccati, F., Pinheiro, F., Gonzalez, D., Carija, A., Navarro, S., Conde-Gimenez, M., Garcia, J., Guardiola, S., Giral, E., Salvatella, X., Sancho, J., Sodupe, M., et al. (2018) Small molecule inhibits alpha-synuclein aggregation, disrupts amyloid fibrils, and prevents degeneration of dopaminergic neurons. *Proc. Natl. Acad. Sci. U. S. A.* **115**, 10481–10486
31. Suzuki, G., Imura, S., Hosokawa, M., Katsumata, R., Nonaka, T., Hisanaga, S. I., Saeki, Y., and Hasegawa, M. (2020) alpha-synuclein strains that cause distinct pathologies differentially inhibit proteasome. *Elife* **9**, e56825

32. Tornquist, M., Michaels, T. C. T., Sanagavarapu, K., Yang, X., Meisl, G., Cohen, S. I. A., Knowles, T. P. J., and Linse, S. (2018) Secondary nucleation in amyloid formation. *Chem. Commun.* **54**, 8667–8684
33. Hansen, C., Angot, E., Bergstrom, A. L., Steiner, J. A., Pieri, L., Paul, G., Outeiro, T. F., Melki, R., Kallunki, P., Fog, K., Li, J. Y., and Brundin, P. (2011) α -Synuclein propagates from mouse brain to grafted dopaminergic neurons and seeds aggregation in cultured human cells. *J. Clin. Invest.* **121**, 715–725
34. Vasili, E., Dominguez-Mejide, A., Flores-Leon, M., Al-Azzani, M., Kanellidi, A., Melki, R., Stefanis, L., and Outeiro, T. F. (2022) Endogenous levels of α -synuclein modulate seeding and aggregation in cultured cells. *Mol. Neurobiol.* **59**, 1273–1284
35. Vaikath, N. N., Erskine, D., Morris, C. M., Majbour, N. K., Vekrellis, K., Li, J. Y., and El-Agnaf, O. M. A. (2019) Heterogeneity in α -synuclein subtypes and their expression in cortical brain tissue lysates from Lewy body diseases and Alzheimer's disease. *Neuropathol. Appl. Neurobiol.* **45**, 597–608
36. Wang, Y., Shi, M., Chung, K. A., Zabetian, C. P., Leverenz, J. B., Berg, D., Srulijes, K., Trojanowski, J. Q., Lee, V. M., Siderowf, A. D., Hurtig, H., Litvan, I., Schiess, M. C., Peskind, E. R., Masuda, M., *et al.* (2012) Phosphorylated α -synuclein in Parkinson's disease. *Sci. Transl. Med.* **4**, 121ra120
37. Walker, D. G., Lue, L. F., Adler, C. H., Shill, H. A., Caviness, J. N., Sabagh, M. N., Akiyama, H., Serrano, G. E., Sue, L. I., Beach, T. G., and Arizona Parkinson Disease, C. (2013) Changes in properties of serine 129 phosphorylated α -synuclein with progression of Lewy-type histopathology in human brains. *Exp. Neurol.* **240**, 190–204
38. Delenclos, M., Farooqi, A. H., Yue, M., Kurti, A., Castanedes-Casey, M., Rousseau, L., Phillips, V., Dickson, D. W., Fryer, J. D., and McLean, P. J. (2017) Neonatal AAV delivery of α -synuclein induces pathology in the adult mouse brain. *Acta Neuropathol. Commun.* **5**, 51
39. Tanaka, M., Collins, S. R., Toyama, B. H., and Weissman, J. S. (2006) The physical basis of how prion conformations determine strain phenotypes. *Nature* **442**, 585–589
40. Yamasaki, T. R., Holmes, B. B., Furman, J. L., Dhavale, D. D., Su, B. W., Song, E. S., Cairns, N. J., Kotzbauer, P. T., and Diamond, M. I. (2019) Parkinson's disease and multiple system atrophy have distinct α -synuclein seed characteristics. *J. Biol. Chem.* **294**, 1045–1058
41. Levin, J., Schmidt, F., Boehm, C., Prix, C., Botzel, K., Ryazanov, S., Leonov, A., Griesinger, C., and Giese, A. (2014) The oligomer modulator anle138b inhibits disease progression in a Parkinson mouse model even with treatment started after disease onset. *Acta Neuropathol.* **127**, 779–780
42. Limbicker, R., Staats, R., Chia, S., Ruggeri, F. S., Mannini, B., Xu, C. K., Perni, M., Cascella, R., Bigi, A., Sasser, L. R., Block, N. R., Wright, A. K., Kreiser, R. P., Custy, E. T., Meisl, G., *et al.* (2021) Squalamine and its derivatives modulate the aggregation of amyloid-beta and α -synuclein and suppress the toxicity of their oligomers. *Front. Neurosci.* **15**, 680026
43. Limbicker, R., Mannini, B., Ruggeri, F. S., Cascella, R., Xu, C. K., Perni, M., Chia, S., Chen, S. W., Habchi, J., Bigi, A., Kreiser, R. P., Wright, A. K., Albright, J. A., Kartanas, T., Kumita, J. R., *et al.* (2020) Trodusquemine displaces protein misfolded oligomers from cell membranes and abrogates their cytotoxicity through a generic mechanism. *Commun. Biol.* **3**, 435
44. Santos, J., Iglesias, V., Santos-Suarez, J., Mangiagalli, M., Brocca, S., Palares, I., and Ventura, S. (2020) pH-dependent aggregation in intrinsically disordered proteins is determined by charge and lipophilicity. *Cells* **9**, 145
45. Uversky, V. N., Li, J., and Fink, A. L. (2001) Evidence for a partially folded intermediate in α -synuclein fibril formation. *J. Biol. Chem.* **276**, 10737–10744
46. McAllister, C., Karymov, M. A., Kawano, Y., Lushnikov, A. Y., Mikheikin, A., Uversky, V. N., and Lyubchenko, Y. L. (2005) Protein interactions and misfolding analyzed by AFM force spectroscopy. *J. Mol. Biol.* **354**, 1028–1042
47. Hoyer, W., Antony, T., Cherny, D., Heim, G., Jovin, T. M., and Subramaniam, V. (2002) Dependence of α -synuclein aggregate morphology on solution conditions. *J. Mol. Biol.* **322**, 383–393
48. Murray, I. V., Giasson, B. I., Quinn, S. M., Koppaka, V., Axelsen, P. H., Ischiropoulos, H., Trojanowski, J. Q., and Lee, V. M. (2003) Role of α -synuclein carboxy-terminus on fibril formation *in vitro*. *Biochemistry* **42**, 8530–8540
49. Gallardo, J., Escalona-Noguero, C., and Sot, B. (2020) Role of α -synuclein regions in nucleation and elongation of amyloid fiber assembly. *ACS Chem. Neurosci.* **11**, 872–879
50. Roeters, S. J., Iyer, A., Pletikapić, G., Kogan, V., Subramaniam, V., and Woutersen, S. (2017) Evidence for intramolecular antiparallel beta-sheet structure in α -synuclein fibrils from a combination of two-dimensional infrared spectroscopy and atomic force microscopy. *Sci. Rep.* **7**, 41051
51. Zhang, S., Liu, Y. Q., Jia, C., Lim, Y. J., Feng, G., Xu, E., Long, H., Kimura, Y., Tao, Y., Zhao, C., Wang, C., Liu, Z., Hu, J. J., Ma, M. R., Liu, Z., *et al.* (2021) Mechanistic basis for receptor-mediated pathological α -synuclein fibril cell-to-cell transmission in Parkinson's disease. *Proc. Natl. Acad. Sci. U. S. A.* **118**, e2011196118
52. Pujols, J., Pena-Diaz, S., Conde-Gimenez, M., Pinheiro, F., Navarro, S., Sancho, J., and Ventura, S. (2017) High-throughput screening methodology to identify α -synuclein aggregation inhibitors. *Int. J. Mol. Sci.* **18**, 478
53. Crespo, R., Villar-Alvarez, E., Taboada, P., Rocha, F. A., Damas, A. M., and Martins, P. M. (2016) What can the kinetics of amyloid fibril formation tell about off-pathway aggregation? *J. Biol. Chem.* **291**, 2018–2032
54. Diaz-Caballero, M., Navarro, S., Fuentes, I., Teixidor, F., and Ventura, S. (2018) Minimalist prion-inspired polar self-assembling peptides. *ACS Nano* **12**, 5394–5407
55. Volpicelli-Daley, L. A., Luk, K. C., and Lee, V. M. (2014) Addition of exogenous α -synuclein preformed fibrils to primary neuronal cultures to seed recruitment of endogenous α -synuclein to Lewy body and Lewy neurite-like aggregates. *Nat. Protoc.* **9**, 2135–2146

4. Concluding remarks

4.1. Chapter 1. High-throughput screening methodology to identify alpha-synuclein aggregation inhibitors

HTS methodologies provide a great opportunity to identify putative drugs directed to proteins that miss a defined three-dimensional structure. Nevertheless, HTS techniques to target protein aggregation usually lack reproducibility and robustness, while also requiring large amounts of protein and time. All in all, the protocol here described provides a robust way to produce substantial amount of α -Syn and to screen large chemical libraries in search of modulators of protein aggregation. Therefore, we can conclude that:

- The expression and purification systems here described constitute an easy-to-implement protocol that provides large amounts of highly pure and nucleic acid free α -Syn.
- The aggregation protocol here developed and optimised, reduces the variability of protein aggregation attributable by sample manipulation.
- By implementing 96-well plates and orbital agitation, we have increased the homogeneity of the sample and the reproducibility among different assays, which can be performed simultaneously.
- Teflon beads significantly accelerate α -Syn aggregation, while reducing variability and the amount of protein required for the assay.
- The applicability of this method was validated by analysing Maybridge HitFinder Collection chemical library with more than 14000 chemically diverse structures.
- Different mechanisms of action (Th-T reduction, aggregation delay or modification of kinetics constants) can be appreciated with this screening protocol.
- This aggregation protocol is also an important tool for the characterization of inhibitors, since can be adapted to carry out dose-response or time-addition studies.

To sum up, this protocol not only provides the basis for setting up a simple screening of anti-aggregational compounds with high accuracy and low errors, but also facilitates the *in vitro* characterisation of these candidates and the distinction of the targeted phase of the aggregation. Even though the presence of teflon beads may not perfectly reproduce *in vivo* aggregation and biased the screening towards aggregated species, it still provides important information of compounds targeting toxic species (as oligomers or fibrils) but not functional monomers in a reasonable period of time.

4.2. Chapter 2. Small molecule inhibits α -Synuclein aggregation, disrupts amyloid fibrils, and prevents degeneration of dopaminergic neurons

Current absence of effective disease-modifying therapies and the abundance of α -Syn inclusions in the affected cells, have turned amyloid aggregation of α -Syn mainstream in the search for treatments for PD. In the present work, we described a detailed *in vitro* and *in vivo* characterisation of the anti-aggregational properties of the small aromatic compound, SC-D. As a result of this study, the following points should be highlighted:

- SC-D inhibits α -Syn aggregation *in vitro* by modulating its autocatalytic rate constant in a 25 %, reducing then the formation of amyloid aggregates in a 53% and increasing t_{50} .
- Its inhibitory potential was validated with orthogonal techniques as light-scattering and TEM, which both conclude that the compound can reduce the number of aggregates.
- The aggregation of familial variants as H50Q and A30P could also be targeted by the administration of SC-D, but the different inhibition levels suggest a conformational/sequential dependent effect.
- Dose-response analysis demonstrated that SC-D is effective even in substoichiometric conditions with a 34 % of Th-T fluorescence reduction in a 7:1 protein:compound ratio.
- PMCA technique evinced that SC-D could target aggregated structures and prevent seeding capacity, but also suggested a putative disaggregational effect. Further Th-T, light-scattering and TEM analysis incubating mature fibrils with SC-D confirmed the disaggregational capacity of the compound.
- According to its capacity to modify the autocatalytic rate constant (accounting for fibril elongation and seeding), SC-D did not present any binding to monomeric and soluble α -Syn, as revealed by NMR. In agreement, docking simulations suggested that the compound could target the core of the fibril.
- Administration of SC-D to cellular and animal models of PD demonstrated that the compound significantly reduced the number of apparent aggregates and the aggregation-mediated neurodegeneration.

Thus, the aromatic nature of SC-D combined with its polar ramifications permitted significant aggregate binding, likely mediated by the hydrophobic aromatic region, and subsequent inhibition and disaggregation, which might be explained by the interaction's competition exerted by the molecule polar ramifications. Such preference against aggregated species might be the underlying cause of its neuroprotective capacity, which turn SC-D into a promising molecule to develop an effective, disease-modifying therapy for PD.

4.3. Chapter 3. ZPD-2, a Small Compound That Inhibits α -Synuclein Amyloid Aggregation and Its Seeded Polymerization

Together with SC-D, our HTS technology rendered a multitude of putative candidates to tackle α -Syn aggregation. The work here described characterised, *in vitro* and *in vivo*, the anti-aggregational mechanism of ZPD-2, an aromatic compound that shares common structural features with SC-D, but interestingly differs in the inhibitory activity. Overall, this research concludes that:

- ZPD-2 modifies the nucleation rate constant and the autocatalytic rate constant, reducing amyloids aggregates by an 80 % and increasing t_{50} up to 8 h. This inhibitory potential is validated with orthogonal techniques as light-scattering or TEM.
- The compound is capable to prevent aggregation at substoichiometric ratio (up to 49 % of inhibition at 7:1 protein:compound ratios), but preferentially targets early and intermediate structures as oligomers or protofibrils.
- Incubation with ZPD-2 significantly reduced the aggregation of H50Q and A30P variants of α -Syn, which favour oligomerisation.

- Seeding reactions were hampered in presence of ZPD-2 but there are not evidences of disaggregating capacity.
- ZPD-2 maintained its inhibitory and anti-seeding capacity in the presence of different strains of α -Syn.
- *In vivo* models of PD revealed that ZPD-2 moderately modulates protein aggregation and its derived neurotoxicity.

In light of this information, we can conclude that, despite sharing similar functional groups, the distribution and amount of the hydrophobic and polar ramifications influence the inhibitory mechanism of the compounds. In this case, all the data provided agree on the fact that ZPD-2 has a great ability to target intermediate structures as oligomers or protofibrils.

4.4. Chapter 4. Inhibition of α -Synuclein Aggregation and Mature Fibril Disassembling With a Minimalistic Compound, ZPDm

Found independently during the HTS analysis, ZPDm constitutes a minimalistic variant of ZPD-2 with better predicted pharmacological properties and a single aromatic ring. This chapter constitutes a detailed *in vitro* and *in vivo* characterisation of the inhibitory mechanism of ZPDm, which concludes that:

- ZPDm reduced the total amount of amyloid α -Syn by a 60 % and delays for 2 h t_{50} by modifying the primary nucleation rate constant. This inhibitory potential was validated with orthogonal techniques as light-scattering and TEM.
- Evaluation of (trifluoromethyl)benzene effect on α -Syn aggregation, revealed that this structure might be a building element of the structure without active effect on protein aggregation. This could be explained by the absence of potent hydrogen bonds donor/acceptors, characteristic of anti-aggregational molecular chaperones.
- As ZPD-2, ZPDm was active at substoichiometric conditions, reducing aggregation a 35 % in a 7:5 protein:compound ratio.
- ZPDm significantly inhibited the aggregation of H50Q and A30P variants, with a higher effect on H50Q aggregation, which presents an increased fibrillation tendency.
- PMCA technique evinced that ZPDm can tackle seeding reaction. Further analysis indicated that ZPDm preferentially targeted aggregated structures and dismantled preformed fibrils of multiple strains.
- *C. elegans* model of PD revealed that the administration of ZPDm at L4 stage is translated into a significant reduction in the number of apparent aggregates on body wall muscle cells.

ZPDm and ZPD-2 share an important part of their chemical structure but clearly differ in their anti-aggregational mechanisms. As both molecules present similar numbers of H-bonds donors/acceptors, the different hydrophobic content might be the responsible for their different affinity for α -Syn aggregates. ZPDm presents better pharmacological properties that make this compound a better candidate than ZPD-2 as an hypothetical treatment. When comparing the *C. elegans* results of SC-D, ZPD-2 and ZPDm we observed that those compounds with the capacity to target large aggregates presented better inhibitory capacities; this could be explained as L4 worms mimic aged PD patients and early and intermediate aggregates would not abound.

4.5. Chapter 5. The small aromatic compound SynuClean-D inhibits the aggregation and seeded polymerization of multiple α -Synuclein strains

Studies of *in vivo* α -Syn aggregates have demonstrated that fibril morphology and properties vary depending on the affected cell or tissue and, in consequence, on the particular synucleinopathy. Assessing whether the inhibitory potential of a compound varies depending on the generated strain has become thus a new challenge. With all this in mind, in this chapter we modified our aggregation protocol to generate multiple strains and evaluate the effect of a compound in detail. As a result of our work, it can be confirmed that:

- The protocol here described generated three diverse strains with different aggregation propensities, morphology, β -sheet content, and degradation resistance.
- Treatment with SC-D clearly inhibited aggregation of all strains but showed a greater effect on those obtained at neutral pH.
- Aggregates generated at neutral pH were capable to significantly seed the aggregation of monomeric α -Syn, whereas acidic fibrils did not show a significant increase in the aggregation rate.
- In presence of SC-D, seeded polymerisation was significantly reduced, but it showed a conformational-dependent effect, which was more potent when α -Syn aggregating under saline conditions.
- SC-D retained its disaggregational capacity in all three strains but the differential effect on the different polymorphs confirmed its conformational-dependent action.
- Cellular analysis proved that the propensity for aggregation propagation depends on the fibril structure, as previously reported. Furthermore, these studies suggested that treatment with SC-D either reduced their transmission capacity or produced a different structure with a lower seeding propensity.

The results derived from this study indicated that α -Syn aggregation is highly regulated by the environmental conditions, but also confirmed SC-D as a pluripotent modulator of protein aggregation. This generic inhibitory capacity may relay on the interactions of SC-D with residues within or close to the NAC domain, which would be crucial for fibril formation in any condition. Despite binding to the core of the fibril, there is a clear conformational dependence of the effect of SC-D, which could be explained by a differential interaction with intermediate species of the reactions. Altogether, SC-D is a promising candidate to treat different synucleinopathies or to develop drug-like molecules with a generic inhibitory capacity.

5. Annex: Supplementary information

- 5.1. Chapter 2. Small molecule inhibits α -Synuclein aggregation, disrupts amyloid fibrils, and prevents degeneration of dopaminergic neurons

Published at Proceedings of the National Academy of Sciences on October 2018

Available in: <https://www.pnas.org/content/115/41/10481.long>



Supplementary Information for

Small molecule inhibits α -Synuclein aggregation, disrupts amyloid fibrils and prevents degeneration of dopaminergic neurons

Jordi Pujols, Samuel Peña-Díaz, Diana F. Lázaro, Francesca Peccati, Francisca Pinheiro, Danilo González, Anita Carija, Susanna Navarro, María Conde-Giménez, Jesús García, Salvador Guardiola, Ernest Giralt, Xavier Salvatella, Javier Sancho, Mariona Sodupe, Tiago F. Outeiro, Esther Dalfó and Salvador Ventura

Salvador Ventura

Email: Salvador.Ventura@uab.es

This PDF file includes:

- Supplementary Information
- Text Figs. S1 to S10
- Table S1
- Captions for movies S1 to S2
- References for SI reference citations

Other supplementary materials for this manuscript include the following:

- Movies S1 to S2

www.pnas.org/cgi/doi/10.1073/pnas.1804198115

Supplementary Information Text

Materials and Methods

Protein Purification

cDNAs corresponding to WT α -Syn and A30P and H50Q mutants were cloned in a pET28(a) plasmid and transformed into an E. coli BL21 DE3 strain. WT α -Syn and its variants were expressed and purified as described previously (1). Samples were lyophilised and kept at -80°C until assayed.

Metabolic stability in human liver microsomes

SC-D at 0.1 μ M final concentration was pre-incubated with pooled human liver microsomes in phosphate buffer (pH 7.4) for 5 min in a 37 °C shaking water-bath (final microsomal protein concentration: 0.1 mg/mL) in duplicate. The reaction was initiated by adding NADPH-generating system and incubated for 0, 15, 30, 45, and 60 min. The reaction was stopped by transferring the incubation mixture to acetonitrile/methanol (1:1, v/v). Samples were then vortexed and centrifuged at 4 °C. Supernatants were used for UPLC-MS/MS analysis on an SCIEX 5500 triple-quadrupole MS (SCIEX, Framingham, Massachusetts, USA). Two reference compounds were tested in parallel: propranolol, which is relatively stable, and verapamil, which is readily metabolized in human liver microsomes.

In vitro aggregation of α -Synuclein

Lyophilized α -Syn was dissolved in sterile PBS 1X to a final concentration of 210 μ M and filtered through 22 μ m membranes to remove α -Syn small protein aggregates. The aggregation reaction was carried out in a 96-well sealed plate. Each well contained 70 μ M α -Syn (WT, A30P or H50Q), 40 μ M Th-T in PBS 1X, a 1/8" diameter teflon polyball (Polysciences Europe GmbH, Eppelheim, Germany) and the absence or presence of compound at 100 μ M in a total volume of 150 μ L. The plate was fixed in an orbital culture shaker Max-Q 4000 (ThermoScientific, Waltham, Massachusetts, USA) and agitated at 100 rpm and 37°C. Th-T fluorescence was measured every 2 h by exciting the samples through a 430–450 nm filter and collecting the emission signal with a 480–510 filter using a

Victor3.0 Multilabel Reader (PerkinElmer, Waltham, Massachusetts, USA). A minimum of three plate replicates were made for each condition and also measurement triplicates were taken for each time point. After compiling the fluoresce signals for each condition and measurement, means and standard error of mean (SEM) were used to fit the aggregation kinetics with equation (1),

$$\text{Equation (1)} \quad \alpha = 1 - \frac{1}{k_b(e^{k_a t} - 1) + 1}$$

where k_b and k_a indicate the homogeneous nucleation rate constant and the secondary rate constant, accounting for fibril elongation and secondary nucleation, respectively (2).

For the analysis of the disaggregation capacity of SC-D, 70 μ M α -Syn was incubated as previously described for four days and the Th-T signal measured. Then, 3.75 μ L of DMSO or SC-D 4 mM in DMSO were added to attain a 100 μ M compound concentration in the assay. The plate was incubated for an additional 24 h and Th-T derived fluorescence signals were measured again.

Transmission Electron Microscopy (TEM)

α -Syn samples were diluted 1:10 in PBS 1X, sonicated for 5 minutes and 5 μ L of the resulting mixture immediately placed on a carbon-coated copper grid. After 5 min, samples were carefully dried with a piece of filter paper to remove the excess of liquid and washed with MiliQ water twice. Then, 5 μ L of a solution of 2% (w/v) uranyl acetate was placed on the top of the grid for 2 min. Uranyl acetate excess was removed with filter paper. Finally, grids were left to air-dry for 10 min. Images were obtained using a Transmission Electron Microscopy Jeol 1400 (Peabody, Massachusetts, USA) operating at an accelerating voltage of 120 kV. A minimum of 30 fields were screened for each sample to obtain representative images.

Light scattering

Total aggregate formation was measured by light scattering adding 120 μ L of pre-aggregated α -Syn into a quartz cuvette. Samples were previously resuspended by carefully vortexing and pipetting and then excited at 300 and 340 nm to collect and 90° scattering collected between 260 to 400 nm in a Cary Eclipse Fluorescence Spectrophotometer (Agilent, Santa Clara, California, USA).

Nanoparticle tracking analysis

End point α -Syn aggregation reactions were collected and diluted 1:100 with MiliQ water to a final volume of 1 mL. The sample was measured by using a Nanosight NS3000 (Malvern Instruments Ltd, Malvern, United Kingdom) recording the light scattering and trajectory of any particle in solution for 1 minute. All samples were measured in triplicate and analysed with NTA3.1 software (Malvern Instruments Ltd, Malvern, United Kingdom).

Protein Misfolding Cyclic Amplification (PMCA)

Lyophilised α -Syn was dissolved in Conversion Buffer (PBS 1X, 1% Triton X-100, 150 mM NaCl), supplemented with Complete Protease Inhibitor Mixture (Roche Applied Science, Penzberg, Germany), to a final concentration of 90 μ M as previously described. Then, 60 μ L of the α -Syn solution was placed in 200- μ L PCR tubes containing 1.0 mm silica beads (Biospec Products, Bartlesville, OK, USA) and the mixture was subjected to 24-hour cycles of 30 s sonication and 30 min incubation at 37°C, using a Misonix 4000 sonicator setted at 70% power. Every 24 h, 1 μ L of PMCA-incubated sample was transferred to a fresh soluble α -Syn samples, repeated for 5 days. Treated samples were prepared by adding SC-D into 200- μ L tubes to a final concentration of 128 μ M, in order to maintain the 0.7:1 α -Syn:SC-D ratio used in original kinetic assays. Control samples were prepared with the corresponding concentration of DMSO (0.26%). All reactions were performed in triplicate.

After each cycle of PMCA, 10 μ L of α -Syn aggregates were diluted to a final volume of 100 μ L with PBS 1X and 40 μ M Th-T. Th-T fluorescence was recorded by exciting at 445 nm and collecting the emission fluorescence between 460 to 600 nm in a Cary Eclipse Fluorescence Spectrophotometer (Agilent, Santa Clara, California, USA).

Proteinase K Digestion

18 μ L of α -Syn aggregates coming from each cycle of PMCA were mixed with 6 μ L of Proteinase K (5 μ g/mL final concentration). After an incubation of 30 minutes at 37°C, 8 μ L of loading buffer containing 1% β -mercaptoethanol were added and the enzyme inactivated by an incubation for 10 min at 95°C in a Thermocell Cooling&Heating Block (BIOER, Hangzhou, Zhejiang Province, China). Afterwards, 7 μ L of each sample were loaded into a Tricine-SDS-PAGE gel together with unstained Protein Standard markers (ThermoFisher Scientific, Waltham, Massachusetts, USA). Gels were stained with Blue safe.

Nuclear Magnetic Resonance

WT 15N-labeled α -Syn was expressed in E. coli BL21 DE3 strain. Cells were previously grown in LB medium until an OD600 of 0.6 was reached. The cultures were centrifuged at 3000 rpm for 15 min and cells resuspended in minimal medium; 750 mL of miliQ water containing 100 μ L CaCl₂ 1M, 2 mL MgSO₄ 2 M, 20 mL glucose 20%, 100 mL vitamins 100x (Sigma-Aldrich, Darmstadt, Germany), 200 mL salts M9 and 1 g 15NH₄ (Cambridge Isotope Laboratories, Inc., Tewksbury, Massachusetts, USA). After 1 h of incubation at 37°C, protein expression was induced with 1 mM IPTG. Protein was purified as previously described (1).

1H-15N HSQC spectra were obtained at 20 °C on a Bruker 600 MHz NMR spectrometer equipped with a cryoprobe in a sample containing 70 μ M 15N-labeled α -Syn, PBS buffer (pH 7.4), 2.5% d₆-DMSO and 10% D₂O in the absence or in the presence of 100 μ M SC-D.

Characterisation of SynuClean-D – Fibril interaction

α -Synuclein fibril model

To predict the binding energy of SC-D on human α -Syn fibrils, a model composed of 10 strands was built based on PDB structure 2N0A (Fig. S9A) (3). The central part of the structure is characterized by parallel, in-register β -sheets with a greek-key topology, while the terminals are flexible loops. The full-length α -Syn strand comprises 140 residues; however, SC-D, with its planar aromatic structure, will interact with the ordered β portion of the fibril rather than with the unstructured flexible loops. For this reason, a reduced model of α -Syn fibril was constructed including only residues 34 to 99 of PDB 2N0A (Fig. S9B). This reduced model, whose validity as a model for the full fibril has been tested with molecular dynamics simulations, has been used in all calculations.

To justify the validity of this approximation, 10 ns molecular dynamics simulations were performed and the RMSD of the backbone was computed for residues 34 to 99 on both the full-length α -Synuclein fibril model (Fig. S9A) and the reduced model (Fig. S9B). Additionally, for the reduced model, a 1 ns and a 100 ns simulations were performed, to assess the stability of the fibrillar structure as a function of the simulation time. Results are reported in Fig. S10, and indicate that along a 10 ns simulation the RMSD evolution is identical for the full and the reduced model, validating our approximation. As far as the stability of the fibril as a function of time is concerned, our simulations revealed that the model of α -Synuclein fibril is only partially stable, as along the 100 ns simulation the high fluctuation of RMSD indicates that important structural deformations take place. This instability is likely due to the small size of the model, which only comprises 10 strands and is hardly representative, in terms of network of weak interactions, of a fully grown α - synuclein fibril. Within the 10 ns simulation, however, the RMSD fluctuation is lower. This observation determined the maximum time of production simulation, which was set to 3 ns just to avoid unphysical structural deformations.

Binding site prediction

To predict the interaction of SC-D with the model of α -Syn fibril we used the Protein Energy Landscape Exploration (PELE) methodology (4, 5). PELE combines a Monte Carlo stochastic approach with protein structure prediction algorithms, and is able, among several options, to predict the binding poses of a small ligand on a protein without any beforehand crystallographic information. The general workflow of PELE is composed of three steps:

i) a localized perturbation (random translation and rotation of the ligand, but it may also involve the backbone of the protein); ii) a side chain sampling based on a rotamer library;

iii) a minimization, involving the full system. The OPLS2005 force field is employed and solvation effects are accounted for with the Generalized Born method (6, 7). Owing to the stochastic nature of PELE, several independent runs need to be performed on the same protein-ligand pair to ensure a full exploration of the conformational space. We ran 150 independent trajectories for the α -Syn/compound pair, providing a satisfactory sampling.

Molecular dynamics simulations indicate that regardless of the fact that SC-D is fully inserted between the parallel β -sheets, it is still in contact with water molecules along the whole simulation. This is not surprising owing to the wealth of polar group that are attached to the aromatic ring, and again corroborates the hypothesis that the main interaction of SC-D with the fibril is of van der Waals type. These interactions are represented as green patches (Fig. S6).

Binding energy calculation

We evaluated the binding energy of the poses predicted by PELE with the MM/GBSA method as implemented in the Amber16 suite (8, 9). In the MM/GBSA method, the binding energy is estimated based on a collection of frames, which were generated with molecular dynamics simulations run with the ff14SB force field, with the ligand topology generated using the General Amber Force Field and atomic partial charges fitted on the electrostatic potential computed at the B3LYP/6-31+G(d,p) level of theory with the Gaussian 09 package (10, 11). The PELE structures are neutralized with the appropriate number of counterions (Na⁺/Cl⁻) and water molecules are added up to a minimum distance of 8 Å

from the protein. The protocol for the molecular dynamics simulations is as follows: i) 2000 steps of minimization; ii) a 200 ps equilibration run in the NVT ensemble rising the temperature from 0 to 100 K, with a 4.0 kcal mol⁻¹ constraint on the backbone, to avoid strong deformations; iii) a 2 ns run in the NPT ensemble, with the temperature rising from 100 to 300 K in the first half, and kept constant to 300 K in the second half, with a 2.0 kcal mol⁻¹ constraint on the backbone, again to avoid strong deformations; iv) 5 independent 3 ns production runs in the NPT ensemble with the temperature kept constant to 300 K, with no constraints. A Langevin thermostat and a Monte Carlo barostat were employed. 20 geometries were evenly sampled from the last 2 ns of each trajectory of the production run, and the resulting 100 structures were used for binding free energy calculations neglecting the entropy term. The free energy values were computed on the ligand/fibril complex trajectory. An ionic strength of 100 mM, which is compatible with that of a biological buffer, was employed, and the igb5 generalized Born model of Amber16 was used. In this model, the Born radii are re-scaled to obtain a better agreement with the electrostatic component of solvation energy calculated by the Poisson-Boltzmann treatment in proteins (12).

Non-covalent interactions prediction

Non-covalent interactions were studied with the NCIPLOT program according to the methodology proposed by Yang and co-workers (13). The reduced density gradient $s(r)$ (Eq. 2) is plotted against the electron density ρ multiplied by the sign of the second eigenvalue of the density Hessian. Peaks in the negative region of the x-axis in Fig. 3C are indicative of attractive interactions, while peaks in the positive regions are indicative of repulsive (non-bonded) contacts.

$$\text{Equation (2)} \quad s(\mathbf{r}) = \frac{1}{2(3\pi^2)^{1/3}} \frac{|\nabla\rho|}{\rho^{4/3}}$$

Cytotoxicity assay

For human neuroglioma cells (H4), 40,000 cells were plated in a 24-well plate. After 24h, cells were treated with different concentrations of the compound or with vehicle (DMSO). Cells were

the fixed after 24h with 4% PFA for 10 min, permeabilized with 0,1% triton X-100 for 20 min, and stained with DAPI (1:5000) for 10 min. With the Olympus IX81-ZDC microscope system, 36 fields were randomly taken with 10x objective, in 6 independent experiments. The number of cells was counted using the Olympus Scan[^]R Image Analysis Software and the results analyzed using Graphpad Prism software (GraphPad Software, La Jolla, California, USA).

For human neuroblastoma cells (SH-SY5Y), 4000 cells/well were seeded into 96 well- plates and cultured in DMEM medium supplemented with 10% FBS. Then, SC-D was added at a range from 10 μ M to 1 mM into each well. Treated and untreated cells were incubated at 37 °C for 72 h. Then, 10 μ L of PrestoBlue[®] reagent (ThermoFisher Scientific, Waltham, Massachusetts, USA) was added and, after an incubation for 10 minutes at 37 °C, the fluorescence emission was recorded at 590 nm by exciting at 560 nm.

In-cell aggregation of endogenous α -Synuclein

Cell Culture

Human neuroglioma cells (H4) were maintained in Opti-MEM I Reduced Serum Medium (Life Technologies-Gibco, Thermo Fisher Scientific, Waltham, Massachusetts, USA) supplemented with 10% fetal bovine serum Gold (FBS) (PAA, Cölbe, Germany) and 1% Penicillin-Streptomycin (PAN, Aidenbach, Germany). Cells were grown at 37 °C with 5% of CO₂ atmosphere.

Cell Transfection

Twenty-four hours prior to transfection, H4 cells were plated in 12-well plates (Costar, Corning, New York). The cells were transiently transfected according to the calcium phosphate method. Equal amounts of plasmids encoding a C-terminally modified α -Syn (SynT construct) were diluted in H₂O and 2.5 M CaCl₂. The mixture was then added dropwise and vigorously mixed into 2xBES-buffered saline solution containing phosphate ions (50 mM BES, 280 mM NaCl, 1.5 mM Na₂HPO₄·xH₂O, pH 6.98). Fresh media was added to the cells during the 20 min of incubation. 16 h after transfection, cells were treated with different concentrations of the compound (1 or 10 μ M). DMSO was used as the vehicle. Finally, at 24 h the cells were fixed and subjected to immunocytochemistry to examine α -Syn inclusions formation.

Immunocytochemistry

After the treatment, cells were fixed with 4% paraformaldehyde for 10 min at room temperature followed by 20 min of permeabilization with 0.1% Triton X-100 (Sigma- Aldrich, Darmstadt, Germany) at room temperature. The cells were blocked in 1.5% normal goat serum (PAA)/PBS for 1 h, and then incubated for 3 h with mouse anti- α -Syn primary antibody (1:1000, BD Transduction Laboratories, USA). Afterwards, cells were washed three times with PBS and incubated with a secondary antibody (Alexa Fluor 488 donkey anti-mouse IgG) for 2 h at room temperature. Finally, cells were stained with Hoechst 33258 (Life Technologies- Invitrogen, Carlsbad, California, USA) (1:5000 in PBS) for 5 min and maintained in PBS for epifluorescence microscopy.

Quantification of α -Synuclein inclusions

Quantifications were performed as previously described (14). Briefly, transfected cells were detected and scored based on the α -Syn inclusions pattern. Results were expressed as the percentage of the total number of transfected cells. At least 50-100 cells were counted per condition.

Caenorhabditis elegans models of PD

Media

Nematodes were cultured and maintained following standard procedures (17). Briefly, animals were synchronized by hypochlorite bleaching, hatched overnight in M9 buffer (3 g/L KH₂PO₄, 6 g/L Na₂HPO₄, 5 g/L NaCl, 1 M MgSO₄), and subsequently cultured at 20

°C on nematode growth medium (NGM) [1 mM CaCl₂, 1 mM MgSO₄, 5 µg/mL cholesterol, 250 M KH₂PO₄ (pH 6.0), 17 g/L Agar, 3 g/L NaCl] plates seeded with the E coli OP50 strain (OD₆₀₀ values between 1.3-1.6).

C. elegans strains

NL5901, unc-119(ed3) III; pkIs2386 [Punc-54::α-Syn::YFP; unc-119(+)] and N2 (Bristol) wild type strains were obtained from the Caenorhabditis elegans Genetic Center (CGC). To analyse α-Syn induced dopaminergic degeneration, we used the strain UA196 (15), gifted generously by the laboratory of Dr Guy Caldwell (Department of Biological Science, The University of Alabama, Tuscaloosa, USA), (sid-1(pk3321); baIn33 [Pdat-1::sid-1, Pmyo-2::mCherry]; baIn11 [Pdat-1::α-Syn; Pdat-1::GFP]). This strain was named Pdat-1::GFP; Pdat-1::α-Syn in the main text.

SynuClean-D administration

SynuClean-D was administered within NGM agar media and within the food source E. coli OP50 strain. Briefly, 100 µM of a stock SC-D in 0.2% Dimethyl sulfoxide (DMSO) was added to liquid warm NGM to a final concentration of 10 µM. 250 µL of the E. coli OP50 strain, containing 10 µM of SC-D or 0.2% of DMSO as control were added to dried plates, allowing the liquid to soak into the plates. Seeded plates were dried 24 hours before transferring the worms. Worms were transferred onto SC-D-seeded plates directly at larval stage L4, exposed to SC-D for 7 days and transferred daily to avoid cross progeny. EGCG was administered in the same manner.

Aggregate quantification

The quantification of aggregates was performed as previously described (16, 17). Briefly, NL5901 pkIs2386 [Punc-54::α-Syn::YFP; unc-119(+)] animals were age-synchronized and left overnight to hatch. L1 animals were grown onto individual NGM plates containing

E. coli OP50 to reach L4 developmental stage. Afterwards, L4 animals were transferred onto SC-D containing plates, while NGM plates containing only DMSO were used as negative control. Worms were transferred daily to avoid cross contamination. Aggregates were counted for each animal staged at L4+7 days in the posterior part. For each independent experiment, thirty 7-days old worms of each treatment were examined under a Nikon Eclipse E800 epifluorescence microscope equipped with an Endow GFP HYQ filter cube (Chroma Technology Corp, Bellows Falls, Vermont USA) and each experiment was performed by triplicate. Aggregates were defined as discrete, bright structures, with boundaries distinguishable from surrounding fluorescence. Measurements of the inclusions were performed using ImageJ software considering the area dimensions.

Thrashing assays

Animals from the strain NL5901 [unc-119(ed3) III; pkIs2386 [Punc-54::α-Syn::YFP; unc-119(+)] (SC-D treated and non-treated) at L4+7 days of development, were placed individually in a drop of M9 buffer and allowed to recover for 120 s (to avoid observing behaviour associated with stress). Afterwards, the number of body bends was recorded for 1 min. Non-treated N2 wild type animals were used as control. Movies of swimming worms were recorded

using a Leica MZFFLIII stereomicroscope at nominal magnification of 30X and the Hamamatsu ORCA-Flash 4.0LT camera at 17 frames per second (17 fps) for 1 min. Bends per minute were obtained with the Worm Tracker plugin (wrMTrack), from the ImageJ software. Thirty animals were counted in each experiment unless stated otherwise. Experiments were carried out in triplicate. Statistical analysis was performed using Graphpad Prism software (GraphPad Software, La Jolla, California, USA).

Blinding of experiments and replicates

Thrashing, or body bending studies were completed such that the experimenter was blind to the genotype of the worms. Strains were given letter codes by another member of the laboratory and the code was not broken until all of the replicates for a particular assay were completed. For all assays, we completed a minimum of three biological replicates per strain.

C. elegans neurodegeneration assays

Worms were analyzed for α -Syn -induced dopaminergic neurodegeneration as described previously (17). Briefly, 20-30 L4 staged animals from the strain UA196 were transferred to SC-D-NGM plates and were grown for seven days after which the dopaminergic cell death induced by the over-expression of α -Syn was analysed by fluorescence. Plates containing only 0.2% DMSO, without SC-D, were used as control. Worms were transferred daily to avoid cross contamination.

The six anterior DA neurons (four CEP and two ADE DA neurons) were scored for neurodegeneration according to previously described criteria (18). Worms were considered normal when all six anterior DA neurons (four CEP (cephalic) and two ADE (anterior deirid) were present without any visible signs of degeneration. If a worm displayed degeneration in at least one of the six neurons, it was scored as exhibiting degeneration. For each independent experiment, thirty worms of each treatment were examined under a Nikon Eclipse E800 epifluorescence microscope equipped with an Endow GFP HYQ filter cube (Chroma Technology Corp, Bellows Falls, Vermont, USA).

Microscopy and imaging

Animals were placed in a 1 mM solution of sodium azide and mounted with a coverslip on a 4% agarose pad. Animals were visualized with a Nikon Eclipse E800 epifluorescence microscope. The system acquires a series of frames at specific Z-axis position (focal plane) using a Z-axis motor device. Animals were examined at 100 \times magnification to examine α -Syn induced DA cell death and at 40X to examine α -Syn apparent aggregates.

Statistical analysis

All graphs were generated with GraphPad Prism 6.0 software (GraphPad Software Inc, La Jolla, California, USA). Data were analysed by two-way ANOVA Tukey test using SPSS software version 20.0 (IBM Analytics, Armonk, NY, United States). All data are shown as means and standard error of mean (SEM). $p < 0.05$ was considered statistically significant. In the graphs *, **, and *** indicate $p < 0.05$, $p < 0.01$ and $p < 0.001$, respectively.

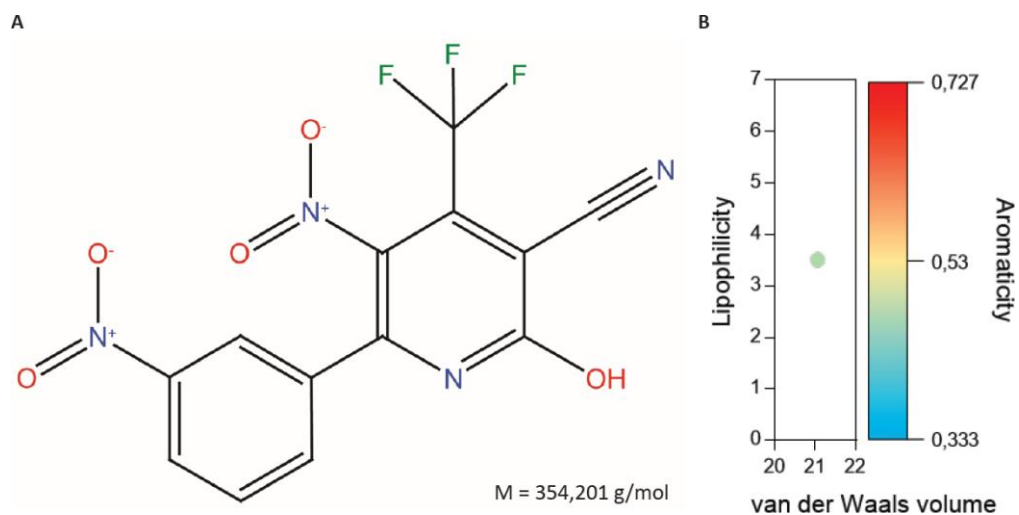


Figure S1. 2-hydroxy-5-nitro-6-(3-nitrophenyl)-4-(trifluoromethyl)nicotinonitrile or SynuClean-D (SC-D). Chemical structure (A) and properties (B) of the compound. Lipophilicity is defined as the Ghose–Crippen octanol/water coefficient (22). The volume corresponds to the sum of atomic van der Waals volumes (23). Aromaticity is defined as the ratio of the number of aromatic atoms to the total number of atoms.

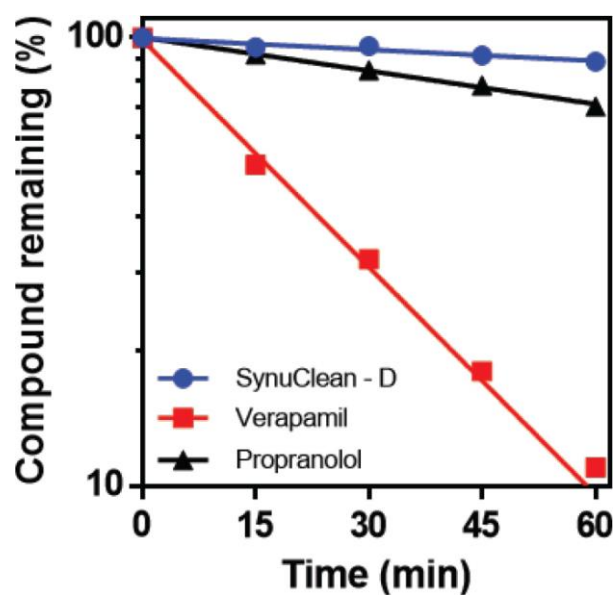


Figure S2. Metabolic stability of SC-D in human liver microsomes. The percentage of remaining compounds is plotted as a function of the incubation time at 37 °C. Propranolol and verapamil are slowly and rapidly metabolized reference compounds, respectively. The data correspond to the mean of two experiments. The calculated T1/2 of SC-D, propranolol and verapamil are 357.2, 119.5 and 19.0 min, respectively. The calculated intrinsic clearance values for SC-D, propranolol and verapamil are 3.9, 11.6 and 73.1 $\mu\text{L}/\text{min}/\text{mg}$, respectively.

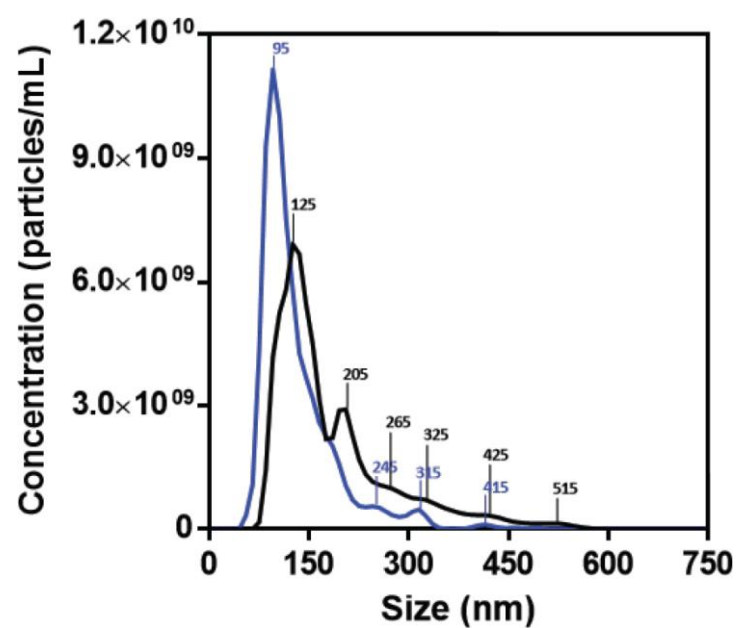


Figure S3. Fibril size characterization. Determination of the different fibril size population in absence (black) and presence (blue) of SC-D by using nanosight system.

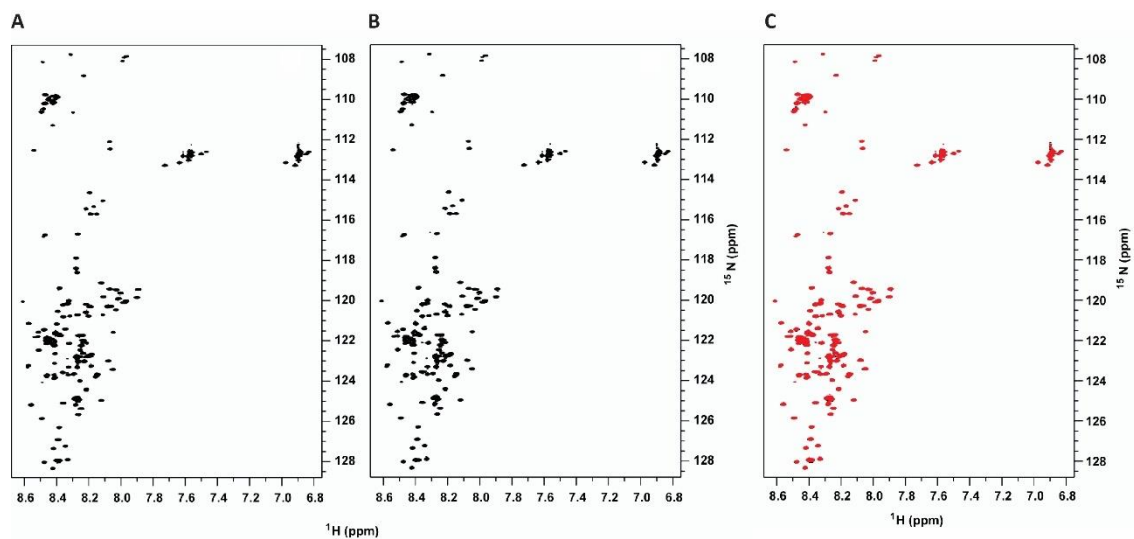


Figure S4. NMR characterisation of SynuClean-D non interaction to α -Synuclein monomer. ^1H - ^{15}N HSQC NMR spectra of ^{15}N -labeled α -Syn ($70\ \mu\text{M}$) in the absence (A) and in the presence (B) of SC-D ($100\ \mu\text{M}$). Superposition of the spectra (C) shown in panels (A) and (B) illustrating that α -Syn exhibits identical NMR spectra in the absence (black contours) and in the presence (red contours) of SC-D.

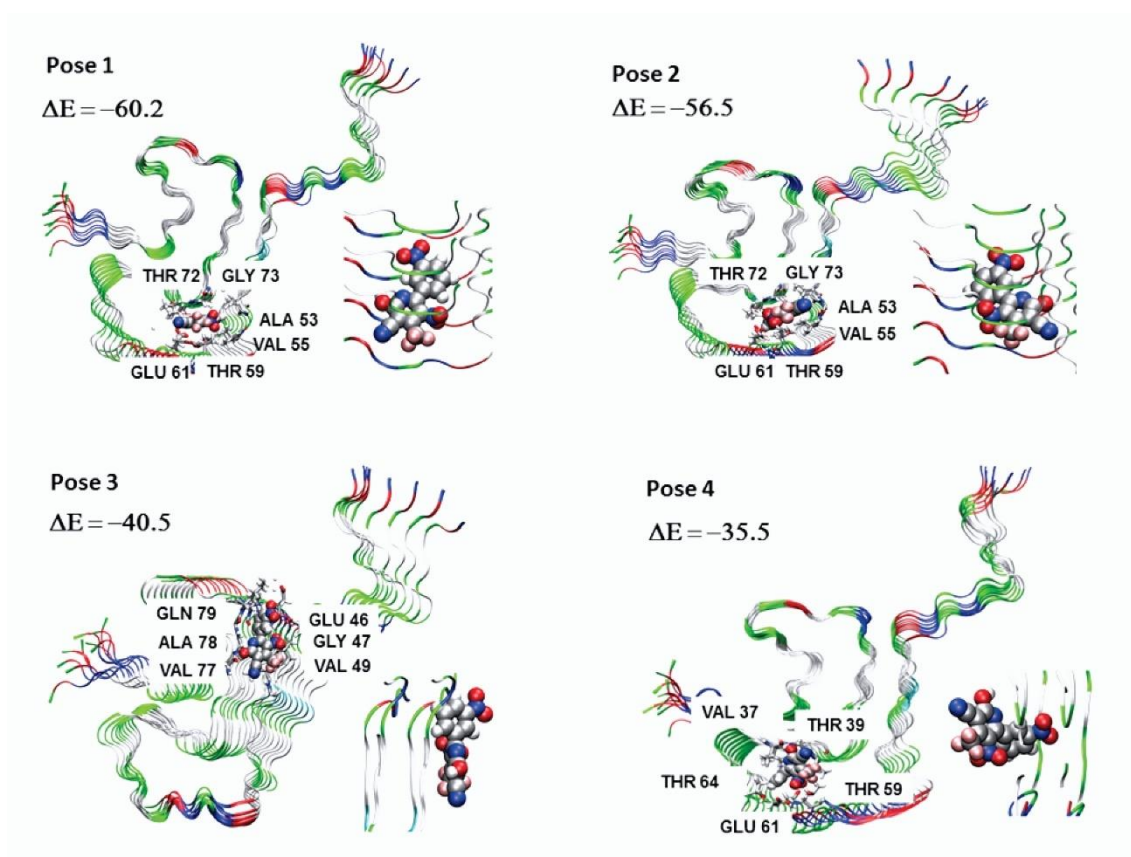


Figure S5. Binding sites prediction. Binding sites predicted by the Protein Energy Landscape Exploration (PELE) methodology. Interaction energies (ΔE) are expressed in kcal mol⁻¹.

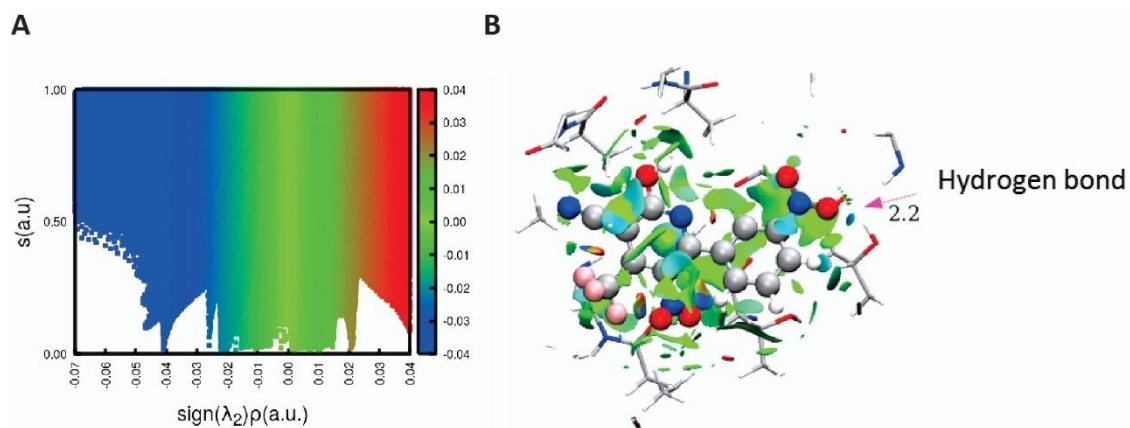


Figure S6. Characterisation of SynuClean-D-fibril interaction. Non-covalent interaction plot (A) and the representation of the non-covalent interactions involving SC- D in preferred binding pose at the PELE geometry (B). Contacts are represented in green. Distances in Å.

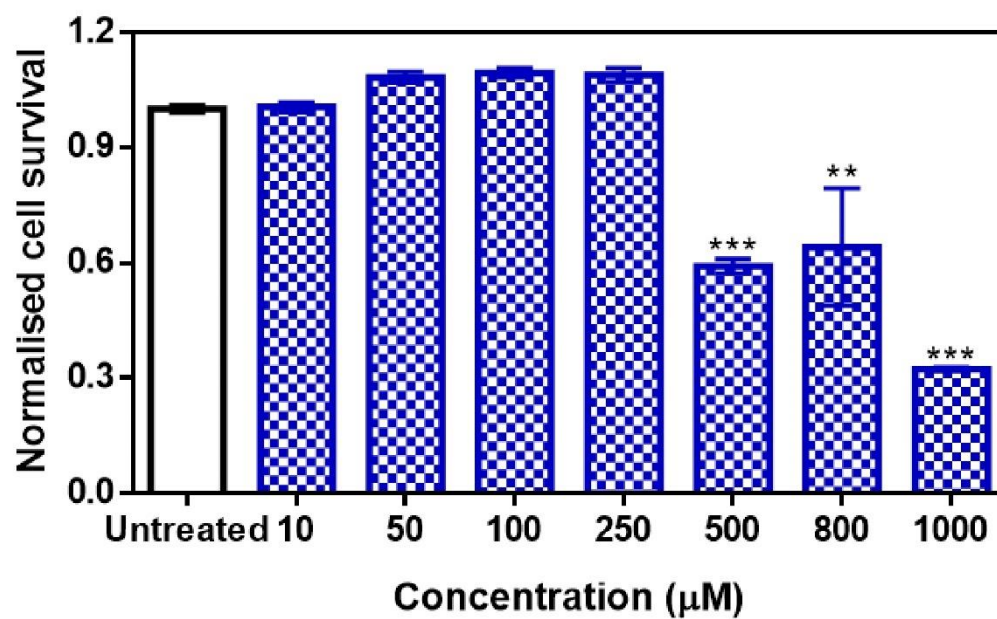


Figure S7. Toxicity of SC-D for neuroblastoma cells. Normalized SH-SY5Y cells survival in the presence of increasing concentrations of SC-D (blue) and without the compound (white).

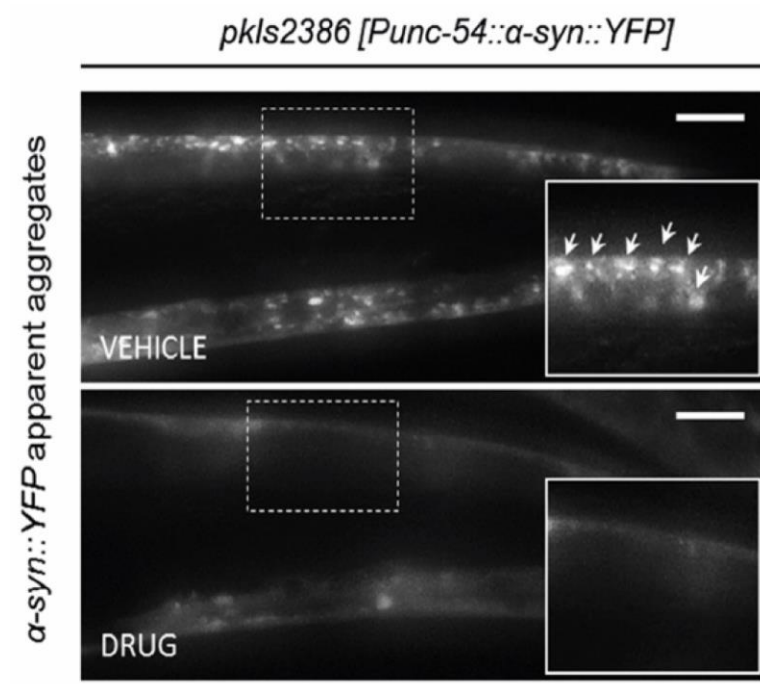


Figure S8. Inhibition effect of the compound in the formation of α -Synuclein inclusions in a *C. elegans* model of PD. Selected images of α -Syn muscle aggregates obtained by epifluorescence microscopy of NL5901 worms treated without (top panel, vehicle) and with SC-D (bottom panel, drug).

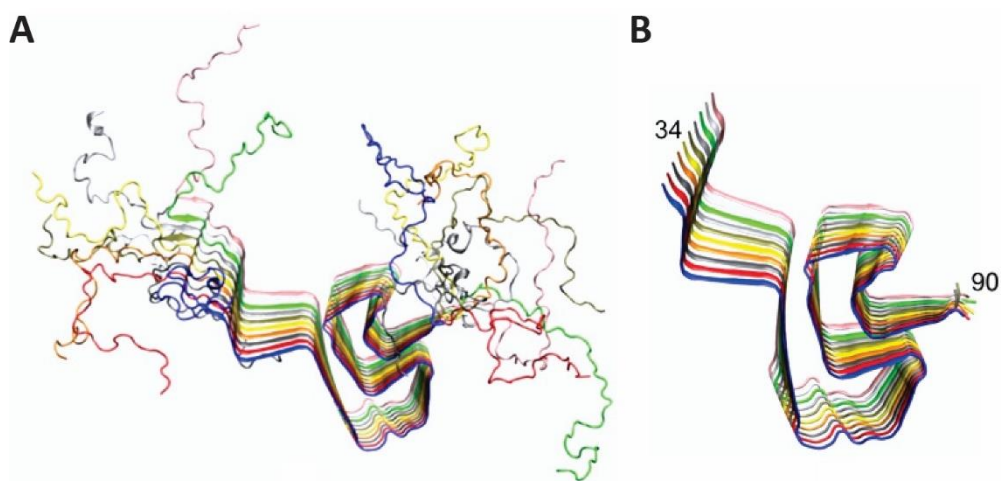


Figure S9. Aggregated structure of human α -Synuclein (PDB code 2N0A). NMR full-length model of human α -Syn fibril (A). Reduced model (B), including residues 34 to 99 of PDB 2N0A employed in the binding site search and binding energy calculations.

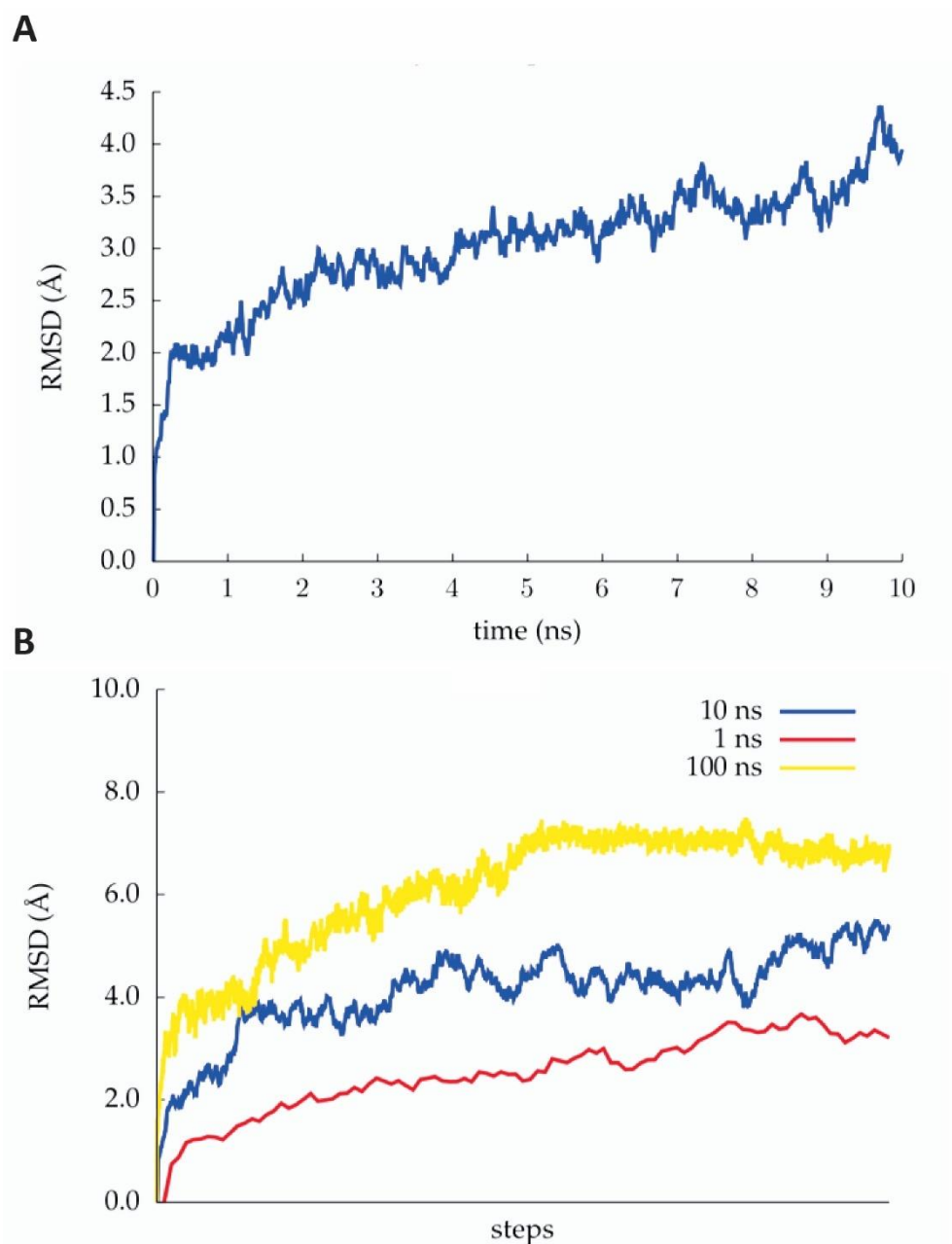


Figure S10. RMSD results of NPT molecular dynamics simulations. Backbone RMSD along 10 ns of NPT molecular dynamics simulation (A) at 300 K of the full α -Synuclein fibril from PDB structure 2N0A, with RMSD computed on residues 34 to 99. Backbone RMSD computed along 1, 10 and 100 ns of NPT molecular dynamics simulations (B) of the reduced α -Syn fibril model comprising residues 34 to 99.

Table S1. Interaction energies values involved in different predicted binding sites. MM/GBSA gas phase binding energy ΔG_{gas} , van der Waals (vdW) and electrostatic contributions (E_{El}), solvation free energy (DDG_{solv}), and binding energy in solution (ΔG_{bind}) for the two internal (1 and 2) and two external (3 and 4) poses of SC-D interacting with the α -Syn fibril model. All energies are in kcal mol⁻¹. Standard deviation is showed in parentheses.

<i>Binding pose</i>	<i>1</i>	<i>2</i>	<i>3</i>	<i>4</i>
ΔG_{gas}	-53.7 (5.4)	-47.1 (9.5)	-40.6 (8.3)	-52.3 (16.6)
vdW	-36.2 (4.5)	-37.1 (4.7)	-25.0 (3.9)	-31.0 (5.0)
E_{El}	-17.5 (4.7)	-10.0 (10.3)	-15.6 (7.0)	-21.3 (13.3)
$D\Delta G_{\text{solv}}$	35.3 (4.6)	32.5 (8.1)	29.2 (6.8)	36.2 (12.2)
ΔG_{bind}	-18.4 (4.1)	-14.6 (3.4)	-11.4 (3.1)	-16.1 (5.7)

Movie S1. Mobility of untreated YFP:: α -Syn worms, at day 7 of adulthood.

Movie S2. Mobility of YFP:: α -Syn worms treated with 10 μ M of SC-D, at day 7 of adulthood.

References

1. Pujols J, et al. (2017) High-Throughput Screening Methodology to Identify Alpha- Synuclein Aggregation Inhibitors. *Int J Mol Sci* 18(3).
2. Crespo R, et al. (2016) What Can the Kinetics of Amyloid Fibril Formation Tell about Off-pathway Aggregation? *J Biol Chem* 291(4):2018-2032.
3. Tuttle MD, et al. (2016) Solid-state NMR structure of a pathogenic fibril of full- length human alpha-synuclein. *Nat Struct Mol Biol* 23(5):409-415.
4. Madadkar-Sobhani A & Guallar V (2013) PELE web server: atomistic study of biomolecular systems at your fingertips. *Nucleic Acids Res* 41(Web Server issue):W322-328.
5. Borrelli KW, Vitalis A, Alcantara R, & Guallar V (2005) PELE: Protein Energy Landscape Exploration. A Novel Monte Carlo Based Technique. *J Chem Theory Comput* 1(6):1304-1311.
6. Onufriev A, Bashford D, & Case DA (2000) Modification of the generalized Born model suitable for macromolecules. *Journal of Physical Chemistry B* 104(15):3712-3720.
7. Jorgensen WL & Tirado-Rives J (1988) The OPLS [optimized potentials for liquid simulations] potential functions for proteins, energy minimizations for crystals of cyclic peptides and crambin. *J Am Chem Soc* 110(6):1657-1666.
8. Salomon-Ferrer R, Case DA, & Walker RC (2013) An overview of the Amber biomolecular simulation package. *Wiley Interdisciplinary Reviews-Computational Molecular Science* 3(2):198-210.
9. Genheden S & Ryde U (2015) The MM/PBSA and MM/GBSA methods to estimate ligand-binding affinities. *Expert Opinion on Drug Discovery* 10(5):449-461.
10. D.A. Case DSC TEC, III, T.A. Darden, R.E. Duke, T.J. Giese, H. Gohlke, A.W. Goetz, D. Greene, N. Homeyer, S. Izadi, A. Kovalenko, T.S. Lee, S. LeGrand, P. Li, C. Lin, J. Liu, T. Luchko, R. Luo, D. Mermelstein, K.M. Merz, G. Monard, H. Nguyen, I. Omelyan, A. Onufriev, F. Pan, R. Qi, D.R. Roe, A. Roitberg, C. Sagui, C.L. Simmerling, W.M. Botello-Smith, J. Swails, R.C. Walker, J. Wang, R.M. Wolf, X. Wu, L. Xiao, D.M. York and P.A. Kollman (2016) AMBER 16. University of California, San Francisco.
11. Wang J, Wolf RM, Caldwell JW, Kollman PA, & Case DA (2004) Development and testing of a general amber force field. *J Comput Chem* 25(9):1157-1174.
12. Feig M, et al. (2004) Performance comparison of generalized born and Poisson methods in the calculation of electrostatic solvation energies for protein structures. *J Comput Chem* 25(2):265-284.
13. Johnson ER, et al. (2010) Revealing noncovalent interactions. *J Am Chem Soc* 132(18):6498-6506.
14. Lazaro DF, et al. (2014) Systematic comparison of the effects of alpha-synuclein mutations on its oligomerization and aggregation. *PLoS Genet* 10(11):e1004741.

15. Harrington AJ, Yacoubian TA, Slone SR, Caldwell KA, & Caldwell GA (2012) Functional analysis of VPS41-mediated neuroprotection in *Caenorhabditis elegans* and mammalian models of Parkinson's disease. *J Neurosci* 32(6):2142-2153.
16. van Ham TJ, et al. (2008) *C. elegans* model identifies genetic modifiers of alpha-synuclein inclusion formation during aging. *PLoS Genet* 4(3):e1000027.
17. Munoz-Lobato F, et al. (2014) Protective role of DNJ-27/ERdj5 in *Caenorhabditis elegans* models of human neurodegenerative diseases. *Antioxid Redox Signal* 20(2):217-235.
18. Cao S, Gelwix CC, Caldwell KA, & Caldwell GA (2005) Torsin-mediated protection from cellular stress in the dopaminergic neurons of *Caenorhabditis elegans*. *J Neurosci* 25(15):3801-3812.

5.2. Chapter 3. ZPD-2, a Small Compound That Inhibits α -Synuclein
Amyloid Aggregation and Its Seeded Polymerization

Published at Frontiers in Molecular Neurosciences on December 2019

Available in: <https://www.frontiersin.org/articles/10.3389/fnmol.2019.00306/full>

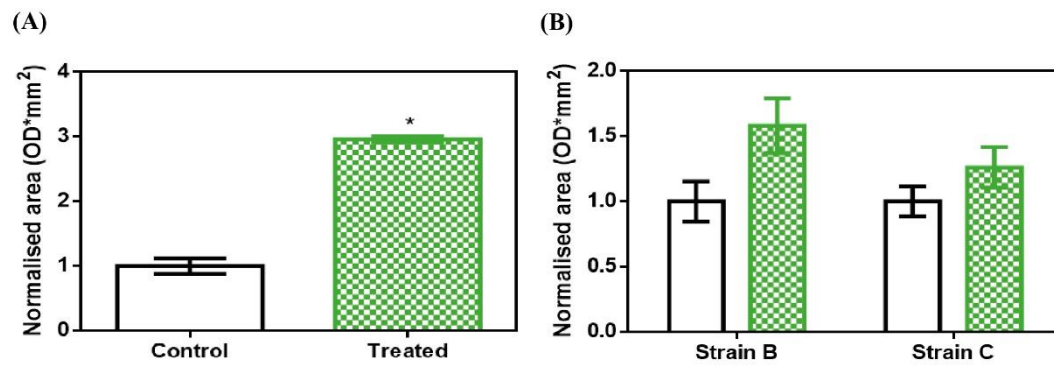


FIGURE S1 | α -Synuclein soluble fraction at the end of the aggregation. (A) Soluble fraction of α -Syn when incubated in absence (black) or presence (green) of ZPD-2 in PBS solution. (B) Soluble fraction of strains B and C at final point of the aggregation when incubated in presence (green) or absence (black) of ZPD-2.

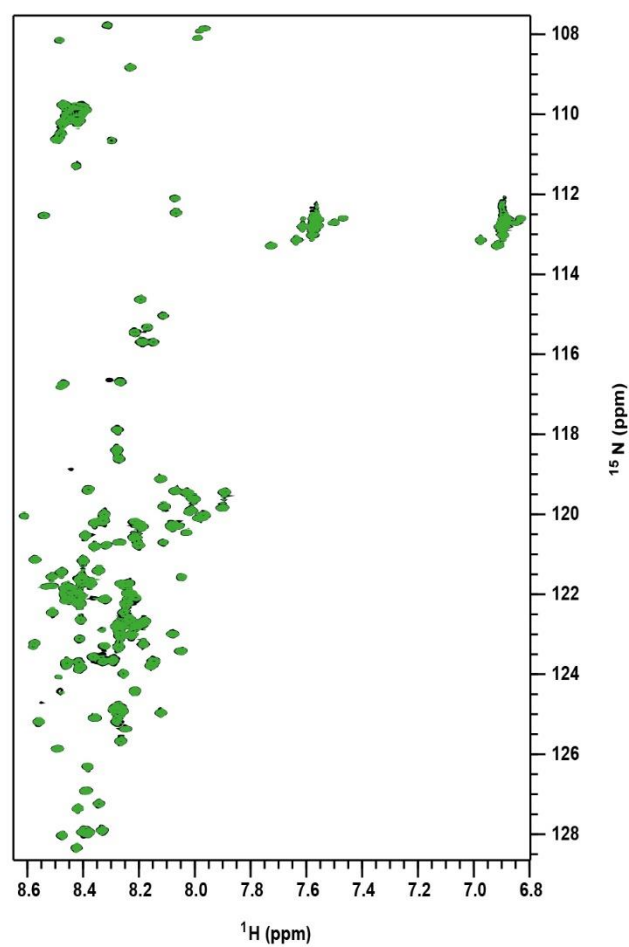


FIGURE S2 | Lack of interaction between monomeric α -Synuclein and ZPD-2 assessed by NMR. Superposition of the ^1H - ^{15}N HSQC NMR spectra of ^{15}N -labeled α -Syn (70 μM) in absence (black) and presence (green) of 100 μM of ZPD-2.

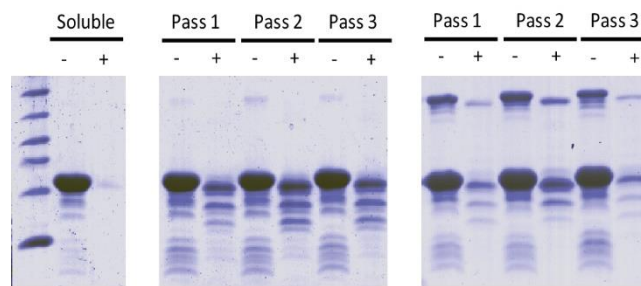


FIGURE S3 | PMCA assay at early stages. Tricine–SDS-PAGE gels of untreated (middle) and ZPD-2-treated (right) PMCA samples before (–) and after (+) being digested with proteinase K. Soluble α -Syn and PMCA steps 1–3 are shown.

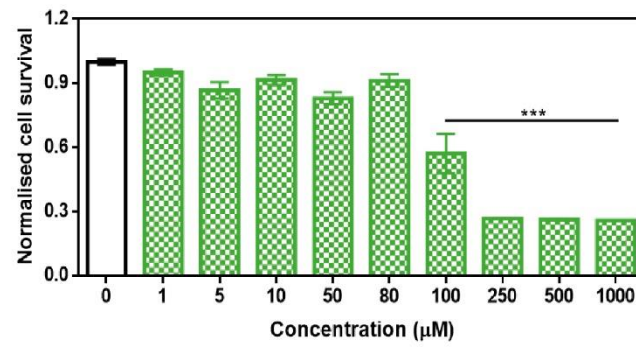


FIGURE S4 | Toxicity assays. Analysis of neuronal cells culture survival in presence of different concentration of ZPD-2. Survival is potted as normalized means. Error bars are shown as standard error of means values, where $p < 0.001$ was indicated by ***.

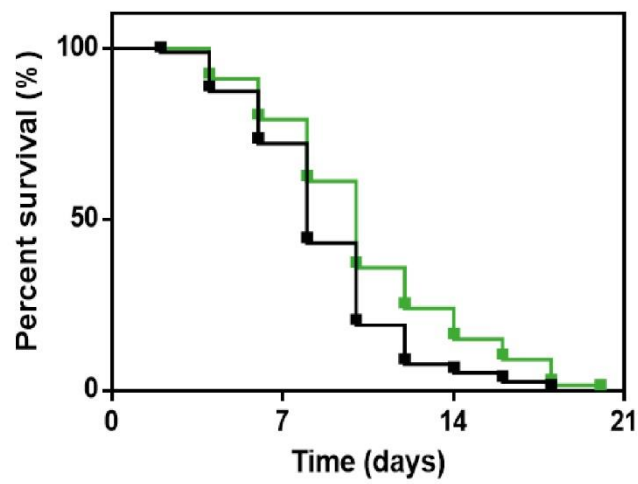


FIGURE S5 | *C. elegans* lifespan analysis. Effect of ZPD-2 treatment (green) on the survival of PD model animals, in comparison with untreated PD worms (black). The data represent the survival ratio (approximately 60–80 animals per group).

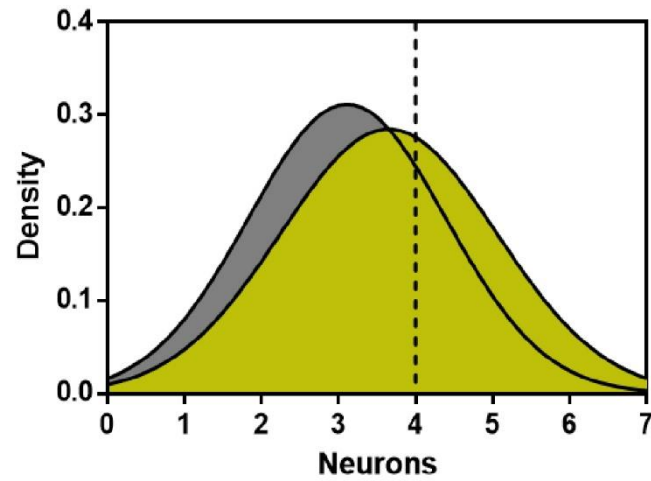
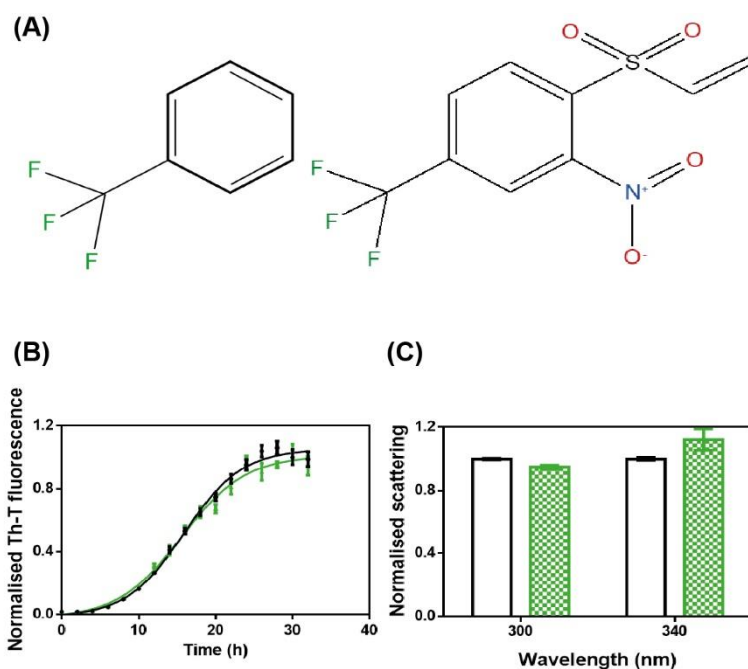


FIGURE S6 | Distribution of functional neurons in the *C. elegans* dopaminergic model. Normal distribution of the remaining functional dopaminergic (DA) neurons in transgenic animals when treated with ZPD-2 (green) or vehicle (gray). The dashed line delimits animals having four or more functional DA neurons.

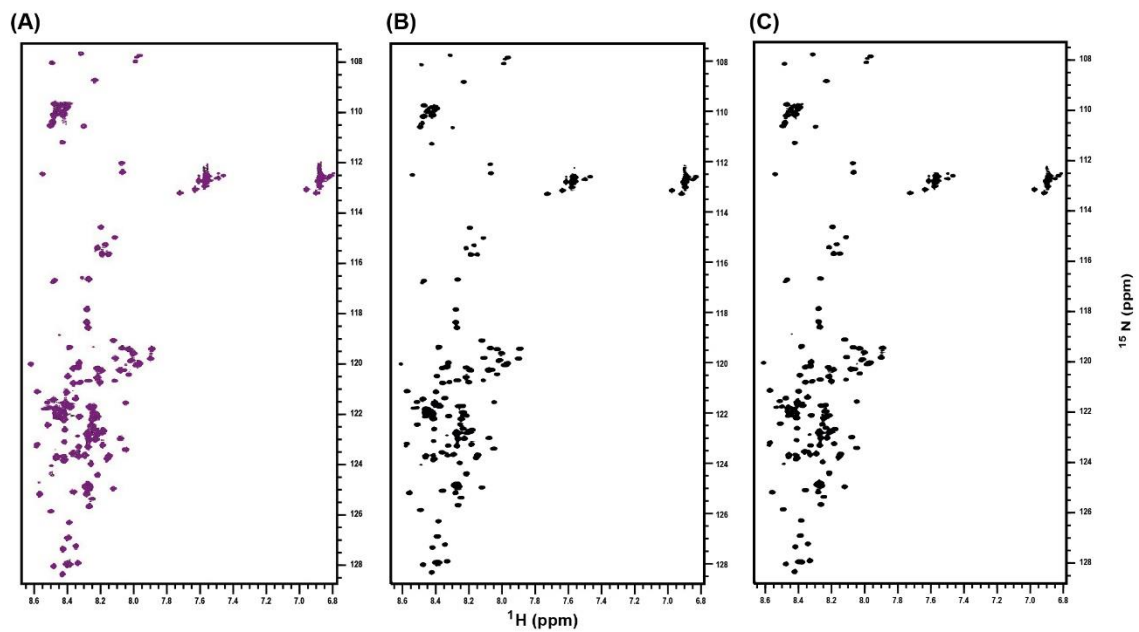
5.3. Chapter 4. Inhibition of α -Synuclein Aggregation and Mature Fibril Disassembling With a Minimalistic Compound, ZPDm

Published at Frontiers in Bioengineering and Biotechnology on October 2020

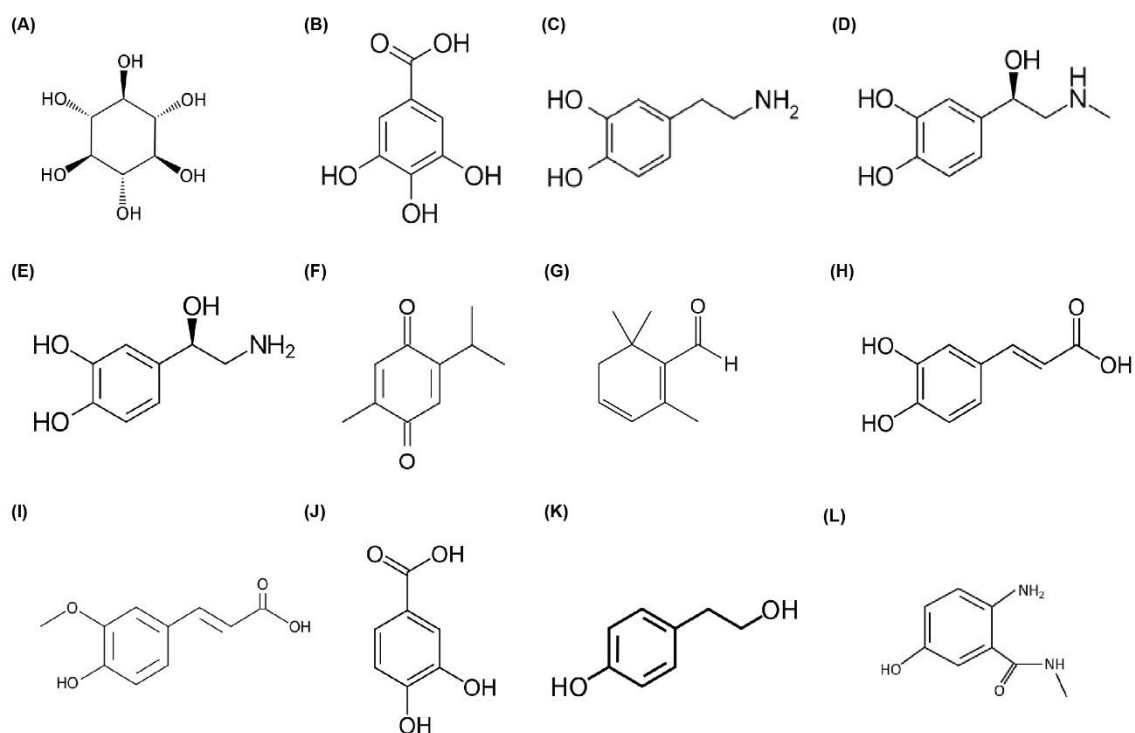
Available in: <https://www.frontiersin.org/articles/10.3389/fbioe.2020.588947/full>



Supplementary Figure 1 | Inhibitory capacity of (trifluoromethyl)benzene. (A) Chemical structures of (trifluoromethyl)benzene, (left) and ZPDm (right). (B) α -Syn aggregation kinetics in the absence (black) and presence (green) of 100 μ M of (trifluoromethyl)benzene followed by Th-T fluorescence. (C) Light-scattering measurements at 300 and 340 nm, in the absence (white) and presence (green) of (trifluoromethyl)benzene.



Supplementary Figure 2 | NMR analysis of ZPDm lack of interaction with monomeric α -Syn. ^1H - ^{15}N HSQC NMR spectra of ^{15}N -labeled α -Syn (70 μM) in the presence (A) and in the absence (B) of ZPDm (100 μM). The superposition of the two NMR spectra is shown in (C).



Supplementary Figure 3 | Chemical structures of different α -Syn aggregation inhibitors with asingle aromatic ring. Chemical structures of (A) scyllo-inositol, (B) gallic acid, (C) dopamine, (D) epinephrine, (E) norepinephrine, (F) thymoquinone, (G) safranal, (H) caffeic acid, (I) ferulic acid, (J) protocatechuic acid, (K) tyrosol, and (L) 576755.

5.4. Chapter 5. The small aromatic compound SynuClean-D inhibits the aggregation and seeded polymerization of multiple α -Synuclein strains

Published at Journal of Biological Chemistry on April 2022

Available in: [https://www.jbc.org/article/S0021-9258\(22\)00342-8/fulltext](https://www.jbc.org/article/S0021-9258(22)00342-8/fulltext)

Supporting information for

The small aromatic compound SynuClean-D inhibits the aggregation and seeded polymerization of multiple α -Synuclein strains

Samuel Peña-Díaz^{a,b,1}, Jordi Pujols^{a,b,1}, Eftychia Vasili^{c,d}, Francisca Pinheiro^{a,b}, Jaime Santos^{a,b}, Zoe Manglano-Artuñedo^{a,b}, Tiago F. Outeiro^{c,d,e,f} and Salvador Ventura^{a,b,g,2}

^a Institut de Biotecnologia i Biomedicina. Universitat Autònoma de Barcelona, 08193-Bellaterra, Spain.

^b Departament de Bioquímica i Biologia Molecular. Universitat Autònoma de Barcelona, 08193-Bellaterra, Spain.

^c Department of Experimental Neurodegeneration, Center for Biostructural Imaging of Neurodegeneration, University Medical Center Göttingen, 37073 Göttingen, Germany.

^d Max Planck Institute for Experimental Medicine, 37075 Göttingen, Germany.

^e Translational and Clinical Research Institute, Faculty of Medical Sciences, Newcastle University, Framlington Place, Newcastle Upon Tyne, NE2 4HH, UK

^f Scientific employee with a honorary contract at Deutsches Zentrum für Neurodegenerative Erkrankungen (DZNE), Göttingen, Germany.

^g ICREA, Passeig Lluís Companys 23, E-08010 Barcelona, Spain.

¹ These authors contributed equally to the work.

² To whom correspondence should be addressed.

Supplementary Figure 1. SynuClean-D. (A) Chemical structure and (B) absorption spectra of SynuClean-D (5-nitro-6-(3-nitrophenyl)-2-oxo-4-(trifluoromethyl)-1*H*-pyridine-3-carbonitrile) in different buffer conditions. Red area indicates the used excitation and emission wavelength of Th-T in aggregation assays.

Supplementary Figure 2. Fibril morphology. (A-F) Representative TEM images of strain A (A and B), strain B (C and D) and strain C (E and F) end-point aggregates. Magnification is 1500X for images A, C and E, and 10000X for images B, D and F. Scale bars corresponds to 2 μ m (A, C and E) and 200 nm (B, D and F), respectively. Discontinuous line delimited squares in low magnification images A, C and E indicate the grid area selected for medium magnification images in B, D and F. Discontinuous line delimited squares in B, D and F indicate the grid area selected for the high magnification images shown in Figure 1D-F (15000X).

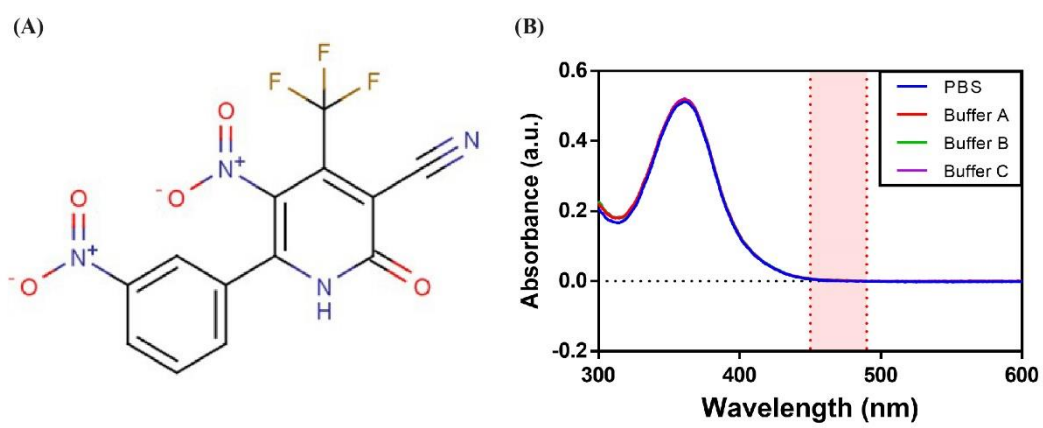
Supplementary Figure 3. Denaturation of strain B and C. Chemical denaturation of mature fibrils of strains B (blue) and C (red) in presence of 4 M urea followed by Th-T fluorescence.

Supplementary Figure 4. Seeds characterisation. (A) Th-T fluorescence measurements of strain B (dotted lines) and strain C (straight lines) fibrils after 0s, 15s, 30s and 60s of sonication. (B) Th-T fluorescence measurements of strain A, strain B and strain C fibrils before (straight lines) and after (dotted lines) 4 rounds of washing with Milli Q water. (C) PK digestion of mature fibrils before and after 4 rounds of washing with Milli Q water. (D) TEM images of mature fibrils before and after 4 rounds of washing with Milli Q water. Scale bars correspond to 200 nm.

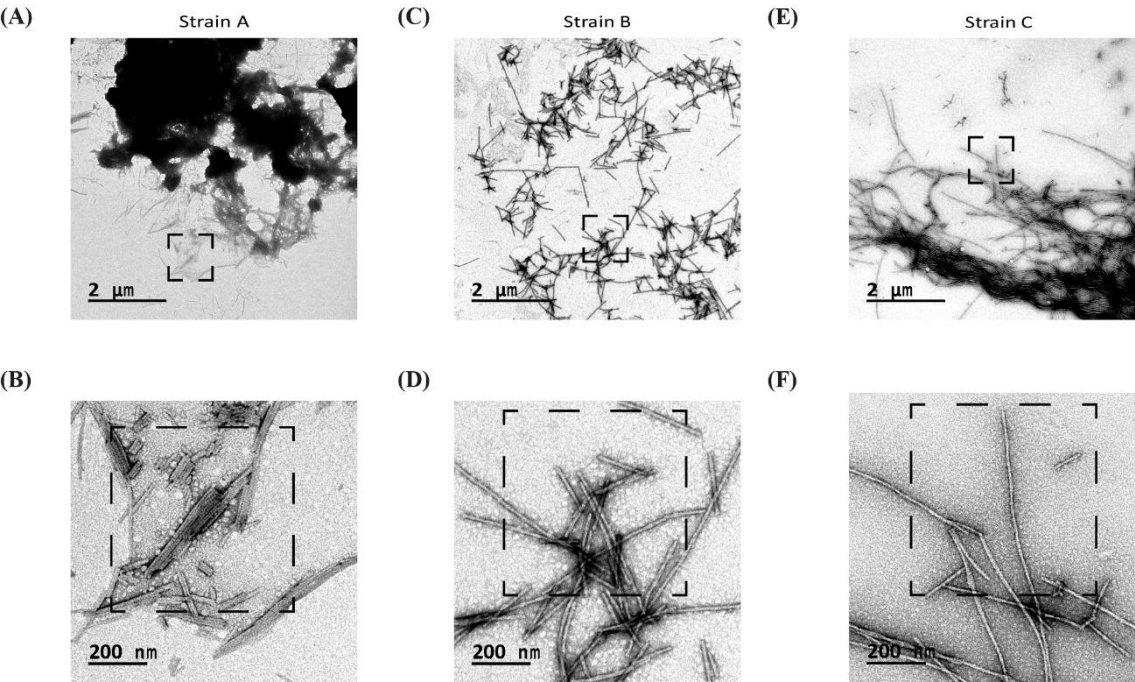
Supplementary Figure 5. Effect of different α -Syn strains in aggregation of endogenously expressed α -Syn-EGFP. Representative images from α -Syn-EGFP expressing stable cell line after treatment with buffers A, B and C (-) or the aggregates (+) generated in these solutions, respectively. Scale bar corresponds to 30 μ m.

Supplementary Figure 6. SynuClean-D interaction with α -Syn fibrillar structures. General (A) and close-up views (B) of the most favourable SC-D binding with fibrils previously predicted by molecular docking. NAC domain is labelled in pink and interacting residues are coloured in blue.

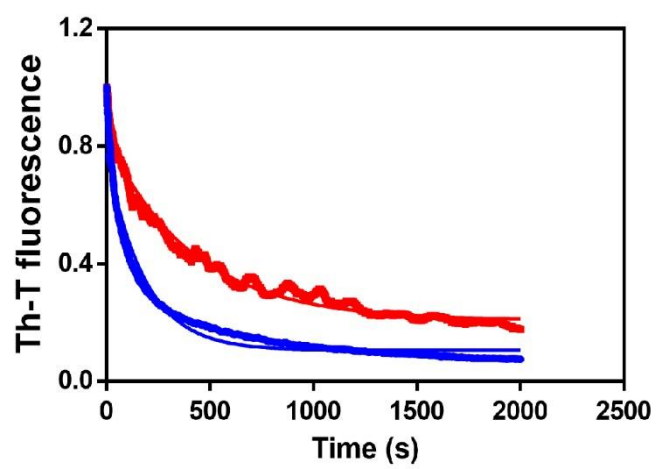
Supplementary figure 1.



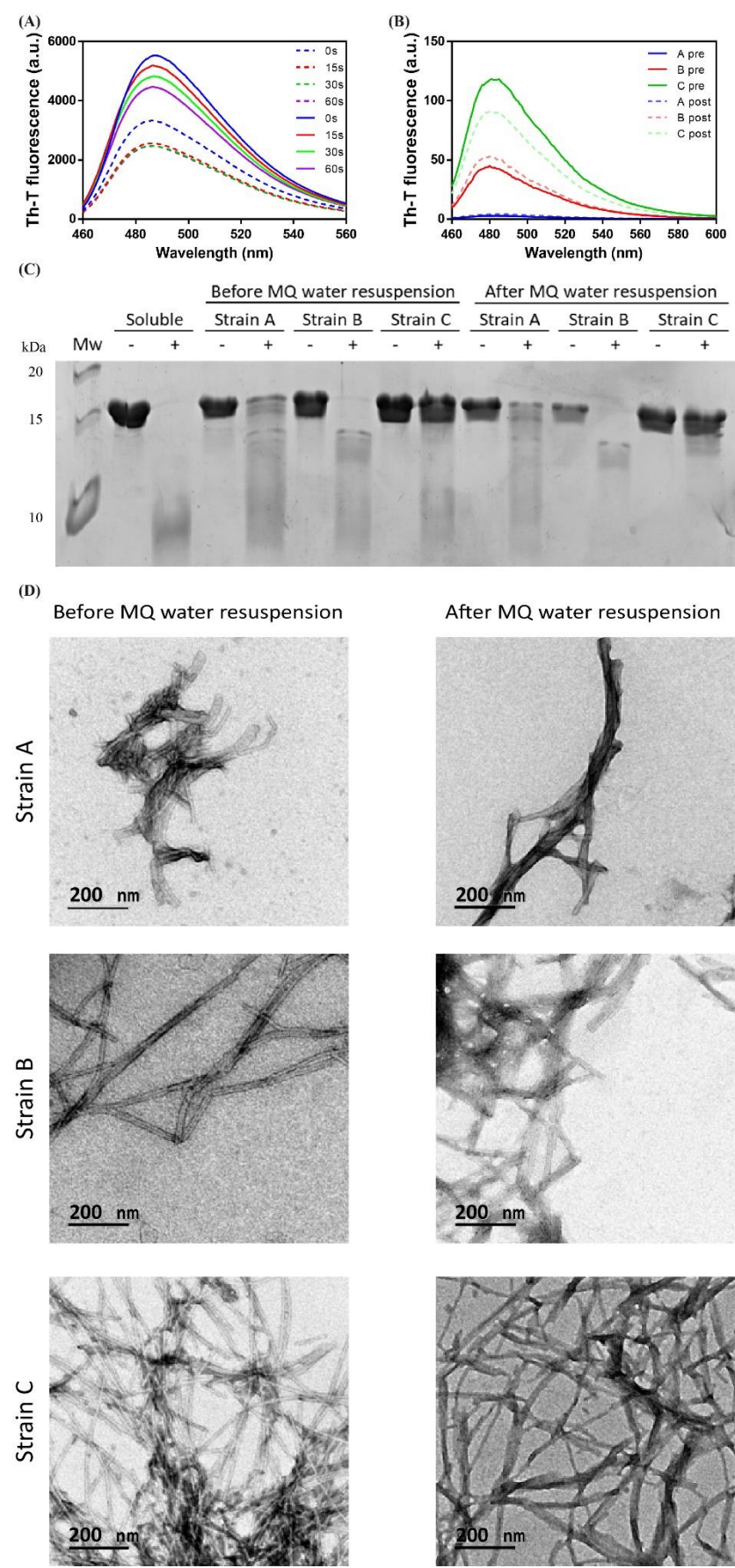
Supplementary figure 2.



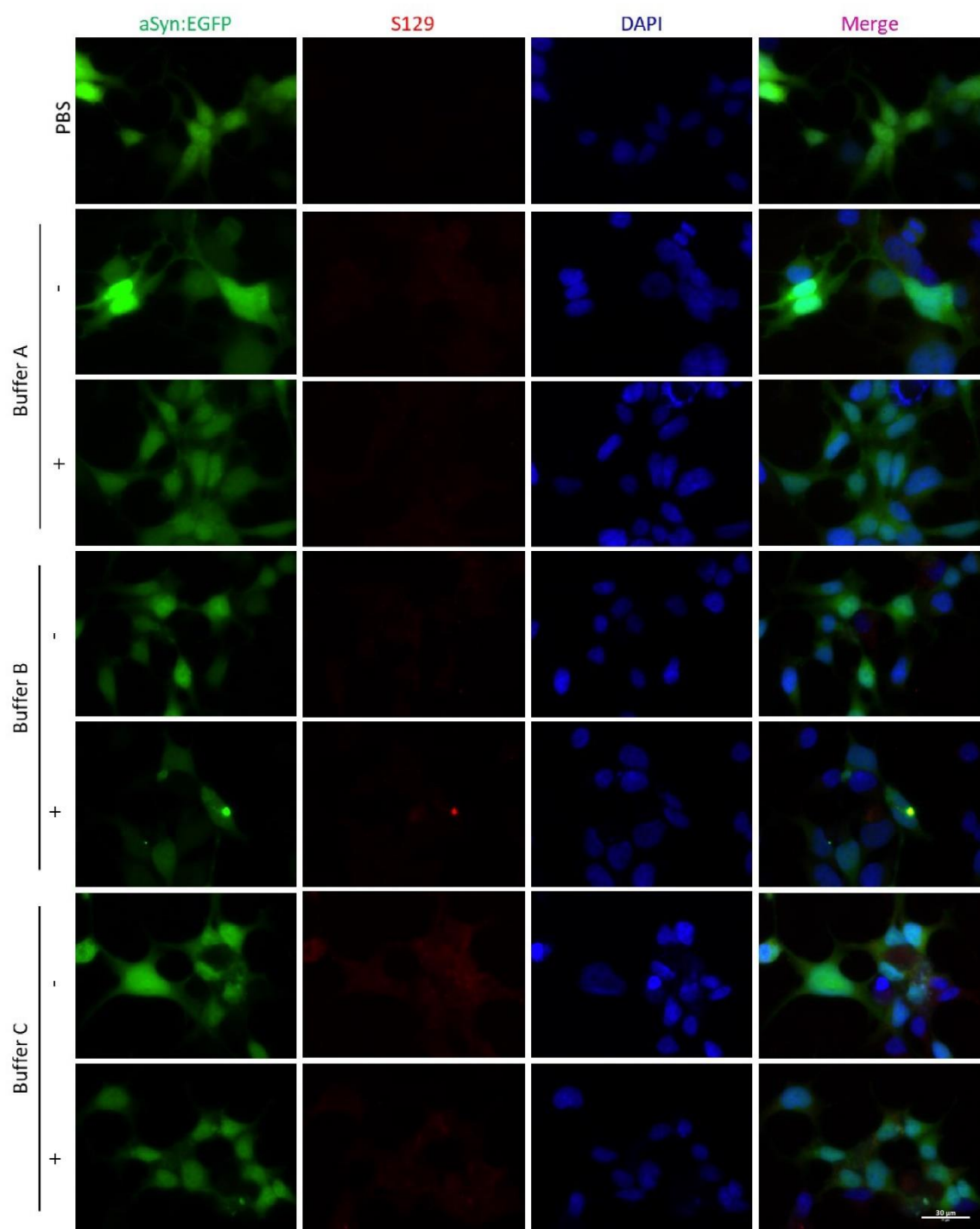
Supplementary figure 3.



Supplementary figure 4.

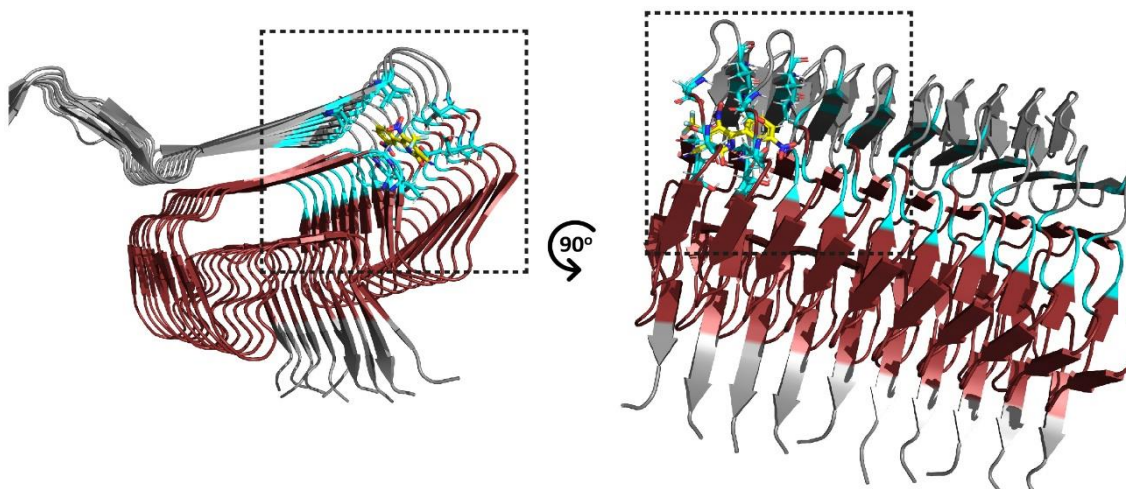


Supplementary figure 5.

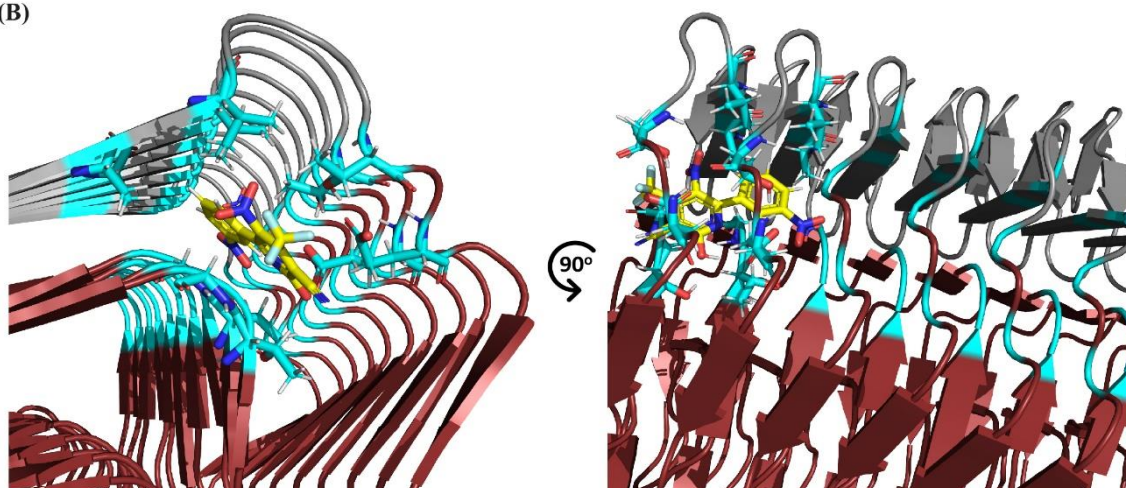


Supplementary figure 6.

(A)



(B)



Supplementary Table 1. Assignment of the secondary structure of aggregated strains. The secondary structure of strains A, B and C aggregates at final point was obtained by measuring ATR-FTIR absorbance in the amide I region, which was acquired and the fitted individual bands after Gaussian deconvolution are indicated

Strain A			Strain B			Strain C		
Band (cm ⁻¹)	Area (%)	Structure	Band (cm ⁻¹)	Area (%)	Structure	Band (cm ⁻¹)	Area (%)	Structure
1628	33	β-sheet (inter)	1627	39	β-sheet (inter)	1624	43	β-sheet (inter)
1645	28	Unordered	1647	28	Unordered	1643	23	Unordered
1666	32	Loop/β-turn	1666	25	Loop/β-turn	1662	25	Loop/β-turn
1686	8	β-turn	1683	8	β-turn	1681	9	β-turn

6. References

- 1 Creighton, T. E. F., W. H. Proteins: Structures and molecular properties. *J. Chem. Technol. Biotechnol.* **62**, doi:10.1002/jctb.280620121 (1992).
- 2 Dobson, C. M. Protein folding and misfolding. *Nature* **426**, 884-890, doi:10.1038/nature02261 (2003).
- 3 Anfinsen, C. B. Principles that govern the folding of protein chains. *Science* **181**, 223-230, doi:10.1126/science.181.4096.223 (1973).
- 4 Eichner, T. & Radford, S. E. A diversity of assembly mechanisms of a generic amyloid fold. *Mol Cell* **43**, 8-18, doi:10.1016/j.molcel.2011.05.012 (2011).
- 5 Knowles, T. P., Vendruscolo, M. & Dobson, C. M. The amyloid state and its association with protein misfolding diseases. *Nat Rev Mol Cell Biol* **15**, 384-396, doi:10.1038/nrm3810 (2014).
- 6 Herczenik, E. & Gebbink, M. F. Molecular and cellular aspects of protein misfolding and disease. *FASEB J* **22**, 2115-2133, doi:10.1096/fj.07-099671 (2008).
- 7 Chiti, F. & Dobson, C. M. Protein misfolding, functional amyloid, and human disease. *Annu Rev Biochem* **75**, 333-366, doi:10.1146/annurev.biochem.75.101304.123901 (2006).
- 8 Luhrs, T. *et al.* 3D structure of Alzheimer's amyloid-beta(1-42) fibrils. *Proceedings of the National Academy of Sciences of the United States of America* **102**, 17342-17347, doi:10.1073/pnas.0506723102 (2005).
- 9 Delacourte, A. & Defossez, A. Alzheimer's disease: Tau proteins, the promoting factors of microtubule assembly, are major components of paired helical filaments. *Journal of the neurological sciences* **76**, 173-186, doi:10.1016/0022-510x(86)90167-x (1986).
- 10 Spillantini, M. G., Crowther, R. A., Jakes, R., Hasegawa, M. & Goedert, M. alpha-Synuclein in filamentous inclusions of Lewy bodies from Parkinson's disease and dementia with lewy bodies. *Proceedings of the National Academy of Sciences of the United States of America* **95**, 6469-6473, doi:10.1073/pnas.95.11.6469 (1998).
- 11 Spillantini, M. G. *et al.* Alpha-synuclein in Lewy bodies. *Nature* **388**, 839-840, doi:10.1038/42166 (1997).
- 12 Anfinsen, C. B., Haber, E., Sela, M. & White, F. H., Jr. The kinetics of formation of native ribonuclease during oxidation of the reduced polypeptide chain. *Proceedings of the National Academy of Sciences of the United States of America* **47**, 1309-1314, doi:10.1073/pnas.47.9.1309 (1961).
- 13 Levinthal, C. Are there pathways for protein folding? *J. Chim. Phys.* **65**, 44-45 (1968).
- 14 Wetlaufer, D. B. Nucleation, rapid folding, and globular intrachain regions in proteins. *Proceedings of the National Academy of Sciences of the United States of America* **70**, 697-701, doi:10.1073/pnas.70.3.697 (1973).

- 15 Karplus, M. & Weaver, D. L. Protein folding dynamics: the diffusion-collision model and experimental data. *Protein Sci* **3**, 650-668, doi:10.1002/pro.5560030413 (1994).
- 16 Karplus, M. & Weaver, D. L. Protein-folding dynamics. *Nature* **260**, 404-406, doi:10.1038/260404a0 (1976).
- 17 Ptitsyn, O. B. & Rashin, A. A. A model of myoglobin self-organization. *Biophys Chem* **3**, 1-20, doi:10.1016/0301-4622(75)80033-0 (1975).
- 18 Tanford, C. Contribution of Hydrophobic Interactions to the Stability of the Globular Conformation of Proteins. *J. Am. Chem. Soc.* **84**, 4240–4247, doi:10.1021/ja00881a009 (1962).
- 19 Kauzmann, W. Some factors in the interpretation of protein denaturation. *Adv Protein Chem* **14**, 1-63, doi:10.1016/s0065-3233(08)60608-7 (1959).
- 20 Jackson, S. E. & Fersht, A. R. Folding of chymotrypsin inhibitor 2. 1. Evidence for a two-state transition. *Biochemistry* **30**, 10428-10435, doi:10.1021/bi00107a010 (1991).
- 21 Itzhaki, L. S., Otzen, D. E. & Fersht, A. R. The structure of the transition state for folding of chymotrypsin inhibitor 2 analysed by protein engineering methods: evidence for a nucleation-condensation mechanism for protein folding. *J Mol Biol* **254**, 260-288, doi:10.1006/jmbi.1995.0616 (1995).
- 22 Fersht, A. R. Optimization of rates of protein folding: the nucleation-condensation mechanism and its implications. *Proceedings of the National Academy of Sciences of the United States of America* **92**, 10869-10873, doi:10.1073/pnas.92.24.10869 (1995).
- 23 Karplus, M. Behind the folding funnel diagram. *Nat Chem Biol* **7**, 401-404, doi:10.1038/nchembio.565 (2011).
- 24 Dobson, C. M., Sali, A. & Karplus, M. Protein Folding: A Perspective from Theory and Experiment. *Angew Chem Int Ed Engl* **37**, 868-893, doi:10.1002/(SICI)1521-3773(19980420)37:7<868::AID-ANIE868>3.0.CO;2-H (1998).
- 25 Shirdel, S. A. & Khalifeh, K. Thermodynamics of protein folding: methodology, data analysis and interpretation of data. *Eur Biophys J* **48**, 305-316, doi:10.1007/s00249-019-01362-7 (2019).
- 26 Dill, K. A. & Chan, H. S. From Levinthal to pathways to funnels. *Nat Struct Biol* **4**, 10-19, doi:10.1038/nsb0197-10 (1997).
- 27 Bartlett, A. I. & Radford, S. E. An expanding arsenal of experimental methods yields an explosion of insights into protein folding mechanisms. *Nature structural & molecular biology* **16**, 582-588, doi:10.1038/nsmb.1592 (2009).
- 28 Dill, K. A. & MacCallum, J. L. The protein-folding problem, 50 years on. *Science* **338**, 1042-1046, doi:10.1126/science.1219021 (2012).
- 29 Jahn, T. R. & Radford, S. E. Folding versus aggregation: polypeptide conformations on competing pathways. *Arch Biochem Biophys* **469**, 100-117, doi:10.1016/j.abb.2007.05.015 (2008).

- 30 Hartl, F. U., Bracher, A. & Hayer-Hartl, M. Molecular chaperones in protein folding and proteostasis. *Nature* **475**, 324-332, doi:10.1038/nature10317 (2011).
- 31 Wright, P. E. & Dyson, H. J. Intrinsically unstructured proteins: re-assessing the protein structure-function paradigm. *J Mol Biol* **293**, 321-331, doi:10.1006/jmbi.1999.3110 (1999).
- 32 Tompa, P. Intrinsically disordered proteins: a 10-year recap. *Trends Biochem Sci* **37**, 509-516, doi:10.1016/j.tibs.2012.08.004 (2012).
- 33 Bahramali, G., Goliaei, B., Minucmehr, Z. & Marashi, S. A. A network biology approach to understanding the importance of chameleon proteins in human physiology and pathology. *Amino acids* **49**, 303-315, doi:10.1007/s00726-016-2361-6 (2017).
- 34 Oldfield, C. J. & Dunker, A. K. Intrinsically disordered proteins and intrinsically disordered protein regions. *Annu Rev Biochem* **83**, 553-584, doi:10.1146/annurev-biochem-072711-164947 (2014).
- 35 Uversky, V. N. Natively unfolded proteins: a point where biology waits for physics. *Protein Sci* **11**, 739-756, doi:10.1110/ps.4210102 (2002).
- 36 Xie, H. *et al.* Functional anthology of intrinsic disorder. 1. Biological processes and functions of proteins with long disordered regions. *J Proteome Res* **6**, 1882-1898, doi:10.1021/pr060392u (2007).
- 37 Spolar, R. S. & Record, M. T., Jr. Coupling of local folding to site-specific binding of proteins to DNA. *Science* **263**, 777-784, doi:10.1126/science.8303294 (1994).
- 38 Dyson, H. J. & Wright, P. E. Coupling of folding and binding for unstructured proteins. *Curr Opin Struct Biol* **12**, 54-60, doi:10.1016/s0959-440x(02)00289-0 (2002).
- 39 Uversky, V. N. Intrinsically disordered proteins and their environment: effects of strong denaturants, temperature, pH, counter ions, membranes, binding partners, osmolytes, and macromolecular crowding. *Protein J* **28**, 305-325, doi:10.1007/s10930-009-9201-4 (2009).
- 40 Tompa, P. & Fuxreiter, M. Fuzzy complexes: polymorphism and structural disorder in protein-protein interactions. *Trends Biochem Sci* **33**, 2-8, doi:10.1016/j.tibs.2007.10.003 (2008).
- 41 Dunker, A. K., Cortese, M. S., Romero, P., Iakoucheva, L. M. & Uversky, V. N. Flexible nets. The roles of intrinsic disorder in protein interaction networks. *FEBS J* **272**, 5129-5148, doi:10.1111/j.1742-4658.2005.04948.x (2005).
- 42 Uversky, V. N. A decade and a half of protein intrinsic disorder: biology still waits for physics. *Protein Sci* **22**, 693-724, doi:10.1002/pro.2261 (2013).
- 43 Tompa, P. Intrinsically unstructured proteins. *Trends Biochem Sci* **27**, 527-533, doi:10.1016/s0968-0004(02)02169-2 (2002).
- 44 Uversky, V. N., Gillespie, J. R. & Fink, A. L. Why are "natively unfolded" proteins unstructured under physiologic conditions? *Proteins* **41**, 415-427, doi:10.1002/1097-0134(20001115)41:3<415::aid-prot130>3.0.co;2-7 (2000).

- 45 Radivojac, P. *et al.* Intrinsic disorder and functional proteomics. *Biophys J* **92**, 1439-1456, doi:10.1529/biophysj.106.094045 (2007).
- 46 Chiti, F. & Dobson, C. M. Protein Misfolding, Amyloid Formation, and Human Disease: A Summary of Progress Over the Last Decade. *Annu Rev Biochem* **86**, 27-68, doi:10.1146/annurev-biochem-061516-045115 (2017).
- 47 Monsellier, E. & Chiti, F. Prevention of amyloid-like aggregation as a driving force of protein evolution. *EMBO Rep* **8**, 737-742, doi:10.1038/sj.embor.7401034 (2007).
- 48 Castillo, V. & Ventura, S. Amyloidogenic regions and interaction surfaces overlap in globular proteins related to conformational diseases. *PLoS Comput Biol* **5**, e1000476, doi:10.1371/journal.pcbi.1000476 (2009).
- 49 Kim, Y. E., Hipp, M. S., Bracher, A., Hayer-Hartl, M. & Hartl, F. U. Molecular chaperone functions in protein folding and proteostasis. *Annu Rev Biochem* **82**, 323-355, doi:10.1146/annurev-biochem-060208-092442 (2013).
- 50 Kampinga, H. H. & Craig, E. A. The HSP70 chaperone machinery: J proteins as drivers of functional specificity. *Nat Rev Mol Cell Biol* **11**, 579-592, doi:10.1038/nrm2941 (2010).
- 51 Rudiger, S., Mayer, M. P., Schneider-Mergener, J. & Bukau, B. Modulation of substrate specificity of the DnaK chaperone by alteration of a hydrophobic arch. *J Mol Biol* **304**, 245-251, doi:10.1006/jmbi.2000.4193 (2000).
- 52 Tartaglia, G. G., Dobson, C. M., Hartl, F. U. & Vendruscolo, M. Physicochemical determinants of chaperone requirements. *J Mol Biol* **400**, 579-588, doi:10.1016/j.jmb.2010.03.066 (2010).
- 53 Kaufman, R. J. *et al.* The unfolded protein response in nutrient sensing and differentiation. *Nat Rev Mol Cell Biol* **3**, 411-421, doi:10.1038/nrm829 (2002).
- 54 Hipp, M. S., Kasturi, P. & Hartl, F. U. The proteostasis network and its decline in ageing. *Nat Rev Mol Cell Biol* **20**, 421-435, doi:10.1038/s41580-019-0101-y (2019).
- 55 Auer, S., Dobson, C. M., Vendruscolo, M. & Maritan, A. Self-templated nucleation in peptide and protein aggregation. *Phys Rev Lett* **101**, 258101, doi:10.1103/PhysRevLett.101.258101 (2008).
- 56 Sabate, R. & Ventura, S. Cross-beta-sheet supersecondary structure in amyloid folds: techniques for detection and characterization. *Methods Mol Biol* **932**, 237-257, doi:10.1007/978-1-62703-065-6_15 (2013).
- 57 Sunde, M. *et al.* Common core structure of amyloid fibrils by synchrotron X-ray diffraction. *J Mol Biol* **273**, 729-739, doi:10.1006/jmbi.1997.1348 (1997).
- 58 Ke, P. C. *et al.* Half a century of amyloids: past, present and future. *Chem Soc Rev* **49**, 5473-5509, doi:10.1039/c9cs00199a (2020).
- 59 Gallardo, R., Ranson, N. A. & Radford, S. E. Amyloid structures: much more than just a cross-beta fold. *Curr Opin Struct Biol* **60**, 7-16, doi:10.1016/j.sbi.2019.09.001 (2020).

- 60 Loquet, A. *et al.* 3D structure determination of amyloid fibrils using solid-state NMR spectroscopy. *Methods* **138-139**, 26-38, doi:10.1016/j.ymeth.2018.03.014 (2018).
- 61 Riek, R. & Eisenberg, D. S. The activities of amyloids from a structural perspective. *Nature* **539**, 227-235, doi:10.1038/nature20416 (2016).
- 62 Nilsson, M. R. Techniques to study amyloid fibril formation in vitro. *Methods* **34**, 151-160, doi:10.1016/j.ymeth.2004.03.012 (2004).
- 63 Hawe, A., Sutter, M. & Jiskoot, W. Extrinsic fluorescent dyes as tools for protein characterization. *Pharm Res* **25**, 1487-1499, doi:10.1007/s11095-007-9516-9 (2008).
- 64 Chiti, F., Stefani, M., Taddei, N., Ramponi, G. & Dobson, C. M. Rationalization of the effects of mutations on peptide and protein aggregation rates. *Nature* **424**, 805-808, doi:10.1038/nature01891 (2003).
- 65 Chiti, F. *et al.* Kinetic partitioning of protein folding and aggregation. *Nat Struct Biol* **9**, 137-143, doi:10.1038/nsb752 (2002).
- 66 Wurth, C., Guimard, N. K. & Hecht, M. H. Mutations that reduce aggregation of the Alzheimer's Abeta42 peptide: an unbiased search for the sequence determinants of Abeta amyloidogenesis. *J Mol Biol* **319**, 1279-1290, doi:10.1016/S0022-2836(02)00399-6 (2002).
- 67 Beerten, J., Schymkowitz, J. & Rousseau, F. Aggregation prone regions and gatekeeping residues in protein sequences. *Curr Top Med Chem* **12**, 2470-2478, doi:10.2174/1568026611212220003 (2012).
- 68 De Baets, G., Van Durme, J., Rousseau, F. & Schymkowitz, J. A genome-wide sequence-structure analysis suggests aggregation gatekeepers constitute an evolutionary constrained functional class. *J Mol Biol* **426**, 2405-2412, doi:10.1016/j.jmb.2014.04.007 (2014).
- 69 Lawrence, M. S., Phillips, K. J. & Liu, D. R. Supercharging proteins can impart unusual resilience. *J Am Chem Soc* **129**, 10110-10112, doi:10.1021/ja071641y (2007).
- 70 West, M. W. *et al.* De novo amyloid proteins from designed combinatorial libraries. *Proceedings of the National Academy of Sciences of the United States of America* **96**, 11211-11216, doi:10.1073/pnas.96.20.11211 (1999).
- 71 Teng, P. K. & Eisenberg, D. Short protein segments can drive a non-fibrillizing protein into the amyloid state. *Protein Eng Des Sel* **22**, 531-536, doi:10.1093/protein/gzp037 (2009).
- 72 Ventura, S. *et al.* Short amino acid stretches can mediate amyloid formation in globular proteins: the Src homology 3 (SH3) case. *Proceedings of the National Academy of Sciences of the United States of America* **101**, 7258-7263, doi:10.1073/pnas.0308249101 (2004).
- 73 Ventura, S. *et al.* Conformational strain in the hydrophobic core and its implications for protein folding and design. *Nat Struct Biol* **9**, 485-493, doi:10.1038/nsb799 (2002).

- 74 Garcia-Pardo, J. *et al.* Amyloid formation by human carboxypeptidase D transthyretin-like domain under physiological conditions. *The Journal of biological chemistry* **289**, 33783-33796, doi:10.1074/jbc.M114.594804 (2014).
- 75 Sanchez de Groot, N., Pallares, I., Aviles, F. X., Vendrell, J. & Ventura, S. Prediction of "hot spots" of aggregation in disease-linked polypeptides. *BMC structural biology* **5**, 18, doi:10.1186/1472-6807-5-18 (2005).
- 76 DuBay, K. F. *et al.* Prediction of the absolute aggregation rates of amyloidogenic polypeptide chains. *J Mol Biol* **341**, 1317-1326, doi:10.1016/j.jmb.2004.06.043 (2004).
- 77 Morel, B., Varela, L., Azuaga, A. I. & Conejero-Lara, F. Environmental conditions affect the kinetics of nucleation of amyloid fibrils and determine their morphology. *Biophys J* **99**, 3801-3810, doi:10.1016/j.bpj.2010.10.039 (2010).
- 78 Wang, W., Nema, S. & Teagarden, D. Protein aggregation--pathways and influencing factors. *Int J Pharm* **390**, 89-99, doi:10.1016/j.ijpharm.2010.02.025 (2010).
- 79 Tedeschi, G. *et al.* Aggregation properties of a disordered protein are tunable by pH and depend on its net charge per residue. *Biochim Biophys Acta Gen Subj* **1861**, 2543-2550, doi:10.1016/j.bbagen.2017.09.002 (2017).
- 80 Griffith, J. S. Self-replication and scrapie. *Nature* **215**, 1043-1044, doi:10.1038/2151043a0 (1967).
- 81 Prusiner, S. B. Novel proteinaceous infectious particles cause scrapie. *Science* **216**, 136-144, doi:10.1126/science.6801762 (1982).
- 82 Jarrett, J. T. & Lansbury, P. T., Jr. Seeding "one-dimensional crystallization" of amyloid: a pathogenic mechanism in Alzheimer's disease and scrapie? *Cell* **73**, 1055-1058, doi:10.1016/0092-8674(93)90635-4 (1993).
- 83 Serio, T. R. *et al.* Nucleated conformational conversion and the replication of conformational information by a prion determinant. *Science* **289**, 1317-1321, doi:10.1126/science.289.5483.1317 (2000).
- 84 Tanaka, M., Collins, S. R., Toyama, B. H. & Weissman, J. S. The physical basis of how prion conformations determine strain phenotypes. *Nature* **442**, 585-589, doi:10.1038/nature04922 (2006).
- 85 Carulla, N. *et al.* Molecular recycling within amyloid fibrils. *Nature* **436**, 554-558, doi:10.1038/nature03986 (2005).
- 86 Cohen, S. I., Vendruscolo, M., Dobson, C. M. & Knowles, T. P. From macroscopic measurements to microscopic mechanisms of protein aggregation. *J Mol Biol* **421**, 160-171, doi:10.1016/j.jmb.2012.02.031 (2012).
- 87 Santos, J. & Ventura, S. Functional Amyloids Germinate in Plants. *Trends Plant Sci* **26**, 7-10, doi:10.1016/j.tplants.2020.10.001 (2021).
- 88 Claessen, D. *et al.* A novel class of secreted hydrophobic proteins is involved in aerial hyphae formation in *Streptomyces coelicolor* by forming amyloid-like fibrils. *Genes Dev* **17**, 1714-1726, doi:10.1101/gad.264303 (2003).

- 89 Chapman, M. R. *et al.* Role of Escherichia coli curli operons in directing amyloid fiber formation. *Science* **295**, 851-855, doi:10.1126/science.1067484 (2002).
- 90 Fowler, D. M. *et al.* Functional amyloid formation within mammalian tissue. *PLoS Biol* **4**, e6, doi:10.1371/journal.pbio.0040006 (2006).
- 91 Otzen, D. & Riek, R. Functional Amyloids. *Cold Spring Harb Perspect Biol* **11**, doi:10.1101/cshperspect.a033860 (2019).
- 92 Barnhart, M. M. & Chapman, M. R. Curli biogenesis and function. *Annu Rev Microbiol* **60**, 131-147, doi:10.1146/annurev.micro.60.080805.142106 (2006).
- 93 Yan, Z., Yin, M., Chen, J. & Li, X. Assembly and substrate recognition of curli biogenesis system. *Nature communications* **11**, 241, doi:10.1038/s41467-019-14145-7 (2020).
- 94 Hammer, N. D., Schmidt, J. C. & Chapman, M. R. The curli nucleator protein, CsgB, contains an amyloidogenic domain that directs CsgA polymerization. *Proceedings of the National Academy of Sciences of the United States of America* **104**, 12494-12499, doi:10.1073/pnas.0703310104 (2007).
- 95 Shu, Q. *et al.* The E. coli CsgB nucleator of curli assembles to beta-sheet oligomers that alter the CsgA fibrillization mechanism. *Proceedings of the National Academy of Sciences of the United States of America* **109**, 6502-6507, doi:10.1073/pnas.1204161109 (2012).
- 96 Cherny, I. *et al.* The formation of Escherichia coli curli amyloid fibrils is mediated by prion-like peptide repeats. *J Mol Biol* **352**, 245-252, doi:10.1016/j.jmb.2005.07.028 (2005).
- 97 Evans, M. L. *et al.* The bacterial curli system possesses a potent and selective inhibitor of amyloid formation. *Mol Cell* **57**, 445-455, doi:10.1016/j.molcel.2014.12.025 (2015).
- 98 Zhang, M., Shi, H., Zhang, X., Zhang, X. & Huang, Y. Cryo-EM structure of the nonameric CsgG-CsgF complex and its implications for controlling curli biogenesis in Enterobacteriaceae. *PLoS Biol* **18**, e3000748, doi:10.1371/journal.pbio.3000748 (2020).
- 99 Evans, M. L. & Chapman, M. R. Curli biogenesis: order out of disorder. *Biochimica et biophysica acta* **1843**, 1551-1558, doi:10.1016/j.bbamcr.2013.09.010 (2014).
- 100 Loferer, H., Hammar, M. & Normark, S. Availability of the fibre subunit CsgA and the nucleator protein CsgB during assembly of fibronectin-binding curli is limited by the intracellular concentration of the novel lipoprotein CsgG. *Mol Microbiol* **26**, 11-23, doi:10.1046/j.1365-2958.1997.5231883.x (1997).
- 101 Dueholm, M. S. *et al.* Functional amyloid in Pseudomonas. *Mol Microbiol* **77**, 1009-1020, doi:10.1111/j.1365-2958.2010.07269.x (2010).
- 102 Zeng, G. *et al.* Functional bacterial amyloid increases Pseudomonas biofilm hydrophobicity and stiffness. *Front Microbiol* **6**, 1099, doi:10.3389/fmicb.2015.01099 (2015).
- 103 Andreasen, M. *et al.* Physical Determinants of Amyloid Assembly in Biofilm Formation. *mBio* **10**, doi:10.1128/mBio.02279-18 (2019).

- 104 Bleem, A. *et al.* Protein Engineering Reveals Mechanisms of Functional Amyloid Formation in *Pseudomonas aeruginosa* Biofilms. *J Mol Biol* **430**, 3751-3763, doi:10.1016/j.jmb.2018.06.043 (2018).
- 105 Nagaraj, M. *et al.* Predicted Loop Regions Promote Aggregation: A Study of Amyloidogenic Domains in the Functional Amyloid FapC. *J Mol Biol* **432**, 2232-2252, doi:10.1016/j.jmb.2020.01.044 (2020).
- 106 Rouse, S. L. *et al.* A new class of hybrid secretion system is employed in *Pseudomonas* amyloid biogenesis. *Nature communications* **8**, 263, doi:10.1038/s41467-017-00361-6 (2017).
- 107 Dueholm, M. S. *et al.* Expression of Fap amyloids in *Pseudomonas aeruginosa*, *P. fluorescens*, and *P. putida* results in aggregation and increased biofilm formation. *Microbiologyopen* **2**, 365-382, doi:10.1002/mbo3.81 (2013).
- 108 Le, K. Y. *et al.* Role of Phenol-Soluble Modulins in *Staphylococcus epidermidis* Biofilm Formation and Infection of Indwelling Medical Devices. *J Mol Biol* **431**, 3015-3027, doi:10.1016/j.jmb.2019.03.030 (2019).
- 109 Gonzalez, D. J. *et al.* Novel phenol-soluble modulin derivatives in community-associated methicillin-resistant *Staphylococcus aureus* identified through imaging mass spectrometry. *The Journal of biological chemistry* **287**, 13889-13898, doi:10.1074/jbc.M112.349860 (2012).
- 110 Peschel, A. & Otto, M. Phenol-soluble modulins and staphylococcal infection. *Nat Rev Microbiol* **11**, 667-673, doi:10.1038/nrmicro3110 (2013).
- 111 Schwartz, K., Syed, A. K., Stephenson, R. E., Rickard, A. H. & Boles, B. R. Functional amyloids composed of phenol soluble modulins stabilize *Staphylococcus aureus* biofilms. *PLoS Pathog* **8**, e1002744, doi:10.1371/journal.ppat.1002744 (2012).
- 112 Salinas, N., Colletier, J. P., Moshe, A. & Landau, M. Extreme amyloid polymorphism in *Staphylococcus aureus* virulent PSMalpha peptides. *Nature communications* **9**, 3512, doi:10.1038/s41467-018-05490-0 (2018).
- 113 Tayeb-Fligelman, E. *et al.* The cytotoxic *Staphylococcus aureus* PSMalpha3 reveals a cross-alpha amyloid-like fibril. *Science* **355**, 831-833, doi:10.1126/science.aaf4901 (2017).
- 114 Taylor, J. D. & Matthews, S. J. New insight into the molecular control of bacterial functional amyloids. *Front Cell Infect Microbiol* **5**, 33, doi:10.3389/fcimb.2015.00033 (2015).
- 115 Tuite, M. F. & Cox, B. S. The genetic control of the formation and propagation of the [PSI⁺] prion of yeast. *Prion* **1**, 101-109, doi:10.4161/pri.1.2.4665 (2007).
- 116 Liebman, S. W. & Sherman, F. Extrachromosomal psi⁺ determinant suppresses nonsense mutations in yeast. *J Bacteriol* **139**, 1068-1071, doi:10.1128/jb.139.3.1068-1071.1979 (1979).

- 117 Firoozan, M., Grant, C. M., Duarte, J. A. & Tuite, M. F. Quantitation of readthrough of termination codons in yeast using a novel gene fusion assay. *Yeast* **7**, 173-183, doi:10.1002/yea.320070211 (1991).
- 118 Serio, T. R. & Lindquist, S. L. [PSI⁺]: an epigenetic modulator of translation termination efficiency. *Annu Rev Cell Dev Biol* **15**, 661-703, doi:10.1146/annurev.cellbio.15.1.661 (1999).
- 119 Glover, J. R. *et al.* Self-seeded fibers formed by Sup35, the protein determinant of [PSI⁺], a heritable prion-like factor of *S. cerevisiae*. *Cell* **89**, 811-819, doi:10.1016/s0092-8674(00)80264-0 (1997).
- 120 King, C. Y. *et al.* Prion-inducing domain 2-114 of yeast Sup35 protein transforms in vitro into amyloid-like filaments. *Proceedings of the National Academy of Sciences of the United States of America* **94**, 6618-6622, doi:10.1073/pnas.94.13.6618 (1997).
- 121 Baxa, U. *et al.* Filaments of the Ure2p prion protein have a cross-beta core structure. *J Struct Biol* **150**, 170-179, doi:10.1016/j.jsb.2005.02.007 (2005).
- 122 Lian, H. Y., Jiang, Y., Zhang, H., Jones, G. W. & Perrett, S. The yeast prion protein Ure2: structure, function and folding. *Biochimica et biophysica acta* **1764**, 535-545, doi:10.1016/j.bbapap.2005.11.016 (2006).
- 123 Taylor, K. L., Cheng, N., Williams, R. W., Steven, A. C. & Wickner, R. B. Prion domain initiation of amyloid formation in vitro from native Ure2p. *Science* **283**, 1339-1343, doi:10.1126/science.283.5406.1339 (1999).
- 124 True, H. L. & Lindquist, S. L. A yeast prion provides a mechanism for genetic variation and phenotypic diversity. *Nature* **407**, 477-483, doi:10.1038/35035005 (2000).
- 125 Chien, P., Weissman, J. S. & DePace, A. H. Emerging principles of conformation-based prion inheritance. *Annu Rev Biochem* **73**, 617-656, doi:10.1146/annurev.biochem.72.121801.161837 (2004).
- 126 True, H. L., Berlin, I. & Lindquist, S. L. Epigenetic regulation of translation reveals hidden genetic variation to produce complex traits. *Nature* **431**, 184-187, doi:10.1038/nature02885 (2004).
- 127 Uptain, S. M. & Lindquist, S. Prions as protein-based genetic elements. *Annu Rev Microbiol* **56**, 703-741, doi:10.1146/annurev.micro.56.013002.100603 (2002).
- 128 Shorter, J. & Lindquist, S. Prions as adaptive conduits of memory and inheritance. *Nat Rev Genet* **6**, 435-450, doi:10.1038/nrg1616 (2005).
- 129 Lindquist, S. *et al.* Amyloid fibres of Sup35 support a prion-like mechanism of inheritance in yeast. *Biochem Soc Trans* **26**, 486-490, doi:10.1042/bst0260486 (1998).
- 130 Wilson, K. A. & Tan-Wilson, A. Proteases catalyzing vicilin cleavage in developing pea (*Pisum sativum* L.) seeds. *J Plant Physiol* **224-225**, 86-94, doi:10.1016/j.jplph.2018.03.015 (2018).
- 131 Antonets, K. S. *et al.* Accumulation of storage proteins in plant seeds is mediated by amyloid formation. *PLoS Biol* **18**, e3000564, doi:10.1371/journal.pbio.3000564 (2020).

- 132 Wehmeyer, N. & Vierling, E. The expression of small heat shock proteins in seeds responds to discrete developmental signals and suggests a general protective role in desiccation tolerance. *Plant Physiol* **122**, 1099-1108, doi:10.1104/pp.122.4.1099 (2000).
- 133 Sano, N. *et al.* Staying Alive: Molecular Aspects of Seed Longevity. *Plant Cell Physiol* **57**, 660-674, doi:10.1093/pcp/pcv186 (2016).
- 134 Berson, J. F., Harper, D. C., Tenza, D., Raposo, G. & Marks, M. S. Pmel17 initiates premelanosome morphogenesis within multivesicular bodies. *Mol Biol Cell* **12**, 3451-3464, doi:10.1091/mbc.12.11.3451 (2001).
- 135 Raposo, G., Tenza, D., Murphy, D. M., Berson, J. F. & Marks, M. S. Distinct protein sorting and localization to premelanosomes, melanosomes, and lysosomes in pigmented melanocytic cells. *J Cell Biol* **152**, 809-824, doi:10.1083/jcb.152.4.809 (2001).
- 136 Berson, J. F. *et al.* Proprotein convertase cleavage liberates a fibrillogenic fragment of a resident glycoprotein to initiate melanosome biogenesis. *J Cell Biol* **161**, 521-533, doi:10.1083/jcb.200302072 (2003).
- 137 Theos, A. C., Truschel, S. T., Raposo, G. & Marks, M. S. The Silver locus product Pmel17/gp100/Silv/ME20: controversial in name and in function. *Pigment Cell Res* **18**, 322-336, doi:10.1111/j.1600-0749.2005.00269.x (2005).
- 138 Pawelek, J. M. & Lerner, A. B. 5,6-Dihydroxyindole is a melanin precursor showing potent cytotoxicity. *Nature* **276**, 626-628, doi:10.1038/276627a0 (1978).
- 139 Maji, S. K. *et al.* Functional amyloids as natural storage of peptide hormones in pituitary secretory granules. *Science* **325**, 328-332, doi:10.1126/science.1173155 (2009).
- 140 Nussbaum, R. L. & Ellis, C. E. Alzheimer's disease and Parkinson's disease. *The New England journal of medicine* **348**, 1356-1364, doi:10.1056/NEJM2003ra020003 (2003).
- 141 Dexter, D. T. & Jenner, P. Parkinson disease: from pathology to molecular disease mechanisms. *Free radical biology & medicine* **62**, 132-144, doi:10.1016/j.freeradbiomed.2013.01.018 (2013).
- 142 Pringsheim, T., Jette, N., Frolkis, A. & Steeves, T. D. The prevalence of Parkinson's disease: a systematic review and meta-analysis. *Movement disorders : official journal of the Movement Disorder Society* **29**, 1583-1590, doi:10.1002/mds.25945 (2014).
- 143 Goetz, C. G. The history of Parkinson's disease: early clinical descriptions and neurological therapies. *Cold Spring Harbor perspectives in medicine* **1**, a008862, doi:10.1101/cshperspect.a008862 (2011).
- 144 Duncan, G. W. *et al.* Health-related quality of life in early Parkinson's disease: the impact of nonmotor symptoms. *Movement disorders : official journal of the Movement Disorder Society* **29**, 195-202, doi:10.1002/mds.25664 (2014).
- 145 Martinez-Martin, P., Rodriguez-Blazquez, C., Kurtis, M. M., Chaudhuri, K. R. & Group, N. V. The impact of non-motor symptoms on health-related quality of life of patients

- with Parkinson's disease. *Movement disorders : official journal of the Movement Disorder Society* **26**, 399-406, doi:10.1002/mds.23462 (2011).
- 146 Marti, M. J., Tolosa, E. & Campdelacreu, J. Clinical overview of the synucleinopathies. *Movement disorders : official journal of the Movement Disorder Society* **18 Suppl 6**, S21-27, doi:10.1002/mds.10559 (2003).
 - 147 Kalia, L. V. & Lang, A. E. Parkinson's disease. *Lancet* **386**, 896-912, doi:10.1016/S0140-6736(14)61393-3 (2015).
 - 148 Cotzias, G. C. L-Dopa for Parkinsonism. *The New England journal of medicine* **278**, 630, doi:10.1056/nejm196803142781127 (1968).
 - 149 Hornykiewicz, O. L-DOPA: from a biologically inactive amino acid to a successful therapeutic agent. *Amino acids* **23**, 65-70, doi:10.1007/s00726-001-0111-9 (2002).
 - 150 Parkinson, J. An essay on the shaking palsy. 1817. *The Journal of neuropsychiatry and clinical neurosciences* **14**, 223-236; discussion 222, doi:10.1176/jnp.14.2.223 (2002).
 - 151 Charcot, J.-M. Leçons sur le maladies du système nerveus. *Bureaux du Progrès Medical Oeuvres Complètes (Tome 1)*. eds A. Delahaye and E. Lecronsniier Paris: Bureaux du Progrès Médical. 155–188. (1872).
 - 152 Blocq, C., Marinescu, G. . Sur un cas de tremblement parkinsonien hémiplégique symptomatique d'une tumeur du pédoncle cérébral. *C. R. Cos. Biol.* **5**, 105-111 (1893).
 - 153 Brissaud, E. Leçons sur les Maladies Nerveuses. *Escondido, CA: Masson & Associates, Inc.* **2** (1899).
 - 154 Trétiakoff, C. D. Contribution à L'étude De L'anatomie Pathologique Du Locus Niger De Soemmering Avec Quelques Deductions Relatives A La Pathogenie Des Troubles Du Tonus Musculaire Et De La Maladie De Parkinson. *Paris: Université de Paris* (1919).
 - 155 Lewy, F. Zur pathologischen anatomie der paralysis agitans. *Dtsch. Z. Nervenheilkd.* **50**, 50-55 (1912).
 - 156 Postuma, R. B. & Berg, D. Advances in markers of prodromal Parkinson disease. *Nature reviews. Neurology* **12**, 622-634, doi:10.1038/nrneurol.2016.152 (2016).
 - 157 Del Rey, N. L. *et al.* Advances in Parkinson's Disease: 200 Years Later. *Frontiers in neuroanatomy* **12**, 113, doi:10.3389/fnana.2018.00113 (2018).
 - 158 Carlsson, A., Lindqvist, M. & Magnusson, T. 3,4-Dihydroxyphenylalanine and 5-hydroxytryptophan as reserpine antagonists. *Nature* **180**, 1200, doi:10.1038/1801200a0 (1957).
 - 159 Ehringer, H. & Hornykiewicz, O. [Distribution of noradrenaline and dopamine (3-hydroxytyramine) in the human brain and their behavior in diseases of the extrapyramidal system]. *Klinische Wochenschrift* **38**, 1236-1239, doi:10.1007/bf01485901 (1960).

- 160 Polymeropoulos, M. H. *et al.* Mutation in the alpha-synuclein gene identified in families with Parkinson's disease. *Science* **276**, 2045-2047, doi:10.1126/science.276.5321.2045 (1997).
- 161 Kruger, R. *et al.* Ala30Pro mutation in the gene encoding alpha-synuclein in Parkinson's disease. *Nature genetics* **18**, 106-108, doi:10.1038/ng0298-106 (1998).
- 162 Athanassiadou, A. *et al.* Genetic analysis of families with Parkinson disease that carry the Ala53Thr mutation in the gene encoding alpha-synuclein. *American journal of human genetics* **65**, 555-558, doi:10.1086/302486 (1999).
- 163 Zarranz, J. J. *et al.* The new mutation, E46K, of alpha-synuclein causes Parkinson and Lewy body dementia. *Annals of neurology* **55**, 164-173, doi:10.1002/ana.10795 (2004).
- 164 Chartier-Harlin, M. C. *et al.* Alpha-synuclein locus duplication as a cause of familial Parkinson's disease. *Lancet* **364**, 1167-1169, doi:10.1016/S0140-6736(04)17103-1 (2004).
- 165 Appel-Cresswell, S. *et al.* Alpha-synuclein p.H50Q, a novel pathogenic mutation for Parkinson's disease. *Movement disorders : official journal of the Movement Disorder Society* **28**, 811-813, doi:10.1002/mds.25421 (2013).
- 166 Kiely, A. P. *et al.* alpha-Synucleinopathy associated with G51D SNCA mutation: a link between Parkinson's disease and multiple system atrophy? *Acta neuropathologica* **125**, 753-769, doi:10.1007/s00401-013-1096-7 (2013).
- 167 Singleton, A. B., Farrer, M. J. & Bonifati, V. The genetics of Parkinson's disease: progress and therapeutic implications. *Movement disorders : official journal of the Movement Disorder Society* **28**, 14-23, doi:10.1002/mds.25249 (2013).
- 168 Kitada, T. *et al.* Mutations in the parkin gene cause autosomal recessive juvenile parkinsonism. *Nature* **392**, 605-608, doi:10.1038/33416 (1998).
- 169 Samaranch, L. *et al.* PINK1-linked parkinsonism is associated with Lewy body pathology. *Brain : a journal of neurology* **133**, 1128-1142, doi:10.1093/brain/awq051 (2010).
- 170 Taipa, R. *et al.* DJ-1 linked parkinsonism (PARK7) is associated with Lewy body pathology. *Brain : a journal of neurology* **139**, 1680-1687, doi:10.1093/brain/aww080 (2016).
- 171 Zimprich, A. *et al.* Mutations in LRRK2 cause autosomal-dominant parkinsonism with pleomorphic pathology. *Neuron* **44**, 601-607, doi:10.1016/j.neuron.2004.11.005 (2004).
- 172 Schober, A. Classic toxin-induced animal models of Parkinson's disease: 6-OHDA and MPTP. *Cell and tissue research* **318**, 215-224, doi:10.1007/s00441-004-0938-y (2004).
- 173 Ko, W. K. D. & Bezard, E. Experimental animal models of Parkinson's disease: A transition from assessing symptomatology to alpha-synuclein targeted disease modification. *Experimental neurology* **298**, 172-179, doi:10.1016/j.expneurol.2017.07.020 (2017).

- 174 Koprach, J. B., Kalia, L. V. & Brotchie, J. M. Animal models of alpha-synucleinopathy for Parkinson disease drug development. *Nature reviews. Neuroscience* **18**, 515-529, doi:10.1038/nrn.2017.75 (2017).
- 175 Lazaro, D. F., Pavlou, M. A. S. & Outeiro, T. F. Cellular models as tools for the study of the role of alpha-synuclein in Parkinson's disease. *Experimental neurology* **298**, 162-171, doi:10.1016/j.expneurol.2017.05.007 (2017).
- 176 Marmion, D. J. & Kordower, J. H. alpha-Synuclein nonhuman primate models of Parkinson's disease. *Journal of neural transmission* **125**, 385-400, doi:10.1007/s00702-017-1720-0 (2018).
- 177 Trigo-Damas, I., Del Rey, N. L. & Blesa, J. Novel models for Parkinson's disease and their impact on future drug discovery. *Expert opinion on drug discovery* **13**, 229-239, doi:10.1080/17460441.2018.1428556 (2018).
- 178 Dehay, B. *et al.* Targeting alpha-synuclein for treatment of Parkinson's disease: mechanistic and therapeutic considerations. *The Lancet. Neurology* **14**, 855-866, doi:10.1016/S1474-4422(15)00006-X (2015).
- 179 Sampson, T. R. *et al.* Gut Microbiota Regulate Motor Deficits and Neuroinflammation in a Model of Parkinson's Disease. *Cell* **167**, 1469-1480 e1412, doi:10.1016/j.cell.2016.11.018 (2016).
- 180 Coune, P. G., Schneider, B. L. & Aebischer, P. Parkinson's disease: gene therapies. *Cold Spring Harbor perspectives in medicine* **2**, a009431, doi:10.1101/cshperspect.a009431 (2012).
- 181 Tolosa, E., Wenning, G. & Poewe, W. The diagnosis of Parkinson's disease. *The Lancet. Neurology* **5**, 75-86, doi:10.1016/S1474-4422(05)70285-4 (2006).
- 182 Postuma, R. B. *et al.* MDS clinical diagnostic criteria for Parkinson's disease. *Movement disorders : official journal of the Movement Disorder Society* **30**, 1591-1601, doi:10.1002/mds.26424 (2015).
- 183 Poewe, W. *et al.* Parkinson disease. *Nature reviews. Disease primers* **3**, 17013, doi:10.1038/nrdp.2017.13 (2017).
- 184 (!!! INVALID CITATION !!! {}).
- 185 Marder, K. S. *et al.* Predictors of parkin mutations in early-onset Parkinson disease: the consortium on risk for early-onset Parkinson disease study. *Arch Neurol* **67**, 731-738, doi:10.1001/archneurol.2010.95 (2010).
- 186 Pont-Sunyer, C. *et al.* The onset of nonmotor symptoms in Parkinson's disease (the ONSET PD study). *Movement disorders : official journal of the Movement Disorder Society* **30**, 229-237, doi:10.1002/mds.26077 (2015).
- 187 Schrag, A., Sauerbier, A. & Chaudhuri, K. R. New clinical trials for nonmotor manifestations of Parkinson's disease. *Movement disorders : official journal of the Movement Disorder Society* **30**, 1490-1504, doi:10.1002/mds.26415 (2015).

- 188 Hinnell, C. *et al.* Nonmotor versus motor symptoms: how much do they matter to health status in Parkinson's disease? *Movement disorders : official journal of the Movement Disorder Society* **27**, 236-241, doi:10.1002/mds.23961 (2012).
- 189 Storch, A. *et al.* Nonmotor fluctuations in Parkinson disease: severity and correlation with motor complications. *Neurology* **80**, 800-809, doi:10.1212/WNL.0b013e318285c0ed (2013).
- 190 Weerkamp, N. J. *et al.* Nonmotor symptoms in nursing home residents with Parkinson's disease: prevalence and effect on quality of life. *J Am Geriatr Soc* **61**, 1714-1721, doi:10.1111/jgs.12458 (2013).
- 191 Kalia, L. V., Brochie, J. M. & Fox, S. H. Novel nondopaminergic targets for motor features of Parkinson's disease: review of recent trials. *Movement disorders : official journal of the Movement Disorder Society* **28**, 131-144, doi:10.1002/mds.25273 (2013).
- 192 Karachi, C. *et al.* Cholinergic mesencephalic neurons are involved in gait and postural disorders in Parkinson disease. *The Journal of clinical investigation* **120**, 2745-2754, doi:10.1172/JCI42642 (2010).
- 193 Hirsch, E. C., Graybiel, A. M., Duyckaerts, C. & Javoy-Agid, F. Neuronal loss in the pedunculopontine tegmental nucleus in Parkinson disease and in progressive supranuclear palsy. *Proceedings of the National Academy of Sciences of the United States of America* **84**, 5976-5980, doi:10.1073/pnas.84.16.5976 (1987).
- 194 Seppi, K. *et al.* The Movement Disorder Society Evidence-Based Medicine Review Update: Treatments for the non-motor symptoms of Parkinson's disease. *Movement disorders : official journal of the Movement Disorder Society* **26 Suppl 3**, S42-80, doi:10.1002/mds.23884 (2011).
- 195 Connolly, B. & Fox, S. H. Treatment of cognitive, psychiatric, and affective disorders associated with Parkinson's disease. *Neurotherapeutics* **11**, 78-91, doi:10.1007/s13311-013-0238-x (2014).
- 196 Mahlknecht, P., Seppi, K. & Poewe, W. The Concept of Prodromal Parkinson's Disease. *J Parkinsons Dis* **5**, 681-697, doi:10.3233/JPD-150685 (2015).
- 197 Salat, D., Noyce, A. J., Schrag, A. & Tolosa, E. Challenges of modifying disease progression in prediagnostic Parkinson's disease. *The Lancet. Neurology* **15**, 637-648, doi:10.1016/S1474-4422(16)00060-0 (2016).
- 198 O'Sullivan, S. S. *et al.* Nonmotor symptoms as presenting complaints in Parkinson's disease: a clinicopathological study. *Movement disorders : official journal of the Movement Disorder Society* **23**, 101-106, doi:10.1002/mds.21813 (2008).
- 199 Hely, M. A., Reid, W. G., Adena, M. A., Halliday, G. M. & Morris, J. G. The Sydney multicenter study of Parkinson's disease: the inevitability of dementia at 20 years. *Movement disorders : official journal of the Movement Disorder Society* **23**, 837-844, doi:10.1002/mds.21956 (2008).
- 200 Hely, M. A., Morris, J. G., Reid, W. G. & Trafficante, R. Sydney Multicenter Study of Parkinson's disease: non-L-dopa-responsive problems dominate at 15 years.

- Movement disorders : official journal of the Movement Disorder Society* **20**, 190-199, doi:10.1002/mds.20324 (2005).
- 201 Noyce, A. J. *et al.* Meta-analysis of early nonmotor features and risk factors for Parkinson disease. *Annals of neurology* **72**, 893-901, doi:10.1002/ana.23687 (2012).
 - 202 Ritz, B., Lee, P. C., Lassen, C. F. & Arah, O. A. Parkinson disease and smoking revisited: ease of quitting is an early sign of the disease. *Neurology* **83**, 1396-1402, doi:10.1212/WNL.0000000000000879 (2014).
 - 203 Papadimitriou, D. *et al.* Motor and Nonmotor Features of Carriers of the p.A53T Alpha-Synuclein Mutation: A Longitudinal Study. *Movement disorders : official journal of the Movement Disorder Society* **31**, 1226-1230, doi:10.1002/mds.26615 (2016).
 - 204 Koros, C., Simitsi, A. & Stefanis, L. Genetics of Parkinson's Disease: Genotype-Phenotype Correlations. *Int Rev Neurobiol* **132**, 197-231, doi:10.1016/bs.irn.2017.01.009 (2017).
 - 205 Somme, J. H. *et al.* Initial neuropsychological impairments in patients with the E46K mutation of the alpha-synuclein gene (PARK 1). *Journal of the neurological sciences* **310**, 86-89, doi:10.1016/j.jns.2011.07.047 (2011).
 - 206 Ghosh, D. *et al.* The newly discovered Parkinson's disease associated Finnish mutation (A53E) attenuates alpha-synuclein aggregation and membrane binding. *Biochemistry* **53**, 6419-6421, doi:10.1021/bi5010365 (2014).
 - 207 Kiely, A. P. *et al.* Distinct clinical and neuropathological features of G51D SNCA mutation cases compared with SNCA duplication and H50Q mutation. *Mol Neurodegener* **10**, 41, doi:10.1186/s13024-015-0038-3 (2015).
 - 208 Lesage, S. *et al.* G51D alpha-synuclein mutation causes a novel parkinsonian-pyramidal syndrome. *Annals of neurology* **73**, 459-471, doi:10.1002/ana.23894 (2013).
 - 209 Tokutake, T. *et al.* Clinical and neuroimaging features of patient with early-onset Parkinson's disease with dementia carrying SNCA p.G51D mutation. *Parkinsonism Relat Disord* **20**, 262-264, doi:10.1016/j.parkreldis.2013.11.008 (2014).
 - 210 Martikainen, M. H., Paivarinta, M., Hietala, M. & Kaasinen, V. Clinical and imaging findings in Parkinson disease associated with the A53E SNCA mutation. *Neurol Genet* **1**, e27, doi:10.1212/NXG.0000000000000027 (2015).
 - 211 Pasanen, P. *et al.* Novel alpha-synuclein mutation A53E associated with atypical multiple system atrophy and Parkinson's disease-type pathology. *Neurobiology of aging* **35**, 2180 e2181-2185, doi:10.1016/j.neurobiolaging.2014.03.024 (2014).
 - 212 Paisan-Ruiz, C. *et al.* Cloning of the gene containing mutations that cause PARK8-linked Parkinson's disease. *Neuron* **44**, 595-600, doi:10.1016/j.neuron.2004.10.023 (2004).
 - 213 Zabetian, C. P. *et al.* A clinic-based study of the LRRK2 gene in Parkinson disease yields new mutations. *Neurology* **65**, 741-744, doi:10.1212/01.wnl.0000172630.22804.73 (2005).

- 214 Lee, S., Imai, Y., Gehrke, S., Liu, S. & Lu, B. The synaptic function of LRRK2. *Biochem Soc Trans* **40**, 1047-1051, doi:10.1042/BST20120113 (2012).
- 215 Rassu, M. *et al.* Role of LRRK2 in the regulation of dopamine receptor trafficking. *PloS one* **12**, e0179082, doi:10.1371/journal.pone.0179082 (2017).
- 216 Bose, A. & Beal, M. F. Mitochondrial dysfunction in Parkinson's disease. *Journal of neurochemistry* **139 Suppl 1**, 216-231, doi:10.1111/jnc.13731 (2016).
- 217 Cookson, M. R. Cellular effects of LRRK2 mutations. *Biochem Soc Trans* **40**, 1070-1073, doi:10.1042/BST20120165 (2012).
- 218 Marras, C. *et al.* Motor and nonmotor heterogeneity of LRRK2-related and idiopathic Parkinson's disease. *Movement disorders : official journal of the Movement Disorder Society* **31**, 1192-1202, doi:10.1002/mds.26614 (2016).
- 219 Pont-Sunyer, C. *et al.* The prodromal phase of leucine-rich repeat kinase 2-associated Parkinson disease: Clinical and imaging Studies. *Movement disorders : official journal of the Movement Disorder Society* **32**, 726-738, doi:10.1002/mds.26964 (2017).
- 220 Healy, D. G. *et al.* Phenotype, genotype, and worldwide genetic penetrance of LRRK2-associated Parkinson's disease: a case-control study. *The Lancet. Neurology* **7**, 583-590, doi:10.1016/S1474-4422(08)70117-0 (2008).
- 221 Lill, C. M. Genetics of Parkinson's disease. *Mol Cell Probes* **30**, 386-396, doi:10.1016/j.mcp.2016.11.001 (2016).
- 222 Thaler, A. *et al.* A "dose" effect of mutations in the GBA gene on Parkinson's disease phenotype. *Parkinsonism Relat Disord* **36**, 47-51, doi:10.1016/j.parkreldis.2016.12.014 (2017).
- 223 Montfort, M., Chabas, A., Vilageliu, L. & Grinberg, D. Functional analysis of 13 GBA mutant alleles identified in Gaucher disease patients: Pathogenic changes and "modifier" polymorphisms. *Hum Mutat* **23**, 567-575, doi:10.1002/humu.20043 (2004).
- 224 Sidransky, E. & Lopez, G. The link between the GBA gene and parkinsonism. *The Lancet. Neurology* **11**, 986-998, doi:10.1016/S1474-4422(12)70190-4 (2012).
- 225 Rocha, E. M. *et al.* Progressive decline of glucocerebrosidase in aging and Parkinson's disease. *Ann Clin Transl Neurol* **2**, 433-438, doi:10.1002/acn3.177 (2015).
- 226 Sidransky, E. *et al.* Multicenter analysis of glucocerebrosidase mutations in Parkinson's disease. *The New England journal of medicine* **361**, 1651-1661, doi:10.1056/NEJMoa0901281 (2009).
- 227 Mazzulli, J. R. *et al.* Gaucher disease glucocerebrosidase and alpha-synuclein form a bidirectional pathogenic loop in synucleinopathies. *Cell* **146**, 37-52, doi:10.1016/j.cell.2011.06.001 (2011).
- 228 Sardi, S. P. *et al.* Augmenting CNS glucocerebrosidase activity as a therapeutic strategy for parkinsonism and other Gaucher-related synucleinopathies. *Proceedings of the National Academy of Sciences of the United States of America* **110**, 3537-3542, doi:10.1073/pnas.1220464110 (2013).

- 229 Riley, B. E. *et al.* Structure and function of Parkin E3 ubiquitin ligase reveals aspects of RING and HECT ligases. *Nature communications* **4**, 1982, doi:10.1038/ncomms2982 (2013).
- 230 Smith, W. W. *et al.* Leucine-rich repeat kinase 2 (LRRK2) interacts with parkin, and mutant LRRK2 induces neuronal degeneration. *Proceedings of the National Academy of Sciences of the United States of America* **102**, 18676-18681, doi:10.1073/pnas.0508052102 (2005).
- 231 Sardi, S. P., Cheng, S. H. & Shihabuddin, L. S. Gaucher-related synucleinopathies: the examination of sporadic neurodegeneration from a rare (disease) angle. *Prog Neurobiol* **125**, 47-62, doi:10.1016/j.pneurobio.2014.12.001 (2015).
- 232 van der Merwe, C., Jalali Sefid Dashti, Z., Christoffels, A., Loos, B. & Bardien, S. Evidence for a common biological pathway linking three Parkinson's disease-causing genes: parkin, PINK1 and DJ-1. *Eur J Neurosci* **41**, 1113-1125, doi:10.1111/ejn.12872 (2015).
- 233 Schneider, S. A. & Alcalay, R. N. Neuropathology of genetic synucleinopathies with parkinsonism: Review of the literature. *Movement disorders : official journal of the Movement Disorder Society* **32**, 1504-1523, doi:10.1002/mds.27193 (2017).
- 234 Bonifati, V. *et al.* Mutations in the DJ-1 gene associated with autosomal recessive early-onset parkinsonism. *Science* **299**, 256-259, doi:10.1126/science.1077209 (2003).
- 235 Lesage, S. *et al.* Loss of VPS13C Function in Autosomal-Recessive Parkinsonism Causes Mitochondrial Dysfunction and Increases PINK1/Parkin-Dependent Mitophagy. *American journal of human genetics* **98**, 500-513, doi:10.1016/j.ajhg.2016.01.014 (2016).
- 236 Pickrell, A. M. & Youle, R. J. The roles of PINK1, parkin, and mitochondrial fidelity in Parkinson's disease. *Neuron* **85**, 257-273, doi:10.1016/j.neuron.2014.12.007 (2015).
- 237 Di Nottia, M. *et al.* DJ-1 modulates mitochondrial response to oxidative stress: clues from a novel diagnosis of PARK7. *Clin Genet* **92**, 18-25, doi:10.1111/cge.12841 (2017).
- 238 Guzman, J. N. *et al.* Oxidant stress evoked by pacemaking in dopaminergic neurons is attenuated by DJ-1. *Nature* **468**, 696-700, doi:10.1038/nature09536 (2010).
- 239 McCoy, M. K. & Cookson, M. R. Mitochondrial quality control and dynamics in Parkinson's disease. *Antioxid Redox Signal* **16**, 869-882, doi:10.1089/ars.2011.4074 10.1089/ars.2011.4019 (2012).
- 240 Valente, E. M. *et al.* Hereditary early-onset Parkinson's disease caused by mutations in PINK1. *Science* **304**, 1158-1160, doi:10.1126/science.1096284 (2004).
- 241 Abou-Sleiman, P. M. *et al.* A heterozygous effect for PINK1 mutations in Parkinson's disease? *Annals of neurology* **60**, 414-419, doi:10.1002/ana.20960 (2006).
- 242 Kim, C. & Lee, S. J. Controlling the mass action of alpha-synuclein in Parkinson's disease. *Journal of neurochemistry* **107**, 303-316, doi:10.1111/j.1471-4159.2008.05612.x (2008).

- 243 Melki, R. Role of Different Alpha-Synuclein Strains in Synucleinopathies, Similarities with other Neurodegenerative Diseases. *J Parkinsons Dis* **5**, 217-227, doi:10.3233/JPD-150543 (2015).
- 244 Kaushik, S. & Cuervo, A. M. Proteostasis and aging. *Nat Med* **21**, 1406-1415, doi:10.1038/nm.4001 (2015).
- 245 Xilouri, M., Brekk, O. R. & Stefanis, L. alpha-Synuclein and protein degradation systems: a reciprocal relationship. *Mol Neurobiol* **47**, 537-551, doi:10.1007/s12035-012-8341-2 (2013).
- 246 Braak, H. *et al.* Staging of brain pathology related to sporadic Parkinson's disease. *Neurobiology of aging* **24**, 197-211, doi:10.1016/s0197-4580(02)00065-9 (2003).
- 247 Angot, E., Steiner, J. A., Hansen, C., Li, J. Y. & Brundin, P. Are synucleinopathies prion-like disorders? *The Lancet. Neurology* **9**, 1128-1138, doi:10.1016/S1474-4422(10)70213-1 (2010).
- 248 Brundin, P., Melki, R. & Kopito, R. Prion-like transmission of protein aggregates in neurodegenerative diseases. *Nat Rev Mol Cell Biol* **11**, 301-307, doi:10.1038/nrm2873 (2010).
- 249 George, S., Rey, N. L., Reichenbach, N., Steiner, J. A. & Brundin, P. alpha-Synuclein: the long distance runner. *Brain Pathol* **23**, 350-357, doi:10.1111/bpa.12046 (2013).
- 250 Brundin, P., Li, J. Y., Holton, J. L., Lindvall, O. & Revesz, T. Research in motion: the enigma of Parkinson's disease pathology spread. *Nature reviews. Neuroscience* **9**, 741-745, doi:10.1038/nrn2477 (2008).
- 251 Xilouri, M., Vogiatzi, T., Vekrellis, K., Park, D. & Stefanis, L. Abberant alpha-synuclein confers toxicity to neurons in part through inhibition of chaperone-mediated autophagy. *PLoS one* **4**, e5515, doi:10.1371/journal.pone.0005515 (2009).
- 252 Volpicelli-Daley, L. A. *et al.* G2019S-LRRK2 Expression Augments alpha-Synuclein Sequestration into Inclusions in Neurons. *The Journal of neuroscience : the official journal of the Society for Neuroscience* **36**, 7415-7427, doi:10.1523/JNEUROSCI.3642-15.2016 (2016).
- 253 Fernandes, H. J. *et al.* ER Stress and Autophagic Perturbations Lead to Elevated Extracellular alpha-Synuclein in GBA-N370S Parkinson's iPSC-Derived Dopamine Neurons. *Stem Cell Reports* **6**, 342-356, doi:10.1016/j.stemcr.2016.01.013 (2016).
- 254 Tang, F. L. *et al.* VPS35 in Dopamine Neurons Is Required for Endosome-to-Golgi Retrieval of Lamp2a, a Receptor of Chaperone-Mediated Autophagy That Is Critical for alpha-Synuclein Degradation and Prevention of Pathogenesis of Parkinson's Disease. *The Journal of neuroscience : the official journal of the Society for Neuroscience* **35**, 10613-10628, doi:10.1523/JNEUROSCI.0042-15.2015 (2015).
- 255 Steele, J. W. *et al.* Latrepirdine stimulates autophagy and reduces accumulation of alpha-synuclein in cells and in mouse brain. *Molecular psychiatry* **18**, 882-888, doi:10.1038/mp.2012.115 (2013).

- 256 Sarkar, S., Davies, J. E., Huang, Z., Tunnacliffe, A. & Rubinsztein, D. C. Trehalose, a novel mTOR-independent autophagy enhancer, accelerates the clearance of mutant huntingtin and alpha-synuclein. *The Journal of biological chemistry* **282**, 5641-5652, doi:10.1074/jbc.M609532200 (2007).
- 257 Emmanouilidou, E., Stefanis, L. & Vekrellis, K. Cell-produced alpha-synuclein oligomers are targeted to, and impair, the 26S proteasome. *Neurobiology of aging* **31**, 953-968, doi:10.1016/j.neurobiolaging.2008.07.008 (2010).
- 258 Zheng, B. *et al.* PGC-1alpha, a potential therapeutic target for early intervention in Parkinson's disease. *Sci Transl Med* **2**, 52ra73, doi:10.1126/scitranslmed.3001059 (2010).
- 259 Devi, L., Raghavendran, V., Prabhu, B. M., Avadhani, N. G. & Anandatheerthavarada, H. K. Mitochondrial import and accumulation of alpha-synuclein impair complex I in human dopaminergic neuronal cultures and Parkinson disease brain. *The Journal of biological chemistry* **283**, 9089-9100, doi:10.1074/jbc.M710012200 (2008).
- 260 Eschbach, J. *et al.* Mutual exacerbation of peroxisome proliferator-activated receptor gamma coactivator 1alpha deregulation and alpha-synuclein oligomerization. *Annals of neurology* **77**, 15-32, doi:10.1002/ana.24294 (2015).
- 261 Dias, V., Junn, E. & Mouradian, M. M. The role of oxidative stress in Parkinson's disease. *J Parkinsons Dis* **3**, 461-491, doi:10.3233/JPD-130230 (2013).
- 262 Bolam, J. P. & Pissadaki, E. K. Living on the edge with too many mouths to feed: why dopamine neurons die. *Movement disorders : official journal of the Movement Disorder Society* **27**, 1478-1483, doi:10.1002/mds.25135 (2012).
- 263 Pissadaki, E. K. & Bolam, J. P. The energy cost of action potential propagation in dopamine neurons: clues to susceptibility in Parkinson's disease. *Front Comput Neurosci* **7**, 13, doi:10.3389/fncom.2013.00013 (2013).
- 264 Surmeier, D. J., Guzman, J. N., Sanchez-Padilla, J. & Schumacker, P. T. The role of calcium and mitochondrial oxidant stress in the loss of substantia nigra pars compacta dopaminergic neurons in Parkinson's disease. *Neuroscience* **198**, 221-231, doi:10.1016/j.neuroscience.2011.08.045 (2011).
- 265 Surmeier, D. J. *et al.* Calcium and Parkinson's disease. *Biochemical and biophysical research communications* **483**, 1013-1019, doi:10.1016/j.bbrc.2016.08.168 (2017).
- 266 Moehle, M. S. & West, A. B. M1 and M2 immune activation in Parkinson's Disease: Foe and ally? *Neuroscience* **302**, 59-73, doi:10.1016/j.neuroscience.2014.11.018 (2015).
- 267 Ransohoff, R. M. How neuroinflammation contributes to neurodegeneration. *Science* **353**, 777-783, doi:10.1126/science.aag2590 (2016).
- 268 Hirsch, E. C. & Hunot, S. Neuroinflammation in Parkinson's disease: a target for neuroprotection? *The Lancet. Neurology* **8**, 382-397, doi:10.1016/S1474-4422(09)70062-6 (2009).
- 269 Gao, H. M. *et al.* Neuroinflammation and oxidation/nitration of alpha-synuclein linked to dopaminergic neurodegeneration. *The Journal of neuroscience : the official journal*

- of the Society for Neuroscience **28**, 7687-7698, doi:10.1523/JNEUROSCI.0143-07.2008 (2008).
- 270 Jao, C. C., Hegde, B. G., Chen, J., Haworth, I. S. & Langen, R. Structure of membrane-bound alpha-synuclein from site-directed spin labeling and computational refinement. *Proceedings of the National Academy of Sciences of the United States of America* **105**, 19666-19671, doi:10.1073/pnas.0807826105 (2008).
 - 271 Bartels, T., Choi, J. G. & Selkoe, D. J. alpha-Synuclein occurs physiologically as a helically folded tetramer that resists aggregation. *Nature* **477**, 107-110, doi:10.1038/nature10324 (2011).
 - 272 Bendor, J. T., Logan, T. P. & Edwards, R. H. The function of alpha-synuclein. *Neuron* **79**, 1044-1066, doi:10.1016/j.neuron.2013.09.004 (2013).
 - 273 Sun, J. *et al.* Functional cooperation of alpha-synuclein and VAMP2 in synaptic vesicle recycling. *Proceedings of the National Academy of Sciences of the United States of America* **116**, 11113-11115, doi:10.1073/pnas.1903049116 (2019).
 - 274 Burre, J. *et al.* Alpha-synuclein promotes SNARE-complex assembly in vivo and in vitro. *Science* **329**, 1663-1667, doi:10.1126/science.1195227 (2010).
 - 275 Burre, J., Sharma, M. & Sudhof, T. C. alpha-Synuclein assembles into higher-order multimers upon membrane binding to promote SNARE complex formation. *Proceedings of the National Academy of Sciences of the United States of America* **111**, E4274-4283, doi:10.1073/pnas.1416598111 (2014).
 - 276 Hallacli, E. *et al.* The Parkinson's disease protein alpha-synuclein is a modulator of processing bodies and mRNA stability. *Cell* **185**, 2035-2056 e2033, doi:10.1016/j.cell.2022.05.008 (2022).
 - 277 Schaser, A. J. *et al.* Alpha-synuclein is a DNA binding protein that modulates DNA repair with implications for Lewy body disorders. *Scientific reports* **9**, 10919, doi:10.1038/s41598-019-47227-z (2019).
 - 278 Fusco, G. *et al.* Direct observation of the three regions in alpha-synuclein that determine its membrane-bound behaviour. *Nature communications* **5**, 3827, doi:10.1038/ncomms4827 (2014).
 - 279 Ulmer, T. S., Bax, A., Cole, N. B. & Nussbaum, R. L. Structure and dynamics of micelle-bound human alpha-synuclein. *The Journal of biological chemistry* **280**, 9595-9603, doi:10.1074/jbc.M411805200 (2005).
 - 280 Zhu, M., Li, J. & Fink, A. L. The association of alpha-synuclein with membranes affects bilayer structure, stability, and fibril formation. *The Journal of biological chemistry* **278**, 40186-40197, doi:10.1074/jbc.M305326200 (2003).
 - 281 Galvagnion, C. *et al.* Chemical properties of lipids strongly affect the kinetics of the membrane-induced aggregation of alpha-synuclein. *Proceedings of the National Academy of Sciences of the United States of America* **113**, 7065-7070, doi:10.1073/pnas.1601899113 (2016).

- 282 Kiechle, M., Grozdanov, V. & Danzer, K. M. The Role of Lipids in the Initiation of alpha-Synuclein Misfolding. *Front Cell Dev Biol* **8**, 562241, doi:10.3389/fcell.2020.562241 (2020).
- 283 O'Leary, E. I. & Lee, J. C. Interplay between alpha-synuclein amyloid formation and membrane structure. *Biochim Biophys Acta Proteins Proteom* **1867**, 483-491, doi:10.1016/j.bbapap.2018.09.012 (2019).
- 284 Doherty, C. P. A. *et al.* A short motif in the N-terminal region of alpha-synuclein is critical for both aggregation and function. *Nature structural & molecular biology* **27**, 249-259, doi:10.1038/s41594-020-0384-x (2020).
- 285 McGlinchey, R. P., Ni, X., Shadish, J. A., Jiang, J. & Lee, J. C. The N terminus of alpha-synuclein dictates fibril formation. *Proceedings of the National Academy of Sciences of the United States of America* **118**, doi:10.1073/pnas.2023487118 (2021).
- 286 Buratti, F. A. *et al.* Aromaticity at position 39 in alpha-synuclein: A modulator of amyloid fibril assembly and membrane-bound conformations. *Protein Sci* **31**, e4360, doi:10.1002/pro.4360 (2022).
- 287 Ueda, K. *et al.* Molecular cloning of cDNA encoding an unrecognized component of amyloid in Alzheimer disease. *Proceedings of the National Academy of Sciences of the United States of America* **90**, 11282-11286, doi:10.1073/pnas.90.23.11282 (1993).
- 288 Wakabayashi, K. *et al.* Accumulation of alpha-synuclein/NACP is a cytopathological feature common to Lewy body disease and multiple system atrophy. *Acta neuropathologica* **96**, 445-452, doi:10.1007/s004010050918 (1998).
- 289 Rodriguez, J. A. *et al.* Structure of the toxic core of alpha-synuclein from invisible crystals. *Nature* **525**, 486-490, doi:10.1038/nature15368 (2015).
- 290 Guerrero-Ferreira, R. *et al.* Cryo-EM structure of alpha-synuclein fibrils. *eLife* **7**, doi:10.7554/eLife.36402 (2018).
- 291 Chakraborty, R. & Chattopadhyay, K. Cryo-Electron Microscopy Uncovers Key Residues within the Core of Alpha-Synuclein Fibrils. *ACS Chem Neurosci* **10**, 1135-1136, doi:10.1021/acschemneuro.9b00090 (2019).
- 292 Izawa, Y. *et al.* Role of C-terminal negative charges and tyrosine residues in fibril formation of alpha-synuclein. *Brain and behavior* **2**, 595-605, doi:10.1002/brb3.86 (2012).
- 293 Baba, M. *et al.* Aggregation of alpha-synuclein in Lewy bodies of sporadic Parkinson's disease and dementia with Lewy bodies. *The American journal of pathology* **152**, 879-884 (1998).
- 294 Tuttle, M. D. *et al.* Solid-state NMR structure of a pathogenic fibril of full-length human alpha-synuclein. *Nature structural & molecular biology* **23**, 409-415, doi:10.1038/nsmb.3194 (2016).
- 295 Gillam, J. E. & MacPhee, C. E. Modelling amyloid fibril formation kinetics: mechanisms of nucleation and growth. *Journal of physics. Condensed matter : an Institute of Physics journal* **25**, 373101, doi:10.1088/0953-8984/25/37/373101 (2013).

- 296 Winner, B. *et al.* In vivo demonstration that alpha-synuclein oligomers are toxic. *Proceedings of the National Academy of Sciences of the United States of America* **108**, 4194-4199, doi:10.1073/pnas.1100976108 (2011).
- 297 Invernizzi, G., Papaleo, E., Sabate, R. & Ventura, S. Protein aggregation: mechanisms and functional consequences. *The international journal of biochemistry & cell biology* **44**, 1541-1554, doi:10.1016/j.biocel.2012.05.023 (2012).
- 298 Marvian, A. T., Koss, D. J., Aliakbari, F., Morshedi, D. & Outeiro, T. F. In vitro models of synucleinopathies: informing on molecular mechanisms and protective strategies. *Journal of neurochemistry* **150**, 535-565, doi:10.1111/jnc.14707 (2019).
- 299 Rutherford, N. J., Moore, B. D., Golde, T. E. & Giasson, B. I. Divergent effects of the H50Q and G51D SNCA mutations on the aggregation of alpha-synuclein. *Journal of neurochemistry* **131**, 859-867, doi:10.1111/jnc.12806 (2014).
- 300 Aguzzi, A., Heikenwalder, M. & Polymenidou, M. Insights into prion strains and neurotoxicity. *Nat Rev Mol Cell Biol* **8**, 552-561, doi:10.1038/nrm2204 (2007).
- 301 Bousset, L. *et al.* Structural and functional characterization of two alpha-synuclein strains. *Nature communications* **4**, 2575, doi:10.1038/ncomms3575 (2013).
- 302 Peelaerts, W. *et al.* alpha-Synuclein strains cause distinct synucleinopathies after local and systemic administration. *Nature* **522**, 340-344, doi:10.1038/nature14547 (2015).
- 303 Yamasaki, T. R. *et al.* Parkinson's disease and multiple system atrophy have distinct alpha-synuclein seed characteristics. *The Journal of biological chemistry* **294**, 1045-1058, doi:10.1074/jbc.RA118.004471 (2019).
- 304 Guerrero-Ferreira, R. *et al.* Two new polymorphic structures of human full-length alpha-synuclein fibrils solved by cryo-electron microscopy. *eLife* **8**, doi:10.7554/eLife.48907 (2019).
- 305 Boyer, D. R. *et al.* Structures of fibrils formed by alpha-synuclein hereditary disease mutant H50Q reveal new polymorphs. *Nature structural & molecular biology* **26**, 1044-1052, doi:10.1038/s41594-019-0322-y (2019).
- 306 Li, B. *et al.* Cryo-EM of full-length alpha-synuclein reveals fibril polymorphs with a common structural kernel. *Nature communications* **9**, 3609, doi:10.1038/s41467-018-05971-2 (2018).
- 307 Schweighauser, M. *et al.* Structures of alpha-synuclein filaments from multiple system atrophy. *Nature* **585**, 464-469, doi:10.1038/s41586-020-2317-6 (2020).
- 308 Shahnawaz, M. *et al.* Discriminating alpha-synuclein strains in Parkinson's disease and multiple system atrophy. *Nature* **578**, 273-277, doi:10.1038/s41586-020-1984-7 (2020).
- 309 Lau, A. *et al.* alpha-Synuclein strains target distinct brain regions and cell types. *Nature neuroscience* **23**, 21-31, doi:10.1038/s41593-019-0541-x (2020).
- 310 Ray, S. *et al.* alpha-Synuclein aggregation nucleates through liquid-liquid phase separation. *Nature chemistry* **12**, 705-716, doi:10.1038/s41557-020-0465-9 (2020).

- 311 Hardenberg, M. C. *et al.* Observation of an alpha-synuclein liquid droplet state and its maturation into Lewy body-like assemblies. *J Mol Cell Biol* **13**, 282-294, doi:10.1093/jmcb/mjaa075 (2021).
- 312 Takamuku, M. *et al.* Evolution of alpha-synuclein conformation ensemble toward amyloid fibril via liquid-liquid phase separation (LLPS) as investigated by dynamic nuclear polarization-enhanced solid-state MAS NMR. *Neurochem Int* **157**, 105345, doi:10.1016/j.neuint.2022.105345 (2022).
- 313 Brangwynne, C. P. *et al.* Germline P granules are liquid droplets that localize by controlled dissolution/condensation. *Science* **324**, 1729-1732, doi:10.1126/science.1172046 (2009).
- 314 Li, X. H., Chavali, P. L., Pancsa, R., Chavali, S. & Babu, M. M. Function and Regulation of Phase-Separated Biological Condensates. *Biochemistry* **57**, 2452-2461, doi:10.1021/acs.biochem.7b01228 (2018).
- 315 Molliex, A. *et al.* Phase separation by low complexity domains promotes stress granule assembly and drives pathological fibrillization. *Cell* **163**, 123-133, doi:10.1016/j.cell.2015.09.015 (2015).
- 316 Berry, J., Weber, S. C., Vaidya, N., Haataja, M. & Brangwynne, C. P. RNA transcription modulates phase transition-driven nuclear body assembly. *Proceedings of the National Academy of Sciences of the United States of America* **112**, E5237-5245, doi:10.1073/pnas.1509317112 (2015).
- 317 Li, P. *et al.* Phase transitions in the assembly of multivalent signalling proteins. *Nature* **483**, 336-340, doi:10.1038/nature10879 (2012).
- 318 Woodruff, J. B. *et al.* The Centrosome Is a Selective Condensate that Nucleates Microtubules by Concentrating Tubulin. *Cell* **169**, 1066-1077 e1010, doi:10.1016/j.cell.2017.05.028 (2017).
- 319 Sawner, A. S. *et al.* Modulating alpha-Synuclein Liquid-Liquid Phase Separation. *Biochemistry* **60**, 3676-3696, doi:10.1021/acs.biochem.1c00434 (2021).
- 320 Huang, S., Xu, B. & Liu, Y. Calcium promotes alpha-synuclein liquid-liquid phase separation to accelerate amyloid aggregation. *Biochemical and biophysical research communications* **603**, 13-20, doi:10.1016/j.bbrc.2022.02.097 (2022).
- 321 Xu, B. *et al.* Manganese promotes alpha-synuclein amyloid aggregation through the induction of protein phase transition. *The Journal of biological chemistry* **298**, 101469, doi:10.1016/j.jbc.2021.101469 (2022).
- 322 Oliva, R. *et al.* Remodeling of the Fibrillation Pathway of alpha-Synuclein by Interaction with Antimicrobial Peptide LL-III. *Chemistry* **27**, 11845-11851, doi:10.1002/chem.202101592 (2021).
- 323 Agarwal, A., Arora, L., Rai, S. K., Avni, A. & Mukhopadhyay, S. Spatiotemporal modulations in heterotypic condensates of prion and alpha-synuclein control phase transitions and amyloid conversion. *Nature communications* **13**, 1154, doi:10.1038/s41467-022-28797-5 (2022).

- 324 Siegert, A. *et al.* Interplay between tau and alpha-synuclein liquid-liquid phase separation. *Protein Sci* **30**, 1326-1336, doi:10.1002/pro.4025 (2021).
- 325 Spillantini, M. G. *et al.* Filamentous alpha-synuclein inclusions link multiple system atrophy with Parkinson's disease and dementia with Lewy bodies. *Neuroscience letters* **251**, 205-208, doi:10.1016/s0304-3940(98)00504-7 (1998).
- 326 Fusco, G. *et al.* Structural basis of membrane disruption and cellular toxicity by alpha-synuclein oligomers. *Science* **358**, 1440-1443, doi:10.1126/science.aan6160 (2017).
- 327 Cremades, N. *et al.* Direct observation of the interconversion of normal and toxic forms of alpha-synuclein. *Cell* **149**, 1048-1059, doi:10.1016/j.cell.2012.03.037 (2012).
- 328 Campioni, S. *et al.* A causative link between the structure of aberrant protein oligomers and their toxicity. *Nat Chem Biol* **6**, 140-147, doi:10.1038/nchembio.283 (2010).
- 329 Cascella, R. *et al.* The release of toxic oligomers from alpha-synuclein fibrils induces dysfunction in neuronal cells. *Nature communications* **12**, 1814, doi:10.1038/s41467-021-21937-3 (2021).
- 330 Gadhe, L. *et al.* Intermediates of alpha-synuclein aggregation: Implications in Parkinson's disease pathogenesis. *Biophys Chem* **281**, 106736, doi:10.1016/j.bpc.2021.106736 (2022).
- 331 Cascella, R., Bigi, A., Cremades, N. & Cecchi, C. Effects of oligomer toxicity, fibril toxicity and fibril spreading in synucleinopathies. *Cell Mol Life Sci* **79**, 174, doi:10.1007/s00018-022-04166-9 (2022).
- 332 Hansen, C. *et al.* alpha-Synuclein propagates from mouse brain to grafted dopaminergic neurons and seeds aggregation in cultured human cells. *The Journal of clinical investigation* **121**, 715-725, doi:10.1172/JCI43366 (2011).
- 333 Rietdijk, C. D., Perez-Pardo, P., Garssen, J., van Wezel, R. J. & Kraneveld, A. D. Exploring Braak's Hypothesis of Parkinson's Disease. *Frontiers in neurology* **8**, 37, doi:10.3389/fneur.2017.00037 (2017).
- 334 Makin, S. Pathology: The prion principle. *Nature* **538**, S13-S16, doi:10.1038/538S13a (2016).
- 335 Bloch, A., Probst, A., Bissig, H., Adams, H. & Tolnay, M. Alpha-synuclein pathology of the spinal and peripheral autonomic nervous system in neurologically unimpaired elderly subjects. *Neuropathology and applied neurobiology* **32**, 284-295, doi:10.1111/j.1365-2990.2006.00727.x (2006).
- 336 Del Tredici, K., Rub, U., De Vos, R. A., Bohl, J. R. & Braak, H. Where does parkinson disease pathology begin in the brain? *J Neuropathol Exp Neurol* **61**, 413-426, doi:10.1093/jnen/61.5.413 (2002).
- 337 Hawkes, C. H., Del Tredici, K. & Braak, H. Parkinson's disease: a dual-hit hypothesis. *Neuropathology and applied neurobiology* **33**, 599-614, doi:10.1111/j.1365-2990.2007.00874.x (2007).

- 338 Doty, R. L. Olfaction in Parkinson's disease and related disorders. *Neurobiology of disease* **46**, 527-552, doi:10.1016/j.nbd.2011.10.026 (2012).
- 339 Jellinger, K. A. A critical evaluation of current staging of alpha-synuclein pathology in Lewy body disorders. *Biochimica et biophysica acta* **1792**, 730-740, doi:10.1016/j.bbadis.2008.07.006 (2009).
- 340 Hughes, A. J., Daniel, S. E. & Lees, A. J. Improved accuracy of clinical diagnosis of Lewy body Parkinson's disease. *Neurology* **57**, 1497-1499, doi:10.1212/wnl.57.8.1497 (2001).
- 341 Goetz, C. G. *et al.* Movement Disorder Society-sponsored revision of the Unified Parkinson's Disease Rating Scale (MDS-UPDRS): scale presentation and clinimetric testing results. *Movement disorders : official journal of the Movement Disorder Society* **23**, 2129-2170, doi:10.1002/mds.22340 (2008).
- 342 Paek, S. H. *et al.* The clinical impact of precise electrode positioning in STN DBS on three-year outcomes. *Journal of the neurological sciences* **327**, 25-31, doi:10.1016/j.jns.2013.01.037 (2013).
- 343 Jankovic, J. & Hunter, C. A double-blind, placebo-controlled and longitudinal study of riluzole in early Parkinson's disease. *Parkinsonism Relat Disord* **8**, 271-276, doi:10.1016/s1353-8020(01)00040-2 (2002).
- 344 Garnett, E. S., Firnau, G. & Nahmias, C. Dopamine visualized in the basal ganglia of living man. *Nature* **305**, 137-138, doi:10.1038/305137a0 (1983).
- 345 Brooks, D. J. & Pavese, N. Imaging biomarkers in Parkinson's disease. *Prog Neurobiol* **95**, 614-628, doi:10.1016/j.pneurobio.2011.08.009 (2011).
- 346 Stoessl, A. J., Lehericy, S. & Strafella, A. P. Imaging insights into basal ganglia function, Parkinson's disease, and dystonia. *Lancet* **384**, 532-544, doi:10.1016/S0140-6736(14)60041-6 (2014).
- 347 Politis, M. Neuroimaging in Parkinson disease: from research setting to clinical practice. *Nature reviews. Neurology* **10**, 708-722, doi:10.1038/nrneurol.2014.205 (2014).
- 348 Delenclos, M., Jones, D. R., McLean, P. J. & Uitti, R. J. Biomarkers in Parkinson's disease: Advances and strategies. *Parkinsonism Relat Disord* **22 Suppl 1**, S106-110, doi:10.1016/j.parkreldis.2015.09.048 (2016).
- 349 Cipriani, S., Chen, X. & Schwarzschild, M. A. Urate: a novel biomarker of Parkinson's disease risk, diagnosis and prognosis. *Biomark Med* **4**, 701-712, doi:10.2217/bmm.10.94 (2010).
- 350 Shi, M. *et al.* Cerebrospinal fluid biomarkers for Parkinson disease diagnosis and progression. *Annals of neurology* **69**, 570-580, doi:10.1002/ana.22311 (2011).
- 351 Eller, M. & Williams, D. R. Biological fluid biomarkers in neurodegenerative parkinsonism. *Nature reviews. Neurology* **5**, 561-570, doi:10.1038/nrneurol.2009.135 (2009).

- 352 Parnetti, L. *et al.* Cerebrospinal fluid biomarkers in Parkinson disease. *Nature reviews. Neurology* **9**, 131-140, doi:10.1038/nrneurol.2013.10 (2013).
- 353 Hong, Z. *et al.* DJ-1 and alpha-synuclein in human cerebrospinal fluid as biomarkers of Parkinson's disease. *Brain : a journal of neurology* **133**, 713-726, doi:10.1093/brain/awq008 (2010).
- 354 Group, P. D. M. C. *et al.* Long-term effectiveness of dopamine agonists and monoamine oxidase B inhibitors compared with levodopa as initial treatment for Parkinson's disease (PD MED): a large, open-label, pragmatic randomised trial. *Lancet* **384**, 1196-1205, doi:10.1016/S0140-6736(14)60683-8 (2014).
- 355 LeWitt, P. A. & Fahn, S. Levodopa therapy for Parkinson disease: A look backward and forward. *Neurology* **86**, S3-12, doi:10.1212/WNL.0000000000002509 (2016).
- 356 Friis, M. L., Paulson, O. B., Hertz, M. M. & Bolwig, T. G. Blood-brain barrier permeability of L-dopa in man. *Eur J Clin Invest* **11**, 231-234, doi:10.1111/j.1365-2362.1981.tb01845.x (1981).
- 357 Marsden, C. D. & Parkes, J. D. Success and problems of long-term levodopa therapy in Parkinson's disease. *Lancet* **1**, 345-349, doi:10.1016/s0140-6736(77)91146-1 (1977).
- 358 Ahlskog, J. E. & Muentert, M. D. Frequency of levodopa-related dyskinesias and motor fluctuations as estimated from the cumulative literature. *Movement disorders : official journal of the Movement Disorder Society* **16**, 448-458, doi:10.1002/mds.1090 (2001).
- 359 Hauser, R. A. *et al.* Ten-year follow-up of Parkinson's disease patients randomized to initial therapy with ropinirole or levodopa. *Movement disorders : official journal of the Movement Disorder Society* **22**, 2409-2417, doi:10.1002/mds.21743 (2007).
- 360 Katzenschlager, R. *et al.* Fourteen-year final report of the randomized PDRG-UK trial comparing three initial treatments in PD. *Neurology* **71**, 474-480, doi:10.1212/01.wnl.0000310812.43352.66 (2008).
- 361 Jenner, P. Molecular mechanisms of L-DOPA-induced dyskinesia. *Nature reviews. Neuroscience* **9**, 665-677, doi:10.1038/nrn2471 (2008).
- 362 Aquino, C. C. & Fox, S. H. Clinical spectrum of levodopa-induced complications. *Movement disorders : official journal of the Movement Disorder Society* **30**, 80-89, doi:10.1002/mds.26125 (2015).
- 363 Shen, H., Kannari, K., Yamato, H., Arai, A. & Matsunaga, M. Effects of benserazide on L-DOPA-derived extracellular dopamine levels and aromatic L-amino acid decarboxylase activity in the striatum of 6-hydroxydopamine-lesioned rats. *Tohoku J Exp Med* **199**, 149-159, doi:10.1620/tjem.199.149 (2003).
- 364 Casacchia, M., Barba, C., Ruggieri, S., Zamponi, A. & Agnoli, A. [Results of prolonged treatment of Parkinson's disease with the L-dopa-benserazide combination]. *Riv Neurol* **44**, 303-330 (1974).
- 365 Rinne, U. K., Sonninen, V. & Siirtola, T. Plasma concentration of levodopa in patients with Parkinson's disease. *Eur Neurol* **10**, 301-310, doi:10.1159/000114285 (1973).

- 366 Mars, H. Metabolic interactions of pyridoxine, levodopa, and carbidopa in Parkinson's disease. *Trans Am Neurol Assoc* **98**, 241-245 (1973).
- 367 Marsden, C. D., Barry, P. E., Parkes, J. D. & Zilkha, K. J. Treatment of Parkinson's disease with levodopa combined with L-alpha-methyldopahydrazine, an inhibitor of extracerebral DOPA decarboxylase. *Journal of neurology, neurosurgery, and psychiatry* **36**, 10-14, doi:10.1136/jnnp.36.1.10 (1973).
- 368 Glasgow, G. L., Henley, J. W. & Willoughby, E. W. L-alpha-methyldopa hydrazine (Carbidopa) combined with L-dopa in the treatment of Parkinson's disease. *Aust N Z J Med* **4**, 373-378, doi:10.1111/j.1445-5994.1974.tb03207.x (1974).
- 369 Muller, T. Catechol-O-methyltransferase inhibitors in Parkinson's disease. *Drugs* **75**, 157-174, doi:10.1007/s40265-014-0343-0 (2015).
- 370 McKenzie, G. M. Proceedings: The effects of COMT inhibitors on behavior and dopamine metabolism. *Psychopharmacol Bull* **10**, 31-38 (1974).
- 371 Ferreira, J. J. *et al.* Opicapone as an adjunct to levodopa in patients with Parkinson's disease and end-of-dose motor fluctuations: a randomised, double-blind, controlled trial. *The Lancet. Neurology* **15**, 154-165, doi:10.1016/S1474-4422(15)00336-1 (2016).
- 372 Mennisto, P. T. Clinical Potential of Catechol-OMethyltransferase (COMT) Inhibitors as Adjuvants in Parkinson's Disease. *CNS Drugs* **1**, 172-179, doi:10.2165/00023210-199401030-00002 (1994).
- 373 Myllyla, V. V., Sotaniemi, K. A., Illi, A., Suominen, K. & Keranen, T. Effect of entacapone, a COMT inhibitor, on the pharmacokinetics of levodopa and on cardiovascular responses in patients with Parkinson's disease. *Eur J Clin Pharmacol* **45**, 419-423, doi:10.1007/BF00315512 (1993).
- 374 Keranen, T. *et al.* The effect of catechol-O-methyl transferase inhibition by entacapone on the pharmacokinetics and metabolism of levodopa in healthy volunteers. *Clinical neuropharmacology* **16**, 145-156, doi:10.1097/00002826-199304000-00007 (1993).
- 375 Maj, J., Rogoz, Z., Skuza, G., Sowinska, H. & Superata, J. Behavioural and neurochemical effects of Ro 40-7592, a new COMT inhibitor with a potential therapeutic activity in Parkinson's disease. *J Neural Transm Park Dis Dement Sect* **2**, 101-112, doi:10.1007/BF02260898 (1990).
- 376 Limousin, P., Pollak, P., Gervason-Tournier, C. L., Hommel, M. & Perret, J. E. Ro 40-7592, a COMT inhibitor, plus levodopa in Parkinson's disease. *Lancet* **341**, 1605, doi:10.1016/0140-6736(93)90750-b (1993).
- 377 Seppi, K. *et al.* Update on treatments for nonmotor symptoms of Parkinson's disease- an evidence-based medicine review. *Movement disorders : official journal of the Movement Disorder Society* **34**, 180-198, doi:10.1002/mds.27602 (2019).
- 378 Fox, S. H. *et al.* The Movement Disorder Society Evidence-Based Medicine Review Update: Treatments for the motor symptoms of Parkinson's disease. *Movement disorders : official journal of the Movement Disorder Society* **26 Suppl 3**, S2-41, doi:10.1002/mds.23829 (2011).

- 379 Poewe, W. H. *et al.* Efficacy of pramipexole and transdermal rotigotine in advanced Parkinson's disease: a double-blind, double-dummy, randomised controlled trial. *The Lancet. Neurology* **6**, 513-520, doi:10.1016/S1474-4422(07)70108-4 (2007).
- 380 Garcia Ruiz, P. J. *et al.* Efficacy of long-term continuous subcutaneous apomorphine infusion in advanced Parkinson's disease with motor fluctuations: a multicenter study. *Movement disorders : official journal of the Movement Disorder Society* **23**, 1130-1136, doi:10.1002/mds.22063 (2008).
- 381 Jankovic, J. & Poewe, W. Therapies in Parkinson's disease. *Curr Opin Neurol* **25**, 433-447, doi:10.1097/WCO.0b013e3283542fc2 (2012).
- 382 Connolly, B. S. & Lang, A. E. Pharmacological treatment of Parkinson disease: a review. *JAMA* **311**, 1670-1683, doi:10.1001/jama.2014.3654 (2014).
- 383 Goldenberg, M. M. Medical management of Parkinson's disease. *P T* **33**, 590-606 (2008).
- 384 Schapira, A. H. Monoamine oxidase B inhibitors for the treatment of Parkinson's disease: a review of symptomatic and potential disease-modifying effects. *CNS Drugs* **25**, 1061-1071, doi:10.2165/11596310-000000000-00000 (2011).
- 385 Chew, Z. X. *et al.* The Role of Monoamine Oxidase B Inhibitors in the Treatment of Parkinson's Disease - An Update. *CNS Neurol Disord Drug Targets*, doi:10.2174/1871527321666211231100255 (2021).
- 386 Alborghetti, M. & Nicoletti, F. Different Generations of Type-B Monoamine Oxidase Inhibitors in Parkinson's Disease: From Bench to Bedside. *Curr Neuroparmacol* **17**, 861-873, doi:10.2174/1570159X16666180830100754 (2019).
- 387 Marmol, S., Feldman, M., Singer, C. & Margolesky, J. Amantadine Revisited: A Contender for Initial Treatment in Parkinson's Disease? *CNS Drugs* **35**, 1141-1152, doi:10.1007/s40263-021-00862-5 (2021).
- 388 Friedman, J. H. & Hershkowitz, D. Clozapine Use in a Movement Disorder Clinic. *Clinical neuropsychopharmacology* **45**, 95-98, doi:10.1097/WNF.0000000000000510 (2022).
- 389 Allen, N. E. *et al.* Interventions for preventing falls in Parkinson's disease. *Cochrane Database Syst Rev* **6**, CD011574, doi:10.1002/14651858.CD011574.pub2 (2022).
- 390 Baba, T. *et al.* Effect of donepezil for dementia prevention in Parkinson's disease with severe hyposmia (The DASH-PD study): A randomized long-term placebo-controlled trial. *EClinicalMedicine* **51**, 101571, doi:10.1016/j.eclinm.2022.101571 (2022).
- 391 Limousin, P. *et al.* Effect of parkinsonian signs and symptoms of bilateral subthalamic nucleus stimulation. *Lancet* **345**, 91-95, doi:10.1016/s0140-6736(95)90062-4 (1995).
- 392 Kalia, S. K., Sankar, T. & Lozano, A. M. Deep brain stimulation for Parkinson's disease and other movement disorders. *Curr Opin Neurol* **26**, 374-380, doi:10.1097/WCO.0b013e3283632d08 (2013).

- 393 Antonini, A., Moro, E., Godeiro, C. & Reichmann, H. Medical and surgical management of advanced Parkinson's disease. *Movement disorders : official journal of the Movement Disorder Society* **33**, 900-908, doi:10.1002/mds.27340 (2018).
- 394 Rodriguez-Oroz, M. C. *et al.* Bilateral deep brain stimulation in Parkinson's disease: a multicentre study with 4 years follow-up. *Brain : a journal of neurology* **128**, 2240-2249, doi:10.1093/brain/awh571 (2005).
- 395 Follett, K. A. *et al.* Pallidal versus subthalamic deep-brain stimulation for Parkinson's disease. *The New England journal of medicine* **362**, 2077-2091, doi:10.1056/NEJMoa0907083 (2010).
- 396 Zibetti, M. *et al.* Beyond nine years of continuous subthalamic nucleus deep brain stimulation in Parkinson's disease. *Movement disorders : official journal of the Movement Disorder Society* **26**, 2327-2334, doi:10.1002/mds.23903 (2011).
- 397 Pujols, J., Pena-Diaz, S., Pallares, I. & Ventura, S. Chemical Chaperones as Novel Drugs for Parkinson's Disease. *Trends in molecular medicine* **26**, 408-421, doi:10.1016/j.molmed.2020.01.005 (2020).
- 398 Alba, R., Bosch, A. & Chillon, M. Gutless adenovirus: last-generation adenovirus for gene therapy. *Gene Ther* **12 Suppl 1**, S18-27, doi:10.1038/sj.gt.3302612 (2005).
- 399 Froelich, S., Tai, A. & Wang, P. Lentiviral vectors for immune cells targeting. *Immunopharmacol Immunotoxicol* **32**, 208-218, doi:10.3109/08923970903420582 (2010).
- 400 Kotterman, M. A. & Schaffer, D. V. Engineering adeno-associated viruses for clinical gene therapy. *Nat Rev Genet* **15**, 445-451, doi:10.1038/nrg3742 (2014).
- 401 LeWitt, P. A. *et al.* AAV2-GAD gene therapy for advanced Parkinson's disease: a double-blind, sham-surgery controlled, randomised trial. *The Lancet. Neurology* **10**, 309-319, doi:10.1016/S1474-4422(11)70039-4 (2011).
- 402 Muramatsu, S. *et al.* Recombinant adeno-associated viral vectors bring gene therapy for Parkinson's disease closer to reality. *Journal of neurology* **249 Suppl 2**, II36-40, doi:10.1007/s00415-002-1207-1 (2002).
- 403 Jarraya, B. *et al.* Dopamine gene therapy for Parkinson's disease in a nonhuman primate without associated dyskinesia. *Sci Transl Med* **1**, 2ra4, doi:10.1126/scitranslmed.3000130 (2009).
- 404 Marks, W. J., Jr. *et al.* Gene delivery of AAV2-neurturin for Parkinson's disease: a double-blind, randomised, controlled trial. *The Lancet. Neurology* **9**, 1164-1172, doi:10.1016/S1474-4422(10)70254-4 (2010).
- 405 Bjorklund, A. *et al.* Towards a neuroprotective gene therapy for Parkinson's disease: use of adenovirus, AAV and lentivirus vectors for gene transfer of GDNF to the nigrostriatal system in the rat Parkinson model. *Brain Res* **886**, 82-98, doi:10.1016/s0006-8993(00)02915-2 (2000).

- 406 Tian, Y. Y. *et al.* Favorable effects of VEGF gene transfer on a rat model of Parkinson disease using adeno-associated viral vectors. *Neuroscience letters* **421**, 239-244, doi:10.1016/j.neulet.2007.05.033 (2007).
- 407 Oh, S. M. *et al.* Combined Nurr1 and Foxa2 roles in the therapy of Parkinson's disease. *EMBO Mol Med* **7**, 510-525, doi:10.15252/emmm.201404610 (2015).
- 408 Rahman, M. U. *et al.* CRISPR-Cas9-Based Technology and Its Relevance to Gene Editing in Parkinson's Disease. *Pharmaceutics* **14**, doi:10.3390/pharmaceutics14061252 (2022).
- 409 Lindvall, O. *et al.* Grafts of fetal dopamine neurons survive and improve motor function in Parkinson's disease. *Science* **247**, 574-577, doi:10.1126/science.2105529 (1990).
- 410 Piccini, P. *et al.* Dopamine release from nigral transplants visualized in vivo in a Parkinson's patient. *Nature neuroscience* **2**, 1137-1140, doi:10.1038/16060 (1999).
- 411 Barker, R. A., Drouin-Ouellet, J. & Parmar, M. Cell-based therapies for Parkinson disease-past insights and future potential. *Nature reviews. Neurology* **11**, 492-503, doi:10.1038/nrneurol.2015.123 (2015).
- 412 Petit, G. H., Olsson, T. T. & Brundin, P. The future of cell therapies and brain repair: Parkinson's disease leads the way. *Neuropathology and applied neurobiology* **40**, 60-70, doi:10.1111/nan.12110 (2014).
- 413 Hauser, R. A. alpha-Synuclein in Parkinson's disease: getting to the core of the matter. *The Lancet. Neurology* **14**, 785-786, doi:10.1016/S1474-4422(15)00136-2 (2015).
- 414 Kingwell, K. Zeroing in on neurodegenerative alpha-synuclein. *Nat Rev Drug Discov* **16**, 371-373, doi:10.1038/nrd.2017.95 (2017).
- 415 Mikitsh, J. L. & Chacko, A. M. Pathways for small molecule delivery to the central nervous system across the blood-brain barrier. *Perspect Medicin Chem* **6**, 11-24, doi:10.4137/PMC.S13384 (2014).
- 416 Li, J., Zhu, M., Manning-Bog, A. B., Di Monte, D. A. & Fink, A. L. Dopamine and L-dopa disaggregate amyloid fibrils: implications for Parkinson's and Alzheimer's disease. *FASEB J* **18**, 962-964, doi:10.1096/fj.03-0770fje (2004).
- 417 Li, H. T. *et al.* Inhibition of alpha-synuclein fibrillization by dopamine analogs via reaction with the amino groups of alpha-synuclein. Implication for dopaminergic neurodegeneration. *FEBS J* **272**, 3661-3672, doi:10.1111/j.1742-4658.2005.04792.x (2005).
- 418 Leong, S. L. *et al.* Formation of dopamine-mediated alpha-synuclein-soluble oligomers requires methionine oxidation. *Free radical biology & medicine* **46**, 1328-1337, doi:10.1016/j.freeradbiomed.2009.02.009 (2009).
- 419 Uversky, V. N. *et al.* Methionine oxidation inhibits fibrillation of human alpha-synuclein in vitro. *FEBS Lett* **517**, 239-244, doi:10.1016/s0014-5793(02)02638-8 (2002).

- 420 Norris, E. H. *et al.* Reversible inhibition of alpha-synuclein fibrillization by dopaminochrome-mediated conformational alterations. *The Journal of biological chemistry* **280**, 21212-21219, doi:10.1074/jbc.M412621200 (2005).
- 421 Latawiec, D. *et al.* Modulation of alpha-synuclein aggregation by dopamine analogs. *PLoS one* **5**, e9234, doi:10.1371/journal.pone.0009234 (2010).
- 422 Herrera, F. E. *et al.* Inhibition of alpha-synuclein fibrillization by dopamine is mediated by interactions with five C-terminal residues and with E83 in the NAC region. *PLoS one* **3**, e3394, doi:10.1371/journal.pone.0003394 (2008).
- 423 Mazzulli, J. R., Armakola, M., Dumoulin, M., Parastatidis, I. & Ischiropoulos, H. Cellular oligomerization of alpha-synuclein is determined by the interaction of oxidized catechols with a C-terminal sequence. *The Journal of biological chemistry* **282**, 31621-31630, doi:10.1074/jbc.M704737200 (2007).
- 424 Dibenedetto, D., Rossetti, G., Caliendo, R. & Carloni, P. A molecular dynamics simulation-based interpretation of nuclear magnetic resonance multidimensional heteronuclear spectra of alpha-synuclein.dopamine adducts. *Biochemistry* **52**, 6672-6683, doi:10.1021/bi400367r (2013).
- 425 Mor, D. E. *et al.* Dopamine induces soluble alpha-synuclein oligomers and nigrostriatal degeneration. *Nature neuroscience* **20**, 1560-1568, doi:10.1038/nn.4641 (2017).
- 426 Mor, D. E., Daniels, M. J. & Ischiropoulos, H. The usual suspects, dopamine and alpha-synuclein, conspire to cause neurodegeneration. *Movement disorders : official journal of the Movement Disorder Society* **34**, 167-179, doi:10.1002/mds.27607 (2019).
- 427 Ono, K. & Yamada, M. Antioxidant compounds have potent anti-fibrillogenic and fibrildestabilizing effects for alpha-synuclein fibrils in vitro. *Journal of neurochemistry* **97**, 105-115, doi:10.1111/j.1471-4159.2006.03707.x (2006).
- 428 Masuda, M. *et al.* Small molecule inhibitors of alpha-synuclein filament assembly. *Biochemistry* **45**, 6085-6094, doi:10.1021/bi0600749 (2006).
- 429 Dhouafli, Z. *et al.* Inhibition of protein misfolding and aggregation by natural phenolic compounds. *Cell Mol Life Sci* **75**, 3521-3538, doi:10.1007/s00018-018-2872-2 (2018).
- 430 Hornedo-Ortega, R. *et al.* Protocatechuic Acid: Inhibition of Fibril Formation, Destabilization of Preformed Fibrils of Amyloid-beta and alpha-Synuclein, and Neuroprotection. *J Agric Food Chem* **64**, 7722-7732, doi:10.1021/acs.jafc.6b03217 (2016).
- 431 Pandey, N., Strider, J., Nolan, W. C., Yan, S. X. & Galvin, J. E. Curcumin inhibits aggregation of alpha-synuclein. *Acta neuropathologica* **115**, 479-489, doi:10.1007/s00401-007-0332-4 (2008).
- 432 Zhu, M. *et al.* The flavonoid baicalein inhibits fibrillation of alpha-synuclein and disaggregates existing fibrils. *The Journal of biological chemistry* **279**, 26846-26857, doi:10.1074/jbc.M403129200 (2004).

- 433 Fazili, N. A. & Naeem, A. Anti-fibrillation potency of caffeic acid against an antidepressant induced fibrillogenesis of human alpha-synuclein: Implications for Parkinson's disease. *Biochimie* **108**, 178-185, doi:10.1016/j.biochi.2014.11.011 (2015).
- 434 Ahmad, B. & Lapidus, L. J. Curcumin prevents aggregation in alpha-synuclein by increasing reconfiguration rate. *The Journal of biological chemistry* **287**, 9193-9199, doi:10.1074/jbc.M111.325548 (2012).
- 435 Ehrnhoefer, D. E. *et al.* EGCG redirects amyloidogenic polypeptides into unstructured, off-pathway oligomers. *Nature structural & molecular biology* **15**, 558-566, doi:10.1038/nsmb.1437 (2008).
- 436 Lorenzen, N. *et al.* How epigallocatechin gallate can inhibit alpha-synuclein oligomer toxicity in vitro. *The Journal of biological chemistry* **289**, 21299-21310, doi:10.1074/jbc.M114.554667 (2014).
- 437 Bieschke, J. *et al.* EGCG remodels mature alpha-synuclein and amyloid-beta fibrils and reduces cellular toxicity. *Proceedings of the National Academy of Sciences of the United States of America* **107**, 7710-7715, doi:10.1073/pnas.0910723107 (2010).
- 438 Singh, P. K. *et al.* Curcumin modulates alpha-synuclein aggregation and toxicity. *ACS Chem Neurosci* **4**, 393-407, doi:10.1021/cn3001203 (2013).
- 439 Ardah, M. T. *et al.* Structure activity relationship of phenolic acid inhibitors of alpha-synuclein fibril formation and toxicity. *Front Aging Neurosci* **6**, 197, doi:10.3389/fnagi.2014.00197 (2014).
- 440 Kujawska, M. & Jodanis-Liebert, J. Polyphenols in Parkinson's Disease: A Systematic Review of In Vivo Studies. *Nutrients* **10**, doi:10.3390/nu10050642 (2018).
- 441 Hu, Q. *et al.* Baicalein inhibits alpha-synuclein oligomer formation and prevents progression of alpha-synuclein accumulation in a rotenone mouse model of Parkinson's disease. *Biochimica et biophysica acta* **1862**, 1883-1890, doi:10.1016/j.bbadis.2016.07.008 (2016).
- 442 Sharma, N. & Nehru, B. Curcumin affords neuroprotection and inhibits alpha-synuclein aggregation in lipopolysaccharide-induced Parkinson's disease model. *Inflammopharmacology* **26**, 349-360, doi:10.1007/s10787-017-0402-8 (2018).
- 443 Ogawa, N. *et al.* MPTP-induced parkinsonian model in mice: biochemistry, pharmacology and behavior. *Eur Neurol* **26 Suppl 1**, 16-23, doi:10.1159/000116351 (1987).
- 444 Jeon, B. S., Jackson-Lewis, V. & Burke, R. E. 6-Hydroxydopamine lesion of the rat substantia nigra: time course and morphology of cell death. *Neurodegeneration* **4**, 131-137, doi:10.1006/neur.1995.0016 (1995).
- 445 Pan-Montojo, F. *et al.* Progression of Parkinson's disease pathology is reproduced by intragastric administration of rotenone in mice. *PloS one* **5**, e8762, doi:10.1371/journal.pone.0008762 (2010).

- 446 Vajragupta, O. *et al.* Manganese complexes of curcumin and its derivatives: evaluation for the radical scavenging ability and neuroprotective activity. *Free radical biology & medicine* **35**, 1632-1644, doi:10.1016/j.freeradbiomed.2003.09.011 (2003).
- 447 Rajeswari, A. & Sabesan, M. Inhibition of monoamine oxidase-B by the polyphenolic compound, curcumin and its metabolite tetrahydrocurcumin, in a model of Parkinson's disease induced by MPTP neurodegeneration in mice. *Inflammopharmacology* **16**, 96-99, doi:10.1007/s10787-007-1614-0 (2008).
- 448 Nagarajan, S., Chellappan, D. R., Chinnaswamy, P. & Thulasingham, S. Ferulic acid pretreatment mitigates MPTP-induced motor impairment and histopathological alterations in C57BL/6 mice. *Pharm Biol* **53**, 1591-1601, doi:10.3109/13880209.2014.993041 (2015).
- 449 Lv, C. *et al.* Effect of Quercetin in the 1-Methyl-4-phenyl-1, 2, 3, 6-tetrahydropyridine-Induced Mouse Model of Parkinson's Disease. *Evid Based Complement Alternat Med* **2012**, 928643, doi:10.1155/2012/928643 (2012).
- 450 Yu, X. *et al.* Assessment of the treatment effect of baicalein on a model of Parkinsonian tremor and elucidation of the mechanism. *Life Sci* **91**, 5-13, doi:10.1016/j.lfs.2012.05.005 (2012).
- 451 Li, S. & Pu, X. P. Neuroprotective effect of kaempferol against a 1-methyl-4-phenyl-1,2,3,6-tetrahydropyridine-induced mouse model of Parkinson's disease. *Biol Pharm Bull* **34**, 1291-1296, doi:10.1248/bpb.34.1291 (2011).
- 452 Lee, E., Park, H. R., Ji, S. T., Lee, Y. & Lee, J. Baicalein attenuates astroglial activation in the 1-methyl-4-phenyl-1,2,3,4-tetrahydropyridine-induced Parkinson's disease model by downregulating the activations of nuclear factor-kappaB, ERK, and JNK. *J Neurosci Res* **92**, 130-139, doi:10.1002/jnr.23307 (2014).
- 453 Chen, M. *et al.* Tea polyphenols alleviate motor impairments, dopaminergic neuronal injury, and cerebral alpha-synuclein aggregation in MPTP-intoxicated parkinsonian monkeys. *Neuroscience* **286**, 383-392, doi:10.1016/j.neuroscience.2014.12.003 (2015).
- 454 Spinelli, K. J., Osterberg, V. R., Meshul, C. K., Soumyanath, A. & Unni, V. K. Curcumin Treatment Improves Motor Behavior in alpha-Synuclein Transgenic Mice. *PloS one* **10**, e0128510, doi:10.1371/journal.pone.0128510 (2015).
- 455 Chen, M. *et al.* Fasudil and its analogs: a new powerful weapon in the long war against central nervous system disorders? *Expert Opin Investig Drugs* **22**, 537-550, doi:10.1517/13543784.2013.778242 (2013).
- 456 He, Q. *et al.* Inhibition of Rho-kinase by Fasudil protects dopamine neurons and attenuates inflammatory response in an intranasal lipopolysaccharide-mediated Parkinson's model. *Eur J Neurosci* **43**, 41-52, doi:10.1111/ejn.13132 (2016).
- 457 Tatenhorst, L. *et al.* Fasudil attenuates aggregation of alpha-synuclein in models of Parkinson's disease. *Acta neuropathologica communications* **4**, 39, doi:10.1186/s40478-016-0310-y (2016).
- 458 Robustelli, P. *et al.* Molecular Basis of Small-Molecule Binding to alpha-Synuclein. *J Am Chem Soc* **144**, 2501-2510, doi:10.1021/jacs.1c07591 (2022).

- 459 Giasson, B. I. *et al.* Neuronal alpha-synucleinopathy with severe movement disorder in mice expressing A53T human alpha-synuclein. *Neuron* **34**, 521-533, doi:10.1016/s0896-6273(02)00682-7 (2002).
- 460 Koprach, J. B., Johnston, T. H., Reyes, M. G., Sun, X. & Brotchie, J. M. Expression of human A53T alpha-synuclein in the rat substantia nigra using a novel AAV1/2 vector produces a rapidly evolving pathology with protein aggregation, dystrophic neurite architecture and nigrostriatal degeneration with potential to model the pathology of Parkinson's disease. *Mol Neurodegener* **5**, 43, doi:10.1186/1750-1326-5-43 (2010).
- 461 Yang, Y. J. *et al.* Fasudil Promotes alpha-Synuclein Clearance in an AAV-Mediated alpha-Synuclein Rat Model of Parkinson's Disease by Autophagy Activation. *J Parkinsons Dis* **10**, 969-979, doi:10.3233/JPD-191909 (2020).
- 462 Wood, J. G., Mirra, S. S., Pollock, N. J. & Binder, L. I. Neurofibrillary tangles of Alzheimer disease share antigenic determinants with the axonal microtubule-associated protein tau (tau). *Proceedings of the National Academy of Sciences of the United States of America* **83**, 4040-4043, doi:10.1073/pnas.83.11.4040 (1986).
- 463 Wischik, C. M., Edwards, P. C., Lai, R. Y., Roth, M. & Harrington, C. R. Selective inhibition of Alzheimer disease-like tau aggregation by phenothiazines. *Proceedings of the National Academy of Sciences of the United States of America* **93**, 11213-11218, doi:10.1073/pnas.93.20.11213 (1996).
- 464 Wischik, C. M. *et al.* Tau aggregation inhibitor therapy: an exploratory phase 2 study in mild or moderate Alzheimer's disease. *J Alzheimers Dis* **44**, 705-720, doi:10.3233/JAD-142874 (2015).
- 465 Gauthier, S. *et al.* Efficacy and safety of tau-aggregation inhibitor therapy in patients with mild or moderate Alzheimer's disease: a randomised, controlled, double-blind, parallel-arm, phase 3 trial. *Lancet* **388**, 2873-2884, doi:10.1016/S0140-6736(16)31275-2 (2016).
- 466 Wilcock, G. K. *et al.* Potential of Low Dose Leuco-Methylthioninium Bis(Hydromethanesulphonate) (LMTM) Monotherapy for Treatment of Mild Alzheimer's Disease: Cohort Analysis as Modified Primary Outcome in a Phase III Clinical Trial. *J Alzheimers Dis* **61**, 435-457, doi:10.3233/JAD-170560 (2018).
- 467 Schwab, K. *et al.* A Protein Aggregation Inhibitor, Leuco-Methylthioninium Bis(Hydromethanesulfonate), Decreases alpha-Synuclein Inclusions in a Transgenic Mouse Model of Synucleinopathy. *Frontiers in molecular neuroscience* **10**, 447, doi:10.3389/fnmol.2017.00447 (2017).
- 468 Frahm, S. *et al.* Alpha-Synuclein transgenic mice, h-alpha-SynL62, display alpha-Syn aggregation and a dopaminergic phenotype reminiscent of Parkinson's disease. *Behav Brain Res* **339**, 153-168, doi:10.1016/j.bbr.2017.11.025 (2018).
- 469 Brycki, B., Koenig, H. & Pospieszny, T. Quaternary Alkylammonium Conjugates of Steroids: Synthesis, Molecular Structure, and Biological Studies. *Molecules* **20**, 20887-20900, doi:10.3390/molecules201119735 (2015).

- 470 Moore, K. S. *et al.* Squalamine: an aminosterol antibiotic from the shark. *Proceedings of the National Academy of Sciences of the United States of America* **90**, 1354-1358, doi:10.1073/pnas.90.4.1354 (1993).
- 471 Khelaifia, S. & Drancourt, M. Susceptibility of archaea to antimicrobial agents: applications to clinical microbiology. *Clin Microbiol Infect* **18**, 841-848, doi:10.1111/j.1469-0691.2012.03913.x (2012).
- 472 Cushnie, T. P., Cushnie, B. & Lamb, A. J. Alkaloids: an overview of their antibacterial, antibiotic-enhancing and antivirulence activities. *Int J Antimicrob Agents* **44**, 377-386, doi:10.1016/j.ijantimicag.2014.06.001 (2014).
- 473 Schlottmann, P. G. *et al.* New Treatment Modalities for Neovascular Age-Related Macular Degeneration. *Asia Pac J Ophthalmol (Phila)* **6**, 514-519, doi:10.22608/APO.2017258 (2017).
- 474 Perni, M. *et al.* A natural product inhibits the initiation of alpha-synuclein aggregation and suppresses its toxicity. *Proceedings of the National Academy of Sciences of the United States of America* **114**, E1009-E1017, doi:10.1073/pnas.1610586114 (2017).
- 475 Yeung, T. *et al.* Membrane phosphatidylserine regulates surface charge and protein localization. *Science* **319**, 210-213, doi:10.1126/science.1152066 (2008).
- 476 Sumioka, A., Yan, D. & Tomita, S. TARP phosphorylation regulates synaptic AMPA receptors through lipid bilayers. *Neuron* **66**, 755-767, doi:10.1016/j.neuron.2010.04.035 (2010).
- 477 Alexander, R. T. *et al.* Membrane surface charge dictates the structure and function of the epithelial Na⁺/H⁺ exchanger. *EMBO J* **30**, 679-691, doi:10.1038/emboj.2010.356 (2011).
- 478 Galvagnion, C. *et al.* Lipid vesicles trigger alpha-synuclein aggregation by stimulating primary nucleation. *Nat Chem Biol* **11**, 229-234, doi:10.1038/nchembio.1750 (2015).
- 479 Limbocker, R. *et al.* Squalamine and Its Derivatives Modulate the Aggregation of Amyloid-beta and alpha-Synuclein and Suppress the Toxicity of Their Oligomers. *Front Neurosci* **15**, 680026, doi:10.3389/fnins.2021.680026 (2021).
- 480 Smith, A. M. *et al.* The protein tyrosine phosphatase 1B inhibitor MSI-1436 stimulates regeneration of heart and multiple other tissues. *NPJ Regen Med* **2**, 4, doi:10.1038/s41536-017-0008-1 (2017).
- 481 Perni, M. *et al.* Multistep Inhibition of alpha-Synuclein Aggregation and Toxicity in Vitro and in Vivo by Trodusquemine. *ACS Chem Biol* **13**, 2308-2319, doi:10.1021/acschembio.8b00466 (2018).
- 482 Limbocker, R. *et al.* Trodusquemine displaces protein misfolded oligomers from cell membranes and abrogates their cytotoxicity through a generic mechanism. *Commun Biol* **3**, 435, doi:10.1038/s42003-020-01140-8 (2020).
- 483 Buell, A. K. *et al.* Solution conditions determine the relative importance of nucleation and growth processes in alpha-synuclein aggregation. *Proceedings of the National*

- Academy of Sciences of the United States of America* **111**, 7671-7676, doi:10.1073/pnas.1315346111 (2014).
- 484 Flagmeier, P. *et al.* Mutations associated with familial Parkinson's disease alter the initiation and amplification steps of alpha-synuclein aggregation. *Proceedings of the National Academy of Sciences of the United States of America* **113**, 10328-10333, doi:10.1073/pnas.1604645113 (2016).
- 485 Brown, J. W. *et al.* beta-Synuclein suppresses both the initiation and amplification steps of alpha-synuclein aggregation via competitive binding to surfaces. *Scientific reports* **6**, 36010, doi:10.1038/srep36010 (2016).
- 486 Chen, S. W. *et al.* Structural characterization of toxic oligomers that are kinetically trapped during alpha-synuclein fibril formation. *Proceedings of the National Academy of Sciences of the United States of America* **112**, E1994-2003, doi:10.1073/pnas.1421204112 (2015).
- 487 Evangelisti, E. *et al.* Binding affinity of amyloid oligomers to cellular membranes is a generic indicator of cellular dysfunction in protein misfolding diseases. *Scientific reports* **6**, 32721, doi:10.1038/srep32721 (2016).
- 488 Prabhudesai, S. *et al.* A novel "molecular tweezer" inhibitor of alpha-synuclein neurotoxicity in vitro and in vivo. *Neurotherapeutics* **9**, 464-476, doi:10.1007/s13311-012-0105-1 (2012).
- 489 Acharya, S. *et al.* Molecular basis for preventing alpha-synuclein aggregation by a molecular tweezer. *The Journal of biological chemistry* **289**, 10727-10737, doi:10.1074/jbc.M113.524520 (2014).
- 490 Rink, E. & Wullimann, M. F. The teleostean (zebrafish) dopaminergic system ascending to the subpallium (striatum) is located in the basal diencephalon (posterior tuberculum). *Brain Res* **889**, 316-330, doi:10.1016/s0006-8993(00)03174-7 (2001).
- 491 Chesselet, M. F. *et al.* A progressive mouse model of Parkinson's disease: the Thy1-aSyn ("Line 61") mice. *Neurotherapeutics* **9**, 297-314, doi:10.1007/s13311-012-0104-2 (2012).
- 492 Richter, F. *et al.* A Molecular Tweezer Ameliorates Motor Deficits in Mice Overexpressing alpha-Synuclein. *Neurotherapeutics* **14**, 1107-1119, doi:10.1007/s13311-017-0544-9 (2017).
- 493 Janezic, S. *et al.* Deficits in dopaminergic transmission precede neuron loss and dysfunction in a new Parkinson model. *Proceedings of the National Academy of Sciences of the United States of America* **110**, E4016-4025, doi:10.1073/pnas.1309143110 (2013).
- 494 Refolo, V. *et al.* Progressive striatonigral degeneration in a transgenic mouse model of multiple system atrophy: translational implications for interventional therapies. *Acta neuropathologica communications* **6**, 2, doi:10.1186/s40478-017-0504-y (2018).
- 495 Bengoa-Vergniory, N. *et al.* CLR01 protects dopaminergic neurons in vitro and in mouse models of Parkinson's disease. *Nature communications* **11**, 4885, doi:10.1038/s41467-020-18689-x (2020).

- 496 Herrera-Vaquero, M. *et al.* The molecular tweezer CLR01 reduces aggregated, pathologic, and seeding-competent alpha-synuclein in experimental multiple system atrophy. *Biochim Biophys Acta Mol Basis Dis* **1865**, 165513, doi:10.1016/j.bbadis.2019.07.007 (2019).
- 497 Sinha, S. *et al.* Lysine-specific molecular tweezers are broad-spectrum inhibitors of assembly and toxicity of amyloid proteins. *J Am Chem Soc* **133**, 16958-16969, doi:10.1021/ja206279b (2011).
- 498 Ferreira, N. *et al.* Molecular tweezers targeting transthyretin amyloidosis. *Neurotherapeutics* **11**, 450-461, doi:10.1007/s13311-013-0256-8 (2014).
- 499 Tsigelny, I. F., Sharikov, Y., Miller, M. A. & Masliah, E. Mechanism of alpha-synuclein oligomerization and membrane interaction: theoretical approach to unstructured proteins studies. *Nanomedicine* **4**, 350-357, doi:10.1016/j.nano.2008.05.005 (2008).
- 500 Tsigelny, I. F. *et al.* Role of alpha-synuclein penetration into the membrane in the mechanisms of oligomer pore formation. *FEBS J* **279**, 1000-1013, doi:10.1111/j.1742-4658.2012.08489.x (2012).
- 501 Wrasidlo, W. *et al.* A de novo compound targeting alpha-synuclein improves deficits in models of Parkinson's disease. *Brain : a journal of neurology* **139**, 3217-3236, doi:10.1093/brain/aww238 (2016).
- 502 Price, D. L. *et al.* The small molecule alpha-synuclein misfolding inhibitor, NPT200-11, produces multiple benefits in an animal model of Parkinson's disease. *Scientific reports* **8**, 16165, doi:10.1038/s41598-018-34490-9 (2018).
- 503 Wagner, J. *et al.* Anle138b: a novel oligomer modulator for disease-modifying therapy of neurodegenerative diseases such as prion and Parkinson's disease. *Acta neuropathologica* **125**, 795-813, doi:10.1007/s00401-013-1114-9 (2013).
- 504 Kurnik, M. *et al.* Potent alpha-Synuclein Aggregation Inhibitors, Identified by High-Throughput Screening, Mainly Target the Monomeric State. *Cell chemical biology* **25**, 1389-1402 e1389, doi:10.1016/j.chembiol.2018.08.005 (2018).
- 505 Hideshima, M. *et al.* Two-step screening method to identify alpha-synuclein aggregation inhibitors for Parkinson's disease. *Scientific reports* **12**, 351, doi:10.1038/s41598-021-04131-9 (2022).
- 506 Staats, R. *et al.* Screening of small molecules using the inhibition of oligomer formation in alpha-synuclein aggregation as a selection parameter. *Commun Chem* **3**, doi:ARTN 191 10.1038/s42004-020-00412-y (2020).
- 507 Deeg, A. A. *et al.* Anle138b and related compounds are aggregation specific fluorescence markers and reveal high affinity binding to alpha-synuclein aggregates. *Biochimica et biophysica acta* **1850**, 1884-1890, doi:10.1016/j.bbagen.2015.05.021 (2015).

- 508 Levin, J. *et al.* The oligomer modulator anle138b inhibits disease progression in a Parkinson mouse model even with treatment started after disease onset. *Acta neuropathologica* **127**, 779-780, doi:10.1007/s00401-014-1265-3 (2014).
- 509 Heras-Garvin, A. *et al.* Anle138b modulates alpha-synuclein oligomerization and prevents motor decline and neurodegeneration in a mouse model of multiple system atrophy. *Movement disorders : official journal of the Movement Disorder Society* **34**, 255-263, doi:10.1002/mds.27562 (2019).
- 510 Fellner, L. *et al.* Anle138b Partly Ameliorates Motor Deficits Despite Failure of Neuroprotection in a Model of Advanced Multiple System Atrophy. *Front Neurosci* **10**, 99, doi:10.3389/fnins.2016.00099 (2016).
- 511 Levin, J. *et al.* Safety, tolerability and pharmacokinetics of the oligomer modulator anle138b with exposure levels sufficient for therapeutic efficacy in a murine Parkinson model: A randomised, double-blind, placebo-controlled phase 1a trial. *EBioMedicine* **80**, 104021, doi:10.1016/j.ebiom.2022.104021 (2022).
- 512 Goedert, M. & Spillantini, M. G. Lewy body diseases and multiple system atrophy as alpha-synucleinopathies. *Molecular psychiatry* **3**, 462-465, doi:10.1038/sj.mp.4000458 (1998).
- 513 Bower, J. H., Maraganore, D. M., McDonnell, S. K. & Rocca, W. A. Incidence of progressive supranuclear palsy and multiple system atrophy in Olmsted County, Minnesota, 1976 to 1990. *Neurology* **49**, 1284-1288, doi:10.1212/wnl.49.5.1284 (1997).
- 514 Jecmenica-Lukic, M., Poewe, W., Tolosa, E. & Wenning, G. K. Premotor signs and symptoms of multiple system atrophy. *The Lancet. Neurology* **11**, 361-368, doi:10.1016/S1474-4422(12)70022-4 (2012).
- 515 McKay, J. H. & Cheshire, W. P. First symptoms in multiple system atrophy. *Clinical autonomic research : official journal of the Clinical Autonomic Research Society* **28**, 215-221, doi:10.1007/s10286-017-0500-0 (2018).
- 516 Kollensperger, M. *et al.* Red flags for multiple system atrophy. *Movement disorders : official journal of the Movement Disorder Society* **23**, 1093-1099, doi:10.1002/mds.21992 (2008).
- 517 Tison, F. *et al.* Pain in multiple system atrophy. *Journal of neurology* **243**, 153-156, doi:10.1007/BF02444007 (1996).
- 518 Kollensperger, M. *et al.* Presentation, diagnosis, and management of multiple system atrophy in Europe: final analysis of the European multiple system atrophy registry. *Movement disorders : official journal of the Movement Disorder Society* **25**, 2604-2612, doi:10.1002/mds.23192 (2010).
- 519 Boesch, S. M., Wenning, G. K., Ransmayr, G. & Poewe, W. Dystonia in multiple system atrophy. *Journal of neurology, neurosurgery, and psychiatry* **72**, 300-303, doi:10.1136/jnnp.72.3.300 (2002).

- 520 Figueroa, J. J. *et al.* Multiple system atrophy: prognostic indicators of survival. *Movement disorders : official journal of the Movement Disorder Society* **29**, 1151-1157, doi:10.1002/mds.25927 (2014).
- 521 Watanabe, H. *et al.* Progression and prognosis in multiple system atrophy: an analysis of 230 Japanese patients. *Brain : a journal of neurology* **125**, 1070-1083, doi:10.1093/brain/awf117 (2002).
- 522 Wenning, G. K. *et al.* The natural history of multiple system atrophy: a prospective European cohort study. *The Lancet. Neurology* **12**, 264-274, doi:10.1016/S1474-4422(12)70327-7 (2013).
- 523 Multiple-System Atrophy Research, C. Mutations in COQ2 in familial and sporadic multiple-system atrophy. *The New England journal of medicine* **369**, 233-244, doi:10.1056/NEJMoa1212115 (2013).
- 524 Ferguson, M. C. *et al.* SHC2 gene copy number in multiple system atrophy (MSA). *Clinical autonomic research : official journal of the Clinical Autonomic Research Society* **24**, 25-30, doi:10.1007/s10286-013-0216-8 (2014).
- 525 Sasaki, H. *et al.* Copy number loss of (src homology 2 domain containing)-transforming protein 2 (SHC2) gene: discordant loss in monozygotic twins and frequent loss in patients with multiple system atrophy. *Molecular brain* **4**, 24, doi:10.1186/1756-6606-4-24 (2011).
- 526 Scholz, S. W. *et al.* SNCA variants are associated with increased risk for multiple system atrophy. *Annals of neurology* **65**, 610-614, doi:10.1002/ana.21685 (2009).
- 527 Al-Chalabi, A. *et al.* Genetic variants of the alpha-synuclein gene SNCA are associated with multiple system atrophy. *PloS one* **4**, e7114, doi:10.1371/journal.pone.0007114 (2009).
- 528 Papp, M. I., Kahn, J. E. & Lantos, P. L. Glial cytoplasmic inclusions in the CNS of patients with multiple system atrophy (striatonigral degeneration, olivopontocerebellar atrophy and Shy-Drager syndrome). *Journal of the neurological sciences* **94**, 79-100, doi:10.1016/0022-510x(89)90219-0 (1989).
- 529 Song, Y. J. *et al.* p25alpha relocates in oligodendroglia from myelin to cytoplasmic inclusions in multiple system atrophy. *The American journal of pathology* **171**, 1291-1303, doi:10.2353/ajpath.2007.070201 (2007).
- 530 Lindersson, E. *et al.* p25alpha Stimulates alpha-synuclein aggregation and is co-localized with aggregated alpha-synuclein in alpha-synucleinopathies. *The Journal of biological chemistry* **280**, 5703-5715, doi:10.1074/jbc.M410409200 (2005).
- 531 Yazawa, I. *et al.* Mouse model of multiple system atrophy alpha-synuclein expression in oligodendrocytes causes glial and neuronal degeneration. *Neuron* **45**, 847-859, doi:10.1016/j.neuron.2005.01.032 (2005).
- 532 Watts, J. C. *et al.* Transmission of multiple system atrophy prions to transgenic mice. *Proceedings of the National Academy of Sciences of the United States of America* **110**, 19555-19560, doi:10.1073/pnas.1318268110 (2013).

- 533 Angot, E. *et al.* Alpha-synuclein cell-to-cell transfer and seeding in grafted dopaminergic neurons in vivo. *PloS one* **7**, e39465, doi:10.1371/journal.pone.0039465 (2012).
- 534 Desplats, P. *et al.* Inclusion formation and neuronal cell death through neuron-to-neuron transmission of alpha-synuclein. *Proceedings of the National Academy of Sciences of the United States of America* **106**, 13010-13015, doi:10.1073/pnas.0903691106 (2009).
- 535 Kuzdas-Wood, D. *et al.* Towards translational therapies for multiple system atrophy. *Prog Neurobiol* **118**, 19-35, doi:10.1016/j.pneurobio.2014.02.007 (2014).
- 536 Gilman, S. *et al.* Second consensus statement on the diagnosis of multiple system atrophy. *Neurology* **71**, 670-676, doi:10.1212/01.wnl.0000324625.00404.15 (2008).
- 537 Wenning, G. K. & Working Group on Atypical Parkinsonism of the Austrian Parkinson's, S. Placebo-controlled trial of amantadine in multiple-system atrophy. *Clinical neuropharmacology* **28**, 225-227, doi:10.1097/01.wnf.0000183240.47960.f0 (2005).
- 538 Mancini, F. *et al.* Double-blind, placebo-controlled study to evaluate the efficacy and safety of botulinum toxin type A in the treatment of drooling in parkinsonism. *Movement disorders : official journal of the Movement Disorder Society* **18**, 685-688, doi:10.1002/mds.10420 (2003).
- 539 Gazulla, J. & Benavente, M. I. [Improvements in the symptoms of olivopontocerebellar atrophy with gabapentin]. *Revista de neurologia* **40**, 285-288 (2005).
- 540 Heo, J. H., Lee, S. T., Chu, K. & Kim, M. The efficacy of combined estrogen and buspirone treatment in olivopontocerebellar atrophy. *Journal of the neurological sciences* **271**, 87-90, doi:10.1016/j.jns.2008.03.016 (2008).
- 541 Boeve, B. F., Silber, M. H. & Ferman, T. J. Melatonin for treatment of REM sleep behavior disorder in neurologic disorders: results in 14 patients. *Sleep medicine* **4**, 281-284, doi:10.1016/s1389-9457(03)00072-8 (2003).
- 542 Jankovic, J. *et al.* Neurogenic orthostatic hypotension: a double-blind, placebo-controlled study with midodrine. *The American journal of medicine* **95**, 38-48, doi:10.1016/0002-9343(93)90230-m (1993).
- 543 Freeman, R., Landsberg, L. & Young, J. The treatment of neurogenic orthostatic hypotension with 3,4-DL-threo-dihydroxyphenylserine: a randomized, placebo-controlled, crossover trial. *Neurology* **53**, 2151-2157, doi:10.1212/wnl.53.9.2151 (1999).
- 544 McKeith, I. G. *et al.* Diagnosis and management of dementia with Lewy bodies: Fourth consensus report of the DLB Consortium. *Neurology* **89**, 88-100, doi:10.1212/WNL.0000000000004058 (2017).
- 545 Gomperts, S. N. Lewy Body Dementias: Dementia With Lewy Bodies and Parkinson Disease Dementia. *Continuum* **22**, 435-463, doi:10.1212/CON.0000000000000309 (2016).

- 546 Berge, G., Sando, S. B., Rongve, A., Aarsland, D. & White, L. R. Apolipoprotein E epsilon2 genotype delays onset of dementia with Lewy bodies in a Norwegian cohort. *Journal of neurology, neurosurgery, and psychiatry* **85**, 1227-1231, doi:10.1136/jnnp-2013-307228 (2014).
- 547 Lerche, S. *et al.* Dementia with lewy bodies: GBA1 mutations are associated with cerebrospinal fluid alpha-synuclein profile. *Movement disorders : official journal of the Movement Disorder Society* **34**, 1069-1073, doi:10.1002/mds.27731 (2019).
- 548 Orme, T., Guerreiro, R. & Bras, J. The Genetics of Dementia with Lewy Bodies: Current Understanding and Future Directions. *Current neurology and neuroscience reports* **18**, 67, doi:10.1007/s11910-018-0874-y (2018).
- 549 Walker, Z., Possin, K. L., Boeve, B. F. & Aarsland, D. Lewy body dementias. *Lancet* **386**, 1683-1697, doi:10.1016/S0140-6736(15)00462-6 (2015).
- 550 Hansen, D., Ling, H., Lashley, T., Holton, J. L. & Warner, T. T. Review: Clinical, neuropathological and genetic features of Lewy body dementias. *Neuropathology and applied neurobiology* **45**, 635-654, doi:10.1111/nan.12554 (2019).
- 551 Duda, J. E. Pathology and neurotransmitter abnormalities of dementia with Lewy bodies. *Dementia and geriatric cognitive disorders* **17 Suppl 1**, 3-14, doi:10.1159/000074677 (2004).
- 552 Villemagne, V. L., Dore, V., Burnham, S. C., Masters, C. L. & Rowe, C. C. Imaging tau and amyloid-beta proteinopathies in Alzheimer disease and other conditions. *Nature reviews. Neurology* **14**, 225-236, doi:10.1038/nrneurol.2018.9 (2018).
- 553 Ruffmann, C. *et al.* Cortical Lewy bodies and Abeta burden are associated with prevalence and timing of dementia in Lewy body diseases. *Neuropathology and applied neurobiology* **42**, 436-450, doi:10.1111/nan.12294 (2016).
- 554 Sierra, M., Gelpi, E., Marti, M. J. & Compta, Y. Lewy- and Alzheimer-type pathologies in midbrain and cerebellum across the Lewy body disorders spectrum. *Neuropathology and applied neurobiology* **42**, 451-462, doi:10.1111/nan.12308 (2016).
- 555 Taylor, J. P. *et al.* New evidence on the management of Lewy body dementia. *The Lancet. Neurology* **19**, 157-169, doi:10.1016/S1474-4422(19)30153-X (2020).
- 556 Walker, Z. & Stevens, T. Dementia with Lewy bodies: clinical characteristics and diagnostic criteria. *Journal of geriatric psychiatry and neurology* **15**, 188-194, doi:10.1177/089198870201500403 (2002).